CSCS
Swiss National Supercomputing Centre

Scientific Report
Scientific Report
entific Report
Report
Scientific Report
Scientific Report
c Report
eport
ort
Scientific

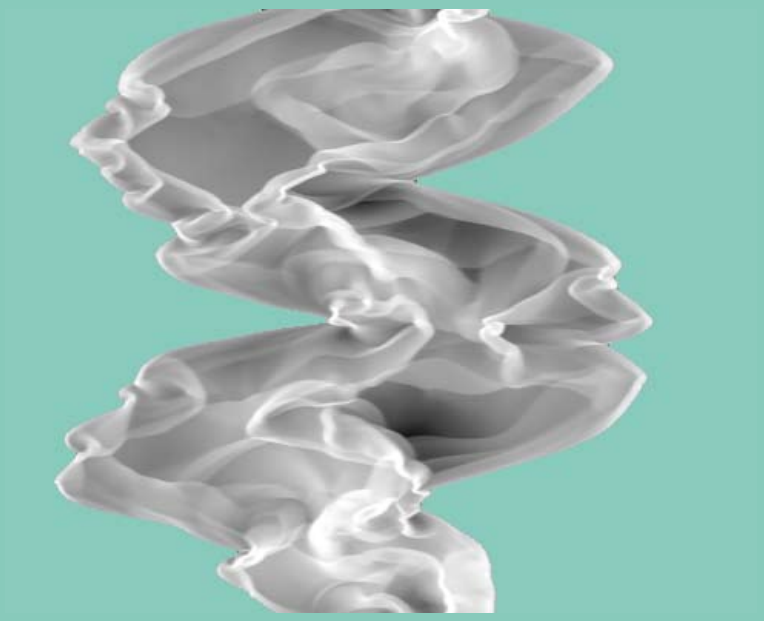

Scientific Report 2006/2007

CSCS
Swiss National Supercomputing Centre

Scientific Report 2006/2007

Content

Editorial by Staatssekretär Mauro Dell' Ambrogio

Mauro Dell' Ambrogio, Segretario di Stato

Una politica tra regionalismo e globalizzazione

L'educazione superiore e la ricerca sono diventate un fattore determinante di sviluppo, non solo a livello nazionale, ma per ogni regione. Istituzioni in questo ambito non solo apportano prestigio, ma contribuiscono direttamente ed indirettamente alla creazione di posti di lavoro qualificati e di attività economiche innovative. Accanto allo sforzo dei governi centrali, investimenti in infrastrutture e personale qualificato per la ricerca sono fatti a buona ragione anche dai poteri pubblici locali, in un contesto competitivo. L'attribuzione su concorso di progetti di ricerca è capace di sovvertire in tempi relativamente brevi le graduatorie d'importanza. Questa competizione si giocava un tempo su scala internazionale o tra pochi centri di uno stesso paese. Con la crescita del numero di studenti e di ricercatori, ogni località può oggi ambire a competere. Sono significative le iniziative nate in pochi anni nelle regioni della Svizzera centrale, del lago Bodanico e dell'Insubria. Lo stesso sviluppo delle scuole universitarie professionali in Svizzera, oltre che come novità tipologica, può essere letto come sfida di località minori alle maggiori.

Questa evoluzione accentua il dilemma postosi già alle origini dello stato federale: se in Svizzera la politica dell'educazione superiore e della ricerca deve concentrare le risorse in pochi poli per una migliore visibilità e attrattiva internazionale, o in molti per diffondere capillarmente le potenzialità di sviluppo. In teoria, il coordinamento da farsi tra Confederazione e Cantoni dovrebbe tendere ad un equilibrio ottimale tra le due tendenze: creare poli di qualità sufficiente a competere internazionalmente, in sedi sufficienti di numero per sostenere uno sviluppo armonico e generalizzato del territorio; fattore quest'ultimo di qualità di vita nei centri medesimi. In pratica, in un sistema federalista prevale la spinta regionalizzatrice. Non solo con la proliferazione dei poli. È significativa la pressione al decentramento esercitata sul settore gestito centralmente per eccellenza: quello delle scuole politecniche federali. Nel quale suscitano talvolta più attenzione le battaglie sul «dove» di quelle sul «cosa» si fa, almeno dal punto di vista della politica.

D'altra parte le risorse centralizzate sono assorbite in misura crescente dalla partecipazione al meccanismo di competizione-distribuzione su scala continentale. Nonostante le apparenze, assistiamo ad una progressiva rinuncia dello Stato nazionale al ruolo di gestore di un sistema competitivo, così come non è più ipotizzabile che esso gestisca un sistema industriale o produttivo in genere. Come l'educazione superiore e la ricerca sono divenute fattori economici decisivi, è inevitabile che si ritrovino in essi i paradigmi della competizione economica: libertà d'intraprendere e competizione su scala globale. La differenza sta nel fatto che i soggetti non sono privati imprenditori, ma enti pubblici, portatori del proprio inter-

esse nazionale o locale in competizione con gli altri. In nome del servizio pubblico o della promozione economica, ogni cantone o città si adopera nell'interesse delle istituzioni sul proprio territorio, poco importa se pubbliche o private e a chi appartenenti.

Una politica nazionale avrebbe già obiettivo ambizioso nella distribuzione intelligente delle risorse comuni. Evitando i paradossi che derivano da approcci settoriali. Il sistema diversificato del quale disponiamo (scuole politecniche federali, università cantonali, scuole universitarie professionali in condivisione tra Cantoni) è nel contempo valore importante per competere e fattore di rischio quando s'interviene per gestirlo o pianificarlo. È ad esempio giustificato che Confederazione e Cantoni insieme pongano un freno al proliferare di offerte didattiche simili in località vicine; ma questo va condotto con visione complessiva, o niente affatto. Non si può per esempio contenere l'offerta di formazioni postgrado nelle scuole universitarie professionali, con argomenti di tipologia, senza considerare le formazioni analoghe offerte da altre istituzioni, almeno dal punto di vista del mercato del lavoro e dell'impatto per lo sviluppo locale. Perché mai master in ingegneria dovrebbero essere offerti largamente a Zurigo e Losanna, per di più a intero costo della Confederazione, e autorizzati invece col contagocce a Lugano, se una SUPSI decide di offrirli a spese principalmente del Cantone ?

La Svizzera è composta da regioni troppo diverse perche possa imporre, per legge federale o accordi intercantonali, tipologie e regole unitarie fondate su di esse. Ciò che può stare accanto, simile ma offerto da istituzioni con diverso profilo in una grande città, può meglio esistere sotto un medesimo tetto istituzionale in una piccola regione. Quella delle tipologie non è scorciatoia praticabile per distribuire equamente le risorse messe in comune, tra l'esigenza di ben figurare nella competizione internazionale e quella di conservare ragionevoli opportunità di crescita in ogni regione.

A policy between regionalism and globalisation

Higher education and research have become a determining factor of national, but also of regional development. Institutions working in this area not only bring prestige, but contribute directly and indirectly to the creation of skilled jobs and innovative eco-nomic activity. Beside the effort of central governments, local public authorities also invest in infrastructure and skilled labour for research purposes for good reasons in a competitive context. The attribution of research projects by competition can eliminate major candidates in relatively short times. In the past this competition took place on an international scale or between a handful of centres within a single country. With the increase in the number of students and researchers, every locality anywhere in the world can today aspire to compete. Significant initiatives have been created in recent years in regions of central Switzerland, Lake Constance and the northern Lombardy. The development of universities of applied sciences in Switzerland not only sets a new trend, but also can be read as a challenge by the smaller localities to larger ones.

This evolution emphasizes the dilemma that arose at the origins of the federal State – whether, in Switzerland, higher education and research policy should concentrate re-sources in just a few centres in order to achieve better visibility and international appeal, or in multiple locations in order to spread the development potential to all the regions. In theory, the coordination to be struck between Confederation and Cantons should tend towards an ideal balance between the two trends by creating a large enough number of centres of sufficient quality to compete internationally, whilst supporting the harmonic and generalised development of the territory, thereby improving the quality of life in the centres themselves. In practice, in a federalist system, the urge to regionalise prevails and not only with the proliferation of centres. The pressure to decentralise exerted on the centrally-managed sector – that of the federal polytechnics par excellence – is significant. In this struggle, more attention is sometimes paid to "where something should be done" than to "what should be done", at least from the policy point of view.

Conversely, centralised resources are increasingly absorbed by participation in the competition-distribution mechanism on a continental scale. Despite appearances, we are witnessing a progressive renunciation by the Nation State of the role of administrator of a competitive system, in the same way as it is no longer possible to imagine that it could administer an industrial or productive system in general. As higher education and research have become decisive economic factors, it is inevitable that they are found to embody the paradigms of economic competition – entrepreneurial freedom and global competition. The difference lies in the fact that the subjects are not private entrepreneurs, but public bodies, bearers of the very national or local interest in the competition with others. In the name of public service or economic promotion, every canton or city strives for the interests of the institutions on its own territory, regardless of whether they are public or private and to whom they may belong.

The intelligent distribution of common resources would already represent an ambitious objective for a national policy and would avoid the paradoxes that derive from sectorial approaches. The diversified system of which we dispose (federal polytechnics, cantonal universities, universities of applied sciences shared between cantons) is at the same time an important asset in order to compete and a risk factor when it comes to administering or planning it. It is, for example, justified that the Confederation and Cantons together place a limit on the proliferation of similar educational of-fers in neighbouring localities; but this must be done with an overall view, or not at all. It is not possible, for

example, to contain the offer of postgraduate education in universities of applied sciences on the grounds of their nature, without considering similar training offered by other institutions, at least from the point of view of the labour market and the impact on local development. Why on earth should a master's in engineering be widely offered in Zurich and Lausanne, moreover entirely at the cost of the Confederation, while it is sparsely authorised in Lugano, if a SUPSI [University of applied sciences of Southern Switzerland] decides to offer them mainly at the expense of the Canton?

The regions of Switzerland are too varied to impose, be it by federal law or intercantonal agreements, unified types of establishments and sets of rules based thereon. Similar offers of different types that exist side by side in a big city, could better exist under a single institutional roof in a small region. The criteria of establishment types is not a feasible shortcut to ensure a fair distribution of common resources between the need to be competitive at the international level and that of conserving reasonable growth opportunities in each region.

ALPS - Advanced Large Projects in Supercomputing

Modeling protein-protein interactions at the atomic level

Dr. Francesco Luigi Gervasio

Project Leader: Prof. Michele Parrinello
Coworkers: Anna Berteotti, Massimiliano Bonomi, Davide Branduardi

Subproject: activation mechanism of Cyclin-dependent kinases

The ALPS project 'Modeling protein-protein interactions at the atomic level' involved both the development of multi-layer parallel algorithms and the study of three relevant biological systems:

1. The aggregation of amyloid fibrils.
2. The activation mechanism of Cyclin-dependent kinases (CDK2,CDK5).
3. The study of HIV protease folding.

Each of these biological systems has been studied as a full scale subproject and each of them yielded very interesting results. In the following I will describe in detail the second subproject, chosen both for the novelty and the relevance of the results obtained.

Cyclin dependent kinases (CDKs) are a biologically and pharmacologically important family of kinase proteins implicated in the eukaryotic cell cycle progression and timing. Malfunctioning of CDKs is at the root of several diseases including cancer and Alzheimer's disease. To be fully active, CDKs require a large-scale closed-to-open switching transition consisting in a rotation of an α-helix of almost 90°, and relocation of the loop that in the closed state hinders the access to the active site. Given the importance of this kinase family, the CDKs activation process has attracted a large interest and has been extensively studied by X-ray crystallography which provided various CDKs complexes both in the active and inactive state. However, the microscopic atomistic details of the activation/deactivation dynamics are still scarce.

We focused on CDK5, a special member of the family which, despite a large sequence identity with the other CDKs shows several important differences. We addressed the microscopic details of the CDK5 open-to-closed transition. To obtain this goal we performed state-of-the-art fully atomistic molecular dynamics simulations with a recently developed powerful sampling technique [1]. This was necessary to overcome the time-scale problem. Indeed, typical atomistic MD simulations on large system like the CDK5 are usually ~10 ns long, while the time-scale of large-scale protein rearrangements is much longer. Many schemes have been developed to overcome this limitation. Most of them are based on a coarse-grained representation of the system.

This approach can be very useful, but obtaining a good coarse-grained representation can be difficult and transferability is an issue. Our recently proposed scheme [1] is able to reconstructing the lowest free energy path that connects a given initial and final state, without having to renounce a fully atomistic description. The method is based on the definition of two variables (s(R) and Z(R)) that are able to describe the position of a point in configurational space relative to a pre-assigned path. The variable s(R) provides the progress of the dynamics along the "template" path while z(R) provides the distance from it. Given a trial path we then run a metadynamics [2] simulation to reconstruct the free energy surface as a function of the two variables.

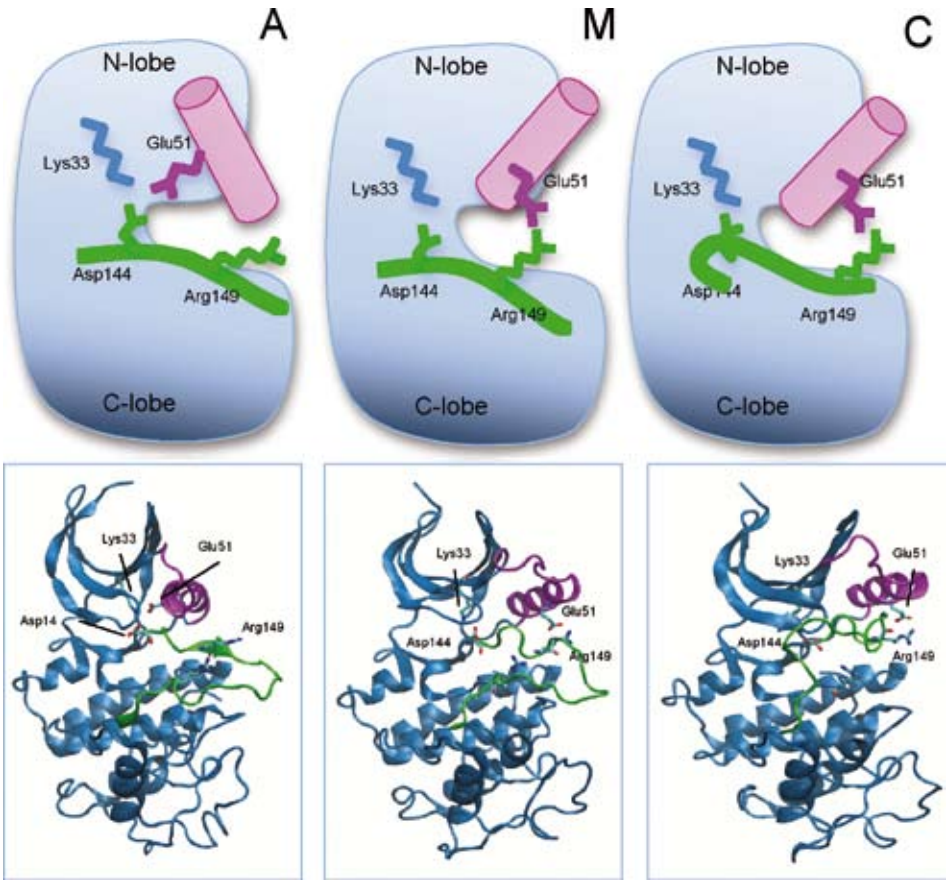

Figure 1: Different conformations of the CDK5. The αC-helix is represented in pink; the T-loop in green. A, active state. Lys33 and Glu51 make a salt bridge. M, metastable intermediate. The salt bridge is broken and a new one between Asp149 and Glu51 is formed. C: closed, inactive state. The T loop blocks the active site.

Eventually, as z(R) increases, this allows non-local searches in the space of paths to be performed. In the case of CDK5, the non-local paths search and the reconstruction of the free energy surface required several long (>100ns) MD trajectories each lasting more than 50,000 cpu hours on the CSCS Cray XT3. But the final result was well worth the cost since this large-scale computational effort enabled us to find for the first time a reaction coordinate between the open and closed state. The activation turns out to be a two-step mechanism. In the first step the αC-helix rotates of about 45°. This event is made possible by the breaking of the salt bridge between Lys33 and Glu51 that anchors αC-helix in its open position. The solvation and the formation of a new salt bridge with Arg149 enables the partial rotation of the αC-helix. In the second step the αC-helix completes its rotation while the T-loop refolds to assume the final closed conformation.

We also estimated the free energy surface associated to the global movement and identified a CDK5 intermediate, which could be exploited for drug design purposes [3]. Our findings are confirmed by an extensive comparison with the available X-ray structures of several homologous CDKs.

References

1. Branduardi, D., Gervasio, F. L. & Parrinello, M. (2007) J. Chem. Phys. 126, 054103.
2. Laio, A. & Parrinello, M. (2002) Proc. Natl. Acad. Sci. U. S. A. 99, 12562-6.
3. Berteotti, A., Cavalli, A., Branduardi, D., Gervasio, F. L., Recanatini, M. and Parrinello, M. Nature Struct. Mol. Biol. Submitted (2008)

Convection and Magnetic Field Generation in the Earth and Other Planets

Prof. Dr. Andrew Jackson (a)

with J. Rotvig (a), M. Evonuk (b), and G. A. Glatzmaier (c)

Institutions:
(a) Institut für Geophysik, Dept Erdwissenschaften, ETH Zürich, Switzerland
(b) Physikalisches Institut, LS Theoretische Physik I, Universität Bayreuth, Germany
(c) Department of Earth and Planetary Sciences, University of California at Santa Cruz, USA

Description

Convection in the liquid parts of planets is the mechanism by which heat is efficiently transported from the interior to the exterior, thus either cooling the planet through time or extracting heat generated internally. We see the signature of convection in the surface patterns of flow on the giant planets such as Jupiter and Saturn, planets that also possess strong magnetic fields. On the Earth, while we cannot see the convection in the liquid core, we can detect the magnetic field with high resolution, observe its changes through time, and via paleomagnetic measurements of the magnetization of rocks, attest to the fact that the magnetic field has been extant for the last 4 billion years.

In order to investigate the possibly turbulent fluid flow at very high rotation rates in the Earth's core and in the giant planets, we conduct numerical simulations of the dynamo equation, Navier-Stokes equation, and heat equation. Our goals are to simulate never before achieved low Ekman number regimes (Ek~10^{-6} and lower), to analyze the scaling of multiple jets in non-magnetic, rotating, and highly supercritical convection, and to perform calculations to gain insight into the mechanisms leading to magnetic polarity reversals.

Achievements

Multiple drifting jets in non-magnetic thermal convection

Rapidly rotating non-magnetic thermal convection in spherical shells is relevant to multiple astrophysical systems. These rotating systems display a weak dependence on the coordinate along the rotation axis. Any obstacle inside the shell, such as the solid inner core within the Earth's liquid iron core, introduces a surface along the rotation axis that separates the dynamics into disconnected regions (see Figure 1). The separating surface, denoted as the tangent cylinder (TC), is an imaginary cylinder along the rotation axis that touches the

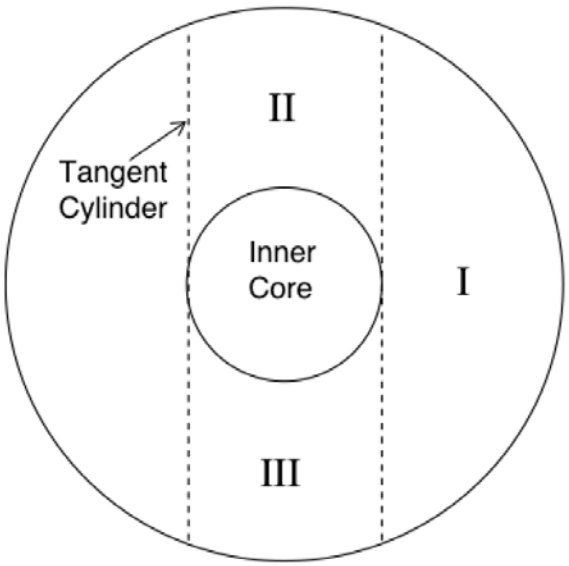

Figure 1: Schematic of regions of the core of the Earth. Region I is an annular region outside the imaginary ``Tangent Cylinder'' defined by the presence of the inner core. Regions II and III are disconnected from one another.

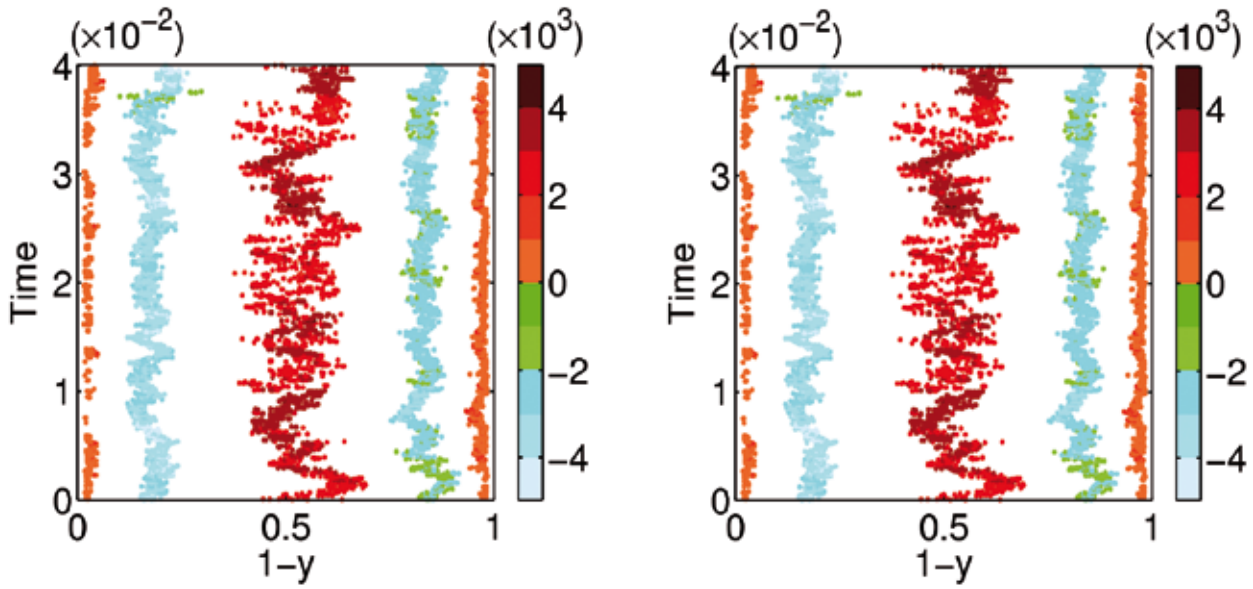

Figure 2: Onset of jet-drift in the 2D model as determined by the radius of curvature of the top and bottom boundary. The position of the zonal flow extrema is shown as function of time. The radius of curvature is infinite and close to minimum, respectively.

inner core. The fluid dynamics interior to the TC is quite different in comparison to the exterior flows. This has important consequences for non-magnetic convection as well as hydrodynamic dynamos, in particular reversing dynamos. Our aim was to investigate the azimuthal flow outside the TC that develops when the flow does not slip at the outer boundary of the shell.

This study reveled a new type of zonal flow outside the tangent cylinder consisting of multiple jets drifting towards the interior, where the number of jets is related to the Rhines length scale and scales as $Ek^{-1/4}$ [1]. At moderate thermal driving, the jet dynamics may be divided into three regions. The central region of the rotating container consists of jets that are drifting towards the TC at a rate that tends to increase towards the tangent cylinder. In the outer region, the azimuthal flow is weak and has no clear jet structure. In the inner region, the jets are changing their width, being created or destroyed, and sometimes change their drift rate abruptly. We also find that variable curvature provides a control on the jet-drift, Figure 2 shows the onset of drift as the curvature is changed. While speculations about possible implications to the geodynamo have been made, direct tests of these are beyond the reach of today's supercomputers.

Reversing geodynamo models

The current geodynamo is being driven by thermal and compositional convection. The presence of the inner core implies efficient buoyancy sources at the inner core boundary. Latent heat and light elements are released at this boundary providing vigorous convection (modeled here by differential heating) that maintains the outer core in an adiabatic state. Before inner core formation, the only energy source available to the geodynamo was thermal heating due to secular cooling and radioactive elements, modeled here by a volumetric heating source. These different driving modes have a large impact on the reversal mechanisms.

In this study we examined the differences between reversing dynamos driven by differential and volumetric heating, respectively, via a filtering method, where the magnetic induction is reduced in various regions to separate dynamo processes (Figure 3). We found that, in the differentially driven dynamos, the flow inside the tangent cylinder plays an important role in the reversals. Meanwhile, in the volumetrically driven dynamos the strength of the

convection inside the tangent cylinder is relatively weak and plays a smaller role in reversals. In fact, for these dynamos a high rotation rate is essential for stabilization of the magnetic dipole, i.e., the occurrence of time intervals where the preferred alignment is along the rotation axis. We have observed that the necessary rotation rate increases as the size of the inner core decreases making this problem harder to solve.

Convection in gas giants without a core

Jupiter and Saturn exhibit an alternating pattern of zonal flows with latitude with a strong eastwardly directed jet at the equator, and alternating eastward and westward jets at higher latitudes. Many numerical simulations in the planetary community have been conducted with varying geometries of thin and thick shells, primarily with constant background density. While the details (directionality and number of jets) may vary, banded structures in highly rotating three-dimensional (3D) bodies are a fairly ubiquitous solution in most simulations. Two possible methods of generating and maintaining a zonal flow with rotation are via vortex-stretching of columns spanning the convection zone and via compressional torque as fluid expands or contracts as it moves radially through a background density profile [2]. Therefore, an important question is if the method that produces bands in numerical simulations, vortex-stretching for the constant background density cases, is the same method that produces bands on the giant planets.

We find in 2D simulations that compressional torque plays an increasingly important role when the Ekman number decreases and rotational effects become dominant [3]. However in 3D, both mechanisms play a role in vorticity generation (Figure 4). In simulations with a background density profile we see the compressional torque term is on the order of 25 times larger than vortex-stretching term near the surface where the jets are maintained. While the vortex-stretching mechanism may still play an important role at depth where the density changes little, or when interacting with the impermeable outer boundary (an unrealistic boundary condition for a giant planet), it appears that the role of density change in generating and maintaining zonal flows is increasingly important as the fluid becomes more turbulent. This indicates vorticity generation via flow through a density profile could be a dominant method of generating differential flow in the giant planets.

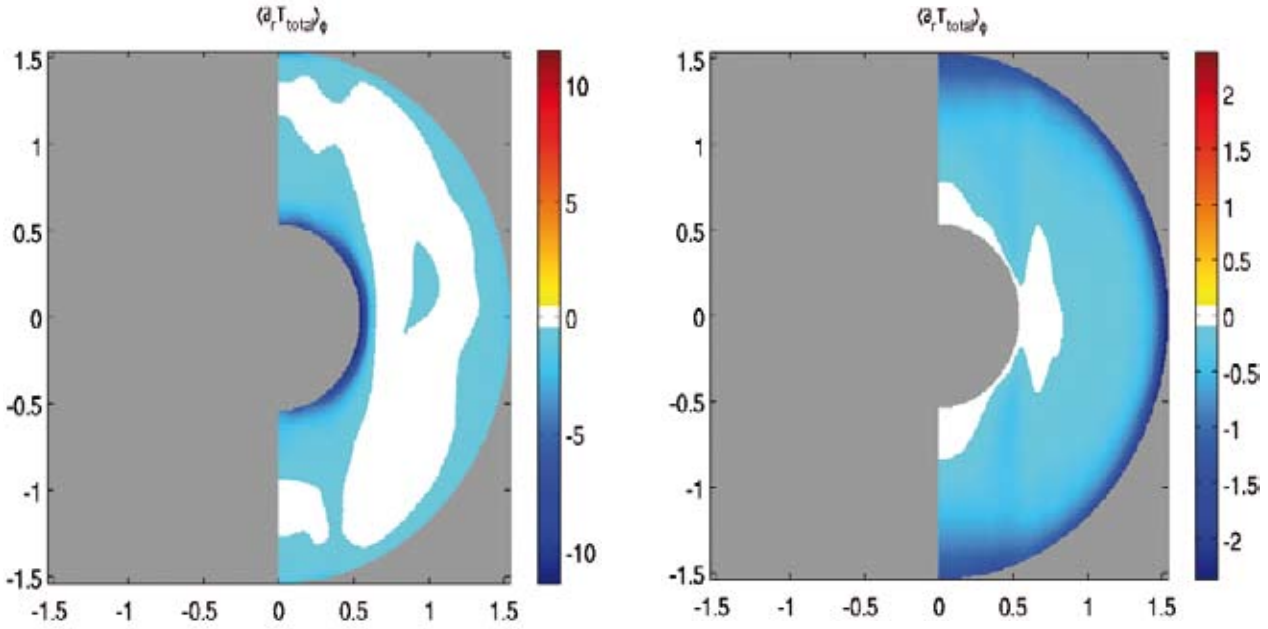

Figure 3: Thermal boundary layers for dynamo A: differentially heated non-reversing dynamo at Ek, Pm, Pr = 3.16x10-4, 4, 1 (left-hand panel), and dynamo B: volumetrically heated non-reversing dynamo at Ek, Pm, Pr = 5.62x10-5, 5, 1.

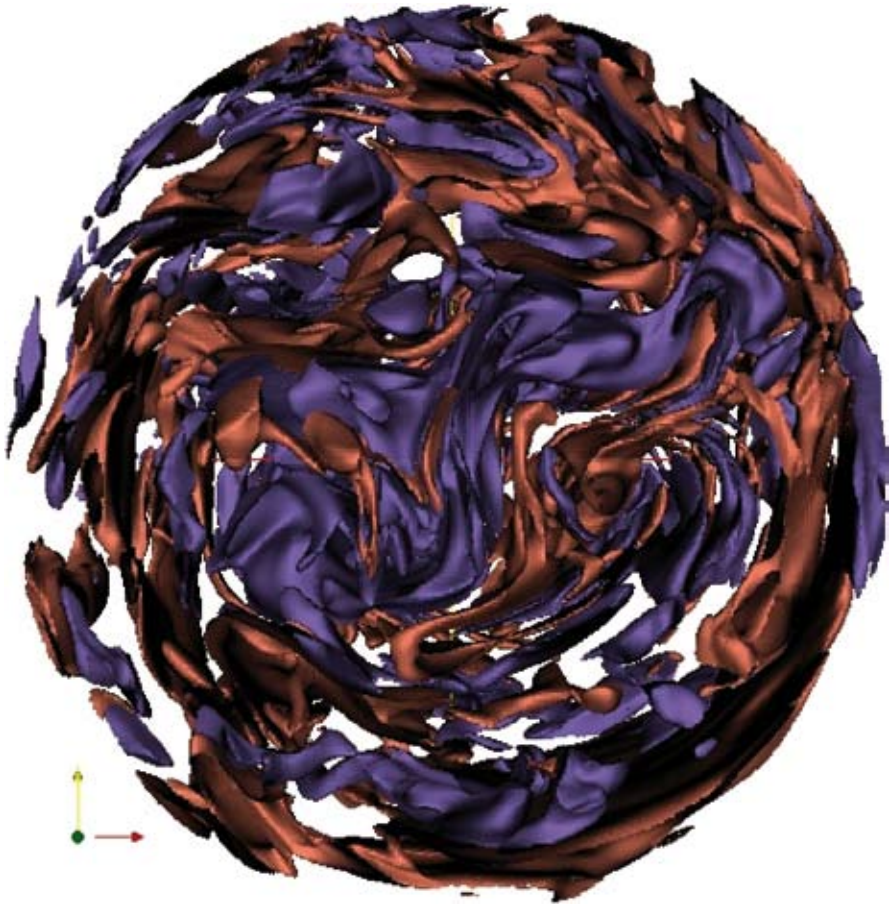

Figure 4: Contours of the vertical vorticity, the z-component of the curl of velocity, viewed from the north. Red indicates positive vorticity, counter-clockwise flow, and blue indicates negative vorticity, clockwise directed flow. Negative vorticity structures spiral in towards the axis of rotation while positive vorticity structures spiral towards the surface of the simulation.

References

1. J. Rotvig, Physcis Review E 2007, 76, 046306, 1-9.
2. G. A. Glatzmaier, M. Evonuk, T. Rogers, Geophysical and Astrophysical Fluid Dynamics, (in the press).
3. M. Evonuk, The Astrophysical Journal 2008, 673: 1154-1159.

Climate Change and the Hydrological Cycle from Global to European/Alpine Scales

Prof. Ulrike Lohmann

Project Leader: Prof. Christoph Schär

ALPS-Climate report 2007-2008

Droughts as well as floods pose major environmental threats for societies and ecosystems. Recent history shows that the central European and Alpine area is particularly vulnerable to variations in the water cycle, as seen in the extended 2003 summer drought or the severe 2002 and 2005 central European and Alpine floods. Improved understanding and predictions of the variations in the global and regional hydrological cycle is therefore vital to protect and secure the basic needs of human societies and ecosystems under changing climates.

High levels of greenhouse gases (GHGs) are a key factor for climate-change projections: by yielding an overall warming of the atmosphere and an increased capability to uptake water vapor, they contribute at the same time to an increased potential for severe storms and heavy precipitation events, but also to droughts and heat waves over land areas through enhanced evaporation rates. Interactions between global circulation patterns and changes in the regional hydrological cycle may play an important part as well. Therefore, climate-change projections need to account for these two factors, as well as for the processes that can impact them. Major uncertainties relative to these issues are lying in the representation of aerosol effects on the hydrological cycle, the parameterization of clouds and convective processes, land-atmosphere interactions, and effects of model resolution in general.

The purpose of the ALPS-Climate project is the build-up of a comprehensive modeling framework at CSCS, addressing these various areas of uncertainty in climate research, and spanning global to high-resolution scales. This is achieved by running two different climate models: one global model (ECHAM5-HAM) and one regional model

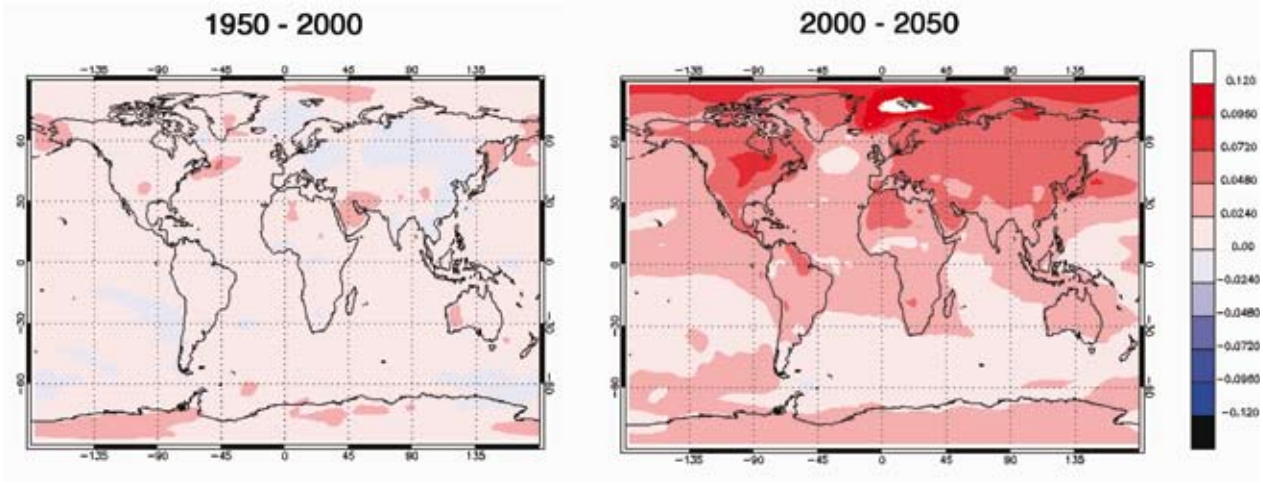

Figure 1: Trends of the temperature at 2 meters (K) for period 1950-2000 (left) and 2000-2050 (right) computed with the global climate model ECHAM-HAM. The global warming for the coming period, in particular around the northern pole, is clearly seen.

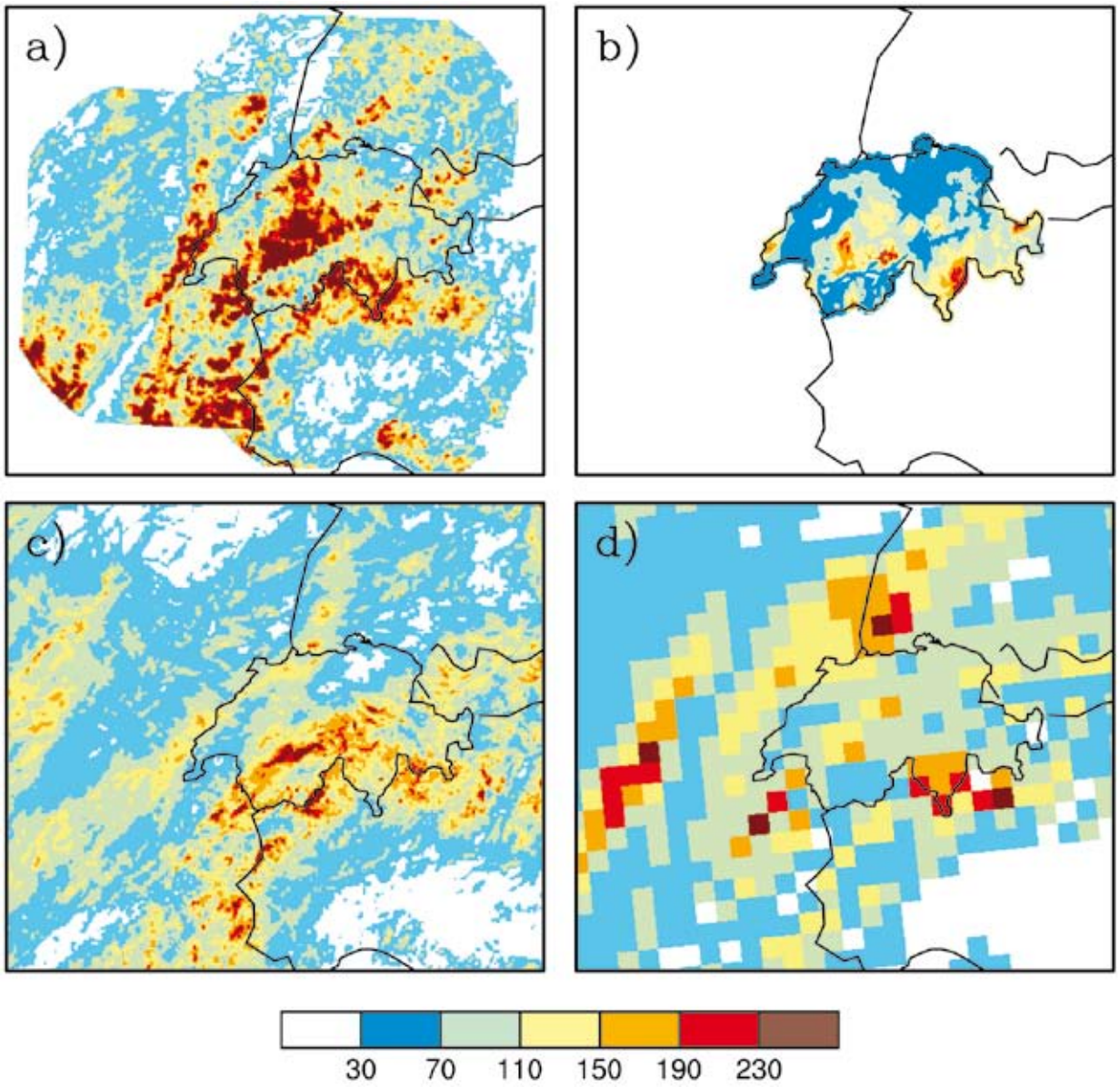

Figure 2: Monthly accumulated precipitation (mm) obtained over Switzerland for a month-long integration (July 2006). Panels show (a) radar precipitation estimates, (b) analysis of conventional rain-gauge data (available for Switzerland only), (c) the cloud-resolving integration, and (d) the driving coarser-resolution simulation. Note the considerable uncertainties regarding observed precipitation in panels (a) and (b).

(CLM) centered over the alpine region, the output of the earlier being used as boundary conditions for the latter.

In addition to the ambitious scientific developments required by the project, ALPS-Climate challenges several aspects of High Performance Computing. On the one hand, it requires very fast computational resources, because both models are run at their respective middle- to high-resolutions limits (both spatial and temporal), but also because many different experiments are required to investigate the role of the relevant parameters. This is achieved by running the models on the Cray XT3 platform for a total of 3.75 MCPUhours over the whole project. On the other hand, the project would not be feasible without fast I/O performances and a huge storage facility. Indeed, both models produce diagnostics for hundreds of climate variables, making the output of these experiments a tremendous wealth of data for the current project but also for many various future studies. This represents a highly valuable investment, which can be directly translated into storage costs:

the project has a total budget of 185 TB of archived data.

Up to now, this project allowed to make important scientific and technical progress, among which one can cite:

- the setup of functional code with specific Cray XT3 optimization to conduct global high-resolution experiments (~1.125 degrees horizontally over 31 vertical levels, 6-hourly output) over 100 years each, including latest advances in the dynamical modeling of the role of aerosols for the climate;
- the successful performance of intermediate experiments using the global model at middle resolutions in both equilibrium and transient modes over 100 years (figure 1), which proved the accuracy of the model and showed good agreement to observations;
- the implementation in the regional model of advanced dynamical aerosol modeling in a consistent manner relative to the global model;
- the successful conduction of transient runs over 100 years using the regional model at a resolution of 25 km;
- the development of an idealized cloud-resolving modeling framework geared towards the studies of extremes in a changing atmospheric environment
- and finally the realization of several short regional cloud-resolving (horizontal resolution of 2 km) climate simulations with durations of months to seasons, demonstrating the potential benefits of using expicit instead of parameterized convection (figure 2).

Despite initial technical and scientific difficulties, ALPS-Climate now reached maturity and already yielded six peer-reviewed articles.

References

1. Lohmann, U., P. Stier, C. Hoose, S. Ferrachat, S. Kloster, E. Roeckner and J. Zhang, Cloud microphysics and aerosol indirect effects in the global climate model ECHAM5-HAM, Atmos. Chem. Phys. 7, 3425-3446, 2007.
2. Brockhaus, P., D. Lüthi and C. Schär, Aspects of the Diurnal Cycle in a Regional Climate Model. Meteorol. Z., 17 (4), 433-443, 2008.
3. Hohenegger, C., P. Brockhaus and C. Schär, Towards climate simulations at cloud-resolving scales. Meteorol. Z., 17 (4), 383-394, 2008.
4. Hohenegger, C., P. Brockhaus, C.S. Bretherton and C. Schär, The soil moisture-precipitation feedback in simulations with explicit and parameterized convection. J. Clim., conditionally accepted, 2008.
5. Kloster, S., F. Dentener, J. Feichter, F. Raes, J. van Aardenne, E. Roeckner, U. Lohmann, P. Stier, and R. Swart, Influence of future air pollution mitigation strategies on total aerosol radiative forcing, Atmos. Chem. Phys. Discuss. 8, 5563-5627, 2008.
6. Lohmann, U, Global anthropogenic aerosol effects on convective clouds in ECHAM5-HAM, Atmos. Chem. Phys. 8, 2115-2131, 2008.

Toward Simulating a Cell Adhesion Site at Angstrom Resolution

Prof. Viola Vogel

Research Team at ETH, D-MatI:
Eileen Puklin-Faucher, Vesa Hytönen,
John Saeger, Henrik Grabner, Samuel Hertig

The focus of this project is to use computational tools (molecular dynamics (MD) and steered molecular dynamics (SMD)) to learn how force is transmitted through force-bearing protein networks that connect the cell exterior via integrins to the contractile cytoskeleton. Our longterm goal is to learn how mechanical forces regulate the formation and subsequent stabilization of cell adhesion sites. To piece together this complex puzzle, we started analyzing the impact of force on the equilibrium structures of proteins and protein fragments that are part of integrin junctions. One of the unsolved questions in cell biology concerns the detailed mechanism by which integrins become activated. While integrin activation has been shown to have a structural origin, which means that the switch from low to high binding affinity occurs via conformational change, no experimental techniques are currently available to reveal the spatiotemporal details of activating structural dynamics. Thanks to the generous allocation of computational resources from CSCS as part of our ALPS project, we are pleased to report substantial progress on our research plan. While the CSCS project only provides for the computational resources, we applied for a competitive SNF grant with the same title and were awarded 461,800 CHF that covers 2 positions, from April 1, 2007 to March 31, 2010. Two new students started and were trained (Henrik Grabner, Samuel Hertig). Thus far, most of our results have been obtained simulating the headpiece of the integrin αvβ3 coupled to the cell adhesion domain of fibronectin (FnIII-10) which is a central extracellular matrix protein. Together with all available structural information, molecular dynamics (MD) and steered molecular dynamics (SMD) allowed us to identity sequential structural events that are tightly coupled to the integrin activation process. Most significantly, the dynamic model of integrin activation derived from these simulations shows how ligand bind is allosterically coupled to remote conformational changes. A comprehensive explanation for two open mysteries how integrins are activated is provided: first, how Ca^{2+}, as opposed to Mg^{2+} or Mn^{2+}, can inhibit integrin activation, and second, how the integrin-fibronectin bond may be switched to high affinity by ligand-mediated tensile force (Puklin-Faucher et al, submitted).

To learn how the integrin activation process is affected by the mutational differences between the different α- and β-integrin subunits, we are now investigating the activation pathway of the integrin αvβ1 headpiece under similar conditions. Starting with the known αvβ3 structure, homology modeling was used to derive the structure for αvβ1 (Henrik Grabner). While previous results led to the observation of spontaneous hinge opening in the integrin beta 3 head piece (Puklin-Faucher et al. 2006), preliminary results show events akin to those found during the integrin beta 3 activation process. Other point mutations that distinguish different integrin subunits from each other will be

tested as well to shed light into their functional roles in the activation process.

Finally, the α6β4 integrin has a unique cytoplasmic tail that contains several domains, two of which are fnIII-like domains. The integrin α6β4 is a mediator for cell adhesion to the extracellular matrix protein laminin. A malfunction in its binding pathway results into the development of the skin disease epidermolysis bullosa (EB). Symptoms include light to heavy skin blistering and large area detachment of the epidermis. Crucial for the integrin function are the intracellular fibronectin modules that are part of the beta 4 integrin tail, which offer a binding site for plectin and thus link the integrin to the cytoskeleton. Distinct mechanical stabilities of those modules might present a regulatory means to control cell-laminin interactions. Additionally, mutations in those modules have been identified to lead to EB. We have used SMD simulations along with mutational analysis to identify key bonds within the integrin β4-FnIII modules that regulate their mechanical stability (Henrik Grabner). The results so far show a direct link between those bonds and the structural stability of the modules. Currently, simulations with known inherited genetic mutations causing EB are being performed.

Since extracellular fibronectin matrix fibers have bungee cord-like characteristics, we are examining the behavior of fibronectin Type I modules when subjected to an external mechanical force. The goal is to determine the extent to which the Type I modules can be extended. Part of these domains are stabilized by disulfide bonds. They stabilize the secondary and tertiary structure by acting as force clamps. The results of the simulations performed so far are exciting: although the disulfide bonds indeed remain intact for all probed forces, the modules show a so far not considered length extension of up to 66%. This change in extension is mainly due to the breaking of hydrogen bonds and the straightening of the terminal loops.

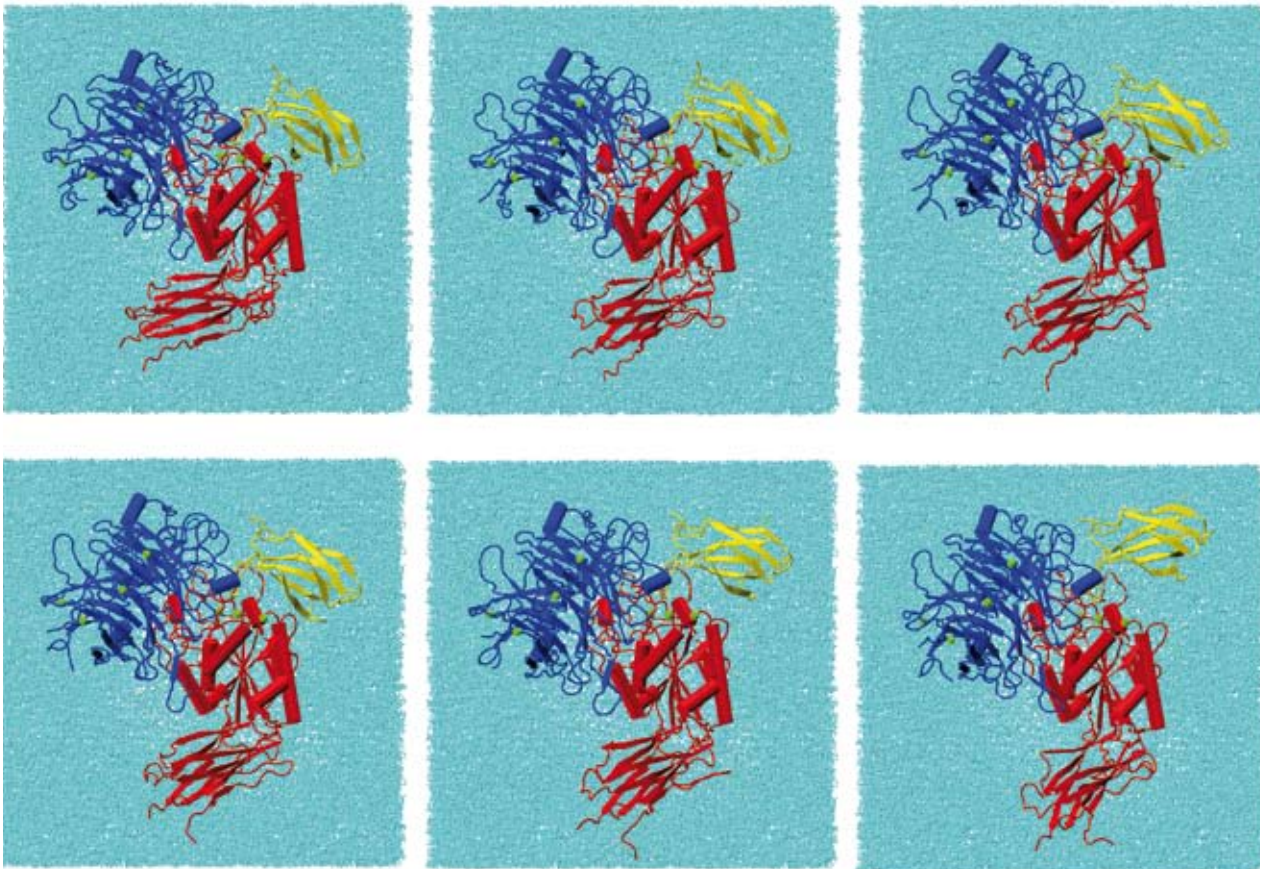

Figure 1: sequential activation process of the αv (blue) β3 (red) integrin head piece coupled to the fibronectin domain FnIII-10 (yellow).

While this project was originally intended as a tutorial for the software VMD/NAMD on an ETH-cluster, we are currently summarizing the results in a manuscript (Samuel Hertig).

The CPU time required for these simulations was far too long for them to be carried out on the ETH cluster exclusively.

Talin is another key protein of integrin junctions. It couples the cytoskeleton to the extracellular matrix via integrins. Here simulations conducted with CSCS resources allowed us to propose a structural mechanism how force might upregulate the recruitment of vinculin to the cell adhesion site. It was found that force-induced the fragmentation of the talin rods into smaller alpha-helix bundles which then facilitated the sequential exposure of the vinculin binding sites. A new mechanism was proposed how force can activate protein binding (alpha-helix swapping) (Hytönen and Vogel 2008).

Finally, in the search for optical mechanosensors to be broadly applied in the life sicneces, we started looking at the unfolding trajectories of the green fluorescent protein, GFP (John Saeger). Various intermediate states were identified in the early unfolding trajectories. Guided by those simulations, we are now investigating experimentally how unfolding of the beta-barral of GFP could impact the spectroscopic properties of the fluorophore (Saeger et al, submitted).

Since several exciting developments are underway driven by Kevin J. Bowers and colleagues and by Klaus Schulten and his colleagues to develop algorithms that will run atomistic simulations about 1000 times faster than what is possible today, we decided to focus on developing largely improved software tools to analyze large trajectories and to test them by analyze in detail the mechanical behavior of the smaller molecular subunits that are part of integrin junctions until the software will become available. The release of the DESMOND software, for example, is planned for late 2008.

Publications

1. Hytönen VP, Vogel V (2008) How force activates talin's vinculin binding sites: SMD reveals a structural mechanism. PLOS Computational Biology. 4: 1-15
2. Puklin-Faucher E, Gao M, Schulten K, Vogel V (2006) How the headpiece hinge angle is opened: New insights into the dynamics of integrin activation. J Cell Biol 175:349-60
3. Puklin-Faucher E., Gao M, Vogel V., The RGD-αVβ3 integrin catch bond, submitted.
4. Saeger J, Hytönen VP, Vogel V, How mechanical tension turns off EGFP and EYFP fluorescence, submitted.
5. Shaw DE, Martin M. Deneroff, Ron O. Dror, Jeffrey S. Kuskin, Richard H. Larson John K. Salmon, Cliff Young, Brannon Batson, Kevin J. Bowers, Jack C. Chao, Michael P. Eastwood Joseph Gagliardo, J. P. Grossman, C. Richard Ho, Douglas J. Ierardi, Istvan Kolossvary, John L. Klepeis Timothy Layman, Christine McLeavey, Mark A. Moraes, Rolf Mueller, Edward C. Priest, Yibing Shan, Jochen Spengler Michael Theobald, Brian Towles, Stanley C. Wang, Anton, a special-purpose machine for molecular dynamics simulation ACM SIGARCH Computer Architecture News, Volume 35, Issue 2, May 2007

LP - Large User Projects

Hydrogenation reactions in heterogeneous enantioselective catalysis

Prof. Alfons Baiker

with A. Vargas and A. Urakawa
Department of Chemistry and Applied Biosciences
ETH Zürich, Switzerland

New materials for heterogeneous enantioselective catalysis

Among the various branches of natural and technical sciences catalysis is of utmost relevance. Due to its ubiquity in chemistry and biology the understanding of its fundamental mechanisms is of basic importance; furthermore it has a broad spectrum of practical applications since most industrial processes involve at least one catalytic step.

Catalysis is also involved in the chemistry of living organisms: it is well known that enzymes are biochemically active catalysts and are the keys for a large range of bio-synthetic and bio-degradation pathways.

When the catalyst is a solid the reactivity occurs at the interface between its surface and a gas or a liquid: we then speak of heterogeneous catalysis. From a technical viewpoint the simplification of catalyst separation and recovery in heterogeneous catalysis makes it economically and environmentally appealing. From a more fundamental standpoint it deals with interface phenomena that are of great importance and interest in biochemistry and material sciences.

One of the most complex and interesting man-made catalytic systems consists in chirally modified supported transition metals, which can be used to produce large enantiomeric excesses in hydrogenation reactions of activated ketones and alkenes[1-5]. The materials resulting from the above mentioned modification possess interesting properties that can be adjusted and tuned according to

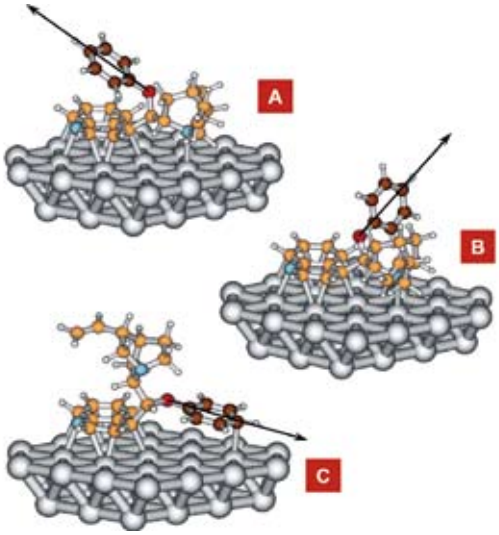

Figure 1: Different surface conformers of O-phenyl-CD. In conformer A the phenyl moiety is out of the chiral pocket, while in conformers B and C it is within the chiral pocket.

a rational choice of the modifier molecule and of the transition metal. Typical chiral surface modifiers for hydrogenation reactions are the alkaloids of the cinchona family. Such molecules are able to anchor on a metal surface thus providing an asymmetric scaffold or chiral site that is able to bias an otherwise asymmetric reaction. Although some experimental techniques do exist that allow the investigation of such surface phenomena[6-7], quantum mechanical simulations are used to complement the knowledge gained by experiment thus allowing detailed molecular insight[8].

The combination of experiments and simulations has allowed the achievement of remarkable insight in the reaction mechanism of this catalytic system8. Following such insight the derivatisation of cinchonidine by means of ether substituents has provided new reaction systems and interesting catalytic materials9. O-phenyl-cinchonidine (PhOCD, Fig. 1) has been shown to have opposite enantioselective properties compared to cinchonidine (CD) in the hydrogenation of activated ketones: while CD yields an R-alcohol, PhOCD yields an S-alcohol9-10. Furthermore the different adsorption potentials of the two chiral modifiers allow for a dynamic exchange of surface chiral sites. As a result the catalytic material can switch its enantioselective properties based on chiral recognition and competing adsorption potentials, thus giving rise to chemically tunable catalysts[9-10].

The investigation of the substituent effect on the O-phenyl moiety has led to the discovery of interesting phenomena. O-(3,5-bis(trifluoromethyl)-phenyl-cinchonidine (tFPhOCD) and O-(3,5-dimethyl-phenyl)-cinchonidine (dMePhOCD) although possessing almost identical van der Waals radii, generate opposite enantiomers when used as chiral surface modifiers in the hydrogenation of activated ketones, while the behaviour of tF-PhOCD and CD are identical (Fig.2). The study of the surface conformational complexity of such molecules on platinum by means of ATR-IR and theoretical modelling revealed that the O-phenyl as well as the O-trimethylsilyl moieties can generate surface conformations having different chiral recognition properties[11-13]. In particular the trifluoromethyl substitution on the phenyl ring can trigger the change in the relative positions between the main skeleton of the alkaloid and chiral pocket, thus critically influencing the resulting enantioselectivity. Such systems, although less refined than biological catalysts, mimic their basic behaviour and chemistry. In fact they use conformational degrees of freedom to change the recognition pattern of a substrate, and the d orbitals of a transition metal to decrease the energy of the transition state.

Interestingly chiral recognition can be also guided by directing groups, as shown in the case of O-(2-pyridyl)-cinchonidine[14]. This modifier, although

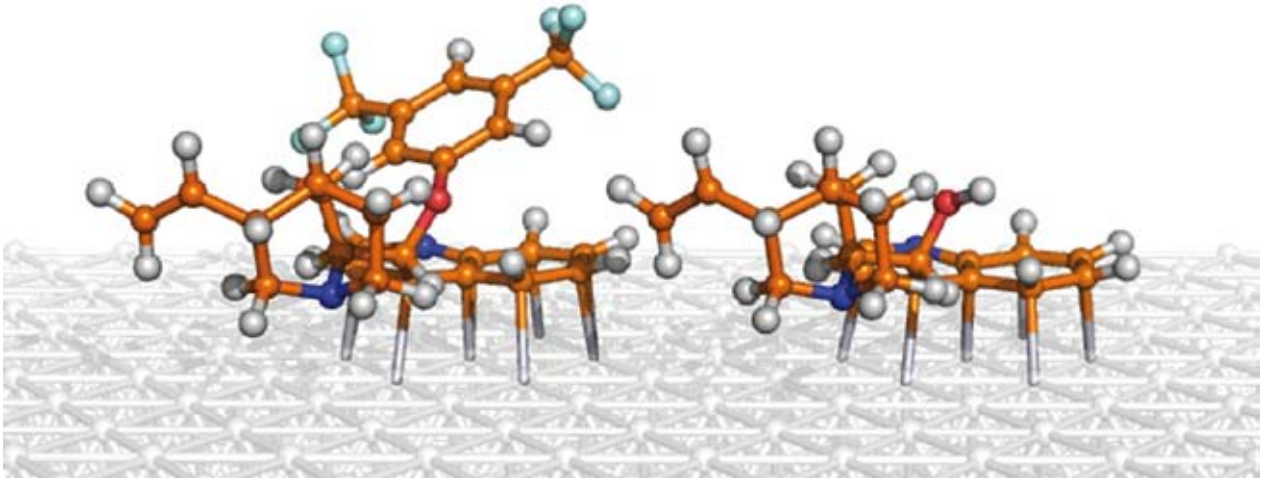

Figure 2: tFPhOCD has a similar chiral pocket to simple CD since the substituted phenyl moiety is removed from the chiral space.

possessing the same van der Waals radius as PhOCD, yields the opposite enantiomer in asymmetric hydrogenation reactions since it seems able to efficiently coordinate the substrate within the chiral space via additional weak intereactions[14]. The phenomenon of chiral recognition of substrates on modified metal surfaces deserves great interest and, as seen above is critically important for the design of functionalized metal surfaces. For this reason in parallel with the investigations above described also docking simulations on a model system (cinchonidine and ketopantolactone, Fig. 3) have been performed[15]. Such simulations allow the identification of docking patterns and give important insight for the design of functionalized inorganic-organic catalytic materials.

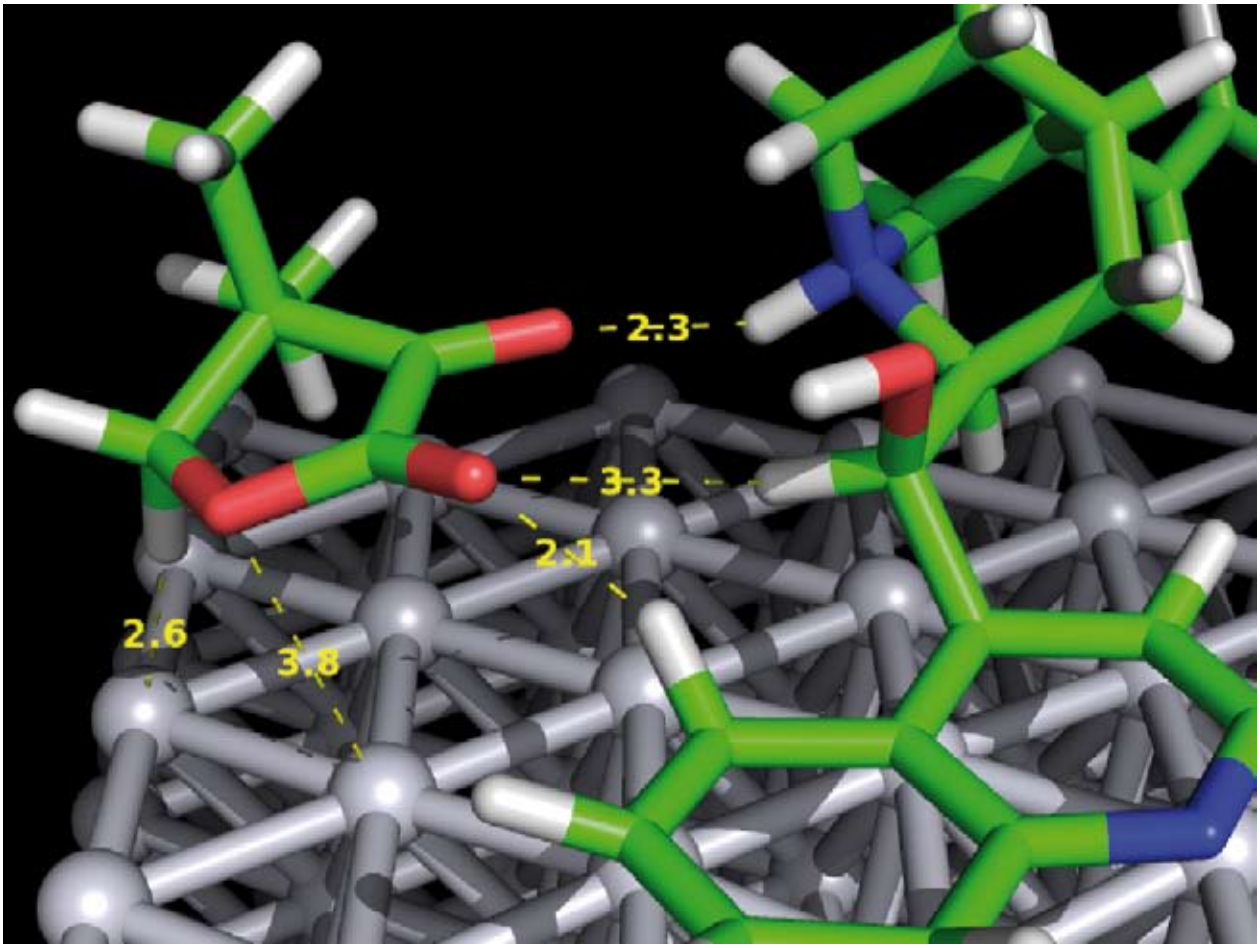

Figure 3: Energetically favourable docking interaction between adsorbed cinchonidine and KPL.

References

1. A. Baiker, Catal. Today 100 (2005) 159.
2. M. Studer, H.U. Blaser, C. Exner, Adv. Synth. Catal. 45 (2003) 345.
3. T. Bürgi, A. Baiker, Acc. Chem. Res. 37 (2004) 909.
4. D. Y. Murzin, P.M. Mäki-Arvela, E. Toukoniitty, T. Salmi, Catal. Rev. 47 (2005) 175.
5. T. Mallat, E. Orglmeister, A. Baiker, Chem. Rev. 107 (2207) 4863.
6. M. vonArx, M. Wahl. T.A. Jung, A. Baiker, Phys. Chem. Chem. Phys. 7 (2005) 273.
7. T. Bürgi, A. Baiker, Adv. Catal. 50 (2006) 227.
8. A. Baiker, A. Vargas, A. Urakawa. Scientific Report 2004/05 of CSCS, p.8-12 and references therein
9. S. Diezi, T. Mallat, A. Szabo, A. Baiker, J. Catal. 228 (2004) 162.
10. N. Bonalumi, A. Vargas, D. Ferri, T. Bürgi, T. Mallat, A. Baiker, J. Am. Chem. Soc. 127 (2005) 8467.
11. A. Vargas, D. Ferri, N. Bonalumi, T. Mallat, A. Baiker, Angew. Chem. Int. Ed. 46/21 (2007) 3905.
12. N. Bonalumi, A. Vargas, D. Ferri, A. Baiker, J. Phys. Chem. C 111 (2007) 9349.
13. N. Bonalumi, A. Vargas, D. Ferri, A. Baiker, Chem. Eur. J. 13 (2007) 9236.
14. F. Hoxha, L. Königsmann, A. Vargas, T. Mallat, A. Baiker, J. Am. Chem. Soc. 129 (2007) 10582.
15. A. Vargas, G. Santarossa, M. Iannuzzi, A. Baiker, J. Phys. Chem. C; 112 (2008) 10200.

Ab initio thermochemistry of large molecules

Dr. Dirk Bakowies

Laboratorium für Phyikalische Chemie
ETH Zürich, Switzerland

Motivation

Thermochemistry is a branch of thermodynamics concerned with the energy balance of chemical reactions. The elements in their standard states define the universal reference, establishing heats of formation as the primary quantity relating the heat content of one compound to that of another. Experimental access is usually provided through combustion calorimetry, supplemented by measurements of heats of vaporization or sublimation. On the theoretical side, heats of formation may be obtained from atomization energies, but *ab initio* predictions to any useful accuracy (say 1-2 kcal/mol) have not been possible even for the smallest chemical systems until about 20 years ago. This is mainly attributable to the large error incurred if electron correlation is not dealt with accurately, as the total atomization of a molecule involves a significant change in electron correlation. Accurate treatment, however, requires expensive calculations using extended basis sets as the electron correlation energy is known to converge very slowly with the size of orbital-based expansions.

Our interest in accurate *ab initio* thermochemical approaches reflects the need for supplying high-quality reference data for semiempirical method development. Traditionally such reference data have been obtained almost exclusively from experiment, but a reliable *ab initio* protocol would offer several advantages: (a) Heats of formation, previously used but theoretically not well justified, can be replaced by more appropriate atomization energies which are easily available only from calculation. (b) The accuracy of experimental data is often hard to quantify, and while many data are very well established, occasionally large errors do occur. (c) Experimental data are entirely unavailable for several important classes of molecules, and, in particular for biologically relevant model systems such as peptides. The latter point is of particular importance as one of the most promising fields of application for improved semiempirical methodology is in biochemistry.

Related work in the literature

A number of research groups have demonstrated that accurate atomization energies can be obtained from composite methods, combining the results from less expensive electron correlation methods extrapolated to the full basis set limit with higher order correlation corrections obtained with medium-sized basis sets. The success of these methods relies on the observation that the complete correlation energy is much more sensitive to basis set saturation than correlation corrections beyond the MP2 or CCSD levels of theory. The focal point analysis introduced by Allen and coworkers,[1] the Wn (Weizmann) protocols of Martin[2] and the recently introduced HEAT protocol[3] are based on such combinations of various levels of theory. These methods have proven to be very accurate, but they are limited to fairly small molecules with just a few heavy atoms as they still require expensive CCSD(T) calculations with sizeable basis

sets. On the other hand, a number of simpler approaches have been introduced by the groups of Pople[4] (G1, G2, G3,...), Petersson[5] (CBS-Q, CBS-q, ...), and Truhlar[6] (MCCM/3, SAC/3). Although these approaches follow similar ideas, they are less demanding computationally and applicable to medium-sized organic molecules with 10 and more heavy atoms. The downside is that they require additional empirical corrections for acceptable accuracy and that these corrections have been determined by calibration with experimental heats of formation for large sets of mostly organic molecules. Such calibration is not entirely satisfactory if the method is supposed to provide high-accuracy reference data, as larger errors may occur occasionally, and, more importantly, as quantities for which the method was not calibrated (such as the atomization energy) may be reproduced less accurately.

Research outline

We are developing fully *ab initio* protocols applicable to large molecules. Our research activities concentrate on two aspects: (a) The convergence behavior of electron correlation energies is analized carefully, employing both results known from analytical theory and a large body of high-quality *ab initio* data. The results of this analysis are used to improve on existing formulas to extrapolate to the complete basis set limit. (b) The bond-separation reaction scheme is implemented in an *ab initio* framework, using only high-level *ab initio* data to correct for systematic errors of more affordable composite approaches. Both aspects of our research have depended heavily on the supercomputing facilities of CSCS to generate the necessary high-quality reference data for analysis and validation.

Extrapolation of electron correlation energies

From the analytical work of Schwartz on helium[7] we know that the correlation energy of two-electron systems converges asymptotically as $f(L)=(L+1)^{-3}$ with the maximum angular momentum L included in the basis set, at least in the limit that perfect radial saturation has been reached. This work has motivated the formulation of various extrapolation techniques, but it can only serve as a guideline. Even if one accepts without proof that the same asymptotic convergence also applies to molecules, a number of further issues affect practical implementations in extrapolation models. One needs to realize that the inverse cubic term is only the leading term of the asymptotic expansion, that different singlet pair energies in N-electron atoms are generally associated with different values of higher expansion coefficients, and that triplet pair energies contribute only with $(L+1)^{-5}$ and higher terms. Further «perturbations» of the asymptotic convergence behavior are caused by the replacement of partial-wave expansions with correlation-consistent basis sets and by the somewhat arbitrary identification of the quantum number L with a particular value of the basis set cardinal number X. All these effects influence the effective convergence behavior which differs from its asymptotic limit for all practical values of X. Thus it appears legitimate to introduce some degree of empiricism and modify extrapolation formulas for optimal agreement with high-level reference data. One way of doing this is to allow for a calibrated exponent β in $f(X)=X^{-\beta}$ that is found to be optimal for a given base and target of extrapolation.

The analysis of a large body of reference data for small to medium-sized first-row molecules (HCNOF) has led to a number of conclusions relevant to the design of thermochemical models:[8] (a) Coupled-cluster (CCSD) treatments always converge faster to the complete basis set limit than perturbational (MP2) treatments. (b) Convergence behavior varies substantially with molecular composition, thus requiring either specialized treatments or large-basis-set calculations for accurate extrapolations. (c) Atomization energies converge less regularly than total energies and require, in general, a different set of optimal extrapolation exponents.

Motivated by observation (b), an improved formula, $f(X)=(X+\xi_i)^{-\beta}$, has been developed for small basis set extrapolations which includes a variable angular momentum offset $\xi=\xi_i$ expressed in terms of a calibrated function relating the number of correlated electrons to the number and type of atoms contributing them (Fig.1).[9] In essence, the offset reflects differences between correlation-consistent basis sets for hydrogen and for first-row atoms. Application of this formula allows for remarkably accurate extrapolations, which are matched by calibrated one-parameter formulas and simple asymptotic limit formulas only if used with significantly larger basis sets. Extensive validation shows that the new formula is robust enough for general application to neutral systems containing hydrogen and all first-row elements from B to Ne.

A new ab *initio* thermochemical protocol

The concept of bond separation reactions (BSRs)[10] may be used in conjunction with appropriate extrapolation techniques to further improve upon low-level treatments of atomization energies. [11] High-level calculations are performed to supply accurate data for a limited set of small parent compounds, essentially reducing the challenging task of calculating accurate atomization energies to the much simpler task of calculating reaction energies. BSRs can be mapped onto a system of corrective bond increments, thus providing for a high-level description of the process of bond dissociation embedded in a lower-level treatment of the perturbation through the chemical environment.

BSRs have often been used before, but their application was limited by the availability of accurate experimental reference data. The use of high level *ab initio* calculations eliminates this restriction, extending the range of possible applications to all molecules for which valence structures can be drawn. Such an approach not only profits from the full potential of BSRs, it also remains truly *ab initio*, as

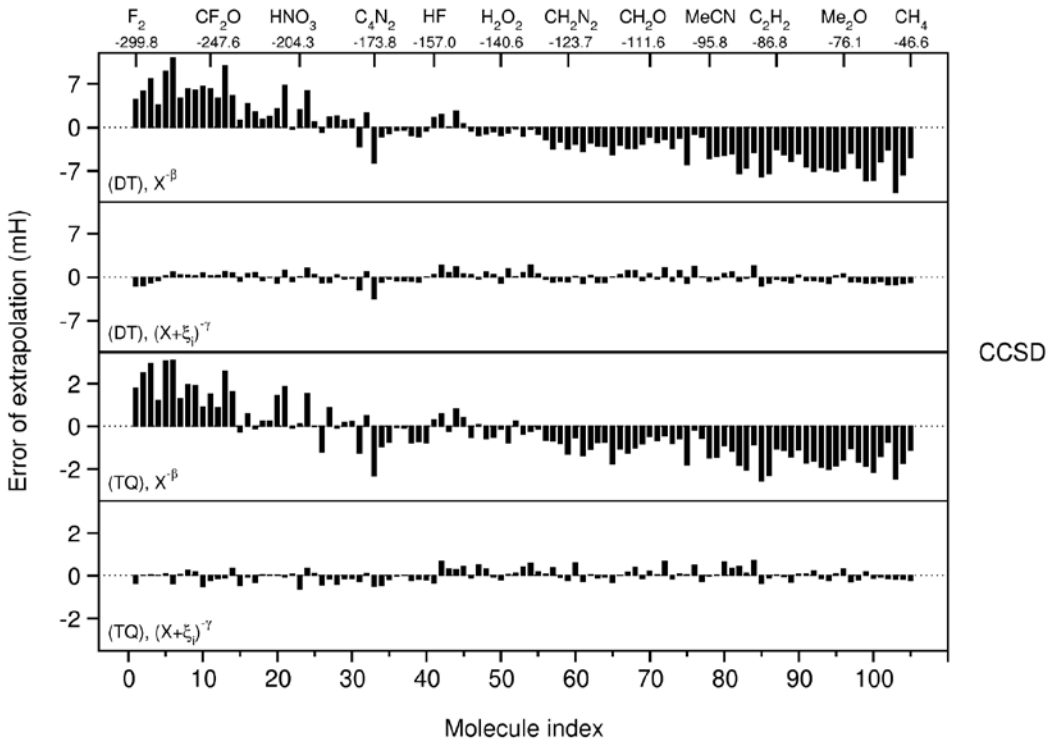

Fig. 1: Extrapolation errors for total correlation energies at the CCSD level as evaluated for a large set of 105 molecules (HCNOF). Molecules have been sorted according to their correlation energy per atom (see top bar for examples), an index that places hydrogen-rich molecules on the right and molecules with electronegative atoms on the left. The upper two panels show extrapolations from double- and triple-zeta basis sets, the lower two panels those from triple- and quadruple-zeta basis sets. The first and third panels refer to the standard one-parameter extrapolation formula, and the second and fourth panels show results for the new extrapolation formula. Energies are given in mH (1 mH ≈ 0.6 kcal/mol).

neither experimental data nor empirical calibration are required. Extensive analysis has shown that BSR corrected low-level atomization energies reproduce high-level reference data quite accurately, not only in total but also component by component, thus largely eliminating the risk of fortuitous error cancellation. Furthermore, good results are obtained not only for „simple organic“ molecules, but also for more complex systems involving, for example, charge-separated valence structures. Corrections beyond the CCSD(T) model are treated under the assumption that the corresponding BSRs are thermoneutral, reducing calculations to simple summations of bond increments. This works extremely well for scalar relativistic corrections and typically provides for reasonable qualitative or semi-quantitative estimates of diagonal Born-Oppenheimer corrections and higher-order electron correlation contributions (Fig. 2). Validation with a large set of experimental heats of formation (neutral, closed shell, HCNOF) shows that the new thermochemical approach is competitive with or even slightly superior to the popular and accurate, but empirically calibrated G3 protocol, at comparable computational cost.[11] Further possible improvements are currently being investigated, and extensions to second-row elements, to ionic systems, and to radicals are planned.

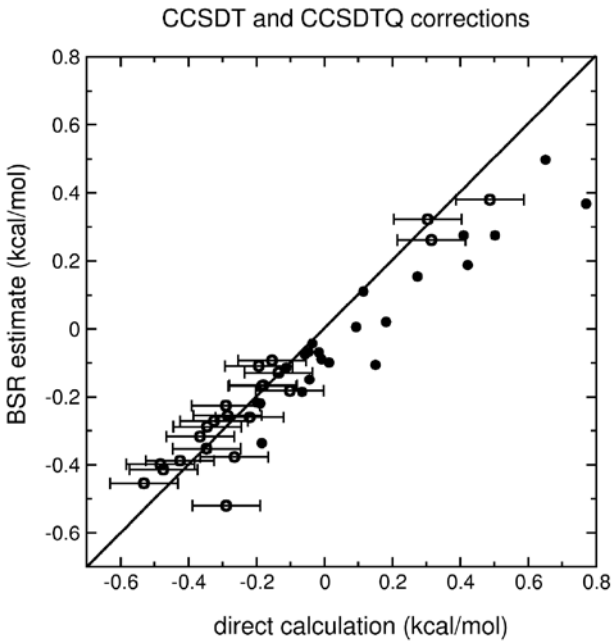

Fig. 2: Comparison between estimated (BSR scheme, assuming thermoneutral reactions) and calculated sums of CCSDTQ-CCSDT and CCSDT-CCSD(T) corrections to atomization energies (44 molecules, HCNOF). Open circles refer to molecules for which full CCSDTQ calculations proved to be unfeasible in which case they were approximated from CCSDT(Q) and CCSDT[Q] results. The error bars of 0.1 kcal/mol indicate the uncertainty expected from a thorough analysis for smaller systems. Note that the BSR estimate involves no fitting or empirical calibration. As the BSRs are assumed to be thermoneutral, however, the estimate reduces to a simple summation over bond increments uniquely determined from precalculated data for a limited set of small parent compounds.

References

1. East, A. L. L.; Allen, W. D. J. Chem. Phys. 1993, 99, 4638.
2. Karton, A.; Rabinovich, E.; Martin, J. M. L.; Ruscic, B. J. Chem. Phys. 2006, 125, 144108.
3. Tajti, A et al J. Chem. Phys. 2004, 121, 11599.
4. Curtiss, L. A.; Redfern, P. C.; Frurip, D. J. Rev. Comp. Chem. 2000, 15, 147.
5. Ochterski, J. W.; Petersson, G. A.; Montgomery Jr., J. A. J. Chem. Phys. 1996, 104, 2598.
6. Lynch, B. J.; Truhlar, D. G. J. Phys. Chem. A 2003, 107, 3898.
7. Schwartz, C. Phys. Rev. 1962, 126, 1015.
8. Bakowies, D. J. Chem. Phys. 2007, 127, 084105.
9. Bakowies, D. J. Chem. Phys. 2007, 127, 164109.
10. Hehre, W. J.; Ditchfield, R.; Radom, L.; Pople, J. A. J. Am. Chem. Soc., 1970, 92, 4796.
11. Bakowies, D. manuscript in preparation.

Climate and Stratospheric Ozone during the 20th century

Stefan Brönnimann

Institute for Atmospheric and Climate Sciences,
ETH Zurich, Switzerland

Outline of the project

The stratosphere plays an important role in the climate system both through dynamical and radiative mechanisms. Understanding these mechanisms is highly relevant for predicting the development of stratospheric ozone as well as for assessing future climate change. The stratosphere exhibits variability in dynamics as well as chemistry on different time scales ranging from day-to-day variability to decadal fluctuations and long-term trends. El Niño Southern Oscillation (ENSO), volcanic eruptions, solar variability or ozone depletion affect stratospheric climate and ozone to a large degree (Hood et al. 1999; Robock 2000; Sassi et al. 2004). The low frequency variability in the stratosphere can be related to tropospheric climate modes such as the Atlantic Multidecadal Oscillation (AMO) or Interdecadal Pacific Oscillation (IPO). Yet, our current understanding of stratospheric variability is largely based on observations and model simulations spanning the past 30 years (see e.g. Eyring et al. 2005), which is hardly enough to address decadal variability. It could be also shown that much larger variations occurred in the first half of the 20th century (Brönnimann et al. 2004).

The aim of this project was to investigate and quantify interannual-to-decadal variability in stratospheric climate and ozone during the whole 20th century using the state of the art chemistry climate model SOCOL ("Solar Climate and Ozone Links") (Egorova et al. 2005). SOCOL has been developed as a combination of a modified version of the middle atmosphere version of ECHAM4 GCM (Manzini and McFarlane 1998) and a modified version of the UIUC (University of Illinois at Urbana-Champaign) atmospheric chemistry-transport model MEZON described in detail by Rozanov et al. (1999). MA-ECHAM4 is a spectral model with T30 horizontal truncation resulting in a grid spacing of about 3.75°; in the vertical direction the model has 39 levels in a hybrid sigma-pressure coordinate system spanning the model atmosphere from the surface to 0.01 hPa. With respect to the standard MA-ECHAM4, the gravity wave source spectrum of the Doppler spread parameterization has been modified. The chemical transport part MEZON simulates 41 chemical species. The calculation of photolysis rates is performed using a look-up table approach covering the spectral band of 120-750 nm. It incorporates parameterized heating rates and absorption coefficients for the very short UV band. The transport of chemical species is performed using a hybrid numerical advection scheme (Zubov et al. 1999). We have introduced a family-based mass fixer scheme for chlorine, bromine and nitrogen species in order to avoid mass loss over the Polar region. The mass fixer for ozone was restricted to the latitude band 40°S – 40°N for the same reason.

The simulations were carried out in transient mode with 9 ensemble members. For the external forcings we used total solar irradiance reconstructions by Lean (2004), HadISST data (Rayner et al. 2003), QBO reconstruction (Brönnimann et al. 2007), stratospheric aerosols (Sato et al. 1993), tropospheric aerosols (Koepke et al. 1997). Data of

greenhouse gases (GHG) and ozone depleting substances (ODS) are obtained from GISS and WMO. Changes in land surface properties were compiled by data of the EDGAR-HYDE database.

Technical details

It was originally planned to perform the 20th century runs on the IBM SP4 machine at CSCS. However, we encountered several problems setting up the model at this environment and found quite slow performance which led us to the decision to continue the project on the Linux-Cluster "Hreidar" at ETH Zurich. To use the granted resource we were planning to perform several short time runs to study the impact of volcanic eruptions upon climate. Since CSCS was switching to the new IBM SP5 "Blanc" beginning in 2007, we were waiting to install SOCOL on this platform. Yet, in the short time range (from the release of "Blanc" till the end of our allocation period) we did not manage to make any model runs.

For little of the simulations we made use of Aria, where we had successfully installed the required postprocessing software, which converts binary data in user-friendly netCDF files.

The output of our century runs is constantly uploaded to the File Archive Server at CSCS. At the moment we have stored 17 TB of data, which will rise to 20 TB until the end of the project.

Up to now the simulations have reached the year of 1980, and hence four fifth of the simulations are completed.

Scientific Results

So far, for the period 1900-1950, we have validated the century runs to various observational data bases. We have analysed a seasonal climatology of SLP and compared it to HadSLP2 data which looked reasonable. Also, January and July climatologies of meridional temperature and mean zonal wind seem to be in line with reanalysis data of ERA 40 for the pre-ozone hole era. The well-known features like the intensification of the polar vortex during the winter hemisphere, the subtropical jets or the cold tropical tropopause layer are in excellent agreement regarding magnitude and sign.

Furthermore, we made comparisons of Total Ozone climatologies at locations where observations are available. Total Ozone series started at Oxford in 1924, at Arosa in 1926, at Tromso in 1935, and at Oslo in 1940. Comparisons with modelled Total Ozone reveal a clear underestimation of the seasonal cycle. When comparing the climatology with satellite data of the late 70s and early 80s, one finds that the meridional gradient in the spring Hemisphere is less steep in SOCOL. The internal variability between the ensemble members is thereby low. The range of minimum and maximum Total Ozone values at these locations is increasing towards higher latitudes in both model and observations.

We have computed the North Atlantic Oscillation index (NAO) and compared it with HadSLP2 data (see Figure 1 a). The within ensemble variability is much higher and therefore not all features on the short-time scale are very well represented. However, the low frequency variability seems to be in line with observations. All ensemble members show the long-term decrease starting in the early 20s. For comparison of the dynamical development at higher altitudes we have made use of reconstructed indices. The investigation of the strength of the polar vortex (not shown) in winter, measured as the 100 hPa geopotential height difference between 75°-90° N and 40°-55° N, revealed a very high internal variability in SOCOL. The vortex seems to be too weak in the 20s and too strong from 1935-45. The very weak event in the early 40s, which is believed to stem from a prevailing El Niño (Brönnimann et al. 2004), is clearly underestimated. Only one ensemble member captured this development. Figure 1 b) shows the development of the strength of the subtropical jet, measured as maximum in the 200 hPa geopotential height in the Northern Hemisphere.

a) b)

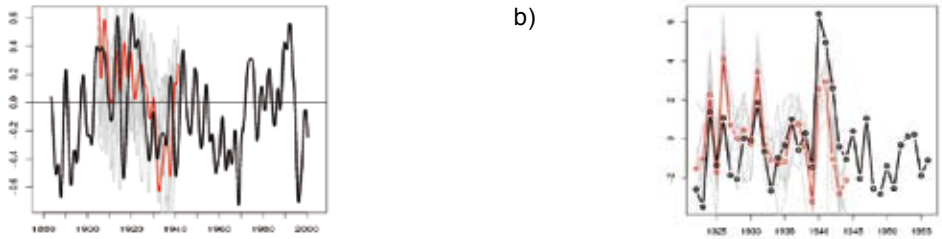

Figure 1: Observed (black) and ensemble mean (red) of a) NAO and b) strength of the subtropical jet (maximum in 200 hPa zonal wind in the Northern Hemisphere, averaged from January to March). The ensemble members are shown in grey.

SOCOL reproduces the observed time series rather well. The ensemble spread is much lower than for the polar vortex.

It is of general interest how volcanic eruptions affect the climate system. Many observational and modelling studies were carried out to study the influence due to Pinatubo eruption in 1991 (Robock 2000). Conclusions from such studies can be used for analysing other similar events. Like Pinatubo the eruption of Santa Maria in October 1902 took place in the Tropics. As in 1991, the reconstructed geopotential height field (Figure 2 b) shows an increased meridional gradient which results in a strengthening of the polar vortex and through downward propagation and intensification of the NAO a winter warming over the European Continent can be observed. SOCOL also features a positive increase of geopotential height over the tropical band and decreased values towards higher latitudes. However, the signal is much less pronounced and statistical significance is missing. Also, the winter warming is not significant.

Out of the century runs we have extracted the solar signal for 1900-1950 as solar maximum minus solar minimum and looked at the ozone response. At all latitudes in the stratosphere SOCOL shows an increase in ozone due to solar variability. This is believed to be a result of intensified photolysis of oxygen. Yet, at higher altitudes ozone depletion takes place. This can be explained by increased photolysis of H2O which leads to an intensification of the HOx destruction cycle. We have compared that feature at the Tropics with observations of SAGE and SBUV and to SOCOL runs over a more recent time period (1975-2000) (see Figure 3). In the middle stratosphere the response between the two different sets of runs looks quite similar. It is still in the range of uncertainty of the observations. However, in the lower stratosphere the increase in ozone in the run over the more recent time period is enhanced whereas at higher altitudes the decrease of ozone is more pronounced in the historical run.

Future steps

The model runs will be finished within the next two months. We will provide several validations using all 100 years. Validation in a process-oriented framework (CCMval project) will also be undertaken. For the analysis we try to estimate internal

a) b)

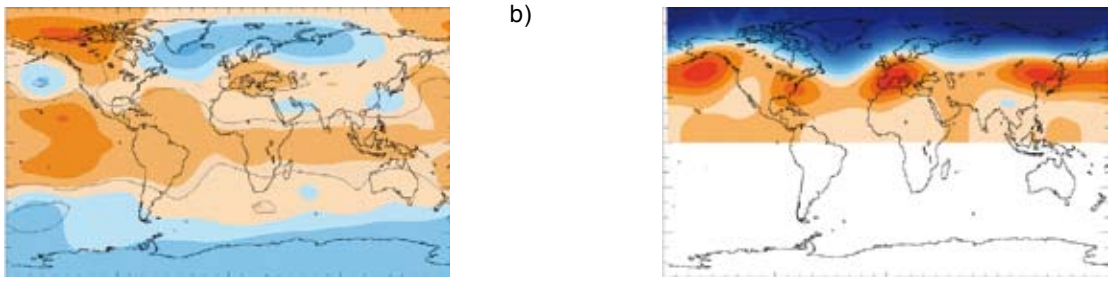

Figure 2: Anomaly of 100 hPa geopotential height averaged over January to March 1903 to a climatology of 1901-1909 for SOCOL (left) and reconstructions of upper-level field (right). Shading means significance on 95% level (student's t-test).

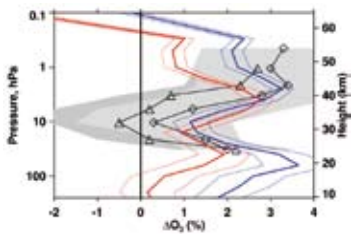

Figure 3: Ozone response (in %) to solar maximum minus solar minimum at the Tropics. Red shows the SOCOL response for the period 1900-1950, blue is the SOCOL response of simulations for 1975-2000. Observations are shown in black (SAGE and SBUV) together with uncertainty range (grey shading).

and external variability. Composites of the winter impact after major volcanic eruptions will be done. However, this also requires studying the effects of other driving and overlaying parameters like El Niños and the phase of the QBO. By using multiple linear regression techniques we try to extract the different forcings and their impact on stratospheric chemical and climate parameters.

References

1. Brönnimann, S., J. L. Annis, C. Vogler and P. D. Jones (2007) Reconstructing the Quasi-Biennial Oscillation back to 1900, Geophys. Res. Lett. (submitted).
2. Brönnimann, S., J. Luterbacher, J. Staehelin, T. M. Svendby, G. Hansen and T. Svenoe (2004): Extreme climate of the global troposphere and stratosphere in 1940-42 related to El Nino, Nature, 431,(7011), 971-974.
3. Egorova, T., E. Rozanov, V. Zubov, E. Manzini, W. Schmutz and T. Peter (2005): Chemistry-climate model SOCOL: a validation of the present-day climatology, Atmospheric Chemistry and Physics, 5, 1557-1576.
4. Eyring, V., D. E. Kinnison and T. G. Shepherd (2005): Overview of planned choupled chemistry-climate simulations to support upcoming ozone and climate assessments, SPARC Newsletter, 25, 11-17.
5. Hood, L., S. Rossi and M. Beulen (1999): Trends in lower stratospheric zonal winds, Rossby wave breaking behavior, and column ozone at northern midlatitudes, Journal of Geophysical Research-Atmospheres, 104,(D20), 24321-24339.
6. Koepke, P., M. Hess, I. Schult and E. P. Shettle (1997): Global Aerosol Data Set, Report No. 243,(Max-Planck-Institut für Meteorologie).
7. Lean, J. (2004): Solar Irradiance Reconstruction, IGBP PAGES/World Data Center for Paleoclimateology Data Contribution
8. Manzini, E. and N. McFarlane (1998): The effect of varying the source spectrum of a gravity wave parameterization in a middle atmosphere general circulation model, Journal of Geophysical Research-Atmospheres, 103,(D24), 31523-31539.
9. Rayner, N. A., D. E. Parker, E. B. Horton, C. K. Folland, L. V. Alexander, D. P. Rowell, E. C. Kent and A. Kaplan (2003): Global analyses of sea surface temperature, sea ice, and night marine air temperature since the late nineteenth century, Journal of Geophysical Research-Atmospheres, 108,(D14), -.
10. Robock, A. (2000): Volcanic eruptions and climate, Reviews of Geophysics, 38,(2), 191-219.
11. Rozanov, E. V., V. A. Zubov, M. E. Schlesinger, F. L. Yang and N. G. Andronova (1999): The UIUC three-dimensional stratospheric chemical transport model: Description and evaluation of the simulated source gases and ozone, Journal of Geophysical Research-Atmospheres, 104,(D9), 11755-11781.
12. Sassi, F., D. Kinnison, B. A. Boville, R. R. Garcia and R. Roble (2004): Effect of El Nino-Southern Oscillation on the dynamical, thermal, and chemical structure of the middle atmosphere, Journal of Geophysical Research-Atmospheres, 109,(D17), -.
13. Sato, M., J. E. Hansen, M. P. Mccormick and J. B. Pollack (1993): Stratospheric Aerosol Optical Depths, 1850-1990, Journal of Geophysical Research-Atmospheres, 98,(D12), 22987-22994.
14. Zubov, V. A., E. V. Rozanov and M. E. Schlesinger (1999): Hybrid scheme for three-dimensional advective transport, Monthly Weather Review, 127,(6), 1335-1346.

Structure and enantiospecificity of chiral nanoparticles and interfaces

Prof. Thomas Bürgi

Institut de Microtechnique, Université de Neuchâtel, Switzerland

Adsorption of molecules on surfaces is of fundamental importance for many processes comprising separation, (bio-)sensing, surface processing, lubrication and heterogeneous catalysis. The conformation of the molecules at the surface can have a pronounced effect on surface properties. However, such information is rather difficult to obtain. A special class of surfaces results from modification by chiral molecules. The resulting chirally modified surfaces have potential for applications in enantioselective separation, detection of enantiomers and heterogeneous enantioselective catalysis (1). The latter effects strongly rely on intermolecular interactions, which depend on the conformation of the adsorbed molecule.

A powerful method for obtaining conformational information is vibrational circular dichroism (VCD), i.e. the differential absorption of left- and right-circularly polarized light by a chiral sample (2). VCD is more sensitive to conformation than conventional infrared absorption spectroscopy. In order to extract that structural information the experimental VCD spectrum has to be compared with theoretical spectra calculated for different conformers. Density functional theory (DFT) calculations have predictive character for VCD spectra of organic molecules (3). An experimental challenge of VCD spectroscopy is the relatively small signals. The anisotropy factors $\Delta A/A = \Delta\varepsilon/\varepsilon$ are typically on the order of 10^{-4} to 10^{-6}. As a consequence measurements on flat surfaces are very difficult, since monolayers give typically rise to very small signals. One way to overcome this obstacle is the use of a high specific surface area material, such as nanoparticles. The latter can be viewed as the nanometer-size analogues of extended flat surfaces. Indeed, we have shown recently that VCD spectra of molecules adsorbed on small metal particles can be measured (4).

In the initial studies we focused on cysteine derivatives such as N-acetyl-L-cysteine (4) and N-isobutyryl-L-cysteine (5). Although valuable information was extracted from these studies the latter systems are not very well suited as benchmark for this new approach to determine adsorbate structures for two reasons: First, the molecules likely exist in several conformations, which “contaminates” the VCD spectrum. Second, and most important, the cysteine derivatives likely interact specifically with the solvent (water). This interaction was not considered in the calculations up to now.

We chose to carefully look at a system that is more rigid and therefore shows less conformational flexibility. A further criterion was solubility in organic solvent in order to prevent specific solvent interactions. Therefore gold nanoparticles covered by 1,1’-binaphthyl-2,2’-dithiol (BINAS) were prepared (6) and their VCD spectra measured and calculated. We used Gaussian03 to calculate the structure and vibrational circular dichroism spectra of the free and the adsorbed molecule by density functional theory (DFT). Figures 1 and 2 show a comparison between experimental and calculated

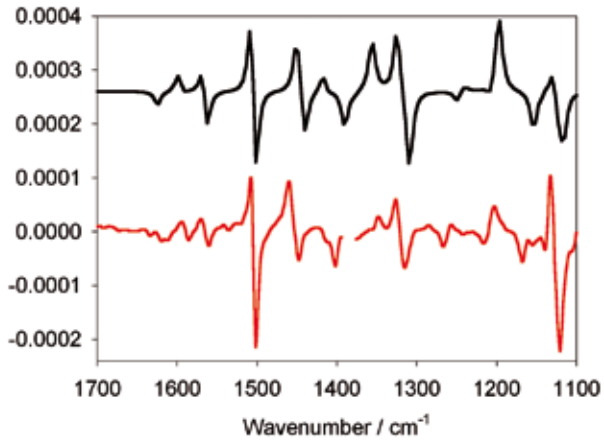

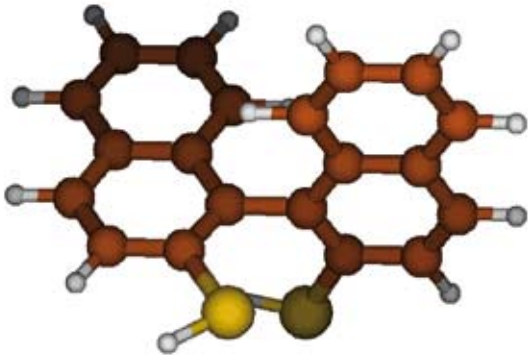

Figure 1: Top. Experimental (red) and calculated (black) VCD spectra of (S)-BINAS. Bottom: Calculated structure. Calculations were performed a the B3PW91 / 6-31G(d,p) level of theory and experiments were performed in CD2Cl2.

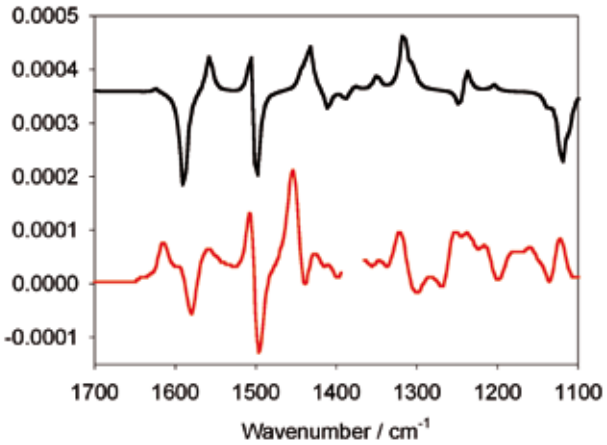

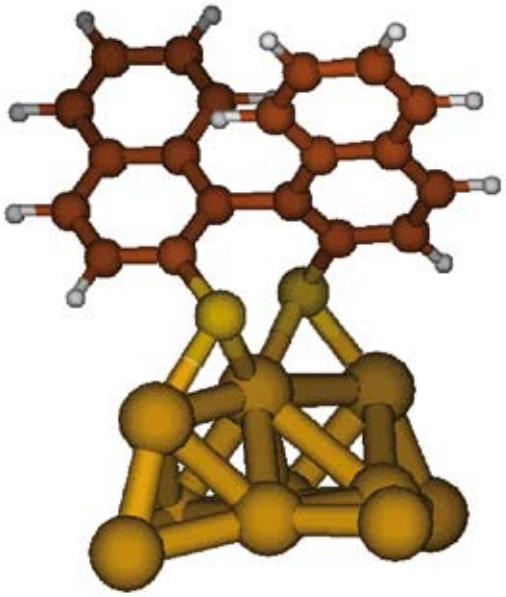

Figure 2: Top. Experimental (red) and calculated (black) VCD spectra of gold nanoparticles covered by R-BINAS. Bottom: Calculated structure of (S)-BINAS adsorbed on a small gold particle. Calculations were performed a the B3PW91 / 6-31G(d,p), LanL2DZ level of theory and experiments were performed in CD2Cl2.

VCD spectra of BINAS (Figure 1) and gold nanoparticles covered by BINAS (Figure 2). The following conclusions can be drawn from this study (7): (i) The VCD spectrum changes drastically upon adsorption of the molecule. (ii) The experimental VCD spectra do not depend on the size of the particles. This shows that the vibrational properties of an adsorbed molecule are of local character. (iii) The experimental and calculated spectra are in excellent agreement, which validates this novel approach to determine the structure of adsorbed molecules.

In addition we addressed the general question of structural evolution of gold particles covered by thiols, as they grow from several to a few tens of gold atoms within the core. Very small gold particles covered by N-acetyl-L-cysteine were separated according to their size by gel electrophoresis. Eight different fractions were collected and

their EXAFS (extended X-ray absorption fine structure) spectra measured at the Swiss Light Source (SLS). These experiments allow the determination of coordination numbers and of distances between atoms. In parallel to the experiments we performed DFT calculations on clusters using Gaussian03 and ADF. The calculations reveal that the sulfur atoms of the adsorbed thiols can enter in between two gold surface atoms. This motif on the particle surface resembles the well known gold – thiol polymer structure. As a consequence the surface region of these nanoparticles is very soft, which is likely to play an important in many applications for which gold nanoparticles are considered nowadays.

Acknowledgment: Financial support by the Swiss National Science Foundation is kindly acknowledged. We also thank the Swiss Light Source (SLS) for beam time.

References

1. Bürgi T., Baiker A. Heterogeneous enantioselective hydrogenation over cinchona alkaloid modified platinum: Mechanistic insight into a complex reaction. Acc. Chem. Res. 2004, 37, 909-917.
2. Nafie LA, Keiderling TA, Stephens PJ. Vibrational circular dichroism, J. Am. Chem. Soc. 1976, 98, 2715-2723.
3. Bürgi T, Urakawa A, Behzadi B, Ernst K-H, Baiker A. Absolute configuration of heptahelicene: A VCD spectroscopy study, New J. Chem. 2004, 28, 332-334.
4. Gautier C, Bürgi T. Vibrational circular dichroism of N-acetyl-L-cysteine protected gold nanoparticles. J. Chem. Soc. Chem. Commun. 2005:5393-5395.
5. Gautier C, Bürgi T. Chiral N-isobutyryl-cysteine protected gold nanoparticles: preparation, size selection and optical activity in the UV-vis and infrared. J. Am. Chem. Soc. 2006, 128:11079-11087.
6. Gautier C, Taras R, Gladiali S, Bürgi T. Chiral BINAS-stabilized gold clusters: Size separation and optical activity in the UV-vis. Chirality, 2008, 20, 486-493.
7. Gautier C, Bürgi T. Manuscript in preparation.

Computaion of Stellarator Coils, Equilibrium, Stability and Transport

Dr. W. Anthony Cooper (a)

with N. Mellet (a), P. Popovich (a), M. Drevlak (b), M. Yu Isaev (c), S. Medvedev (d), M. Mikhailov (c), A. Subbotin (c), A. Martynov (d)

(a) Centre de Recherches en Physique des Plasmas, EPF Lausanne, Switzerland
(b) Max-Planck Institut für Plasmaphysik, Greifswald, Germany
(c) Nuclear Research Institute, Russian Research Centre „Kurchatov Institute“, Moscow, Russian Federation
(d) Keldysh Institute of Applied Mathematics, Russian Academy of Sciences, Moscow, Russian Federation

Description

The increasing costs of fossil fuels and their harmful impact on climate change lead inevitably to a serious consideration of clean long term energy production alternatives that can adequately satisfy the requirements of an industrial society. Nuclear fusion offers a very relevant solution to the future energy needs of the world. The ITER experimental reactor facility under construction in Cadarache, France constitutes an essential first step for the evaluation of nuclear fusion as a viable power generation source. Stellarator systems represent an alternative magnetic confinement concept that allows more flexibility with respect to the conflicting physics and engineering criteria that must be satisfied at the expense of a more complicated geometrical structure. Typically, physics properties that must be optimised are the volume average of the plasma <ß> (the ration of the kinetic pressure to the magnetic pressure of the confining fields) imposed by local and global deal magnetohydrodynamic (MHD) instabilities [1], the robustness of the magnetic field structure to changes in pressure and current, the confinement of α-particles long enough that they deposit the bulk of their birth energies in the background [2], the confinement of the plasma thermal energy to guarantee sustainability of the burn conditions, etc. Engineering criteria include modularity of the coil system, constraints on coil curvature radii, accessibility of heating and diagnostic systems to plasma, blanket design conditions to capture and shield the energetic neutrons resulting from the fusion reactions, etc.

Diverse physics criteria must be simultaneously satisfied to determine satisfactory fusion confinement systems. This is undertaken through an optimization of the plasma boundary to satisfy criteria like MHD stability at high <β>, robustness of the magnetic field structure with respect to changes in <β>, vacuum magnetic well, satisfactory confinement of α-particles, poloidal pseudosymmetry of the magnetic field spectrum and poloidal closure of contours of the second adiabatic invariant have yielded $\mathcal{J}_{\|}$-optimised stellarator configurations. Conditions for which the dipole secondary current vanishes have been explored which retain the quasi-isodynamic properties which are characterised by the poloidal closure of the second adiabatic invariant for all classes of trapped particles as shown in Fig. 1. Additional heating is required in a fusion reactor to ignite the plasma, after which the burn should be self sustained. The three-dimensional global wave propagation code (LEMan; Low frequency ElectroMagnetic code) [3] which in-

cludes finite parallel electric field effects (hence electron inertia) has been applied in the Alfvén frequency range in 2D and 3D geometry, but has been limited so far to 2D tokamak and simple mirror systems in the ion cyclotron range of frequencies. Furthermore, the auxiliary heating can distort the particle distribution functions and drive a pressure anisotropy. The effect of this anisotropy on the MHD equilibrium and stability properties warrants detailed evaluation. Tokamak stability properties that are relevant for ITER require detailed investigation.

Achievements

Optimization of Quasi-Isodynamic Stellarator Configurations

Novel geometry quasi-isodynamic ("qi") stellarator configurations have been devised with vanishing dipole secondary current in the plasma. In a first step, model investigations were undertaken to identify the Fourier spectrum of the magnetic field strength which simultaneously satisfied the "qi" and zero dipole current conditions. Secondly, the geometry at the boundary corresponding to such a magnetic field spectrum was found showing the cross sections were purely elliptical therefore displaying an absence of magnetic well. In the last stage, some boundary magnetic surfaces were generated for which the plasma was stable to Mercier, resistive interchange and strong symmetric ballooning criteria which were also close to "qi". The magnetic field strength at the outermost flux surface for this configuration is depicted in Fig. 2.

Electromagnetic Wave Propagation and Absorption in 3D Plasmas

The LEMan code has been adapted to run on an IBM-P5 cluster. As the memory is shared between all processors of a single node, Open MP was used to obtain an efficient parallelisation of the solver. But MPI is still used for the communication between the nodes. The code is now able to reach

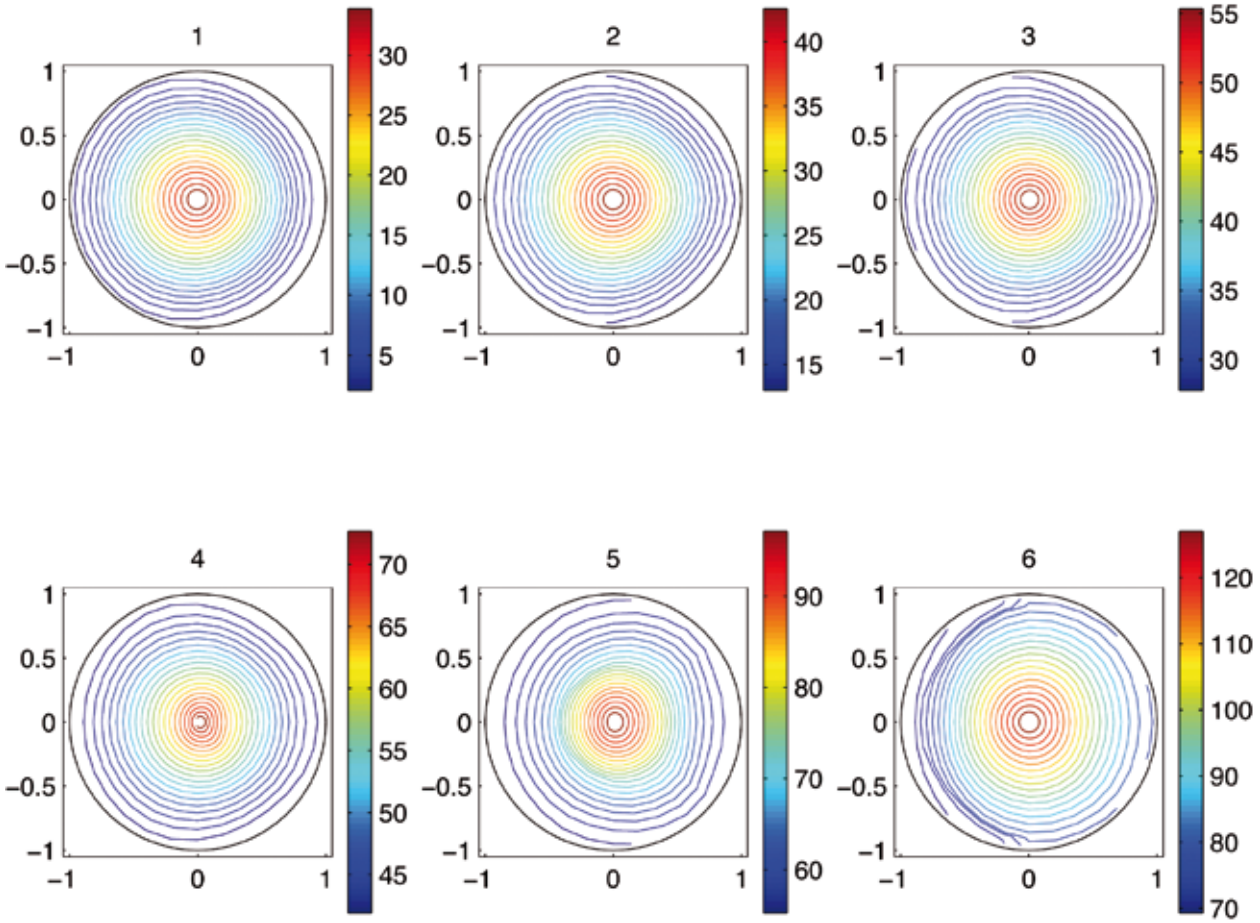

Figure 1

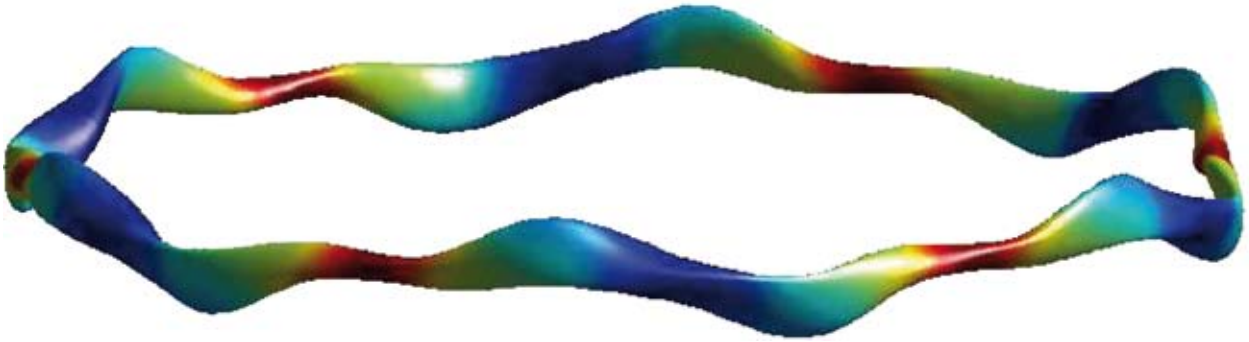

Figure 2

a total of 2000 Fourier modes for the description of the perturbed field. This should allow simulations in the ion cyclotron frequency domain for a wider range of stellarators. As an example, the normal component of the electric field in a 6-period quasi-isodynamic stellarator is displayed in Fig. 3. The computation of the warm dielectric tensor with exact determination of the parallel wave vector has been optimised to reach good convergence with an improvement of the CPU time dependence on the Fourier mode spectrum. This was accomplished by avoiding the computation of negligible terms. A comparison between the versions with exact computation and with different approximated parallel wave vectors has been performed in the case of a JET equilibrium. It points out the importance of this quantity to influence results, the approximation being more or less appropriate for the different cases considered (e.g. inside the gap or the continuum).

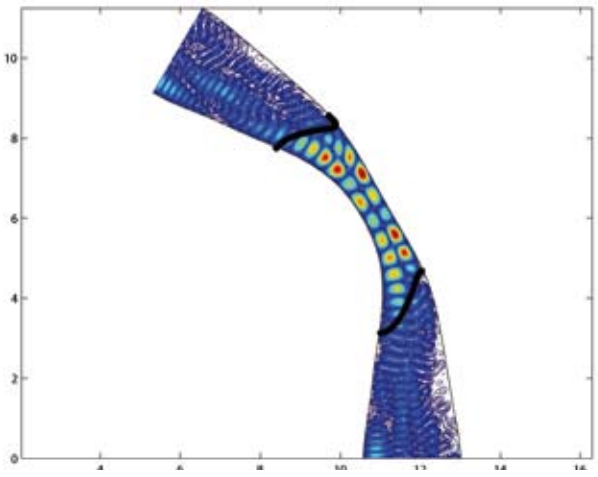

Figure 3

Fluid Magnetohydrodynamic Stability in a Heliotron with Anisotropic Fast Particles

The fluid stability models with anisotropic fast particle species implemented in the TERPSICHORE code have been applied to investigate the properties of on-axis and off-axis hot particle deposition and large parallel versus large perpendicular pressure anisotropy in a Heliotron system. With central deposition, the non interacting hot particle model predicts stability at beta=4% (contributing 1/3 of the total beta) while the fully interacting model also predicts stability properties in both models and yields similar results is significantly more unstable. Typical magnetic field strength contours and perpendicular hot particle pressure distributions for high field and low field side deposition are shown at three cross sections of a heliotron device in Fig. 3. The mode structures are core-localised for the non interacting model and more edge-localised in the fully interacting hot particle model.

Unstructured grid ideal magnetohydrodynamic stability code

Several options to impose the ideal MHD condition E . B = 0 were explored in the unstructured grid n =0 stability code. The node-wise condition was found to be sensitive to the way of weighting of the unknown toroidal electric field and in general giving less regular results when the normal electric field (tangential velocity field) strongly changes across the magnetic surface (plasma-vacuum interface and internal separatrix in the

doublet configurations). The cell-wise conditions E.B = 0 look more flexible because of discontinuous normal electric field projections for the basis edge functions. However a consistent way to do this is still to be found. The code performance with the node-wise E.B = 0 condition is quite reasonable in cases of smooth eigenfunctions for reversed current configurations. The n = 0 stability of analytic equilibria with rectangular cross-section was investigated. The majority of the configurations were found unstable except dipole type equilibria with the separatrix aligned with the minor axis of the plasma cross-section.

Acknowledgements

We would like to thank the support staff of the Swiss National Supercomputing Centre as well as the on-site NEC application analysts for the kind support provided to this project. This project has been partially sponsored by Euratom and the Swiss National Science Foundation.

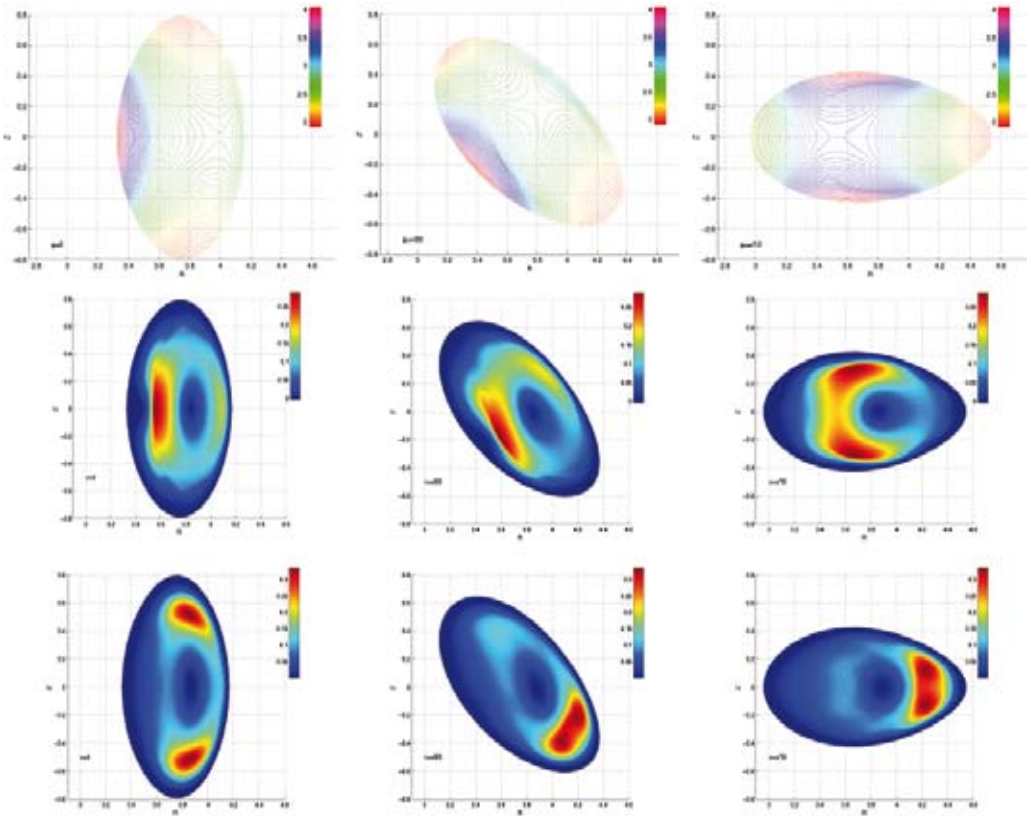

Figure 4

References

1. D.V. Anderson, W.A. Cooper, R. Gruber, S. Merazzi, U. Schwenn; Methods for the efficient calculation of the (MHD) magnetohydrodynamic stability properties of magnetically confined fusion plasmas; International J. Supercomp. Appl. 4 (1990) 34-47.
2. W. Lotz, P. Merkel, J. Nührenberg, E. Strumberger; Collisionless α-particles, confinement in stellarators, Plasma Phy. Control. Fusion 34 (1992) 1037-1052
3. P. Popovich, W.A. Cooper, L. Villard; Three-dimensional full wave propagation for cold plasma; Fusion Science and Technol, 46 (2004) 342-347.
4. W.A. Cooper, J.P. Graves, M. Jucker, K.Y. Watanabe, Y. Narushima, T. Yamaguchi; Fluid magnetohydrodynamic stability in a Heliotron with anisotropic fast particle species; Plasma Phy. Control. Fusion 49 (1007) 1177-1191.

Computational Science and Engineering in Microelectronics and Optoelectronics

Prof. Wolfgang Fichtner

Integrated Systems Laboratory, ETH Zürich, Switzerland

Project Overveiw

In nanoelectronics, Computational Science and Engineering is an established methodology in research as well in development. Physics based process simulation (simulation of the manufacturing technology) and device simulation (simulation of the operating of semiconductor devices) is known as „Technology CAD“ (TCAD). The benefit of TCAD is not only of technical and economic nature (reduction of the very expensive experimental runs in the development phase, time-to-market of integrated circuits), it is also of great importance for science and findings: physical simulations make it possible to have an insight view in manufacturing processes or devices operating during transient and very fast events, which is closed to experimental techniques. Due to the continuous miniaturization of technology and devices, there is a great challenge for research in TCAD (3D simulations, transient events in the pico second regime, complex material structures).

The project is structured in 2 research topics:

- Molecular Dynamics: Ab Initio Simulation of Semiconductor Processing Physics
- Device Physics: Device Simulation in Nanoelectronics

Molecular Dynamics

The ongoing miniaturization of integrated circuits requires an increasingly detailed understanding of the physical processes during manufacturing. For the accurate modeling of dopant diffusion and activation, phenomenological models must be complemented and eventually even replaced with models based on atomic-level physics. However, it is currently not possible to determine the relevant physical properties of the involved defects by experimental methods alone. The general goal of this project is to investigate these defects by means of ab initio simulations and to apply the results to advanced process simulations.

Ab Initio Investigation of Phosphorus Clustering in Silicon

Personnel:	Beat Sahli, Kilian Vollenweider
Funding:	KTI 8349.1 NMPP ATOMDIFF, Synopsys
Partners:	Synopsys Pilot Users: AMAT, Fujitsu, NEC, Samsung, STM, VSEA

Phosphorus is heavily used as dopant in state-of-the-art integrated circuit technologies. Phosphorus clustering and diffusion play a central role in the manufacturing process. The physical properties on the atomic level of relevant phosphorus-related defects in silicon were investigated by ab initio calculations based on density functional theory using the Vienna Ab initio Simulation Package (VASP). Selected clusters including up to one vacancy or up to two interstitials and up to four phosphorus atoms were considered: I, V, P, P2, P3, PI, PI2, P2I, P3I, PV, P2V, P3V and P4V. The selection of defects was based on the needs of state-of-the-art TCAD

models for dopant diffusion and activation. For each defect type the charge states from -4 to +4 were investigated (if they exist). The simulations were performed with supercells containing 216 atoms. From the total energies calculated with VASP, the formation energies and the binding energies of the defects were derived.

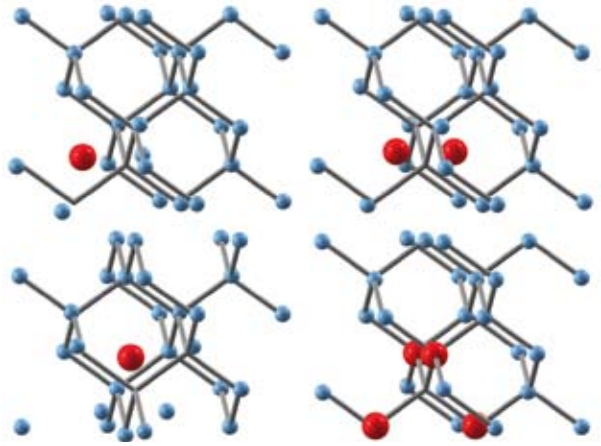

Figure 1: Four clusters containing phosphorus atoms. From top left to bottom right: PI, P2I, PI2, P4V. The silicon atoms are shown in blue, the phosphorus atoms in red and a reference lattice in gray.

Device Physics

Because of the ongoing miniaturization, the traditional continuum based device simulation approach must be complemented or replaced with more advanced methods. Our Monte Carlo simulator with full band and one- and many-particle approaches and self-consistent simulation allows a more accurate treatment of the relevant physical effects within the quasi-classical transport approximation. For the smallest devices, a simulator based on the quantum transport approach is required.

New One-Particle Monte-Carlo Method

Personnel: Simon Brugger, Andreas Schenk
Funding: Fujitsu,
SNF 200021-109393 NEQUATTRO
Partners: Fujitsu, Synopsys

The current-based one-particle Monte-Carlo (MC) method introduced and implemented in the SimnIC device simulator has been optimized and efficiently parallelized on shared memory architectures as well as distributed memory architectures.

A small library has been designed to avoid slow-downs due to the inherent stochastic nature of MC simulations. Using this library, processors which have already finished the computation of their part of the simulation are able to help other processors, and this with a negligibly small overhead. This allow quasi-ideal speed-ups on shared memory architectures (e.g. on the Cray XT3 at CSCS Manno). To improve the statistics in regions where the particle density is inherently low, an algorithm has been developed to automatically adapt the statistical weight of the particles during a simulation.

These improvements permit to compute a full I-V curve using the MC method without restarting for each point from a drift-diffusion or energy-balance solution, putting therefore the MC method on the level of usability of the standard transport models.

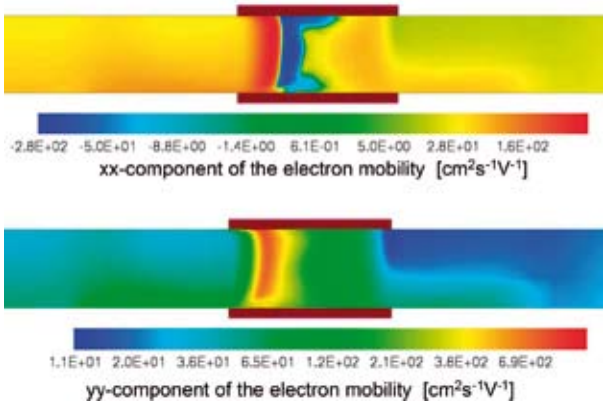

Figure 2: Top: Component of the mobility in transport direction as function of the position in a 24 nm double-gate MOSFET at Vg=1.1 V and Vd=1.2 V. Bottom: Component of the mobility perpendicular to the transport direction. One can see a strong anisotropy in the mobility tensor.

Full-Band Simulations of Si Nanowire Transistors

Personnel: Mathieu Luisier
Funding: SNF 200021-109393 NEQUATTRO

Semiconductor nanowires are possible candidate to replace the actual MOSFET since they can act both as active devices or as device connectors.

Recently, with an individual nanowire, nanoscale field-effect transistors have been realized. As the active dimensions of these nanodevices are approaching the atomic scale, their transport properties must be treated on a quantum mechanical level.

Using the semi-empirical sp3d5s* nearest-neighbor tight-binding method, full-band (FB) simulations of Si triple-gate nanowire transistors are performed for different crystal orientations such as [100], [110], [111], and [112] in the ballistic regime. The three-dimensional (3D) electrostatics (Poisson's equation) is solved self-consistently with the FB transport calculation.

Results for a 2.1 nm x 2.1 nm Si nanowire surrounded by 1 nm tick oxide layers show that [110] is the channel orientation that offers the highest ON-current, followed by [100], [112], and finally [111].

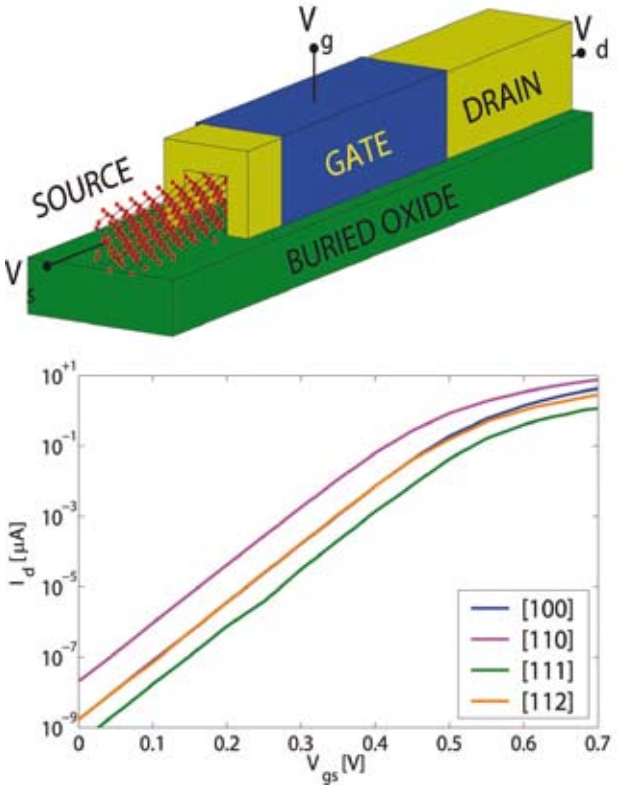

Figure 3: Top: Schematic view of a n-doped triple-gate nanowire transistor deposed on a buried oxide.Bottom: Full-band characteristics of the above transistor with different channel orientations.

Multilevel Incomplete LU-Factorizations in Semiconductor Device Simulation

Personnel: Stefan Röllin

Funding: SNF 200021-107945 ROBUST

The solution of large sparse linear systems is an important task in semiconductor device simulation. Due to time and memory constraints, direct solvers are not suited for these systems and only iterative solvers are able to provide the solution in a reasonable time. An iterative solver consists of different ingredients. Examples are symmetric and asymmetric permutations and scalings or Krylov subspace methods such as BiCGstab or GMRes. But of utmost importance is a suitable preconditioner that speeds up the convergence significantly.

There are a lot of different preconditioners known in the literature. The most effective and most robust problem-independent preconditioning techniques are probably incomplete LU-factorizations (ILU). There are several kinds of these preconditioners known in the literature. Multilevel ILU-methods are the most recent variants of incomplete factorizations and one expects that they are more robust than older, simpler versions.

The multilevel ILU-methods have been investigated for various semiconductor device simulations from both 2D and 3D. In particular, a large comparison has been made with LU-factorizations based on a drop tolerance. This variant led to the best performance in terms of computing time in the past. The gathered results indicate that the multilevel method leads to better convergence, if the preconditioners have about the same fill. Unfortunately, the overall time for a multilevel preconditioner is higher. The reason is that its construction is quite expensive.

Inverse modelling to monitor source regions of air pollutants in Europe

Dr. Doris Folini

with S. Ubl and P. Kaufmann, MeteoSwiss, Switzerland

Frame of the project

Various climate relevant gases (greenhouse effect, ozone layer depletion) are emitted more or less continuously into the earth's atmosphere. The release of some of these gases is regulated or banned by the Montreal- and Kyoto-protocols. Given their climate impact and the need to verify the imposed regulations on some of them, monitoring the emission of such gases is of key importance and the motivation for our project. The 'traditional' way is to compile emission inventories based on sales numbers, taxes etc. However, for various substances this procedure yields unsatisfying results or is barely feasible at all.

In our project we follow an alternative approach which relies on numerical models to derive regionally resolved emission estimates from long term concentration measurements of trace gases taken at a few permanent measurement sites. The basic idea is to use an atmospheric transport model to link emissions and measured concentrations and then to determine a regionally resolved emission scenario such that the long term (several years) concentration measurements are best reproduced.

On the European scale, we use as transport model the Lagrangian Particle Dispersion Model (LPDM) of MeteoSwiss.

One advantage of this approach is its relative independence. Data from a few monitoring sites is used instead of data from national reports. Also, the approach allows fast reaction to newly developed chemical substances. As soon as a new substance can be measured, emission estimates become possible. 'Traditional' inventories take a few years to include a new substance.

The ultimate goal is to derive regionally resolved emission maps for various gaseous substances, in particular halocarbons. Substances of this class are listed in both the Montreal- and Kyoto-protocol. Nevertheless, 'traditional' inventory data is relatively scarce, partly due to the existing wide variety of substances. From a modeling point of view they are attractive as their chemical reaction time scales are much longer than the relevant transport time scales.

Lagrangian particle dispersion model

To model atmospheric transport of passive tracers, like halocarbons, we use the LPDM of MeteoSwiss in backward mode [1,2]. In this model, a large number of particles are released at one point (the measurement site) during some time (the measurement period) and are then traced backward in time. Their motion is governed by meteorological wind fields plus a turbulent velocity component. The wind fields stem from the COSMO model of MeteoSwiss and are given on a grid with 7km x 7km horizontal spacing and 45 vertical levels. The turbulent velocity component is obtained as the solution of a Langevin equation.

As output of the LPDM we get a 3D residence time map which, in essence, gives the probability that

an air parcel reaches the measurement site during the measurement period. From this 3D data we can extract a 2D footprint: the residence time at each horizontal grid point, integrated over a boundary layer height of typically 500 m. The footprint gives a probability map (Fig. 1) of what boundary layer air (polluted air) will reach the measurement site. It contains information on how well a region can be monitored by a particular measuring site.

The high Alpine site Jungfraujoch

High altitude sites are particularly suited for emission monitoring as they are reached by both, atmospheric background air masses at one time and polluted boundary layer air at other times. In the case of Jungfraujoch (3580 m asl), this allows to estimate the net contribution from central Europe to the measured concentrations. Running an atmospheric transport model for this site is, however, demanding because of the complex topography. Consequently, it is crucial to analyze the performance of our LPDM under these conditions.

A first step in our project thus consisted of a sensitivity study [3]. Using 50 km x 50 km gridded inventory data for carbon monoxide (CO) from EMEP (http://www.emep.int), CO concentrations were computed for Jungfraujoch for the years 2003 to 2005 and compared with measured data. Average concentrations agree well; the correlation between modeled and measured concentrations is better in winter where r = 0.6 is reached. Variation of model input parameters within reasonable limits was found to result in 50% variation of modeled concentrations on the one sigma level. Consequently, robust inversion techniques will be needed for the envisaged emission estimates.

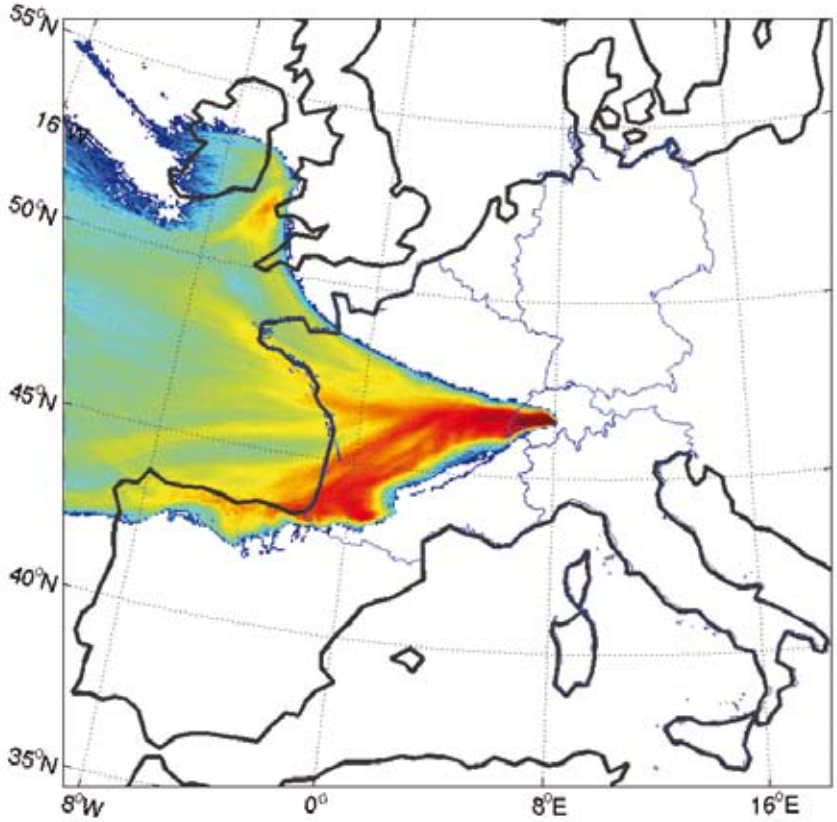

Figure 1: Footprint for station Jungfraujoch, July 4, 2002, measurement period between 03:00 and 06:00. Measured concentrations during this time contain signatures of sources that are located in the western part of Switzerland and in the central part of France. Red indicates high residence time, blue is low residence time.

Region of influence of measurement sites

For the interpretation of measured concentrations in terms of European emissions, quantitative knowledge about the region of influence (ROI) of a measurement site is crucial. A second part of our project deals with this aspect [4]. Modeled CO concentrations were computed for 13 European measurement sites that are generally considered as remote. The ROIs of individual sites, defined as the area whose surface emissions account for 80% of modeled CO concentrations, were found to typically cover an area of a few times 10^5 km^2. To achieve good geographical coverage, measurement sites should not be separated by much more than 600 km from one another, less if the sites are separated by a mountain range. Together, the 13 sites cover an area of $1.5 \cdot 10^6$ km^2, illustrated in Fig. 2. The spatial inhomogeneity of CO surface emissions accounts for 20% to 80% of the total variability of modeled CO concentration time series; the rest is due to changing atmospheric transport patterns. Time dependent emissions have a 25% effect on modeled concentrations. The results demonstrate that CO concentrations contain ample information on the spatial and temporal distribution of emission sources, which may be extracted by inverse modeling. The same is likely true for halocarbons, whose emissions are closely related to human activity and which, like CO, have a life time that is long compared to typical European transport time scales.

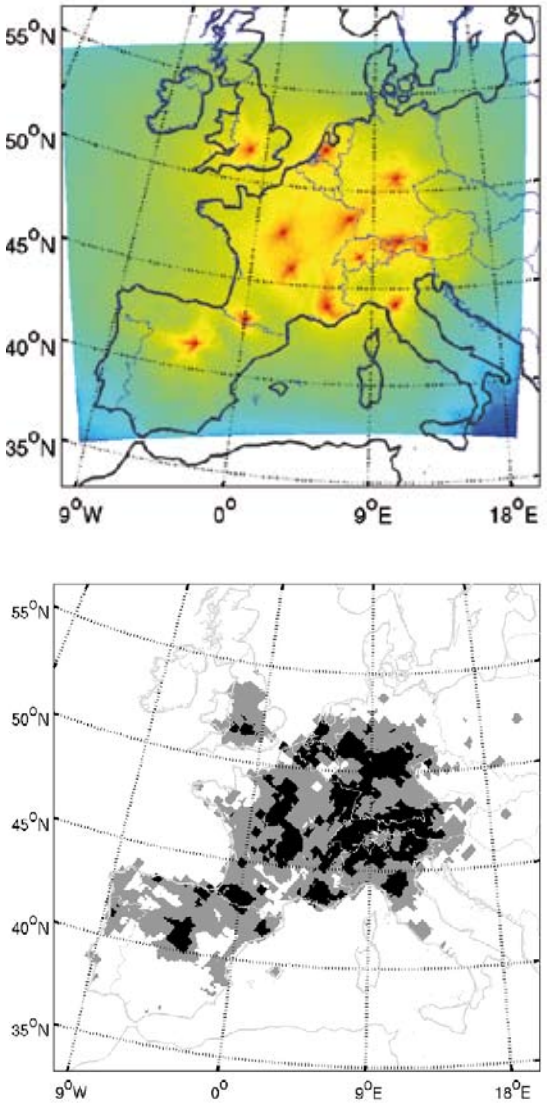

Figure 2: Annual average footprint for the year 2005 for 13 remote European measurement sites (top) and the CO surface emissions accounting for 50% (black) and 80% (gray) of modeled CO at the 13 sites (bottom).

Emission maps from inverse modeling

Currently, we work on the analysis of footprint data from 70 remote European measurement sites. Among them are those few sites that measure halocarbons and can be used for corresponding emission estimates. The 70 sites allow us, within the frame of modeled CO concentrations, to quantitatively examine the quality of emission estimates obtained by inverse modeling. In particular, we want to answer how estimated surface emission are affected by uncertainties in the transport model and by the configuration of the measurement network. The result will also allow us to judge the quality of the halocarbon emission estimates.

References

1. H. Glaab, B. Fay, and I. Jacobsen, Evaluation of the emergency dispersion model at the Deutscher Wetterdienst using ETEX data, Atmospheric Environment 32, (1998) 4359-4366.
2. S. Ubl, Backward Lagrangian particle modeling: applications for a high Alpine measurement site, PhD thesis, ETH No 16282, (2005).
3. D. Folini, S. Ubl, P. Kaufmann, Lagrangian particle dispersion modeling for the high Alpine site Jungfraujoch, Journal of Geophysical Research, accepted.
4. D. Folini, S. Ubl, P. Kaufmann, S. Henne, Region of influence of 13 European measurement sites based on modeled CO mixing ratios, Journal of Geophysical Research, submitted.

Detecting planets by the Gap they create in the dust layer of a protoplanetary disk

Dr. Laure Fouchet

Institute of Astronomy, ETH Zürich, Switzerland

Introduction

Over the last 12 years, 287 planet candidates have been detected (see http://exoplanet.eu/).

This has raised a renewed interest for theories of planet formation. At the first stages of this process is the dynamical evolution of small (micron size) to large (meter size) dust grains/boulders as influenced by the gas component of the protoplanetary disk. This bears issues on how those grains can grow to planetesimal sizes (kilometer size) and how observations of the dust continuum at millimeter wavelengths can be interpreted. Here, we study the interaction of gas and dust in a protoplanetary disk and, especially, how a forming planet could be detected in the dust layer. The complexity of such a system requires high resolution computation.

Standard protoplanetary disk

A standard protoplanetary disk results from the collapse of a molecular cloud. We consider the case of a 1 solar mass star surrounded by a 0.01 solar mass gaseous disk that extends to 160 AU (1 AU is the distance between the Earth and the Sun) and has a an aspect ratio (vertical extent H divided by distance to the star r) of H/r = 0.05. The disk's temperature is imposed by the central star and has a decreasing radial profile while it stays constant in the vertical direction. This is called locally isothermal. The temperature at 100 AU is of order 10 K.

Two phases: gas and dust

A protoplanetary disk is composed by 1% in mass of dust coming from the collapse of the molecular cloud. We call dust, any refractory material such as silicates, ices or PAHs. We model the disk as composed of two fluids, gas and dust the second one being pressureless. Dust needs to achieve a Keplerian velocity ($v_{Kep} = (GM_*/r)^{1/2}$, with G the gravitational constant, M_* the mass of the central star and r, the distance of the grain to the star). The gas, on the other hand is supported by a pressure gradient directed away from the star and can achieve a slightly subkeplerian velocity (10^{-3} less than Keplerian in practice). Therefore, dust constantly feels a headwind by the gas and is slowed down.

Gas-dust coupling

The coupling between gas and dust is achieved through aerodynamic drag with stopping time given by this expression : $t_s = (\rho_d\ s) / (\rho_g\ c_s)$ (Weidenschilling, 1977; Stepinski & Valageas, 1996). Here, ρd refers to the intrinsic density of a dust grain (~ 1 g/cm³ of ices, ~ 3 g/cm³ for silicates), s is the radius of a dust grain considered as compact and spherical, ρ_g is the gas density and c_s the soundspeed. The stopping time is the time it takes for a dust grain to be slowed down to the gas velocity. It varies with dust size and, for our choice of disk parameters, is maximum in the range 1 mm to 1 cm. This leads to dust settling to the midplane and spiraling inwards to the star. More generally, dust concentrates in pressure maxima as shown by Haghighipour & Boss (2003).

Planet-disk interactions

We now consider a 5 Jupiter mass planet located 40 AU from the star. This planet triggers density waves in the disk. Because the disk has a close to keplerian velocity field, the waves become spiral. They are indeed launched with the planet's velocity and therefore, they are speeded up in the internal disk and slowed down in the external one. These waves can be seen on Picture 1. When the planet is heavy enough as in our case, waves dissipate as shocks in the disk and transfer angular momentum. In the inner disk, the surrounding gas is slowed down and has to flow towards the star. In the outer disk it is the other way around, and, as a result, a density drop called gap is built at the orbit of the planet. This gap can also be seen on picture 1. The transfer of angular momentum between planet and disk also leads to radial migration of the planet towards the star, but it is beyond the scope of our study to analyse it.

Numerical tool

We now investigate the structure of the gap in the dust layer by means of 3D, two fluid, locally isothermal, non self-gravitating SPH simulations. This is a follow up to the Fouchet et al. (2007) study. SPH stands for Smoothed Particles Hydrodynamics. It is a Lagrangian technique where particles are followed in their motion as opposed to the Eulerian technique where quantities such as density field are computed on a grid. In SPH, the SPH superparticles are considered as interpolation points for the underlying field of a given physical quantity (density, velocity...) and this quantity is smoothed over a given number of so called neighbours, i.e. particles that are closer than a given distance called smoothing length. This length is chosen so as to have a roughly constant number of neighbours. The star is a fixed gravitational potential while the planet is a gravitational potential orbiting on a fixed circular orbit around the star (the planet only responds to the gravity of the star but not that of the disk, therefore, we cannot investigate the planet migration directly). This problem can only be treated by 3D, two-fluid simulations because the disk-planet interaction is non-axisymmetric (the x-y plane has to be computed), the gas-dust coupling implies dust settling (the r-z plane has to be computed) and dust has a different dynamics than that of gas (we need two fluids).

Gap structure in the dust layer

We show that dust piles up at the edges of the gap because it is the location of a pressure maximum. For the studied size range (100 microns to 10 cm), dust does not cross the gap, and therefore, the pile up at the outer edge increases with time as the reservoir of dust in the outer parts of the disk fills it. For 1 and 10 cm grains, we notice grains trapped in corotation. The gap is now too wide for them to go either in the inner disk or in the outer one while the gap is opening. They stay at the orbit of the planet until they get accreted by the latter. Although we consider the same system in each case (same stellar, planet and disk masses), with varying only the grain size, we obtain differ-

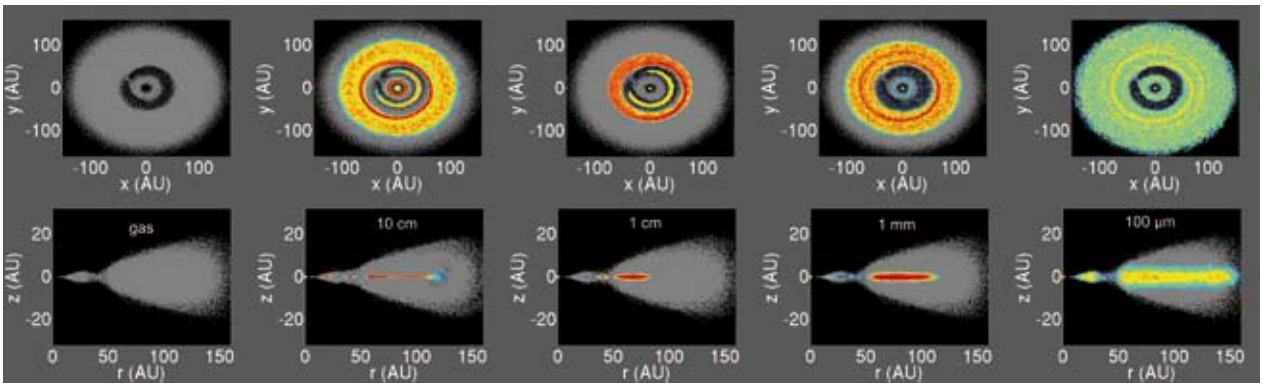

Figure 1. Top row: Disk seen top on, bottom row, disk seen edge on. Grey is gas, color is dust (according to density). From left to right: gas, 10 cm, 1 cm, 1 mm and 100 microns grains. Dust settling is visible in the bottom row while dust radial migration is seen on the top row.

ent structures: gap for 100 microns grains, inner hole for 1 mm grains, non-axisymmetric ring for 1 and 10 cm grains.

Synthetic images and observations

This raises issues how to detect forming planets embedded in their native disk. The planet itself is too faint to be directly detected, but the gap it produces could be observed with future facilities such as ALMA (Atacama Large Millimeter Array) where interferometry is used to observe faint objects such as disks. A study with only gas run by Wolf & D'angelo (2005) showed that the gap produced by a 1 Jupiter mass planet orbiting at 5 AU from a solar mass star at 140 parsecs away from us (typical for the star forming regions) could be observed by ALMA. But these simulations were run considering only gas under the hypothesis well mixed gas and dust. We produce synthetic images at the wavelength of 1.3 mm (see Picture 2) and show that particles trapped in corotation appear in these images and also that the external edge of the gap is brighter than in the well mixed case making it easier to observe. We claim that, given the particular dynamics of dust as compared to gas, a gap is easier to detect in the dust layer than in the gaseous one and, in this way, lighter planets can be detected.

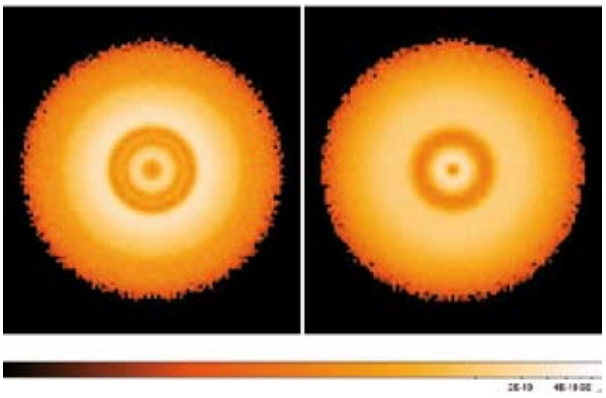

Figure 2: Caption. Synthetic images at 1.3 mm. Left: using data from the numerical simulations for each different grain size. Right: using only data for the gas and assuming gas and dust is well mixed.

References.

1. Fouchet, L.; Maddison, S. T.; Gonzalez, J.-F.; Murray, J. R., A&A, 474, 1037 (2007)
2. Haghighipour, N.; Boss, A. P., ApJ, 598, 1301 (2003)
3. Stepinski, T. F.; Valageas, P., A&A, 309, 301 (1996)
4. Weidenschilling, S., MNRAS, 180, 57 (1977)
5. Wolf, S.; D'Angelo, G., ApJ, 619, 114 (2005)

Charge transfer and oxidative damage to DNA

Dr. Francesco Luigi Gervasio

Computational Science LUI Department of Chemistry and Applied Biosciences, ETH Zurich 6900 Lugano, Switzerland

In the last decade, charge transfer in DNA has been the subject of intense theoretical and experimental investigation [1, 2]. This renewed interest is due to the fact that DNA-based components are envisaged for use in molecular electronic devices [3] and to the role played by DNA's conductivity in oxidatively generated damage and, possibly, repair mechanisms [4]. Accordingly, a number of experiments on both dry and wet DNA molecules have been performed. These experiments provided seemingly contradictory results, ranging from a highly conducting wire [5] and a proximity induced superconductor [6] to a semiconductor[7] or an insulator[8].

Such experiments are technically difficult since they require handling of single molecules or small bundles of DNA and fine control of their contact to the metallic leads and to the supporting surfaces. Despite experimental difficulties, a general consensus has been reached [1]. In particular, experiments on chemically modified or photosensitizer intercalated DNA have demonstrated that wet DNA and DNA bundles can carry charge. On the other hand, long DNA helices deposited on mica surfaces or in dry conditions were found to be insulators or wide-bandgap semiconductors [7]. As discussed in Ref. [8], charge transport in duplex DNA can occur via a coherent single step transport from donor to acceptor (superexchange limit) or multistep charge hopping [9]. Both mechanisms have been observed in wet DNA experiments, where the charge is injected site-selectively by introducing some modification into the DNA and a charge sink is created by the introduction of a modified base or of a GGG sequence[1]. To make things more difficult, DNA oxidation acts as a parasite event that traps charges on the bases.

On the basis of experimental and theoretical evidence different localization and transport mechanisms have been proposed: a change in the tilt angle of the bases, a rearrangement of the solvation shell, a fluctuation in the position of counter-ions and a change in the protonation state of G [10]. The importance of the polarization of the solvent shell has been shown to play a fundamental role in the charge transfer, at least in poly(A:T) [11]. The ion-gated charge hopping mechanism was proposed from first-principles simulations that showed a correlation between the charge localization and the position of the counterion, and it was supported by indirect experimental evidence [12]. The proton-coupled charge transfer mechanism received most attention and different groups found experimental and theoretical supporting evidence [13–14]. In this scenario the charge hopping is linked to the proton transfer from G to C.

The present work completes a long-ongoing supercomputing project on charge transfer in DNA [10,15-20]. By performing large-scale self-interaction-corrected density functional theory (DFT) calculations on a fiber Z-DNA and DFT/MM calculations on B-DNA in water solution we obtained new evidence substantiating the importance of proton

transfer in poly(G:C) and of water rearrangement in poly(A:T).

The full quantum calculations on the polyd(GpCp) fiber have shown that the hole can indeed be localized by a proton transfer from G to C [15,18]. This result has been confirmed on the B-DNA in solution, where we observed the charge transfer from a GGG to a G site upon deprotonation of the latter [17]. To do that we performed a metadynamics simulation. Our goal was to understand how a hole, which is initially localized on the stacked GGG triplet, reversibly hops to a different isolated G, separated from the GGG by an AT bridge. We start adding energy to the H1 of the isolated guanine that initially has no radicalic character.

As the reaction proceeds, the proton is transferred from this G base to the nearby paired C base and, simultaneously, the H4 proton belonging to C is transferred to G. This double proton exchange makes the final state energetically more favorable than a single proton transfer.

In poly(A:T) proton transfer is not possible. In this case the water rearrangement plays a fundamental role in charge hopping.[20] Indeed we found that transport along the A-T bridge involves the breaking and formation of water-nitrogen hydrogen bonds in the first solvation shell occurring on the order of the simulation timescale (ps). Moreover, we found that the positive charge can be delocalized on different DNA bases. However a rearrangement of the solvation shell around the electron-depleted nitrogen atoms induces an energetically favorable localization of the charge, helping to reconcile seemingly contradictory theoretical predictions that the positive charge can be both delocalized and localized [20].

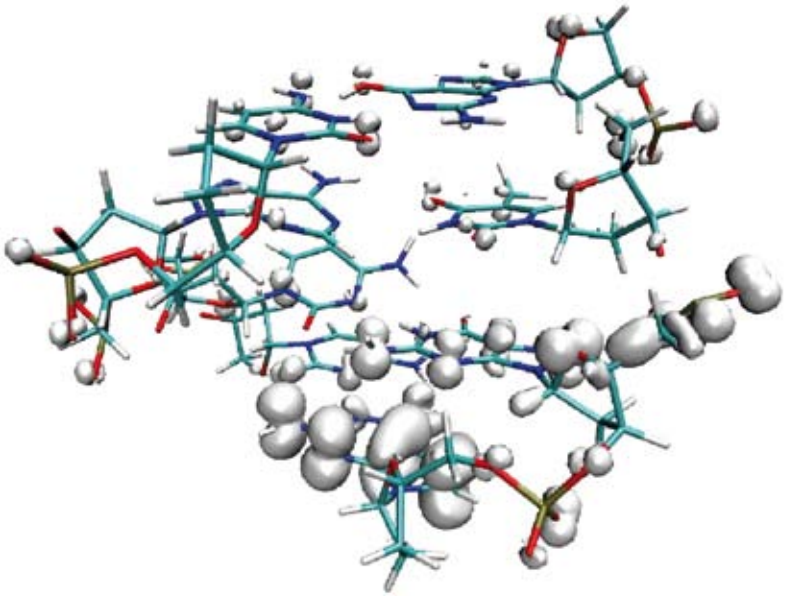

Figure 1: Details of the three-dimensional structure of the B-DNA 38-mer and of the spin density isosurface (in white) associated with the radical cation state during the hole transfer from GGG to the isolated G.

References

1. G. B. Schuster, ed., Longe-Range Charge Transfer in DNA I, vol. 236 of Topics in Current Chemistry (Springer-Verlag, Heidelberg, 2004).
2. G. B. Schuster, ed., Longe-Range Charge Transfer in DNA II, vol. 237 of Topics in Current Chemistry (Springer-Verlag, Heidelberg, 2004).
3. S. O. Kelley, N. M. Jackson, M. G. Hill, and J. K. Barton, Angew. Chem. Int. Ed. 38, 941 (1999).
4. E. M. Boon, Proc. Natl. Acad. Sci. U.S.A. 100, 12543 (2003).
5. R. Holmlin, P. Dandliker, and J. Barton, Angew. Chem. Int. Ed. 36, 2714 (1997).
6. A. Y. Kasumov, M. Kociak, S. Gueron, B. Reulet, V. T. Volkov, D. V. Klinov, and H. Bouchiat, Science 291, 280 (2001).
7. D. Porath, A. Bezryadin, S. deVries, and C. Dekker, Nature 403, 635 (2000).
8. M. Bixon, J. Jortner, Chem. Phys. 319, 273–282 (2005).
9. G.B. Schuster, Acc. Chem. Res. 33, 253–260 (2000).
10. F.L. Gervasio, A. Laio, M. Iannuzzi, M. Parrinello, Chem. Eur. J. 10, 4846–4852 (2004).
11. E.M. Conwell, Proc. Natl. Acad. Sci. USA 102 (25) (2005) 8795–8799.
12. R.N. Barnett, C.L. Cleveland, A. Joy, U. Landman, G. Schuster, Science 94, 567–571 (2001).
13. B. Giese, S. Wessely, Chem. Commun. 20, 2108–2109 (2001).
14. V. Shafirovich, A. Dourandin, N.E. Geacintov, J. Phys. Chem. B 105, 8431–8435 (2001).
15. F.L. Gervasio,M. Boero, A. Laio, M. Parrinello, Phys. Rev. Lett. 94, 158103 (2005).
16. F. L. Gervasio, P. Carloni, and M. Parrinello, Phys. Rev. Lett. 89, 108102 (2002).
17. F.L. Gervasio, M. Boero, M. Parrinello, Angew. Chem. Int. Ed. 45, 5606–5609 (2006).
18. M. Boero, F. L. Gervasio and M. Parrinello. Mol. Simul., 33, 57 - 60 (2007).
19. F. L. Gervasio. Comput. Phys. Commun., 177, 27-29, 2007.
20. Y. A. Mantz, F. L. Gervasio, T. Laino, and M. Parrinello. Phys. Rev. Lett., 99, 058104 (2007).

Atomistic simulations and electronic structure

Prof. Stefan Goedecker

Department of Physics and Astronomy, University of Basel, Switzerland

Our investigations during the last 2 years focused on two subjects:

- The development of wavelet based algorithms for electronic structure calculations and electrostatic problems
- Global geometry optimization to find structures of clusters, nano-structures and biomolecules

Within the context of a European project we have developed a wavelet based density functional electronic structure program. It uses a set of orthogonal Daubechies wavelets to represent the Kohn-Sham wavefunctions. Like plane waves, wavelets are a systematic basis set, but in contrast to plane waves wavelets they allow for adaptivity.

Our wavelet program has three resolution levels in the simulation box. Regions that are void of basis function because they are far away from any atom, low resolution regions in the tail region of the wavefunctions and high resolution in the region where bonding occurs.

Because of their adaptivity the number of degrees of freedom is greatly reduced compared to plane waves for molecular systems. As a consequence, both the memory requirements and CPU times are reduced significantly. The wavelet program is available within the ABINIT package or in a standalone version. The program is well optimized and gives excellent parallel efficiency on parallel computers with a large band width between the processors such as the Cray in Manno. On this machine we can assign one processor per electronic orbital to get the shortest execution time without sacrificing more than 15 percent of the CPU time to communication.

Most of the CPU time is spent in linear algebra and convolution routines. For the linear algebra we use BLAS and the convolutions were especifically tuned for the opteron processor and run at two Gflops.

Using wavelet based algorithms we have also developed several algorithms to solve electrostatic problems both for continuous charge distributions and point particles. All these methods have in common that they solve the integral equation for the potential directly by convolution methods with the exact boundary condition. We have implemented free boundary conditions and surface boundary conditions, i.e. periodicity in two directions and free boundary conditions in one direction. The algorithms for continuous charge distributions are used within our wavelet electronic structure program and the algorithms for point particles are used to simulate interfaces and surfaces of ionic crystals.

Using the Minima hopping method we have generated a very large number of realistic silicon tip structures for use in Atomic Force Microscopy. We have also studied the interaction of these tip structures with silicon surfaces when they approach the surface or retract from it.

In this context our realistic tip structures reveal significant differences to the much smaller model tip structures that were used in previous simulations. We have observed many sudden rearrangements of the atoms in the tip when the distance to the surface changes. These rearrangements give rise to hysteresis which in turn is responsible for the dissipation effects. Using these tip structures we were for the first time able to explain the experimentally observed dissipation in a quantitatively correct way.

In order to understand kinetic effects in silicon clusters and silicon tip structures we have determined a large number of first order saddle points (transition states) on the potential energy surface using the dimer method. We are at present comparing barrier heights obtained by different methods, namely tight binding schemes, density functional methods and quantum Monte Carlo methods.

We have also started to study the structure of AFM tips made out of ionic materials such as NaCl or KBr. We have found a strikingly different behavior compared to the silicon tips we have studied previously and we are at present investigating the consequences of these differences.

Using minima hopping as a global optimization method we succeeded in folding proteins. We have obtained all the standard elementary patterns such as alpha helices, beta sheets and loops. Unfortunately, the global minima of the free energy that we found were in general not the experimental native state. We believe that force fields do not give the required precision to predict protein structure and we are at present investigating in detail the weakness of standard force fields such as OPLS and Amber by comparing structures obtained by these force fields and by density functional calculations.

We have investigated the structure of small medium size silicon clusters using global geometry optimization. We have found many new low energy structures and, in particular, we have found that the lowest isomers are very close in energy. Since low energy isomers differ in energy only by a few mHartree, finite temperature and isotope effects can change the energetic ordering of these systems. A well defined structure does thus not exist. These initial investigations were based on the dual minima hopping method where an approximate but fast method is combined with a more accurate and more costly density functional method.

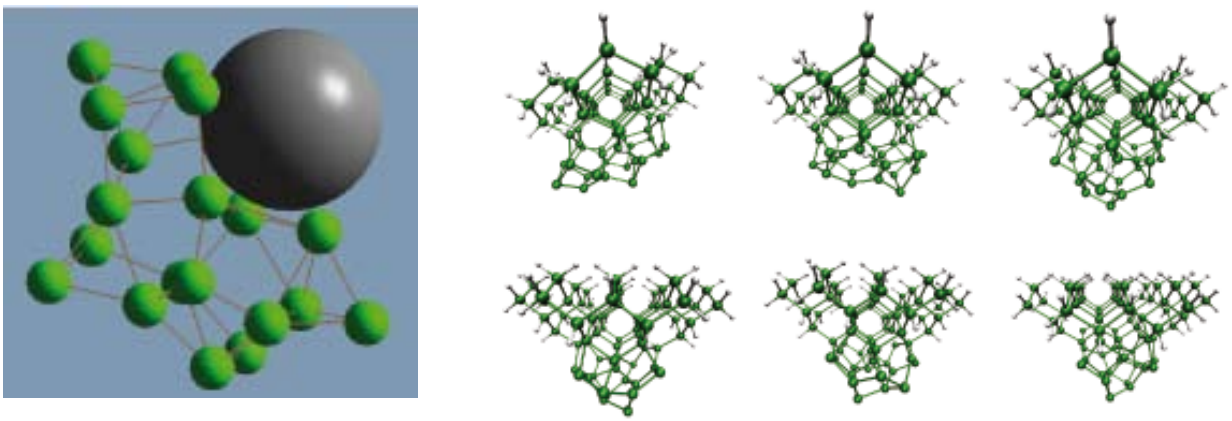

Figure 1: A low energy structure of a Ca@Si_20 cluster (left); 6 complex silicon tip structures for use in atomic force microscopy (right).

Since fast methods such as Tight Binding are available only for few systems we were limited to pure silicon clusters. In order to overcome this limitation we have recently started to do fully density functional based global geometry optimization for small clusters that might play an important role in nano sciences. To do so we have combined our new wavelet based electronic structure program with the minima hopping algorithm.

We have investigated structures proposed in the literature for endohedral metal atom doped silicon clusters and we found that all these structures are metastable. Energy was in all cases lowered significantly if the initial beautiful cage structure was destroyed and the metal atom moved outside of the cage.

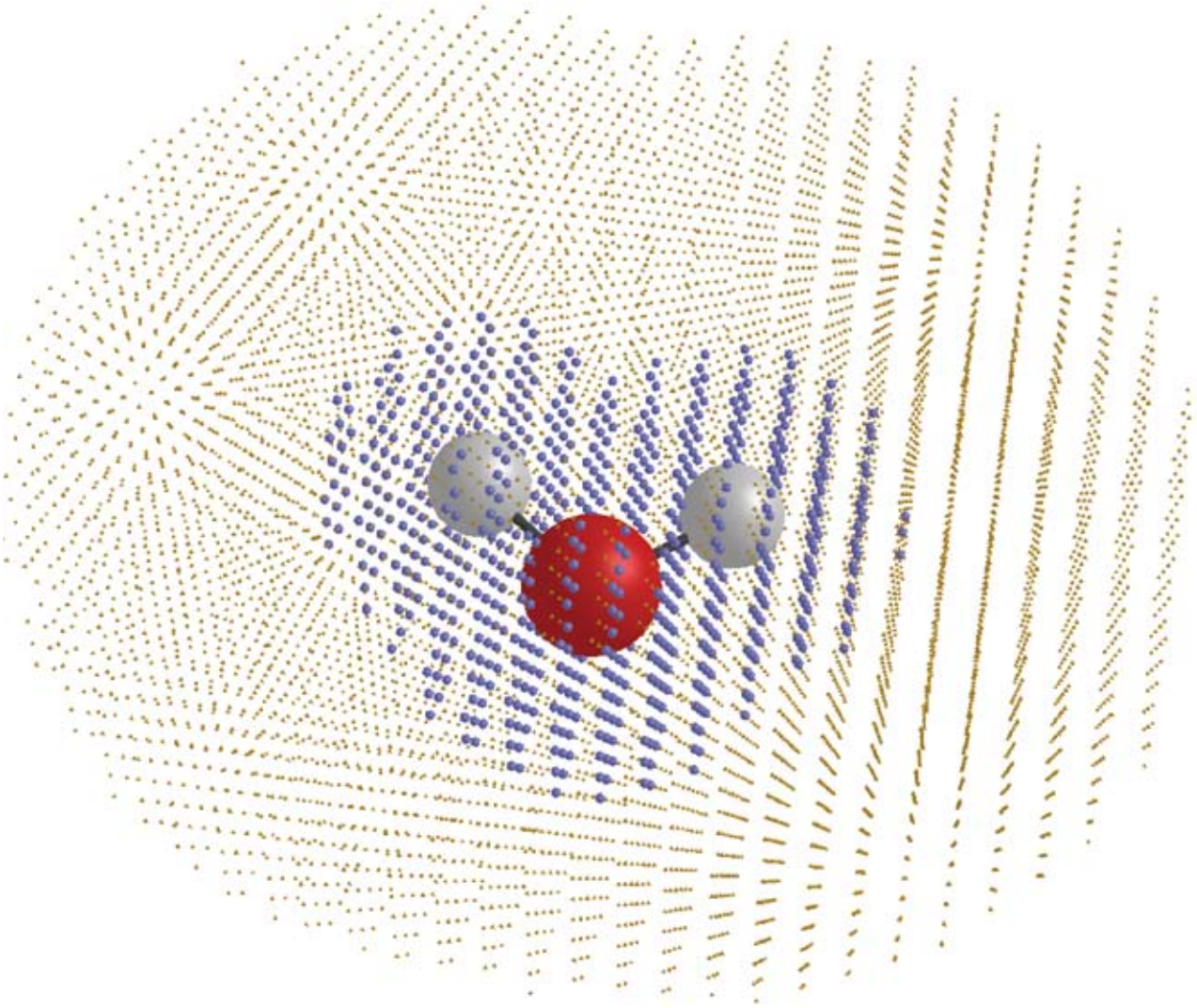

Figure 2: The adaptive wavelet grid around a water molecule.

References

1. Genovese L., Neelov A., Goedecker S, Deutsch T., Ghasemi S.A., Zilberberg O., Bergman A., Rayson M. and Schneider R.: Daubechies wavelets as a basis set for density functional pseudopotential calculations: J. Chem. Phys. 129, 014109 (2008).
2. Ghasemi S.A., Goedecker S., Lenosky T., Hug H., MeierE., Baratoff A.: Dissipation in non-contact atomic force microscopy arising from realistic tip structures, Phys. Rev. Lett. 100, 236106 (2008).
3. Roy S., Goedecker S., and Hellmann V.: A Bell-Evans-Polanyi principle for molecular dynamics trajectories and its implications for global optimization, Phys. rev. E 77, 056707 (2008).
4. Pou P., Ghasemi S.A., Jelinek P., Goedecker S. and Lenosky T.: Structure and Stability of Semiconductor Tip Apexes for Atomic Force Microscopy, submitted to PRB
5. Ghasemi S.A., Neelov A., and Goedecker S.: A particle-particle, particle-density algorithm for the calculation of electrostatic interactions of particles with slablike geometry, J. Chem. Phys. 127, 224102 (2007)
6. Genovese L., Deutsch T., and Goedecker S.: Efficient and accurate three-dimensional Poisson solver for surface problems, J. Chem. Phys. {\bf 127}, 054704 (2007)
7. Neelov S., Ghasemi S.A., and Goedecker S.: Particle-particle, particle-scaling function algorithm for electrostatic problems in free boundary conditions, J. Chem. Phys. {\bf 127}, 024109 (2007)
8. Hellmann W., Hennig R. G., Goedecker S., Umrigar C. J., Delley B., and Lenosky T.: Questioning the existence of a well defined ground state for silicon clusters, Phys. Rev. B {\bf 75}, 085411 (2007)
9. Genovese L., Deutsch T., Neelov A., Goedecker S., and Beylkin G.: Efficient solution of Poisson's equation with free boundary conditions, J. Chem. Phys. {\bf 125}, 074105 (2006)

Full QCD with 2+1 Light Chiral Fermions

Prof. Dr. Peter Hasenfratz

with Dr. F. Niedermayer; Institute of Theoretical Physics, University of Bern

Description

Quantum Chromodynamics (QCD) is the microscopic theory describing the strong interaction of elementary particles as proton, neutron, pion, etc. At low energies the corresponding coupling is large hence perturbation theory is not applicable here.

The microscopic theory contains only a few numbers as input parameters, an overall scale and the quark masses. At zero quark masses QCD becomes invariant with respect to the so-called chiral symmetry, and one expects that this symmetry would be broken spontaneously.

In the real world chiral symmetry is explicitly broken by the non-zero quark masses, but this breaking is small (for the light quarks) and can be considered as a small perturbation. The corresponding phenomenological description of the strong dynamics is given by the low energy effective Lagrangian, containing many phenomenological parameters, the low energy constants. These parameters can be determined from experiments (hadron masses, scattering length, etc.). On the other hand, lattice QCD can predict these phenomenological constants based on its few fundamental parameters.

In the standard formulation of lattice QCD the chiral symmetry is explicitly broken by discretization errors. Recent theoretical developments allowed to construct a formalism where this symmetry remains intact even at finite lattice spacing (at zero quark mass).

We use in our simulations an action which has small discretization errors in the measured quantities and has good chiral properties. This allows us to run simulations at relatively coarse lattices (with a lattice spacing up to 0.15 fm) and small quark masses, making the extrapolation to the physical situation more reliable. We simulated first the system without dynamical quarks (in the so-called quenched approximation) and got very encouraging results: the action indeed has produced small scaling and chiral symmetry violations.

In this project we simulated QCD with 2+1 dynamical quarks (corresponding closely to the real physical situation where one has three light quarks, the u, d and s quarks (u and d having nearly degenerate masses). The simulations were performed on CRAY XT3 at CSCS, on an SGI Altix machine at LRZ in Munich and on PC clusters in Bern, in the framework of the Bern-Graz-Regensburg collaboration.

We simulated the system at a lattice spacing of 0.13 fm, the size of the box was 1.6 fm, with the quark masses 16 MeV and 137 MeV for the u,d and s quarks, respectively. The box size and the quark masses were in the range when one can apply results of chiral perturbation theory. The good chiral properties of our action allows to separate configurations according to their topological

charge, and in turn, to compare to the results of the Random Matrix Theory (RMT). This describes the distribution of the eigenvalues of the Dirac operator for a system close to the chiral limit. As shown in Figure 1, our data are in agreement with the RMT predictions for the ratios of the eigenvalues in different topological sectors. (Here nu denotes the topological charge and k stays for the k-th eigenvalue). Comparing the actual distributions we get one of the basic low energy constant, the quark condensate,
Sigma= (255(9)MeV)^3
which is in agreement with the expectations.

The other important low energy constant, the pion decay constant F, can be obtained from the correlator of two pseudoscalar densities. Figure 2 shows our results for the correlation function together with a fit to the theoretical prediction of chiral perturbation theory. The fit gives for F a value of 90 MeV, which also agrees with the experimental values.

The analysis of our data is not completed yet, and we would like to increase the statistics on this lattice size. In order to investigate the finite-size effects and the discretization errors we also intend to extend the simulations to larger lattices and smaller lattice spacings.

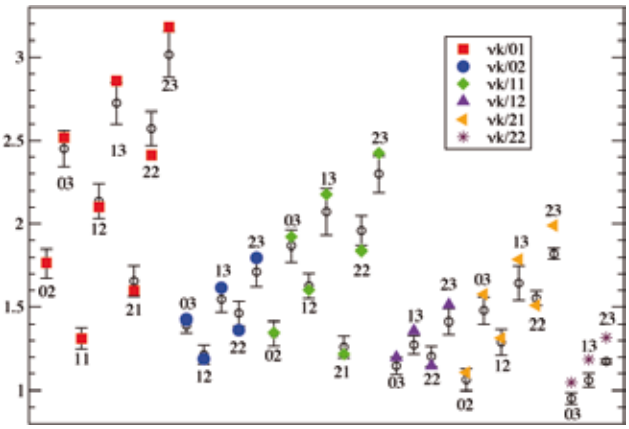

Figure 1: Ratios of expectation values of the k-th eigenvalue in the sector with topological charge nu, compared to the predictions of the Random Matrix Theory. The different symbols refer to the denominator while nu, k of the numerator is indicated at the data points. For example, the highest ratio with value ~3 in the figure refers to $<\lambda_{23}>/<\lambda_{01}>$. *The comparison with the RMT gives the quark condensate.*

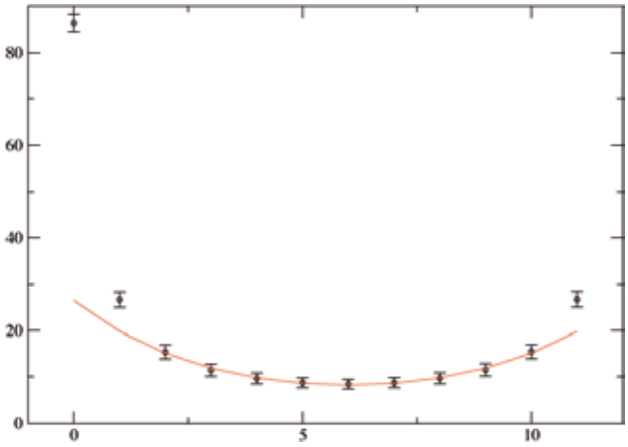

Figure.2: Data obtained for the pseudoscalar correlator function C(t) Are compared to the prediction of the low-energy effective action. The fit gives for the pion decay constant the value F ~ 90 MeV

Photophysics and photochemistry of transition metal compounds: theoretical approaches

Prof. Andreas Hauser

with L. M. Lawson Daku and A. Vargas
Département de chimie physique, Université de Genève, Switzerland

Description

Photophysical and photochemical properties of transition metal compounds are increasingly being made use of in advanced technological applications. It is thus of more than just academic interest to achieve an in-depth understanding of the fundamental photophysical and photochemical processes, such as laser-induced luminescence, intersystem crossing (ISC), internal conversion, excitation energy transfer or light-induced electron transfer, and the parameters which govern their rates and quantum efficiencies. Our research interests are focussed on establishing relationships between structural, electronic and energetic parameters, and the dynamics of elementary radiationless processes at a molecular level, using time-dependent optical spectroscopy in condensed media at temperatures between 4.2 and 300 K along with theoretical methods based on density-functional theory (DFT).

Achievements

The resources allocated to our project during 2006-2007 allowed significant progresses in the understanding of the photophysics of several transition metal complexes to be achieved. Within the framework of spin crossover in d^7 cobalt(II) imine complexes [1], DFT was applied to the characterisation of the geometric, energetic and optical properties of $[Co(bpy)_3]^{2+}$ (bpy = 2,2'-bipyridine) in the high-spin (HS) and the Jahn-Teller (JT) active low-spin (LS) states [2].This complex is an intermediate-field complex with normally a HS ground state and a low-lying excited LS state. However, when $[Co(bpy)_3]^{2+}$ is incorporated into zeolite-Y supercages or into the cavities of three-dimensional oxalate networks, the LS state becomes the ground state and the complex exhibits spin crossover [3]. The results [2] obtained with the 11 state-of-the-art GGA, meta-GGA and hybrid functionals used for the characterization of the geometry and the energetics of the isolated complex within either spin state are consistent with one another and in good agreement with experiment. This thus allowed us to gain new insight into the trigonal splitting of the HS state and into the JT effect in the LS state, which was shown to be dynamic, in agreement with experiment. Most functionals however fail to correctly predict the HS state as the ground state of the isolated $[Co(bpy)_3]^{2+}$ complex. Still, reliable results are obtained with the OLYP, HCTH, B3LYP* and O3LYP functionals. The optical properties of $[Co(bpy)_3]^{2+}$ are a relevant means for monitoring the spin state of the complex in different environment. For $[Co(bpy)_3]^{2+}$ in the two spin states, they could be successfully analyzed on the basis of LR-TDDFT electronic excitations calculations. In particular, the very good agreement of the calculated absorption and circular dichroism (CD) spectra and with the available experimental results (Figure 1) allowed a clear-cut assignment of the chirality of the complex in the sample studied by CD spectroscopy [2].

Other studies that could be successfully completed during the allocation period include the

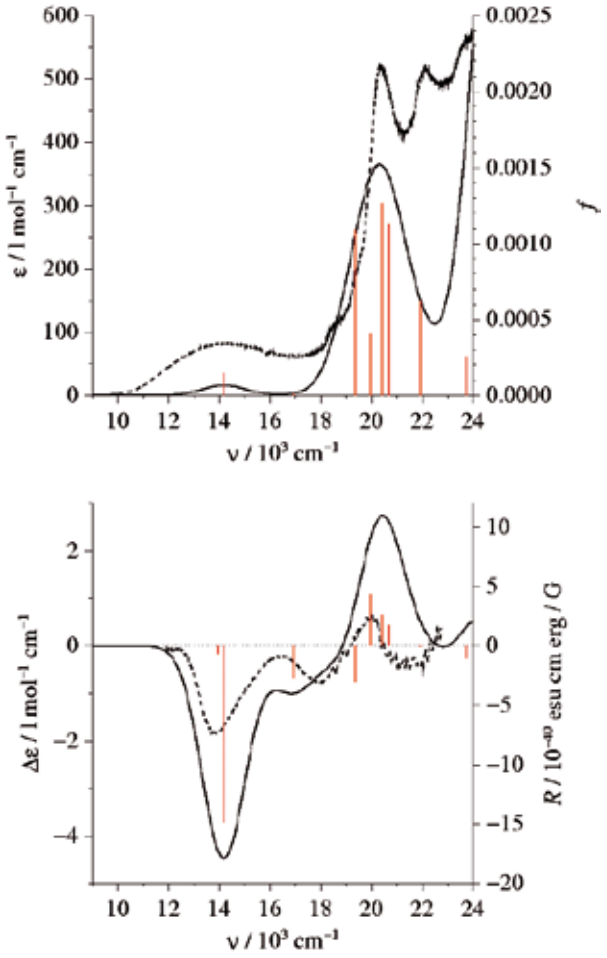

Figure 1: Calculated absorption (top) and CD (bottom) spectra of LS Λ-$[Co(bpy)_3]^{2+}$. The dashed lines are the experimental single-crystal absorption and CD spectra of $[Co(bpy)_3][LiRh(ox)_3]$, recorded at 11 and 15 K, respectively. Taken from Ref. [2]

characterization of iron(II) complexes within the framework of spin crossover and related phenomena [4,5]; the investigation of the bistability of transition metal complexes of bridled chiroporphyrins that can act as nanotweezers [6]; the ab initio static and molecular dynamics study of the 4-styrylpyridine ligand within the framework of the light-induced spin-state change phenomenon [7]; and the first-principles study of the pressure dependence of the structural and vibrational properties of the ternary metal hydride Ca_2RuH_6 [8]

The environment can have a dramatic influence on the electronic properties of transition metal complexes. Thus, those of the $[M(bpy)_3]^{2+}$ complexes, (M = Co, Fe, Ru), can be fine-tuned by doping them into inert host lattices, and the effects of the guest-host interactions at the origin of the changes induced by varying the environment can be rationalized in term of the chemical pressure exerted by the host on the guest [3]. In order to go beyond the chemical pressure image and have a detailed picture of the effective interactions, we have started the DFT study of the influence of the second coordination sphere on the properties of the zeolite-Y encapsulted $[M(bpy)_3]^{2+}$ complexes, (M = Co, Fe, Ru), using the supramolecular model shown in Figure 2.

In the recently completed study of $[Fe(bpy)_3]^{2+}$@Y

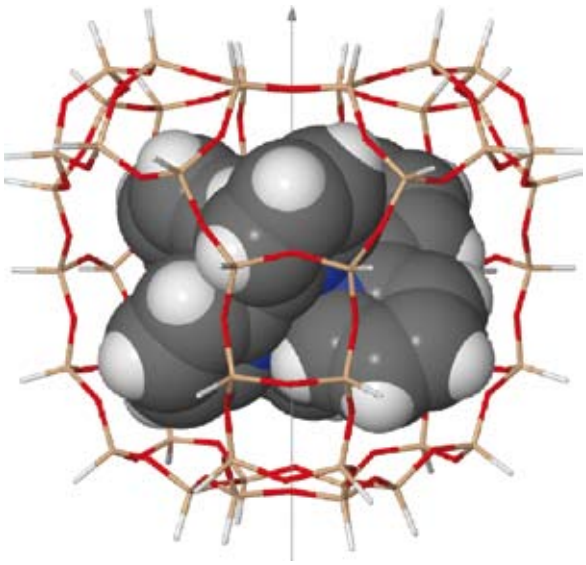

Figure 2: Supramolecular model used for investigating guest-host interactions in $[M(bpy)_3]^{2+}$@Y compounds, (M = Co, Fe, Ru).

[9], we have gained insight into the influence of encapsulation on the geometry and on the ^{57}Fe quadrupole splitting of the LS $[Fe(bpy)_3]^{2+}$ complex in the LS and the HS states. Although the functionals used perform very differently with regard to the determination of the HS-LS energy difference ΔE_{HL}, they consistently predict an increase of ΔEHL upon encapsulation of $\Delta(\Delta E_{HL})$ = 3000±1000 cm^{-1}, which corresponds to an experienced chemical pressure of P_c = 30±10 kbar, and which could be analyzed in terms of the steric and orbital contributions to the bonding interactions between the complex and the supercage. Using for the HS-LS energy difference in the isolated complex the re-

cently determined ab initio (CASPT2) best estimate of 3700 ±1000 cm^{-1} [10], we obtain for ΔE_{HL} in $[Fe(bpy)_3]^{2+}$@Y the first-ever reported estimate of ΔE_{HL} = 6700±2500 cm^{-1}, which is supported by the study of the low-temperature kinetics dynamics of the HS -> LS relaxation that follows the light-induced population of the HS state $[Fe(bpy)_3]^{2+}$@Y [9].

References

1. I. Krivokapic, M. Zerara, M. Lawson Daku, A. Vargas, C. Enachescu, C. Ambrus, P. Tregenna-Piggott, N. Amstutz, E. Krausz, A. Hauser, Coord. Chem. Rev. 2007, 251, 364.
2. A. Vargas, M. Zerara, E. Krausz, A. Hauser, L. M. Lawson Daku, J. Chem. Theory Comput. 2006, 2, 1342.
3. A. Hauser, N. Amstutz, S. Delahaye, A. Sadki, S. Schenker, R. Sieber. M. Zerara, Structure and Bonding 2004, 106, 81.
4. A. Hauser, C. Enacescu, M. Lawson Daku, A. Vargas, N. Amstutz , Coord. Chem. Rev. 2006, 250, 1642.
5. S. Bonhommeau, T. Guillon, L. M. Lawson Daku, P. Demont, J. Sanchez Costa, J.-F. Létard, G. Molnár, A. Bousseksou, Angew. Chem. Int. Ed. 2006, 45, 1625.
6. (a) G. Maheut, A. Castaings, J. Pécaut, L. M. Lawson Daku, G. Pescitelli, L. Di Bari, J.-C. Marchon, J. Am. Chem. Soc. 2006, 128, 6347; (b) L. M. Lawson Daku, A. Castaings, J.-C. Marchon, in revision.
7. L. M. Lawson Daku, J. Linares, M.-L. Boillot: (a), ChemPhysChem 2007, 8, 1402; (b) in preparation.
8. L. M. Lawson Daku, H. Hagemann, Phys. Rev. B 2007, 76, 014118.
9. A. Vargas, I. Krivokapic, A. Hauser, L. M. Lawson Daku, submitted .
10. K. Pierloot, S. Vancoillie: (a) J. Chem. Phys. 2006, 125, 124303; (b) ibid. 2008, 128, 034104.

Development and Application of ab initio Molecular Dynamics Methods

Prof. Jürg Hutter

Institute of Physical Chemistry
University of Zurich, Switzerland

General Description

The basic theme of our research is development and application of novel methods in computational chemistry. The focus is on large systems, mostly in the condensed phase and on density functional theory. The systems studied range from simple liquids to chemical reactions in complex solvents. We are leading group in the development of the software package CP2K (cp2k.berlios.de). This software is freely available to the scientific community and widely used.

Ab initio molecular dynamics simulations need large amounts of computer time. Fortunately, our computer codes are highly optimized and can make efficient use of almost all kinds of modern computer architectures from vector machines to massively parallel computers.

Atomistic models for dye-sensitized solar cells

The goal of this project is to create an atomistic picture of the processes in dye sensitized solar cells (DSSC) using classical force field models as well as density functional theory (DFT) methods. We take all components (semiconductor, dye, solvent, electrolyte) explicitly into account.

Nevertheless, before the full system is modeled explicitly, it is crucial to probe and understand the interactions between the various components of such a cell. We were able to create a force field model for the solvent-semiconductor interface and to gain insight in this system.

Further aspects studied were the effect of the surface on the distribution of solvated ions. First simulations indicated an unexpected behavior where contrary to predictions from continuum electrostatics the ion distribution is very structured and strongly influenced by the ion type.

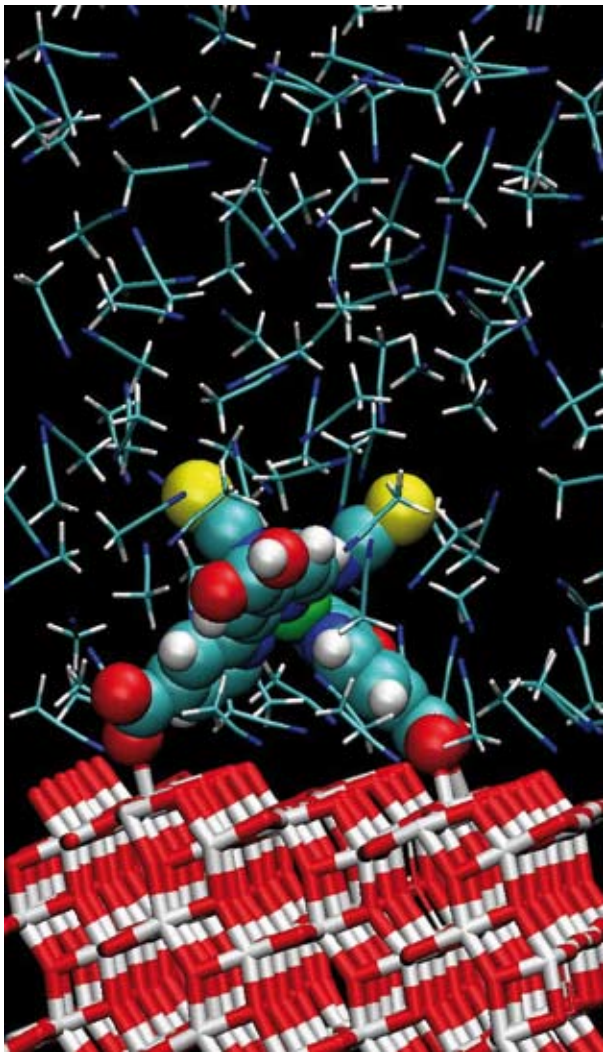

Figure 1: Snapshot of a model system for dye-sensitized solar cells.

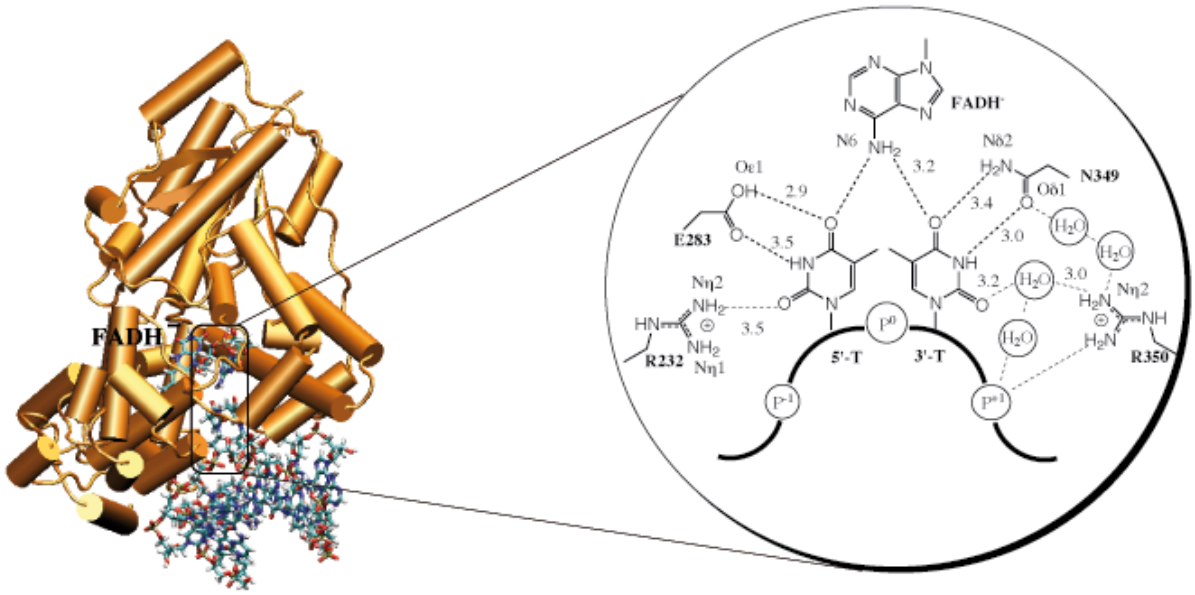

Figure 2: DNA photolyase from Anacystis nidulans bound to double starnded DNA with a CPD lesion. Characteristic interaction distances from classical potentials and the X-ray structures (in brackets) are shown in the inset.

To get a first indicator for the most favorable binding sites we focused on calculating the relative stabilities of a single dye molecule binding to the anatase(101) surface. A problem we had to overcome was the self-interaction error (SIC) in DFT, which caused the system to be metallic instead of a semiconductor.

We solved this problem by applying the DFT+U method in which the SIC is corrected by adding a Hubbard-potential to the Hamiltonian adding a penalty potential for fractional charges.

For the further characterization of the different binding modes we calculated the vibrational spectra of the different configurations. In order to calculate these spectra with a reasonable effort we implemented a mode selective vibrational analysis tool into CP2K. The different binding mode found in our calculations could open a different and more efficient path for electron transfer from the dye to the surface and in this way explain the experimental result for the deprotonated dye to cause a higher photo voltage.

DNA damage and repair

Ultraviolet (UV) light, in particular UV-B radiation (290-320 nm), endangers all forms of life by promoting the formation of genotoxic photoproducts of DNA. The most abundant damage caused to DNA is the cyclobutane pyrimidine dimer (CPD), formed between two adjacent pyrimidine nucleobases, mainly thymine, via a [2 + 2] photo cycloaddition. This lesion formation plays a crucial role in the initiation of UV-induced skin cancer. Experimental and theoretical investigations have shown evidence for a self-repair mechanism in DNA under UV light exposure. However, this autocatalytic process is not an efficient channel for cells to repair the CPD lesion.

Although many theoretical studies have attempted to elucidate the details of the repair mechanism, which are difficult to uncover by experimental means alone, none of them studied the CPD repair reaction in the presence of the specific groups of the DNA photolyase active site. Recently, the thymine dimer radical anion splitting of the photo activated self-repair process in DNA was investigated by QM/MM calculations. We showed that in

the self-repair process the mechanism of the splitting of the cyclobutane ring is asynchronously concerted: the breaking of the C5-C5' bond is spontaneous upon electron uptake and is subsequently followed by the C6-C6' bond cleavage. While C5-C5' bond breaking is barrierless, C6-C6' bond breaking is characterized by a free energy barrier of 2.5 kcal/mol.

We have investigated the dynamics of the splitting of the thymine dimer radical anion within the DNA photolyase active site, using a mixed quantum mechanical/molecular mechanics (QM/MM) method and performing Born-Oppenheimer (BO) molecular dynamics. This work provides the first modeling of the repair reaction in the presence of the protein environment. Similar to the findings for the self-repair reaction, the statistical analysis of the performed trajectories identifies the enzyme-catalyzed repair reaction as an asynchronous concerted mechanism, in which the breaking of the C5-C5,Äô bond is spontaneous upon electron uptake and is subsequently followed by barrierless C6-C6' cleavage.

Towards linear scaling ab initio molecular dynamics

Localized orbitals have a long history in quantum chemistry and solid state physics. They have been used to study chemical bonding and many electric properties and recently new computational approaches based on localized orbitals have emerged, where the complexity of the calculation increases only linearly with system size.

Early developments of localization schemes have focused on the minimization of an appropriate functional of the orbitals, such as the Boys-Foster minimal spread of the orbital centroids. We introduced a sparseness function that aims at providing a representation of the orbitals as maximally sparse as possible. One possibility to achieve this goal is to seek the solution whose orbitals have minimal l1-norm. We exploit the invariance of the total energy with respect to unitary transformation of the occupied orbitals to parameterize such a sparseness function. The l1-norm needs to be smoothened to have at least a continuous first derivative, allowing gradient based algorithms to be employed.

An important aspect is that the computational cost of the proposed algorithm scales linearly with the number of basis functions for sufficiently large systems. The proposed sparseness function provides, in conjunction with the efficient orbital based total energy minimization scheme described below, a powerful linear scaling method.

Efficient and accurate calculations of ground state properties of materials is one of the most important problems in electronic structure theory. In Hartree-Fock or Kohn-Sham density functional theory the ground state energy is calculated through an iterative minimization of the energy functional with respect to the orthogonal single-particle orbitals. In one class of methods the effective Hamiltonian is diagonalized in each iteration. The orthonormal eigenfunctions determine the occupied orbitals and the electron density, from which a new potential and Hamiltonian is constructed. This procedure is repeated until a stationary self-consistent field (SCF) solution is found.

A second class of methods proceeds by a direct minimization of the electronic energy functional. This approach requires the single-particle orbitals to be constrained by orthogonality. We implemented and tested a direct minimization method for a non-orthogonal basis set that has been inspired by the efficient orbital transformation (OT) method and the iterative refinement technique for the approximate factorization of a matrix inverse.
The orbital transformation based on the refinement expansion maps the constrained energy functional to an approximate unconstrained func-

tional, which is valid in a neighborhood of an orthogonal but approximate solution. A conjugate gradient scheme can then be used to find the ground state orbitals from the minimization of a sequence of approximate unconstrained functionals. The proposed direct total energy minimization scheme has been found to be efficient, robust and numerically stable.

References

1. F. Schiffmann, J. Hutter, J. VandeVondele; Atomistic simulations of a solid/liquid interface: a combined force field and first principles approach to the structure and dynamics of acetonitrile near an anatase surface; J. Physics-Condensed Matter 20, 064206 (2008)
2. V. Weber, J. Hutter; A smooth l(1)-norm sparseness function for orbital based linear scaling total energy minimization J. Chem. Phys. 128, 064107 (2008)
3. V. Weber, J. VandeVondele, J. Hutter, A.M.N. Niklasson; Direct energy functional minimization under orthogonality constraints J. Chem. Phys. 128, 084113 (2008)
4. F. Masson, T. Laino, I. Tavernelli, U. Rothlisberger, J. Hutter; Computational Study of Thymine Dimer Radical Anion Splitting in the Self-Repair Process of Duplex DNA, J. Am. Chem. Soc. 130, 3443-3450 (2008).
5. F. Masson, T. Laino, U. Rothlisberger, J. Hutter; A QM/MM Investigation of Thymine Dimer Radical Anion Splitting Catalyzed by DNA Photolyase, submitted for publication

Modelling CARBOn Cycle CLIMate Feedbacks (CARBOCLIM)

Dr. Fortunat Joos

with Thomas Frölicher, Marco Steinacher
Climate and Environmental Physics, Physics Institute, University of Bern, Switzerland

The Project

Motivation: The presently observed and projected future climate change poses a significant risk to the human society. Adequate response strategies to mitigate greenhouse gas emissions and to adapt to climate change require scientific information based on our best understanding of the Earth System. The project CARBOCLIM is targeted to provide such information. The recent award of the Noble Price for Peace to the Intergovernmental Panel on Climate Change highlights the socio-economic importance of climate change research.

Scientific Background: Carbon dioxide (CO2) is the most important anthropogenic greenhouse gas and its radiative forcing contributes significantly to current and future global warming. CO2 is emitted through burning of fossil fuel and due to land use and land use change activities. Presently, about half of the current carbon emissions stays airborne, whereas the rest is taken up by the ocean and the land biosphere. The atmospheric CO2 rise and climate change would proceed at much higher rates than observed if these natural sinks were not operating. It is key for climate change projections to understand how the present marine and terrestrial carbon sinks will evolve in the future and how climate change itself will affect atmospheric CO2.

Marine (and terrestrial) ecosystems will be affected in a variety of ways by global warming. Marine ecosystem changes are likely to change the biogeochemical cycling of carbon and other elements (nitrogen, iron, silica etc) within the ocean and to feed back on the evolution of atmospheric CO2 and climate. The uptake of the acid CO2 by the ocean lowers the pH of seawater and increases the aquatic concentrations of CO2, [CO2], and of bicarbonate, [HCO3-], whereas the concentration of the carbonate ion, [CO3--], is lowered. Many marine organisms produce a shell consisting of calcite or aragonite (two different forms of the mineral CaCO3). Recent projections reveal that aragonite will become undersaturated over the coming decades in the Arctic (Steinacher 2007) and the Southern Ocean (Orr et al., 2005). Then, the aragonite shells of many species (e.g. pteropods) will be prone to dissolution.

Goals: The specific goal of CARBOCLIM is to perform simulations with the fully coupled ocean-atmosphere climate-carbon cycle model over the industrial period and over this century to study carbon cycle-climate interactions. The understanding of the coupling between the carbon cycle and the physical climate system is a prerequisite for global warming projections. The main focus of CARBOCLIM is on the ocean carbon cycle. The uptake of anthropogenic carbon, the impact of carbon cycle climate feedbacks on ocean CO2 uptake, the role of ocean acidification and marine ecosystem changes and the variability of oxygen and other tracers are investigated. CARBOCLIM is addressing spatial scales ranging from regional to the global and temporal scales ranging from seasonal to centennial. An important focus of

CARBOCLIM is on contrasting seasonal to decadal variability simulated by the model and reconstructed from observations with projected decadal-to-millennial scale anthropogenic changes. Understanding the role of internal and forced system variability is crucial to attribute observed changes to individual drivers and mechanisms.

Tools: The primary research tool in the Large User Project CARBOCLIM is the Climate System Model (CSM1.4-carbon) developed by the National Centre for Atmospheric Research (NCAR), Boulder. CSM1.4-carbon is a state-of-the-art 3-dimensional coupled atmosphere-ocean climate-carbon cycle model. The NCAR CSM1.4-carbon is an important pillar of our model hierarchy that also includes different cost-efficient reduced form Earth System models. The model hierarchy allows us to investigate the Earth System from the regional to the global scale and over the past million years to the next millennia, thereby utilizing information from the past and the present for improved predictability of the future.

Partners: CARBOCLIM is a contribution by the Earth System – Biogeochemical Modelling group of the division of Climate and Environmental Physics (CEP), University of Bern, to two European projects within the Framework Programme Six: the Integrated Project CARBOOCEAN and the Network of Excellence EUR-OCEANS. Both projects have started in 2005 and last until end of 2009 and 2008, respectively. A follow-up project under the 7. Framework Programme, the European Project on Ocean Acidification, starts in May 2008. CARBOCLIM is part of a collaboration with NCAR, formalised through an NCAR affiliate scientist position of the project leader. The Swiss National Science Foundation contributes to local infrastructure and by funding a PhD student. Last, but not least, the support by the CSCS-Swiss National Supercomputing Centre is essential to carry out the massively parallel simulations and to archive the output data.

Achievements: In 2007 and the first four month of 2008, the group has contributed 21 publications on carbon cycle-climate change issues to the peer-reviewed literature. The group leader has been involved in the Assessment Report Four of the Intergovernmental Panel on Climate Change as a lead author of the Paleoclimate chapter and the Technical Summary and as member of the drafting team for the Working Group I Summary for Policy Makers. Work with CSM1.4-carbon includes inter alia the analysis of climate simulations covering the past 1300 years (Ammann et al. 2007) to investigate the contribution of solar and volcanic forcing to Northern Hemisphere temperature variability, a set of six ensemble simulations over the industrial period and the 21th century to analyse variability and trends in climate, the carbon cycle, and marine biological productivity (Steinacher 2007, Frölicher et al. 2008, Schneider et al. 2008).

What is next? An analysis of CSM1.4-carbon simulations covering the next five hundred years to document the long-term impact of the human perturbation is underway. The European Integrated Project on Ocean Acidification is ready to start and simulation protocols addressing the specific needs and requirement to study human-induced ocean acidification (Orr et al. 2005) and its climatic, biogeochemical and ecosystem consequences will be developed by the project partners in the coming months. New simulations will be started to address the impacts of a potential future freshwater release from Greenland ice sheet melting for climate, ocean circulation, the global carbon cycle and atmospheric CO2. The CSM1.4-carbon will be updated with the new coupled climate-carbon cycle model that is currently under testing at NCAR.

Selected Highlights

Continued human-induced greenhouse gas emissions cause atmospheric greenhouse gas concentrations to rise, global warming to accelerate, and oceanic oxygen concentration to decrease over this century.

Global warming projections suggest a considerable decrease in mean ocean oxygen inventory over the century. However, our results demonstrate that the large decadal variations in oceanic oxygen make the detection of human-induced oxygen changes and their attribution to anthropogenic forcing not yet possible.

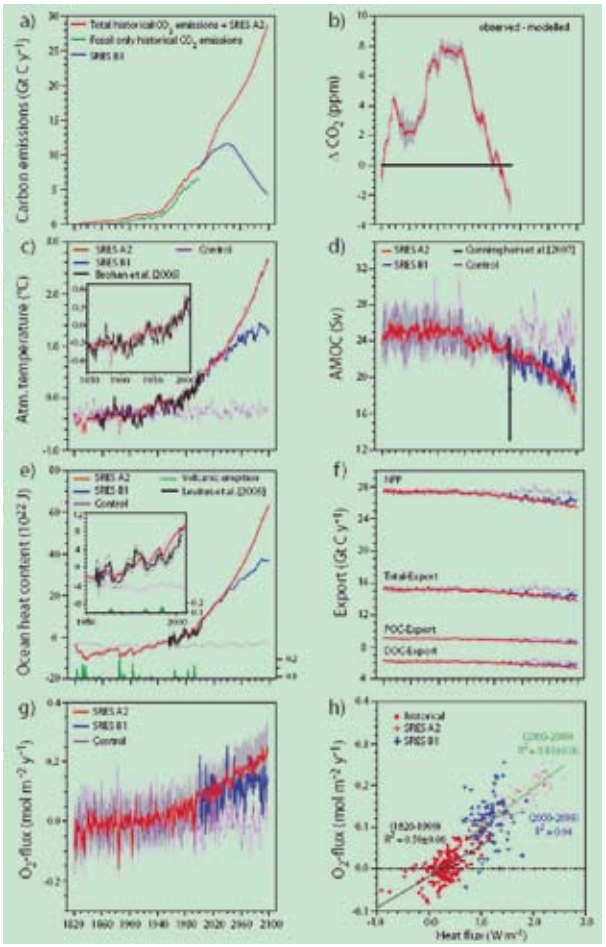

Figure 1: Results from simulations over the period 1820 to 2100 with the NCAR CSM1.4-carbon for two selected emission scenarios. a) prescribed carbon emissions; b) the difference between modelled and observed atmospheric CO2 for the historical period is small; c) simulated global mean surface air temperature is rising and the observation-based record (black) is reproduced; d) the Atlantic Meridional Overturning Circulation is projected to decrease; d) Ocean heat content is projected to rise; e) global marine biological export production slightly decreases; f) the ocean is loosing oxygen to the atmosphere; g) the sea-to-air oxygen flux is linked to ocean heat uptake (Frölicher et al. 2008).

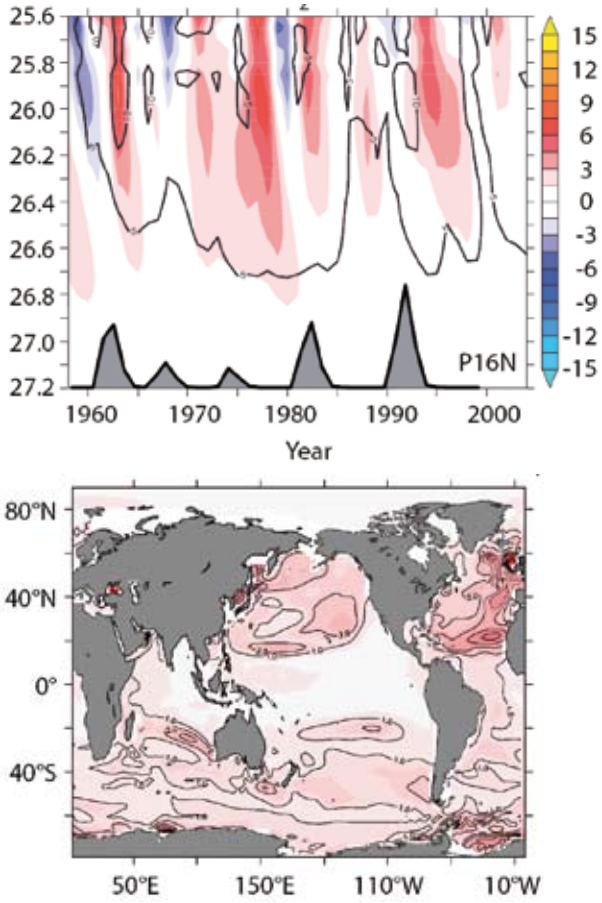

Figure 2: top) Volcanic eruptions and resulting forcing (gray) force variability in dissolved oxygen in the North Pacific. Colours indicate oxygen changes in µmol/kg. Contour lines denote one standard deviation among the six ensemble members. bottom) Decadal variability in Apparent Oxygen Utilization, displayed as one standard deviation of the ensemble simulation. Contours are every 0.5 µmol/kg and data are ploted on a constant density surface (1026.6 kg m-3) (Frölicher et al. 2008).

References

1. Ammann, C. M., F. Joos, D. S. Schimel, B. L. Otto-Bliesner, and R. A. Tomas. 2007. Solar influence on climate during the past millennium: results from transient simulations with the NCAR Climate System Model. Proc Natl Acad Sci USA 104:3713-3718.
2. Frölicher, T. L., F. Joos, G. K. Plattner, M. Steinacher, and S. C. Doney. 2008. Variability and trends in oceanic oxygen: Detection and attribution using a coupled carbon cycle-climate model ensemble. Climate Dynamics
3. Orr, J. C., V. J. Fabry, O. Aumont, L. Bopp, S. C. Doney, R. A. Feely, A. Gnanadesikan, N. Gruber, A. Ishida, F. Joos, R. M. Key, K. Lindsay, E. Maier-Reimer, R. Matear, P. Monfray, A. Mouchet, R. G. Najjar, G. K. Plattner, K. B. Rodgers, C. L. Sabine, J. L. Sarmiento, R. Schlitzer, R. D. Slater, I. J. Totterdell, M. F. Weirig, Y. Yamanaka, and A. Yool. 2005. Anthropogenic ocean acidification over the twenty-first century and its impact on calcifying organisms. Nature 437:681-686.
4. Schneider, B., L. Bopp, M. Gehlen, J. Segschneider, T. L. Frölicher, P. Cadule, P. Friedlingstein, S. Doney, M. J. Behrenfels, and F. Joos. 2008. Climate-induced interannual variability of marine primary and export production in three global coupled climate carbon cycle models. Biogeosciences 5:597-614.
5. Steinacher, M. 2007. Ocean acidification and changes in marine productivity in simulations with the fully coupled 3-D climate model CSM1.4-carbon. diploma. University of Bern, Bern.

Numerical Simulation of Transitional, Turbulent and Multiphase Flows

Prof. Leonhard Kleiser

Institute of Fluid Dynamics, ETH Zurich, Switzerland

The group of Prof. Kleiser is concerned with computational fluid dynamics (CFD). A major part of the computational studies involve Direct Numerical Simulations (DNS) and Large-Eddy Simulations (LES) of turbulent and transitional flows.

The DNS approach to turbulent flow computation resolves all relevant space and time scales and permits high-fidelity flow simulations without using any turbulence model assumptions. However, the application of DNS is presently restricted to prototype flows at low and moderate Reynolds numbers due to the wide range of scales present in turbulent flows and the corresponding immense numerical resolution requirements. In the LES approach, only the large scales are resolved, while the effect of the small ones is accounted for by a subgrid turbulence model. Computationally, LES is typically much less expensive than DNS (e.g. needing only order 1% of the computing time), enabling also the simulation of turbulent flows at higher Reynolds numbers.

1. Large-Eddy Simulation of compressible wall-bounded and massively separated flows

To be able to predict complex unsteady flow fields

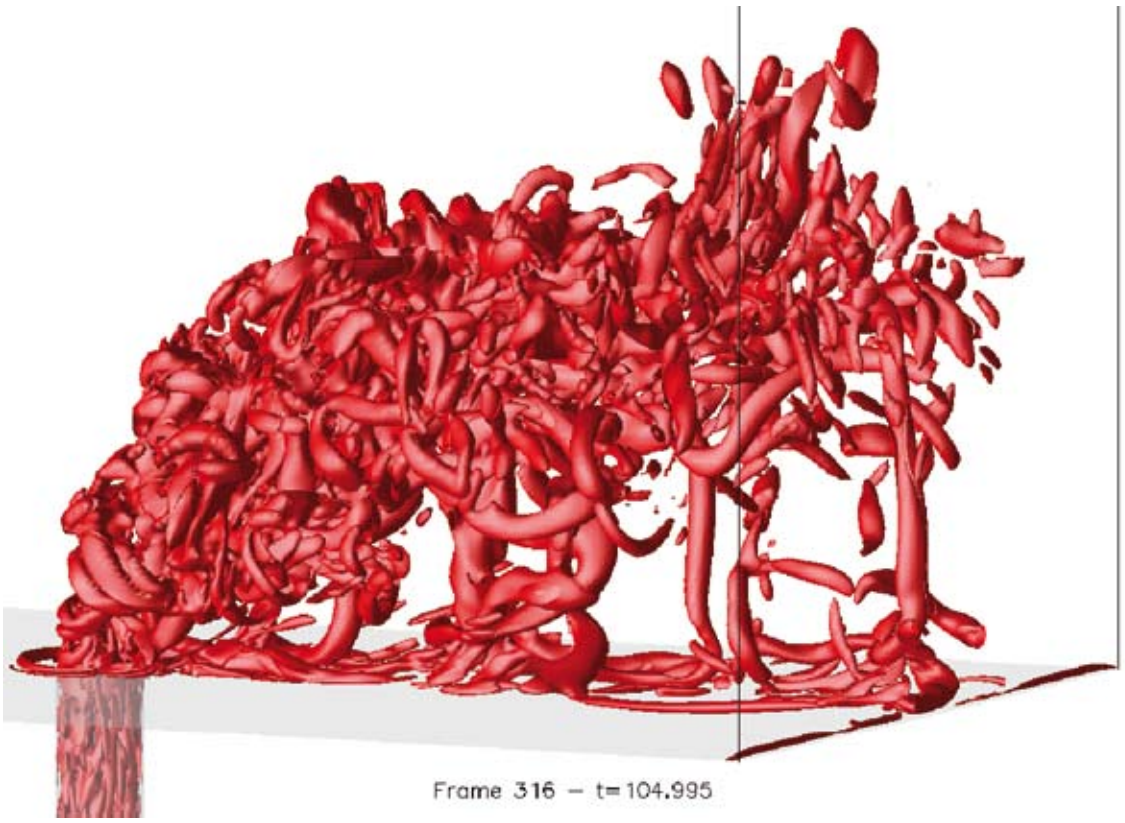

Figure 1: Vortex structures of a jet-in-crossflow configuration

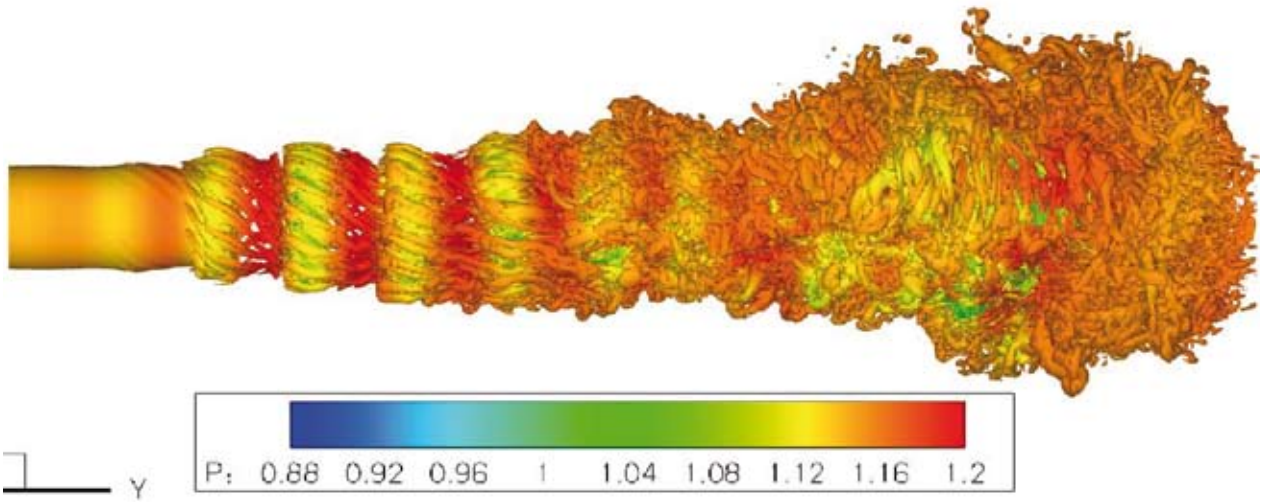

Figure 2: Vortex structures of a swirling jet flow (color indicates the pressure)

in an efficient manner, we implemented the subgrid-scale model ADM (Approximate Deconvolution Model) in an industrial-type finite volume code (NSMB), including an extension to flexible multiblock geometries. After the successful validation using the canonical periodic-hill channel configuration, we shifted focus to a flow case of more industrial relevance. Our current research focuses on a turbulent jet issuing into an oncoming boundary layer. This so-called ”jet in crossflow” (JICF) configuration is a problem occurring in a wide variety of applications such as film cooling of turbomachinery blades, fuel injection in combustors, plumes of smoke stacks or vertical/short take-off and landing (V/STOL) aircraft. To assess the validity of our simulation approach, a generic JICF configuration consisting of a turbulent round jet issuing perpendicularly into a laminar boundary layer was investigated at two different jet-to-crossflow velocity ratios. The obtained mean-flow results agree well with experimental and numerical reference data. Sophisticated visualisations of the mean and instantaneous flow fields reveal the relevant flow structure and dynamics, especially the complex vortex systems in the near-field of the mixing region.

2. Large-Eddy Simulation of swirling jet flows

In this project the capability of advanced LES methods for prediction of swirling flows is investigated and a better understanding of the complex flow physics of swirling jet flow is sought. Compressible circular swirling jets exhibit instability and transition features that differ fundamentally from their swirl-free counterparts. A detailed analysis was performed to examine the effects of different parameters such as Reynolds number, Mach number, swirl and/or co-flow intensity. It was shown that the addition of a modest amount of swirl significantly enhances the maximum growth rate in circular mixing layers. To simulate such swirling jet flows we used a compressible Navier-Stokes solver with the ADM subgrid-scale model. In these simulations, the inflow is defined by a laminar compressible boundary layer solution superimposed with instability modes from linear stability theory.

3. Computational aeroacoustics

Our work in the field of computational aeroacoustic (CAA) focuses on the prediction of aeroacoustic noise from jet flows using LES. As a subgrid-scale model we employ the Approximate Deconvolution Model (ADM). In previous work, a comparative study of DNS and LES with ADM of a compressible transitional rectangular jet at a subsonic Mach number was performed and very good predictive capabilities of the LES were demonstrated. Presently, we investigate a round jet flow

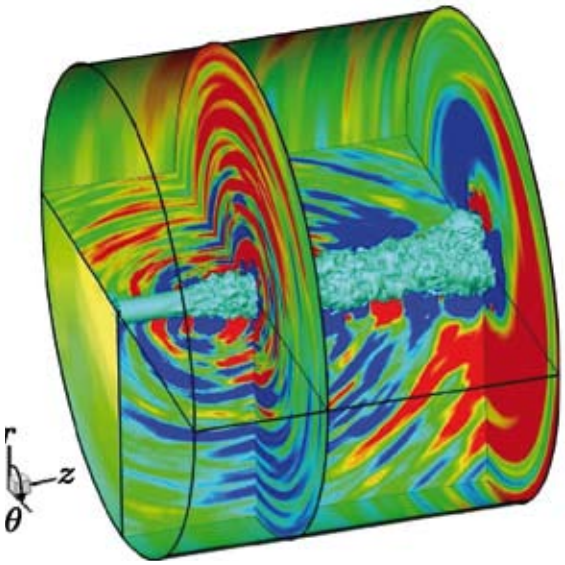

Figure 3: Visualization of a transitional jet flow with acoustic waves (the blue isosurface near the center indicates axial velocity of 25% of the maximum jet velocity)

and its associated noise for a moderate Reynolds number and a high subsonic Mach number. To this end, a DNS/LES code developed for cylindrical geometries is applied for simulations of circular jet flows with direct computation of noise radiation into the near field.

4. Turbulent spot propagation in compressible boundary layers

Research on turbulent spots in supersonic boundary layers has gained a lot of interest in recent years. We investigate turbulent spots for high Mach number boundary-layer flows with the focus on spot growth rates, skin friction and heat transfer. Different spot-triggering mechanisms are compared with respect to similarity of the developing turbulent region.

The simulations are carried out with a high-order finite-difference code using ADM for the non-resolved scales. A set of data quantifying turbulent spot growth has been compiled. This data is useful also for the modelling of transition in RANS flow solvers handling complex flow cases.

5. Simulation of particle-laden flows

This sub-project is concerned with the direct numerical simulation of disperse two–phase flows, in which a large number of small particles are suspended in a carrier fluid. We consider dilute sus-

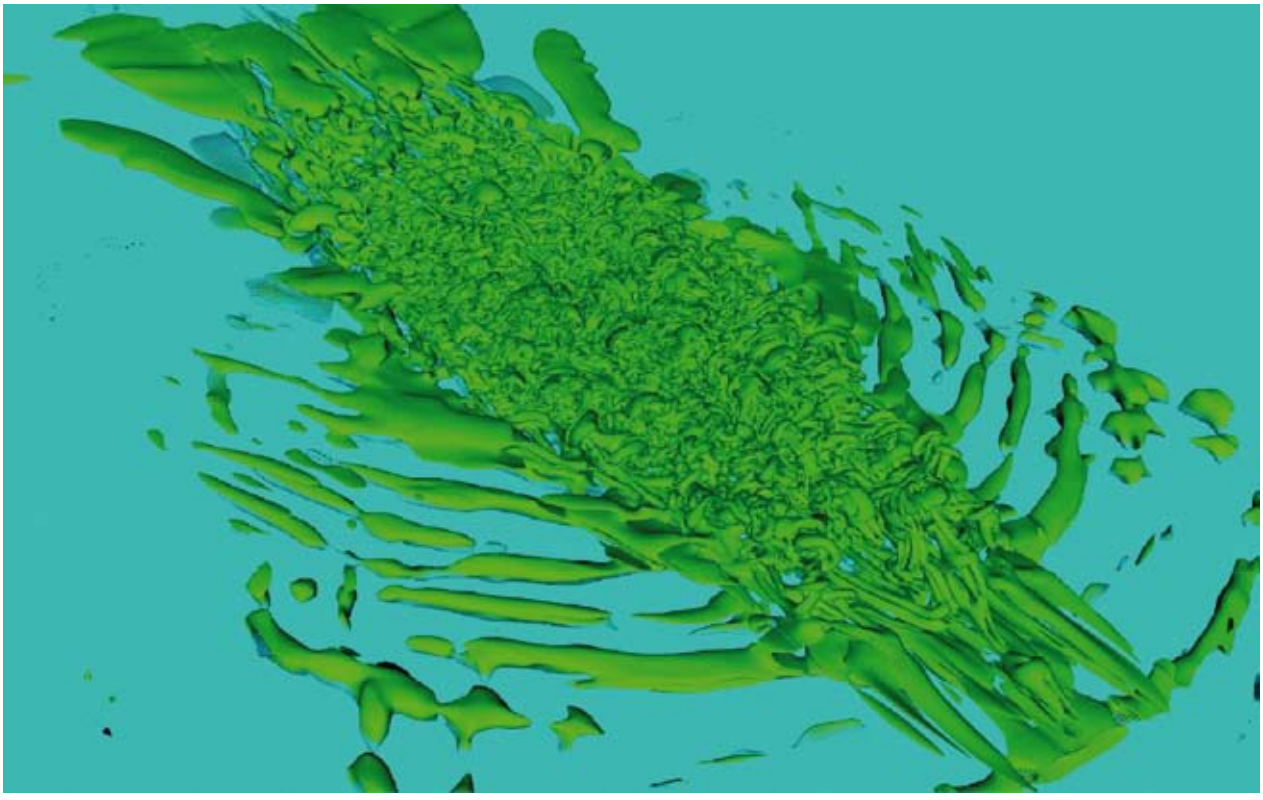

Figure 4: Turbulent spot in a transonic boundary layer (vortex structures colored by velocity magnitude)

pensions, i.e. flows with small particle concentrations where the particle–fluid interaction is the predominant process while direct particle–particle interactions are neglected (two–way coupling). Turbulent, wall-bounded particle-laden attached and separated flows were investigated using the setup of a plane channel and a backward-facing step. To account for the wall–particle interaction, models of this process were extended and refined. Two-way coupling for the particulate flow was implemented allowing for studies of turbulence modification. It has been confirmed for the plane channel flow that particle feedback causes the turbulence intensities to become more non-isotropic as the particle loading is increased. The particles tend to increase the characteristic length scales of the fluctuations in the streamwise velocity, which reduces the transfer of energy between the streamwise and the transverse velocity components. The particle concentration exhibits a maximum close to the wall and a slight increase in the middle of the channel.

6. Development of a massively-parallel high-order solver for incompressible flows

We developed a new simulation code for the incompressible Navier-Stokes equations which is based on a high-order finite-difference discretization in space and a semi-implicit integration scheme in time. The elliptical problem is solved in an iterative manner, employing a Krylov subspace method (BiCGstab) combined with multigrid preconditioning.

This scheme is well suited for the use on distributed-memory machines and leads to a good scalability up to several billions of grid points and even more unknowns. To this end the computational domain is decomposed into small blocks which have to communicate only with their nearest neighbours. The code has been tested on up to 2048 processor cores of the Cray XT3 (corresponding to approximately 12 billion unknowns). It will be used for direct and large-eddy simulations of multiphase flows like particle-driven gravity currents or estuary mouth environments.

Simulating Quantum States of Matter

Dr. Andreas Läuchli

with Julien Sudan and Andreas Lüscher,
IRRMA, EPF Lausanne, Switzerland
Christian May and Matthias Troyer,
Theoretische Physik, ETH Zürich, Switzerland

In our project we perform numerical simulations of strongly correlated quantum lattice models. We are currently interested in quantum spin systems with competing (i.e. frustrated) interactions, more specifically we address the question of what kind of orders possibly emerge out of the vastly degenerate classical ground state manifold upon the inclusion of large quantum fluctuations.

Furthermore we study ultracold atomic gases in optical lattices under non-equilibrium conditions, which offer a unique lab for the exploration of novel aspects of quantum many body systems. Finally we also worked on an accurate description of quantum dot structures based on density functional theory.

The method employed is mostly exact diagonalization, where huge eigenvalue and matrix exponential problems are solved based on matrix free Krylov algorithms (typical matrix dimensions are 10^9). These codes have been developed in our research group and scale very well on the SMP machines at CSCS. In addition we also use quantum monte carlo methods as well as density functional codes (c.f. subproject C).

A) Spin nematic order in low-dimensional quantum spin systems

Using mean-field theory, exact diagonalizations and SU(3) flavour theory, we have precisely mapped out the phase diagram of the S=1 bilinear-biquadratic Heisenberg model on the triangular lattice in a magnetic field, with emphasis on the quadrupolar phases and their excitations [1]. In particular, we showed that ferroquadrupolar order can coexist with short-range helical magnetic order, and that the antiferroquadrupolar phase is characterized by a remarkable 2/3 magnetization plateau, in which one site per triangle retains quadrupolar order while the other two are polarized along the field. Our results on quadrupolar spin order provide a natural explanation for the unconventional magnetism of the recently discussed S=1 compound $NiGa_2S_4$ [2].

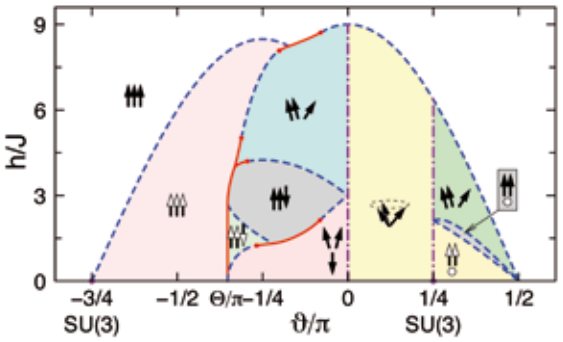

Figure 1 : Phase diagram of the bilinear-biquadratic spin one model on the triangular lattice as a function of the interaction ratio and an external magnetic field. The phases with empty arrows denote phases of spin quadrupolar nature.

B) Non-equilibrium dynamics of strongly correlated quantum systems

We investigated the time evolution of correlations in strongly interacting bosonic atoms following a quench from the superfluid to the Mott insulator [3]. For large values of the final interaction

strength the system approaches a distinctly non-equilibrium steady state that bares strong memory of the initial conditions. In contrast, when the final interaction strength is comparable to the initial interactions, the correlations are rather close to those at thermal equilibrium. The existence of two distinct non-equilibrium regimes is quite surprising. We relate this phenomenon to the role of quasi-particle interactions in the Mott insulator.

Next we investigated the spreading of information after the sudden parameter change [4]. In particular, we studied the time-evolution of correlations and entanglement following a quench. The investigated quantities show a light-cone like evolution, i.e. the spreading with a finite velocity. We discuss the relation of this velocity to other characteristic velocities of the system, like the sound velocity. The entanglement is investigated using two different measures. The von-Neuman entropy and mutual information. Whereas the von-Neumann entropy grows rapidly with time, the mutual information between two small sub-systems can as well decrease after an initial rise.

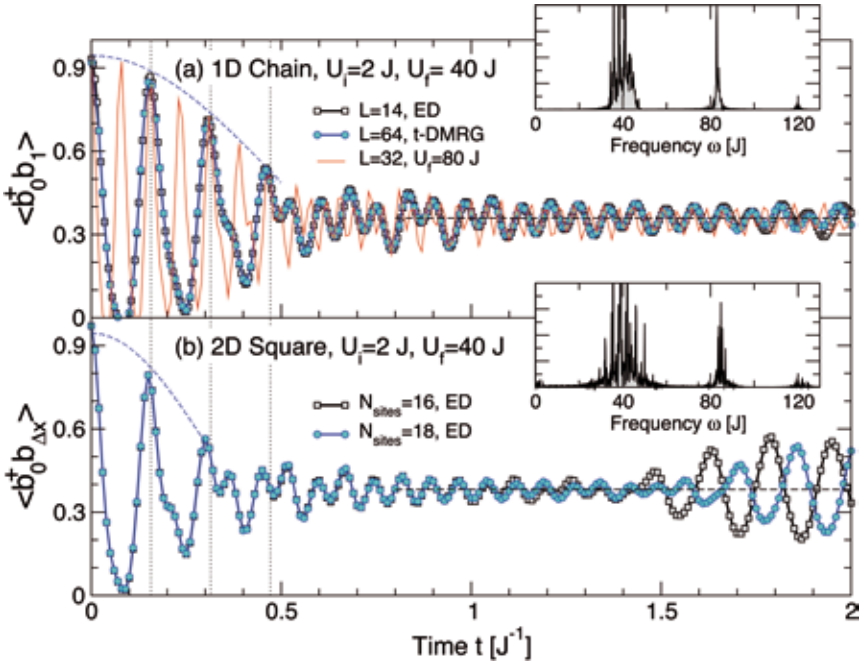

Figure 2: Relaxation of the nearest-neighbor coherence <b⁺b> in a one- and two-dimensional optical lattice after a sudden quench of the interactions from the superfluid regime to the Mott insulating region.

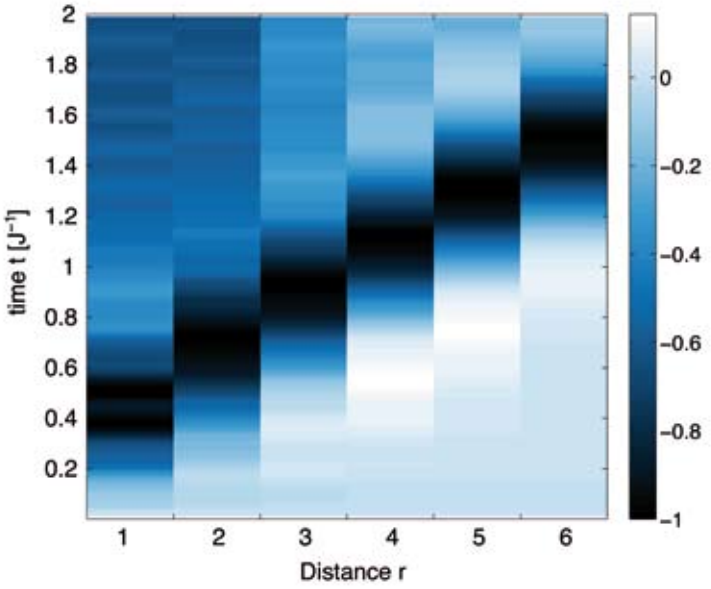

Figue 3: Space-time plot of the density-density correlations after the quench. The signal propagates on a light-cone, illustrating nicely how non-relativistic quantum mechanics satisfies causality.

C) Self-consistent DFT simulations of Quantum Dot Structures

The goal of the project is to calculate self-consistently the potential landscape in III/V semiconductor heterostructures which are nanostructured by atomic force microscope lithography. Using Density Functional Theory, our simulations determine the electronic wave functions in arbitrary devices manufactured using the aforementioned technique. Evaluation of our results and comparison with experiments allows us to determine the sensitive parameters of the system.

From a computational point of view, this requires the solution of both large eigenvalue problems and linear equation systems. For these tasks, efficient algorithms are known which scale well to a large number of processors.

Once having acquired the capability to solve the Schroedinger and Poisson equations self-consistently in three dimensions, we will be in a position to investigate the energy spectrum of an arbitrary semiconductor quantum dot using realistic potential landscapes. On the one hand, this will enable us to ameliorate our understanding of quantum dot physics; on the other hand, it will allow us to develop design tools for enhanced tunnel-coupled quantum devices [5] [6].

References

1. A. Läuchli, F. Mila and K. Penc, Phys. Rev. Lett. 97, 087205 (2006).
2. S. Nakatsuji et al., Science 309, 1697 (2005).
3. C. Kollath, A. Läuchli, and E. Altman, Phys. Rev. Lett. 98, 180601 (2007).
4. A. Läuchli and C. Kollath, J. Stat. Mech. (2008) P01010
5. C.P. May, M. Troyer, and K. Ensslin, Phys. Rev. B 76, 235321 (2007).
6. C. May, K. Ensslin and M. Troyer, Journal of Computer-Aided Materials Design 14(1), 91 (2007).

Wind field simulations and snow drift modelling over steep terrain

Dr. Michael Lehning

Swiss Federal Institute for Forest, Snow and Landscape Research WSL, Davos, Switzerland

Abstract

Snowdrift in alpine terrain is an important factor in avalanche formation and the local water balance. In order to model drifting and blowing snow, accurate microscale windfields are required. The objective of this work is to compute accurate microscale windfields for the modelling of snowdrift and for increasing our understanding on surface energy and mass exchange in mountainous complex terrain. Windfields are computed with the Advance Regional Prediction System (ARPS). ARPS is a meteorological model using the Large Eddy Simulations (LES) method. For the first time, one-way nested LES simulations could be made, which produced mean flow patterns and resolved turbulence patterns comparable to the measured wind and turbulence statistics during a field campaign. To achieve this goal, artificial turbulence was generated by offline ARPS runs with periodic boundary conditions (BCs) and these fields were superimposed on the lateral BCs for the nested run. The method could be adopted as a general method to achieve small scale nested LES simulations with realistically resolved turbulence.

Objectives

The objective of this work has been to compute very high resolution wind fields over complex mountainous terrain with a resolution as fine as 25m, in order to model the transport and redistribution of snow under the influence of wind.

Very high resolution wind fields are required, since the processes driving wind transport of snow take place at spatial scales of a few meters and are located close to the surface. In order to reach the fine resolution of 25m, a grid nesting technique is required.

The high resolution wind fields will have further use to increase our understanding of hydrologic and ecologic processes in high Alpine catchments.

Methods

The ridge of interest is located in the region of Davos, Grisons, Switzerland. This ridge is about 1200 m long, 150 m above the surrounding topography and the width of the ridge is approximately 300 m. Gaudergrat is oriented roughly North to South and the prevailing winds are blowing from West to North-West during cold front events (when snowdrift is happening) which makes it almost ideal for airflow over mountainous terrain studies. At SLF, airflow simulations over the Gaudergrat have already been carried out (Raderschall et al., 2008) using the meteorological model ARPS, developed by the Centre for Analysis and Prediction of Storms (CAPS) of the University of Oklahoma. It can be used in a Large Eddy Simulations (LES) configuration to solve the three-dimensional compressible non-hydrostatic filtered Navier-Stokes equations. ARPS is run in its parallel version, using the MPI communication libraries.

ARPS was initialised using a single sounding, i.e. a homogeneous atmosphere, with periodic bound-

ary conditions. The mean characteristics of the flow over the ridge were well reproduced but showed a high sensitivity of the flow to initial and boundary conditions and the flow became quickly instable. In order to improve the initialisation and boundary conditions specification, ARPS is now run in a one-way nesting configuration using the MeteoSwiss Alpine Model aLMo outputs.
In the current study, this method has been successfully used to reproduce wind fields over the Gaudergrat during one day of the measurement campaign: GAUDEX 2003 (GAUDergrat EXperiment: Lewis et al., 2008).

In order to predict the snow erosion and deposition patterns, 3 models are coupled. aLMo outputs, with a resolution of 7km, are interpolated on the coarsest and largest ARPS grid. This first step provides initial and time-dependent boundary conditions for the ARPS grid with resolution 1.6km. aLMo analyses are updated on a one-hour interval basis. ARPS is then run on 4 additional nested domains, whose horizontal resolutions are 1.6 km, 400m, 100m and 25m respectively (Figure1). The topography of the ridge starts to be well resolved with a resolution equal or finer than 100m. The update interval for lateral boundaries conditions is kept at 1 hour. Finally the micro scale (25m resolution) wind fields produced by ARPS will be used to drive the high resolution snow surface processes model Alpine3D, an Alpine surface process model developed at SLF for the modeling processes at the snow surface in complex alpine terrain (Lehning et al., 2008).

The accuracy of ARPS wind fields is validated and checked by comparisons with measurements obtained from an extensive field campaign : the GAUDergrat EXperiment 2003 (Lewis et al., 2008). Two days with relatively strong winds and similar

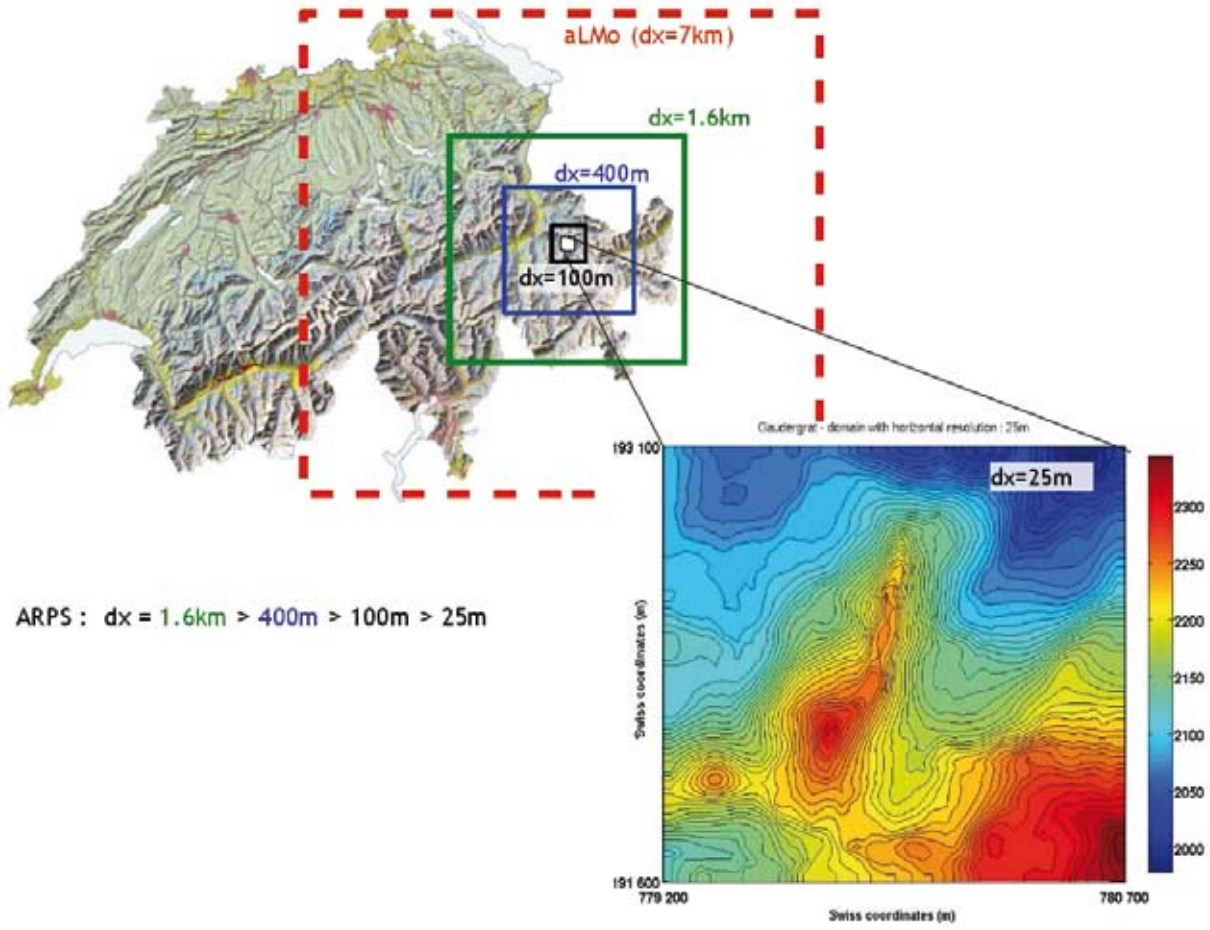

Figure 1: Overview of the nested domains, starting with a resolution of 7km down to 25m.

to winter conditions have been computed for comparisons.

Results

The mean wind features observed during Gaudex (Lewis et al., 2008) are also represented in the model results. The cross-ridge flow appears independently of the inflow wind direction (Figure 2), where the inflow wind direction is respectively South-West. At lower altitudes, flow parallel to the ridge predominate on both sides of the ridge. The

The downscaling system producing high resolution windfields an Alpine ridge based on the operational aLMo numerical weather forecast shows good agreement with measurements for mean flow quantities. However the one-way nesting technique constrains the development of initial perturbations in limited area models and the interpolation of the external boundary conditions lack fine scale turbulence. The implementation of boundary condition perturbations allows the model to resolve the flow explicitly up to smaller scales of

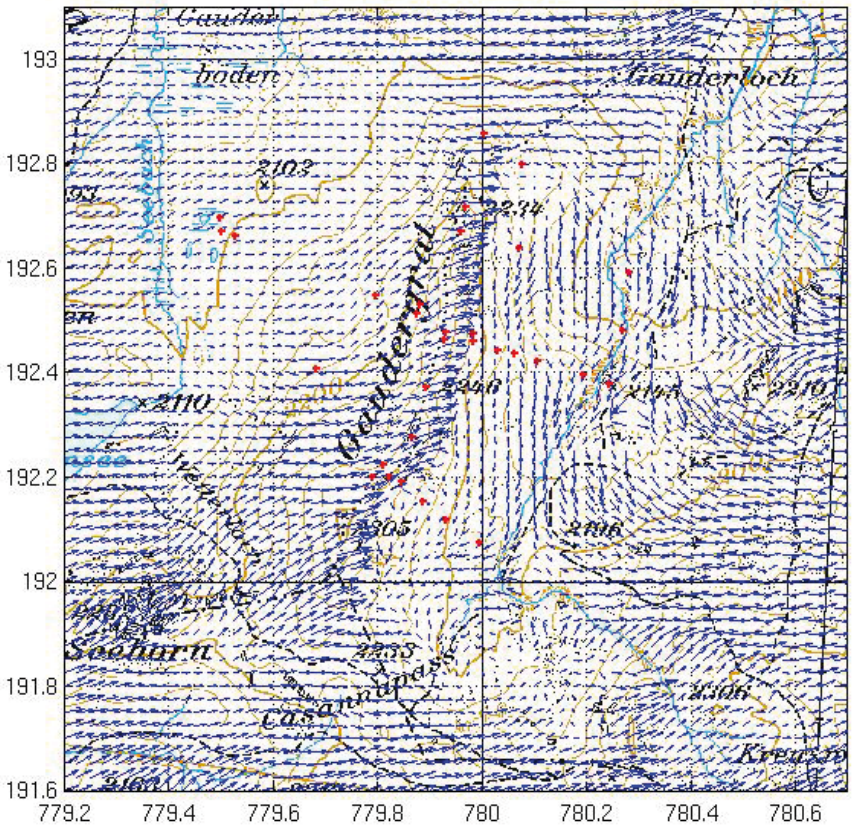

Figure 2: Windfiled from the finest grid results (dx=25m) at the first level above the surface, on August 18, 2003. (absisse and ordinate are swiss coordinates in km)

flow separation from the ridge crest on the lee slope is well represented, as well as the reattachment further near the foot of the lee slope.
The mean flow features are also quantitatively in good agreement for day of relatively strong wind, like on the 18th of August 2003 (Figure 3).
However some features are difficult to capture, such as the change in katabatic flows, as for example in figure 3, between 16:00 and 18:00.

motion. These new boundary conditions do not modify the mean flow and the TKE distribution correspond to the observations. In agreement with the observations, the normalized TKE vertical profiles from ARPS (see Figure 4) show that there is more TKE in the windward side and at the crest than in the lee slope where the recirculation occurs. The work described here is summarized in Faure et al. (submitted).

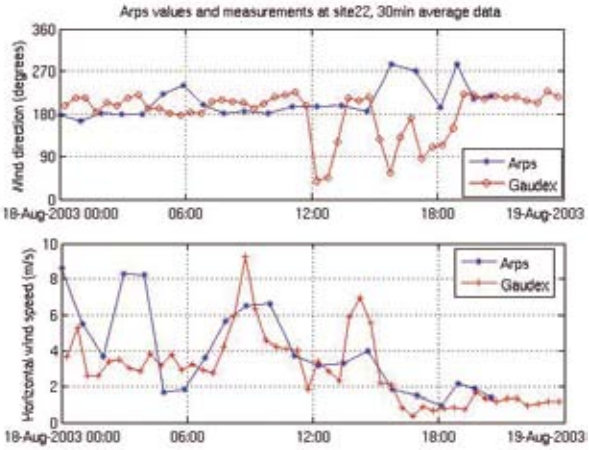

Figure 3: Time series of wind directions (above) and speeds (bellow) at measurment site 22 on Aug. 18, 2003

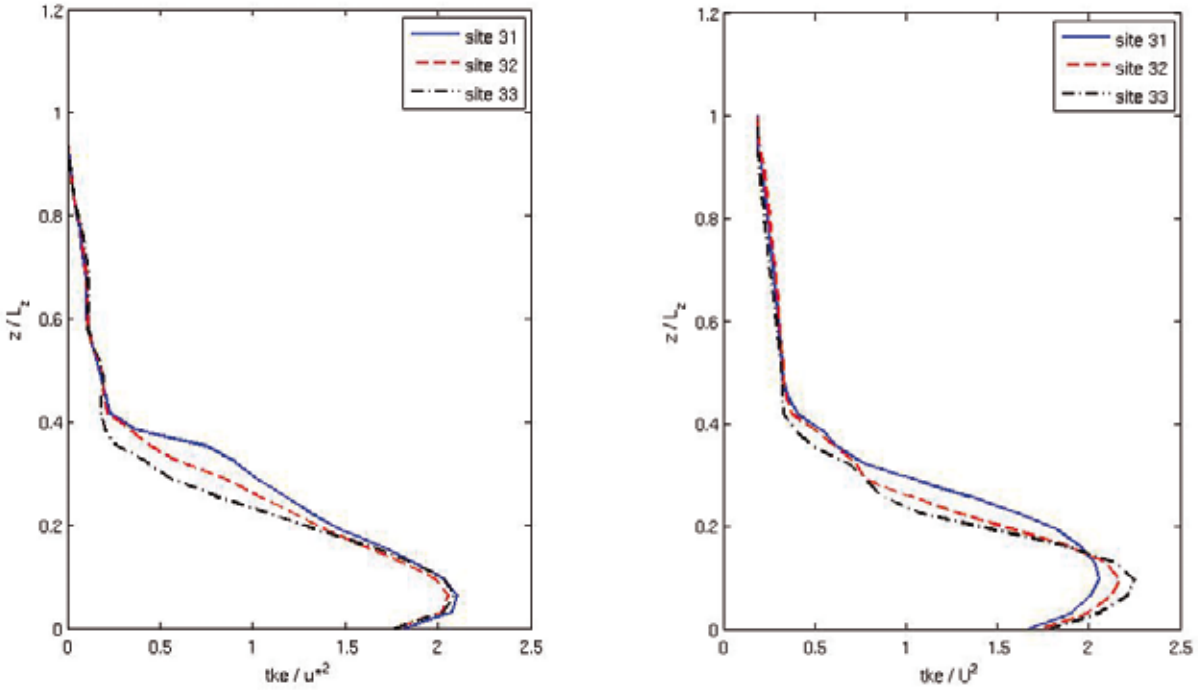

Figure 4: Normalised TKE profiles on the windward side (site 33), at crest (site 32), in the leeward side (site 31), using the one-way nested boundary forcing (left) and the modified boundary conditions (rigth)

References

1. Faure, F., Lehning, M., Lewis, H., Mobbs, S., Bou-Zeid, E., Parlange, M., in preparation. Nested large-eddy simulations of airflow over a steep ridge, Atmos. Env., submitted.
2. Lehning, M., Löwe, H., Ryser, M., Raderschall, N., 2008. Inhomogeneous precipitation distribution and snow transport in steep terrain, Water Resources Res.,/44, W07404 doi:10.1029/2007WR006545.
3. Lewis, H.W., Mobbs, S.D., Lehning M., 2008. Observations of cross-ridge flows across steep terrain, Q.J.R.Meteorol.Soc., 134, 801-816, doi: 10.1002/qj.259.
4. Raderschall, N., Lehning, M., Schär, C., 2008. Fine scale modelling of the boundary layer wind field over steep topography, Wat. Res. Res., in press.

Computational investigation of complex hydrides for hydrogen storage

Dr. Zbigniew Łodziana

Swiss Federal Laboratories for Materials Testing and Research (EMPA), Duebendorf, Switzerland

Overview

At present societal wealth are based mainly on fossil fuels. Their limited resources induced growing interest in the research toward economy based clean and highly abundant energy carriers, like hydrogen. Hydrogen storage in safe and compact ways is one of the most demanding obstacles for widespread introduction of this fuel. The target goals for the hydrogen storage were defined in the so called „freedom car" vision, where hydrogen storage capacity of weight 10.8% is expected in 2015. Solid-state hydrogen storage in so-called complex hydrides is considered as the most promising solution of hydrogen storage problem.

The main objective of this project is to develop theoretical insight that can support practical search for novel efficient hydrogen storage media. Complex hydrides are iono-covalent compounds where hydrogen is covalently bounded to atoms like aluminum or boron. These complexes form ionic crystals balanced by counter cation of metal. An experimental study of these compounds is difficult due to low scattering crossection of light elements, and difficulties in synthesis process.

Quantum mechanical methods serve as important complementary research tools to study complex hydrides on the atomic level [1]. In the present project we use density functional theory and statistical mechanics methods to study stability of novel compounds and the role of catalyst in decomposition and synthesis of known complex hydrides.

Achievements.

Stability and structure of new light complex hydrides is the first step to characterization of promising materials for hydrogen storage, like $Ca(BH_4)_2$ or $Mg(BH_4)_2$. These compounds were successfully synthesized (by wet chemical methods) in last two years. Experimental characterization of $Mg(BH_4)_2$ revealed unusually complex crystal structure (more than 300 atoms per primitive unit cell)[2]. A large ambiguity of the structural properties were reported for $Ca(BH_4)_2$. Calculations of the formation energy of possible candidate structures of $Ca(BH_4)_2$ and calculations of vibrational entropy combined with neutron and X-ray diffraction studies allowed us unequivocal description of low and high temperature phases of this compound [3]. This study enabled us to show that $Ca(BH_4)_2$ exist in pure form thus further studies of this compound as material for hydrogen storage is justified. Schematic view of the $Ca(BH_4)_2$ structure is shown in Fig.1, as an example of complex hydride. For the complex structure of $Mg(BH_4)_2$ we have proposed new combinatorial method of searching for the stable low energy phases [4]. Several new structures were proposed, including structures that are simpler than those found experimentally.

Catalytic decomposition and synthesis of complex hydrides like $NaAlH_4$ or $LiBH_4$ is not understood on the microscopic level, even for sodium alanate, the compound that is extensively studied over last ten years. We have shown that Ti atoms might be

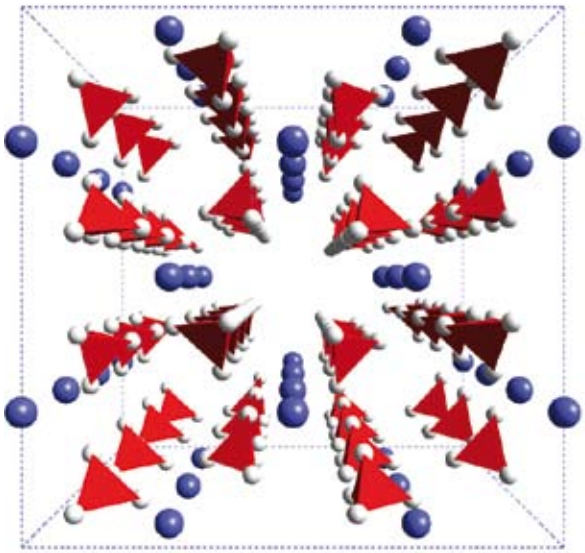

Figure 1: Schematic view of the calcium borohydrie ($Ca(BH_4)_2$). Blue spheres represent calcium, red tetrahedrons are for BH_4 groups.

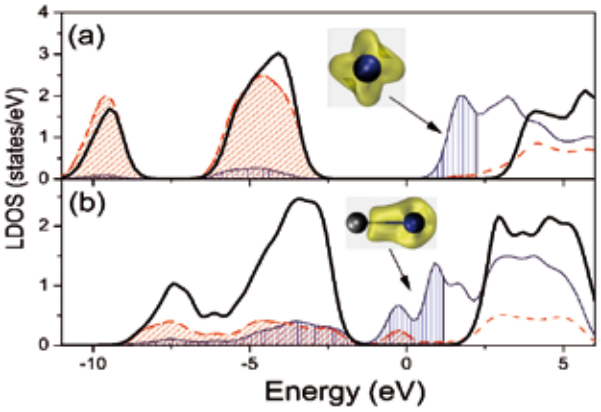

Figure 2: Local density of states LDOS (dashed line) projected on B in $LiBH_4$ (a) and Al in NaAlH4 (b) ions that are closest to neutral interstitial Ti catalyst. The DOS (per formula unit) for undoped samples are shown by thick solid lines and LDOS projected on Ti are shown by thin solid lines for the reference. The top of the valence bands are aligned with respect to pure complex hydrides, shaded regions indicate occupied states for doped systems. The insert shows the real space projection of neutral Ti gap states. Smaller (blue) sphere is for Ti, larger (gray) for Al.

stable in the bulk of $NaAlH_4$ when Ti has high oxidation states [5]. This fact was overlooked in the recent literature.

By combined density functional studies and thermodynamic considerations about Ti related and native defects in lithium borohydride and sodium alanate we have shown that Ti atoms introduced into bulk of $LiBH_4$ are thermodynamically unfavorable for all their oxidation states, while high oxidation states of Ti^{n+} cations are thermodynamically stable in the bulk of $NaAlH_4$[6]. Ti catalyst introduced into sodium alanate forms bond to Al ions, while in lithium borohydride catalyst remains electronically separated in the interstitial position, see Fig. 2.

Neutral hydrogen vacancies and H interstitials or cation vacancies are less stable than their charged counterparts in both compounds. The electronic band alignment in $LiBH_4$ and $NaAlH_4$ is different. In sodium alanate formation of native defects leads to changes of coordination number of aluminum, while in lithium borohydride BH_4 groups change their orientation but B-H bonds remain intact.

Reliability and accuracy of density functional approach applied to complex hydrides was demonstrated by direct comparison of Raman studies and calculations of the vibrational properties of $LiBH_4$ [7].

Our research efforts are focused on proper description of the stability and kinetics of charged and neutral defects in complex hydrides with large electronic band gap by combination of density functional theory and thermodynamics methods.

References

1. Z. Łodziana and T. Vegge, Phys. Rev. Lett. 93, 145501 (2004).
2. R. Cerny, Y. Filinchuk, H. Hagemann, and K. Yvon, Angew. Chem. Int. Ed., 46, 1 (2007).
3. F. Buchter, Z. Łodziana, A. Remhof, O. Friedrichs, A. Borgschulte, Ph. Mauron, and A. Züttel, Structure of $Ca(BD_4)_2$ β-phase from combined neutron and synchrotron X-ray powder diffraction data and density functional calculations., J. Phys. Chem B.; 112, 8042 (2008).
4. J. Voss, J. S. Hummelshøj, Z. Łodziana, and T. Vegge, Structural stability and decomposition of $Mg(BH_4)_2$ isomorphs – an ab initio free energy study, submitted
5. Z. Łodziana and A. Züttel, Titanium cations in sodium alanate, J. Alloys Comp. Letters, doi:10.1016/j.jallcom.2008.03.140.
6. Z. Łodziana , Titanium and native defects in $LiBH_4$ and $NaAlH_4$, submitted
7. A.-M. Racu, J. Schoenes, Z. Łodziana, A. Borgschulte, A. Züttel, High-resolution Raman spectroscopy study of phonon modes in LiBH4 and LiBD4, submitted

Numerical lattice gauge theory

Prof. Martin Lüscher

CERN Physics Department, Geneva, Switzerland

Lattice QCD

The mathematical theory of the strong interactions, Quantum Chromodynamics (QCD), is an elegant quantum field theory which is largely specified by its field content and symmetry properties. In this theory, the only adjustable parameters are the quark-gluon coupling constant and the masses of the quarks. All strong-interaction phenomena, such as the spectrum of baryons and mesons, are then in principle calculable in terms of these. QCD is thus an extremely predictive theory.

On the other hand, the non-linearities of the basic QCD equations are such that the theory cannot be solved analytically, and its verification therefore depends on approximations and often also on ad hoc physical modeling. The basic properties of the nucleons, for example, still have not been reliably calculated from first principles.

The lattice formulation of QCD provides a solid framework in which such computations can be performed using numerical simulations. No uncontrolled approximations need to be made here, but the computations are technically demanding for various reasons. In particular, the fermi statistics of the quarks forbids a direct application of importance sampling methods and the fact that the masses of the light quarks are much smaller than the typical hadronic scales still is an important source of difficulty.

Technical achievements

The simulations performed at the CSCS are part of a long-term project whose goal is to turn lattice QCD into a reliable quantitative tool. Eventually this will allow the theory to be tested accurately in many different ways. The development of efficient simulation algorithms and adapted computational strategies plays a key role in this endeavor.

For the light quarks, the currently preferred simulation algorithms are all based on the so-called Hybrid Monte Carlo (HMC) algorithm. As the quark masses are lowered towards their physical values, this algorithm however becomes increasingly inefficient . Moreover, the simulations may run into instabilities and may violate the requirement of ergodicity in this case. The problem was investigated in the course of the project and it was shown that the range of stability includes the large-volume regime of QCD [1]. This is a rather encouraging outcome since the large-volume regime is, in practice, the most relevant one.

Similarly to the well-known solvers for sparse linear systems, the HMC algorithm can be preconditioned and be accelerated in this way by a large factor. In this context domain-decomposition ideas were only recently introduced and led to a simulation algorithm that is now referred to as the DD-HMC algorithm [2]. The project at the CSCS partly served to validate this algorithm under realistic conditions. As it turns out, the algorithm is highly efficient and makes lattice QCD simulations much more feasible than they were before, particularly so at small sea-quark masses and on large lattices [3,4]. Moreover, the algorithm parallelizes very well and runs on hundreds of processors with nearly no parallelization losses.

The latest development in this general direction is the demonstration that the low quark modes in QCD can be deflated using domain-decomposed deflation projectors [5,6]. As a result a significant further acceleration and a flat scaling behavior of the simulations with respect to the masses of the light quarks are achieved, a result that appeared to be totally unreachable only a few years ago.

First physics results

The immediate output of the simulations that were performed at the CSCS are ensembles of statistically independent field configurations that represent the QCD functional integral at the chosen lattice parameters, coupling constant and sea-quark masses. These field configurations are stored at CERN and will allow many different physical quantities to be computed without further simulations.

So far only some first studies of this kind were performed [3]. In particular, the dependence of the pseudo-scalar meson masses and decay constants on the quark masses were calculated and compared with the behavior expected from chiral perturbation theory. Perhaps the most important outcome here is that the squares of the meson masses turn out to scale nearly linearly with the quark masses up to meson masses of about 500 MeV.

This result quite impressively shows that the simulations are now finally able to reach the chiral regime of QCD where the effects of the spontaneous breaking of chiral symmetry determine much of the low-energy dynamics of the theory. Another outcome of these first studies was, however, that simulations at still smaller quark masses will need to be performed in order to allow the data for the decay constants to be safely extrapolated to the chiral limit.

Impact and future of the project

Although the project no longer makes use of the CSCS facilities, it has not been terminated and now became part of the recently launched Coordinated Lattice Simulations (CLS) effort [7]. The goal of this community effort is to combine the human and computer resources of several specialized teams in Europe in order to share the load of the simulations while allowing many different physics projects to be pursued using the generated representative ensembles of fields.

The CLS teams use the same (now publicly available) DD-HMC simulation code [8] on all machines that are accessible to them. Currently these are various PC clusters, IBM Blue Gene computers and the Mare Nostrum computer. The code is the one that was partly developed in the course of the CSCS project. It includes all improvements added in the last two years and has gone through many validation cycles. Being able to guarantee the correctness and high efficiency of the basic simulation code is essential for the CLS effort and will allow the CLS teams to remain competitive in the coming years.

References

1. L. Del Debbio, L. Giusti, M. Lüscher, R. Petronzio, N. Tantalo, Stability of lattice QCD simulations and the thermodynamic limit, JHEP 0602 (2006) 011
2. M. Lüscher, Schwarz-preconditioned HMC algorithm for two-flavour lattice QCD, Comput. Phys. Commun.165 (2005) 199
3. L. Del Debbio, L. Giusti, M. Lüscher, R. Petronzio, N. Tantalo, QCD with light Wilson quarks on fine lattices. I. First experiences and physics results, JHEP 0702 (2007) 056
4. L. Del Debbio, L. Giusti, M. Lüscher, R. Petronzio, N. Tantalo, QCD with light Wilson quarks on fine lattices. II. DD-HMC simulations and data analysis, JHEP 0702 (2007) 082
5. M. Lüscher, Local coherence and deflation of the low quark modes in lattice QCD, JHEP 0707 (2007) 081
6. M. Lüscher, Deflation acceleration of lattice QCD simulations, JHEP 0712 (2007) 011.
7. https://twiki.cern.ch/twiki/bin/view/CLS/WebHome
8. http://cern.ch/luscher/DD-HMC

Investigation of size effect on structural strength in concrete

Hau-Kit Man

with Prof. Dr. J.G.M. Van Mier, Institute for Building Materials, Department of Civil, Environmental and Geomatic Engineering, ETH Zürich, Switzerland

In this project a computational approach is used to study size effects on fracture of concrete. Fracture simulation of concrete was performed with the goal to understand the fracture mechanism of this and other quasi-brittle materials also addressed as “geo-materials”. Fracture of these materials is a complicated process to understand. To understand this process on the meso level (aggregate level), a simple three-dimensional model from statistical physics is used.

In the beam lattice model, the material is represented by a network of one-dimensional Bernoulli beams. As said, the main goal of this model is to get insight into the fracture mechanism in concrete. The model is a simple and efficient tool for understanding the fracture behavior of quasi-brittle heterogeneous solids, which is simulated by a sequential removal of elements in each loading step as soon as the strength exceeds a certain fracture law (here a simple tensile strength threshold).

At the same time the concrete microstructure should be represented as accurately as possible in the numerical model. At meso-level (size range between 10^{-1} m and 10^{-3} m) concrete is a heterogeneous and highly disordered material (Figure 1), consisting of aggregates, cement matrix and the bond zone.
The first computations and fracture simulations, which were performed at the CSCS on a CRAY XT3, were with a simplified 3D model where the aggregates are represented as spheres [1]. It resembles real concrete to some extent, but obviously some of the complexity of the material is omitted. For example the aggregate geometries are in reality far from spherical: the grains are usually broken or oval shaped (see Figure 1).

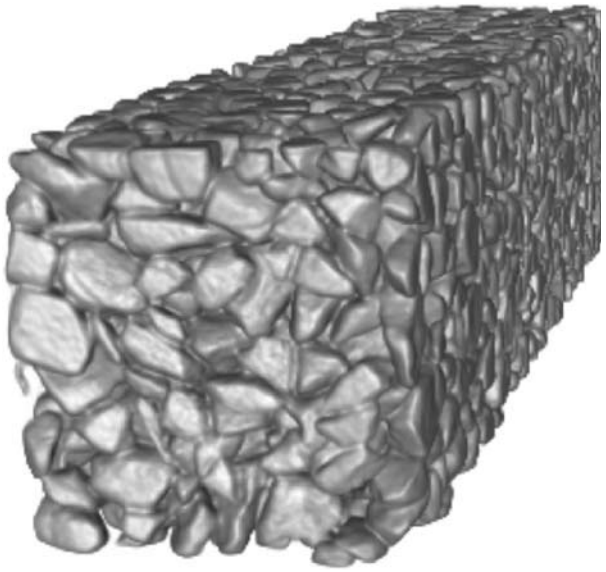

Figure 1: CT-Scan of the concrete microstructure [3]. In this picture the aggregate structure and its distribution is visible.

Consequently, a further step was made to include much more detail into the model. A procedure is developed to model concrete as accurately as possible based on the output from computed tomography experiments. The aggregate distribution can be derived directly from real specimens. Concrete prisms are scanned at Zurich University Hospital on an advanced CT-scanner. The derived microstructure of concrete is mapped into the numerical model. With this method the aggregate shapes are modeled more realistically. The real shapes of pores (Figure 2, [2])

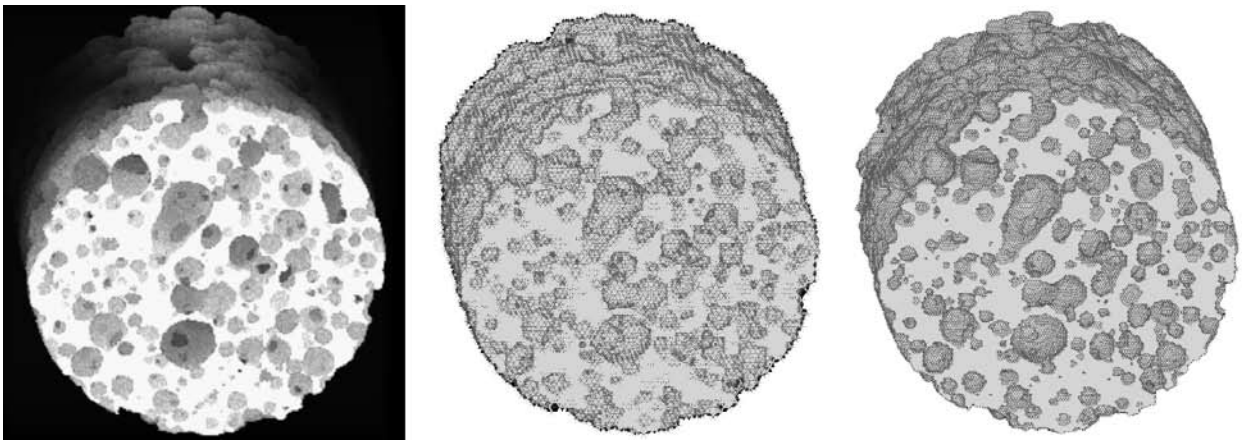

Figure 2: Comparison of the microstructure of foamed cement paste) and 3D lattice model (in two different resolutions, lattice beam length equal to 0.1mm and 0.05mm respectively) (from [2])

and/or the shapes of the aggregates ([3]-[5]) can be included into the numerical model with a certain degree of accuracy, i.e. depending on the size of the projected lattice. Fracture simulations on concrete can now be performed with a simplified or with a more sophisticated microstructure.

The size effect on strength is investigated on prisms loaded in 3-point bending (see Figure 3). Size/scale effects in quasi-brittle materials differ from those in brittle materials, which is the reason for the present study. It is known that the structural strength varies with size, but not exactly how this would be when the material structure changes. Most existing laws are empirical in nature and do not consider the effects from material composition.

To study these effects, a three-dimensional lattice model of concrete subjected to three-point bending is. The specimens are scaled in all three sizes (scaling in length, height and thickness). In every step the specimen size is doubled in all three dimensions. The volume of the largest concrete specimen is 512 times larger compared to the volume of the smallest specimen. Investigations of size effects in 3D are computationally very demanding. Huge computing capacity is needed to simulate fracture. Because of these requirements, numerical size effect study is mostly (for computational convenience) carried out in 2D (i.e. scaling in height and length) only.

In that respect the present project is an improvement as well since wall effects can be included.

In various papers, different analysis on (numerical) concrete were presented. Parameters such as aggregate density (P_k) and the various aggregate shapes are varied: a size effect study on bending strength on concrete with different particle densities and ideal spherical aggregates [1], whereas in [3]-[5] concrete containing realistic aggregate shapes is used.

Figure 3 illustrates the fracture process on concrete with coarse shaped aggregates with four different specimen sizes. In the simulations the typical fracture response observed in laboratory experiments was found: At peak load, many microcracks can be found in the lower part of the beams (Figure 3 left), during softening behavior macrocrack growth occurs (Figure 3 right), which is subsequently followed by bridging.

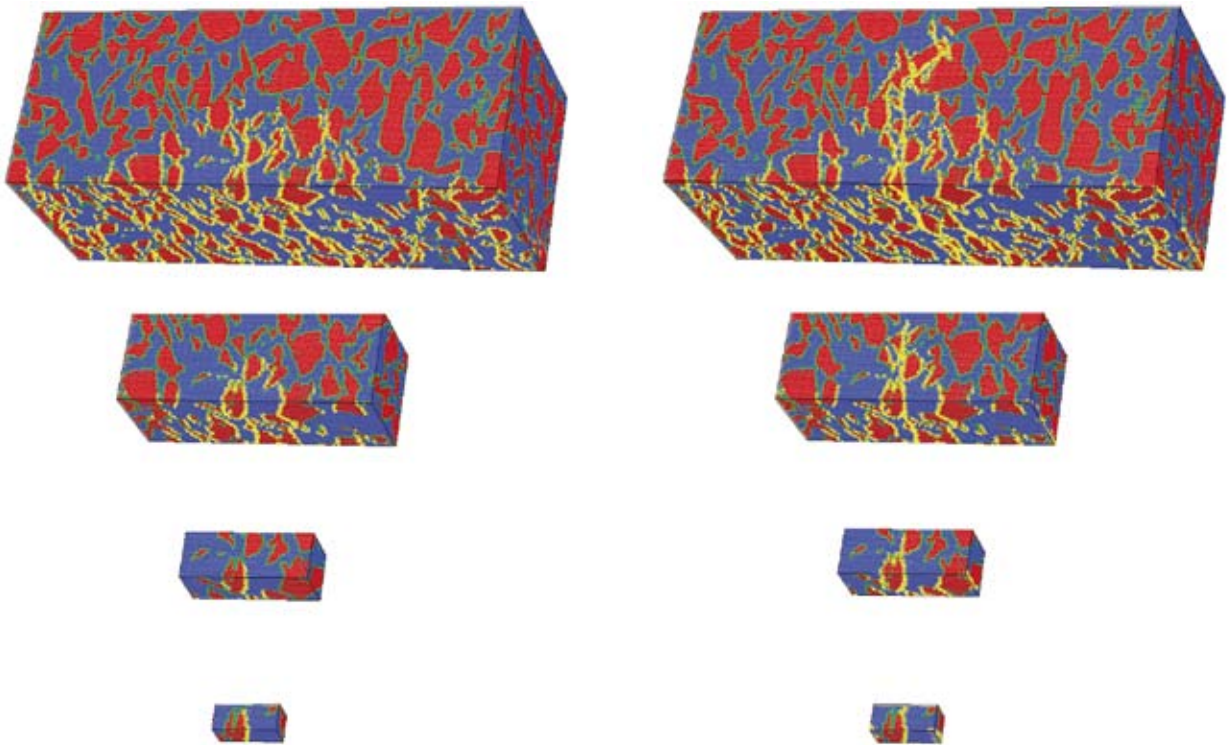

Figure 3: Cracking in concrete at different loading stages (blue: cement matrix, red: aggregate, green: interface zone, yellow: crack; from [3])
Figure 3 left: at maximum load; Figure 3 right: crack localization in the post peak regime

Results from [1], [3]-[6]:

- The comparison of crack processes show that the results from three-dimensional analysis with different P_k compare qualitatively quite well to results obtained with a two-dimensional model.
- Fracture behavior is different depending on aggregate shapes
- From the analysis done, a size effect on global strength can be observed. The bending (structural) strength decreases with increasing specimen size. Depending on the aggregate density P_k, and the aggregate shape, the exponents (slopes on strength vs. specimen size diagram) lie somewhere between the Weibull theory (-1/6) and the linear elastic fracture mechanics (-1/2).
- Investigation of 2D- scaling (which is most frequently done when size-effect models are developed) and different variations of 3D- scaling: it was shown that for each variation different slopes in the log (σ)-log (Height) diagram, but if all curves were gathered in a log (σ) – log (Volume) diagram, all different lines collapsed along a single line, resulting that size-effect must be expressed in terms of log(σ) vs. log(Volume) diagrams instead of log(s) vs. log(Height), which makes the formulation more general [6]

References

1. H.-K. Man and J.G.M. van Mier. Influence of Particle Density on 3D Size Effects in Numerical Concrete. Mechanics of Materials, 40(6):470-486, 2007.
2. D. Meyer, H.-K. Man and J.G.M. van Mier. Fracture of foamed cement paste. A combined experimental and numerical study. In Proceedings IUTAM Symposium on 'Mechanical Properties of Cellular Materials', (Zhao, H. and Fleck, N.A., eds.) LMT-Cachan, Paris, France, September 17-21, 2007. Kluwer Academic Publishers. Dordrecht. In press, 2008.
3. J.G.M. van Mier and H.-K. Man. Some Notes on Microcracking, Softening, Localization and Size Effects, International Journal of Damage Mechanics, Special Issue commemorating D. Krajcinovic. accepted, 2008.
4. H.-K. Man and J.G.M. van Mier. On the relationship between damage distribution and size effect on concrete strength and fracture energy. Submitted, 2008.
5. S. Simioni, and T. Tschenett. Analysis of Size-Effects on Fracture Strength for Concretes Containing Realistic Aggregate Particles, BSc-Thesis, Department of Civil, Environmental and Geomatic Engineering, ETH Zürich, 2007.
6. H.-K. Man and J.G.M. van Mier. Size and Shape Effects of Fracture Strength of Concrete, in Fracture Mechanics of Concrete and Concrete Structures (FraMCoS-6), eds. Carpinteri, A., Gambarova, P., Ferro, G. And Plizarri, G., Taylor & Francis Group, London, 39-44. 2007

Computational Crystallography and Mineral Physics

Prof. Dr. Artem R. Oganov

with Y. Ma, A. Lyakhov, D. Adams, K. Hassdenteufel, D.Y. Jung, C.W. Glass, F. Zhang, Y. Xie; Sabbatical guest: A. Garcia

Laboratory of Crystallography, Department of Materials ETH Zurich, Switzerland

Using ab initio simulations, we study the structure and properties of minerals and other systems of fundamental interest at high pressures and temperatures. The main hallmarks of our approach are the use of highly accurate methods (e.g., the all-electron PAW methodology) and efficient state-of-the-art codes (VASP and ABINIT), development and application of our own computational method, the evolutionary algorithm USPEX [1-3] for crystal structure prediction, and active collaboration with experimentalists (in Japan, France, USA, Russia, Switzerland).

Development of the USPEX method for crystal structure prediction: This groundbreaking methodological development now enable ab initio prediction of complex crystal structures given only the chemical composition (see Figure 1). Apart from the original papers [1-3] describing the method and its initial applications and tests, we have published several detailed reviews [4-6]. More recently, in collaboration with Mario Valle, a powerful fingerprinting method was developed [7,3], which enables efficient data analysis (Fig. 2) and, when incorporated within USPEX, improves its performance.

Using USPEX, we have systematically explored high-pressure behaviour of many elements and compounds [1,2,4-6,8-13]. These studies have uncovered new phenomena occurring under pressure (auotionisation of elements, formation of non-nuclear charge density maxima, etc.) and clarified processes occurring inside planetary interiors. For instance, we have disproved [6] the old idea that heat is produced by gravitational sinking of diamond formed in the interior of Neptune by pressure-induced decomposition of CH_4. We have elucidated the dominant forms of carbon inside the Earth [1,10]. In one of our papers [4] we addressed the validity of the jellium model, which has formerly been used to predict the existence of a new type of insulating solids made of metallic clusters – we found these predictions incorrect. As a result, predictions of the jellium model (commonly used in nanoscience) have to be taken with great care and scepticism.

Studying the high-pressure behaviour of metals [8,9,14-16] we have been able to link the emergent structural complexity of alkali metals with Fermi surface nesting and phonon instabilities. Metal-insulator transitions were found to be a particularly challenging topic – for example, the bonding in the metallic (yet molecular) ζ-phase of oxygen remains enigmatic. Studying quasicrystals at normal and high pressure, we found no evidence for well-defined clusters (such clusters were often hypothesised to explain the structure and bonding of quasicrystals). Unexpectedly, we found that for many metals there are elastic anomalies, which density functional theory cannot reproduce very accurately – this occurs when a metal is close to a

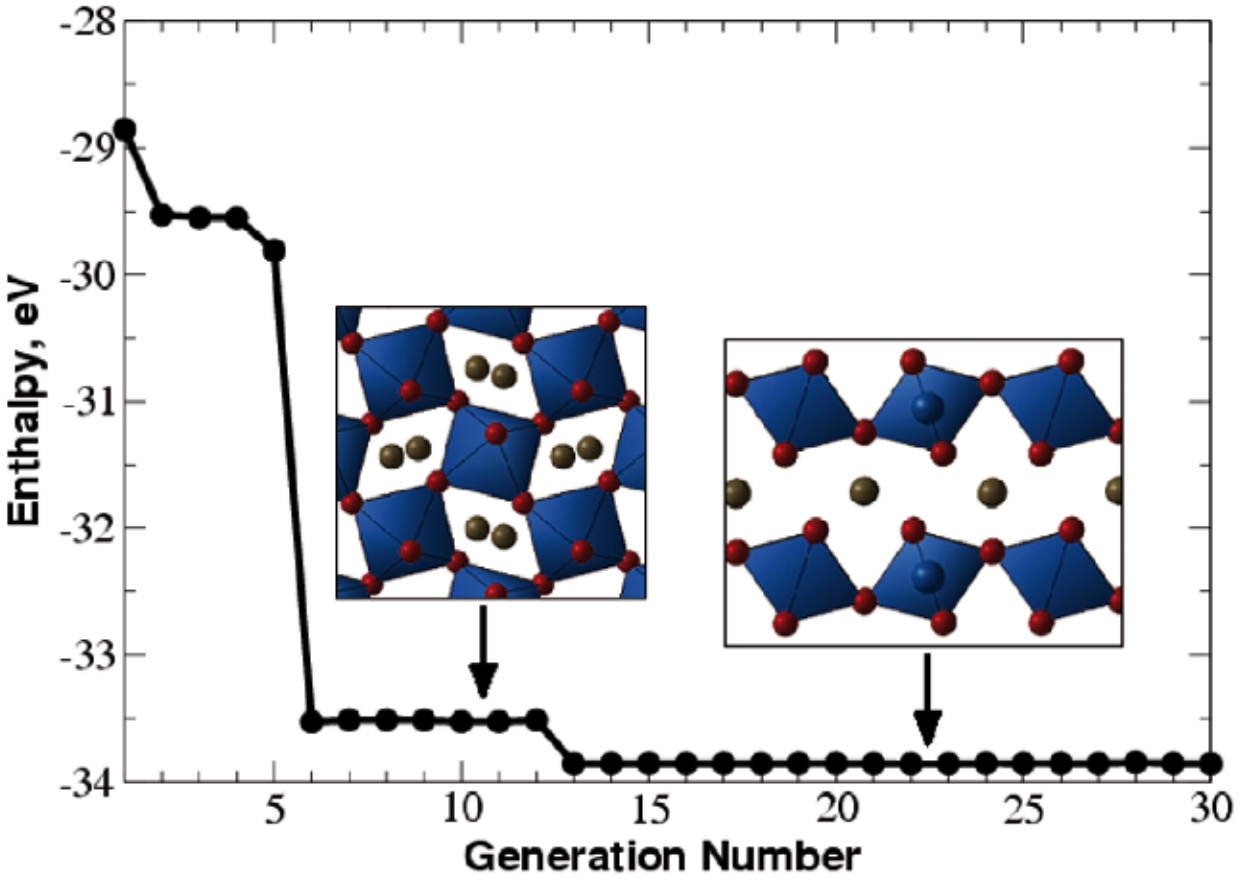

Figure 1: Prediction of the crystal structure of $MgSiO_3$ at 120 GPa (20 atoms/cell) [2]. Enthalpy (per 20 atoms) of the best structure as a function of generation. Insets show the perovskite and post-perovskite structures (blue polyhedra – SiO_6 octahedra; gray spheres – Mg atoms). This simulation used no experimental information and illustrates that our method can find both the stable and low-energy metastable structures in a single simulation.

Lifshitz transition, and a very clear example is vanadium [14].

In collaboration with R. Martonak we have continued to explore phase transition mechanisms and plastic deformation of crystals. Using the improved version of metadynamics [17] we studied pressure-induced reconstructions in SiO_2 and found an unexpected plane-sliding mechanism [17,18]. Studies of the Earth's mantle minerals [19-23] also brought us major surprises. We have proposed high electrical conductivity of $MgSiO_3$ post-perovskite as the explanation for the observed variations of the length of day [19]. Controversial topics, such as the thermal behaviour of $CaSiO_3$ perovskite [20], defect structures and valence and spin states of iron impurities in mantle silicated [21,22] have been addressed – and we have been able to resolve many of the contradictions between previous experimental and theoretical results. A review of deep Earth mineralogy [23] was published.

Detailed thermodynamic studies [24.25] have enabled us to create the most accurate pressure scales available today. High-pressure thermodynamics was reviewed in [26]. The accuracy of thermodynamic predictions of density-functional perturbation theory under pressure was experimentally verified in [27]. We have also been involved in studies of high-pressure isosymmetric phase transitions in molecular crystals [28], where our ab initio simulations have been crucial for interpreting experimental results.

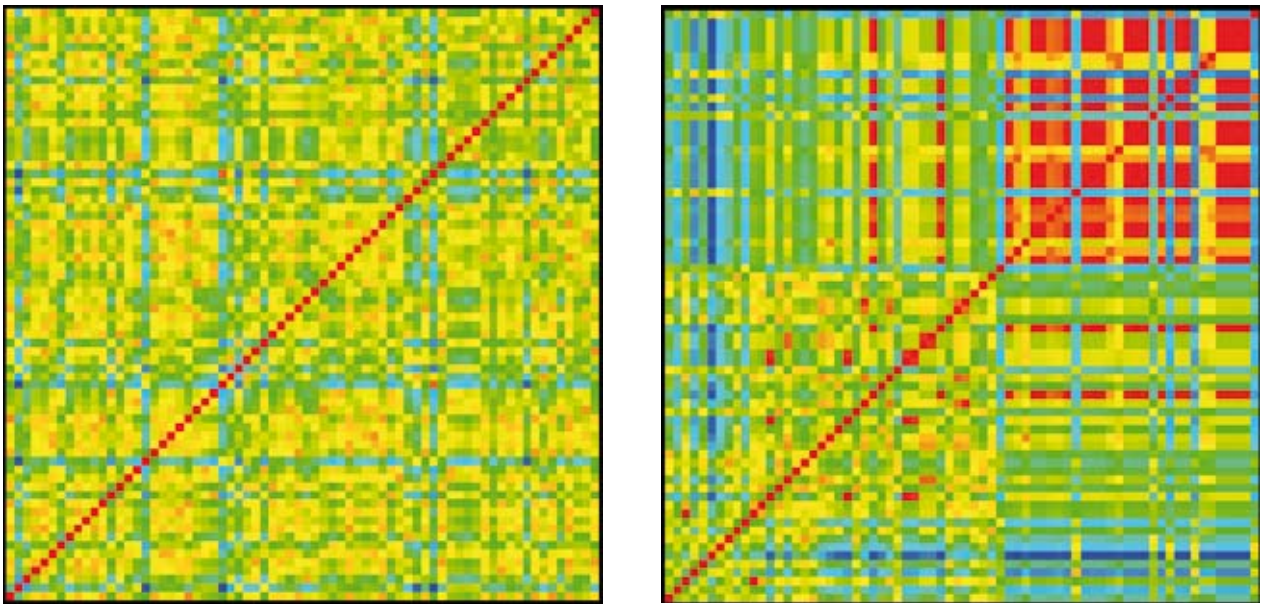

Figure 2: Similarity matrices for (left) random sampling run, (right) evolutionary run with USPEX for GaAs (8 atoms/cell). Matrix dimensions are 70x70. The evolutionary simulation used a generation size of 10 structures. From [6].

Publications in 2006-2007

1. Oganov A.R., Glass C.W., Ono S. (2006). High-pressure phases of $CaCO_3$: crystal structure prediction and experiment. Earth Planet. Sci. Lett. 241, 95-103.
2. Oganov A.R., Glass C.W. (2006). Crystal structure prediction using ab initio evolutionary techniques: principles and applications. J. Chem. Phys. 124, art. 244704.
3. Glass C.W., Oganov A.R., Hansen N. (2006). USPEX – evolutionary crystal structure prediction. Comp. Phys. Comm. 175, 713-720.
4. Oganov A.R., Glass C.W. (2008). Evolutionary crystal structure prediction as a tool in materials design. J. Phys.: Cond. Mattter 20, art. 064210 (invited paper).
5. Martoňák R., Oganov A.R., Glass C.W. (2007). Crystal structure prediction and simulations of structural transformations: metadynamics and evolutionary algorithms. Phase Transitions 80, 277-298.
6. Oganov A.R., Ma Y., Glass C.W., Valle M. (2007). Evolutionary crystal structure prediction: overview of the USPEX method and some of its applications. Psi-k Newsletter, number 84, Highlight of the Month, 142-171 (invited review).
7. Valle M., Oganov A.R. (2008). Crystal structure classifier for an evolutionary algorithm structure predictor. IEEE VAST, in press.
8. Ma Y.-M., Oganov A.R., Glass C.W. (2007). Structure of the metallic ζ-phase of oxygen and isosymmetric nature of the ε-ζ phase transition: Ab initio simulations. Phys. Rev. B76, art. 064101.
9. Ma Y., Oganov A.R., Xie Y. (2008). High pressure structures of lithium, potassium, and rubidium predicted by ab initio evolutionary algorithm. Phys. Rev. B, in press.
10. Oganov A.R., Ono S., Ma Y., Glass C.W., Garcia A. (2008). Novel high-pressure structures of $MgCO_3$, $CaCO_3$ and CO_2 and their role in the Earth's lower mantle. Earth Planet. Sci. Lett., in press.
11. Oganov A.R., Glass C.W., Ma Y.-Z., Ma Y.-M., Chen J. (2008). New high-pressure form of elemental boron. Nature, under review.
12. Ono S., Oganov A.R., Brodholt J.P., Vocadlo L., Wood I.G., Glass C.W., Côté A.S., Price G.D. (2008). High-pressure phase transformations of FeS: novel phases at conditions of planetary cores. Earth Planet. Sci. Lett., under review.

13. Li Q., Wang M., Oganov A.R., Cui T., Ma Y., Zou G. (2008). Crystal structures of superhard BC_2N predicted by ab initio simulations. Submitted to Phys. Rev. B.
14. Koci L., Ma Y., Oganov A.R., Souvatzis P., Ahuja R. (2008). Anomalous elastic behavior of superconducting metals at high pressure. Phys. Rev. B, in press.
15. Hassdenteufel K.H., Oganov A.R., Steurer W., Katrich S. (2007). Ab initio study of the W-phase of Al-Co-Ni, an approximant of the decagonal Al-Co-Ni quasicrystal. Phys. Rev. B75, art. 144115.
16. Xie Y., Tse J.S., Cui T., Oganov A.R., He Z., Ma Y., Zou G. (2007). Electronic and phonon instabilities in face-centered cubic alkali metals under pressure. Phys. Rev. B75, art. 064102.
17. Martoňák R., Donadio D., Oganov A.R., Parrinello M. (2006). Crystal structure transformations in SiO_2 from classical and ab initio metadynamics. Nature Materials 5, 623-626.
18. Martoňák R., Donadio D., Oganov A.R., Parrinello M. (2007). 4- to 6- coordinated silica: transformation pathways from metadynamics. Phys. Rev. B76, art. 014120.
19. Ono S., Oganov A.R., Koyama T., Shimizu H. (2006). Stability and compressibility of high-pressure phase of Al_2O_3 up to 200 GPa: implications for electrical conductivity at the base of the lower mantle. Earth Planet. Sci. Lett. 246, 326-335.
20. Adams D.J., Oganov A.R. (2006). Ab initio molecular dynamics study of $CaSiO_3$ perovskite at P-T conditions of Earth's lower mantle. Phys. Rev. B73, 184106.
21. Zhang F., Oganov A.R. (2006). Mechanisms of Al^{3+} incorporation in $MgSiO_3$ post-perovskite at high pressures. Earth Planet. Sci. Lett. 248, 54-61.
22. Zhang F., Oganov A.R. (2006). Valence and spin states of iron impurities in mantle-forming silicates. Earth Planet. Sci. Lett. 249, 436-443.
23. Pushcharovsky D.Yu., Oganov A.R. (2006). Structural transformations of minerals in deep geospheres: a review. Crystallography Reports 51, 767-777.
24. Dorogokupets P.I., Oganov A.R. (2007). Ruby, metals, and MgO as alternative pressure scales: A semiempirical description of shock-wave, ultrasonic, x-ray, and thermochemical data at high temperatures and pressures. Phys. Rev. B75, art. 024115.
25. Dorogokupets P.I., Oganov A.R. (2006). Equations of state of Al, Au, Cu, Pt, Ta and W and the revised ruby pressure scale. Doklady Earth Sciences 410, 1091-1095.
26. Oganov A.R. (2007). Thermodynamics, phase transitions, equations of state and elasticity of minerals at high pressures and temperatures. Treatise on Geophysics, vol. 2 (Mineral Physics, edited by G.D. Price), 121-152.
27. Ghose S., Krisch M., Oganov A.R., Beraud A., Bossak A., Gulve R., Seelaboyina R., Yang H., Saxena S.K. (2006). Lattice dynamics of MgO at high pressure: theory and experiment. Phys. Rev. Lett. 96, art. 035507.
28. Boldyreva E.V., Ahsbahs H., Chernyshev V.V., Ivashevskaya S.N., Oganov A.R. (2006). Effect of hydrostatic pressure on the crystal structure of sodium oxalate: X-ray diffraction study and ab initio simulations. Z. Krist. 221, 186-197.

Large Eddy Simulations of urban canopy flows

Prof. Marc Parlange

with Nikki Vercauteren, Yue Uyang and Chad Higgins.

Laboratory of Environmental Fluid Mechanics and Hydrology, EPF Lausanne, Switzerland

Introduction

In most numerical simulations of high Reynolds number turbulent flow, which includes atmospheric flows over urban canopies, grid spacings far exceed the viscous scale at which turbulent kinetic energy is dissipated into heat. To overcome this obstacle, Large eddy simulation (LES) explicitly resolves turbulent large-scale motions with a characteristic size larger than the filter size Δ, while motions with a characteristic size smaller than Δ (subgrid-scales, SGS) are parameterized. Thus, LES relies on a set of closure models to account for the turbulent motions occurring at small, numerically unresolved, (the so-called subgrid) scales. In LES of the atmospheric boundary layer (ABL), these scales typically occur at lengths smaller than tens of meters (Lilly 1967, Mason, 1994, Lesieur and Metais, 1996, and Meneveau and Katz, 2000), and are responsible for mixing and large-scale interactions that tend to transfer kinetic energy down the turbulent energy cascade. This transfer must be reproduced accurately by subgrid-scale (SGS) closures to prevent over damping of the resolved scales, or insufficient damping which can lead to spurious instabilities. A successful LES must take into account proper subgrid scale physics so as to achieve this balance. Lilly (1967) was the first to combine this insight with concepts from the phenomenological theory of 3D turbulence to provide quantitative answers to several important parameterization issues in LES.

The LES equations for momentum transport are obtained by spatially filtering the Navier-Stokes and continuity equations. At very high Reynolds number when the effects of molecular viscosity can be neglected, the filtered equations are:

$$\frac{\partial \tilde{u}_i}{\partial t} + u_j \frac{\partial \tilde{u}_i}{\partial x_j} = -\frac{1}{\rho}\frac{\partial \tilde{p}}{\partial x_i} - \frac{\partial \tau_{ij}}{\partial x_j} \qquad (1.1)$$

$$\frac{\partial \tilde{u}_i}{\partial x_i} = 0$$

where ~ represents spatial filtering, $\tilde{u}_i$ is the filered velocity, p is the pressure, t is time, x_i is the spatial coordinate.

$$\tau_{ij} = \tilde{u}_i u_j - \tilde{u}_i \tilde{u}_j, \qquad (1.2)$$

is the SGS stress and must be parameterized. The formulation of τ_{ij} reflects the multiple length scales that are inherent to turbulence (the above having filtered products and products of filtered velocity), and its three-dimensional properties (the SGS stress being a second rank tensor). Closure requires that τ_{ij} be expressed in terms of resolved scale variables, constrained by Galilean-invariant properties of the resolved fields or domain geometry. For the following simulations the next generation Lagrangian scale dependent subgrid scale model was used where τ_{ij} is modeled as:

$$\tau_{ij} = -c_s^2 \Delta^2 |\tilde{\mathbf{S}}| \tilde{S}_{ij} \quad (1.3)$$

and the coefficient c_s is found dynamically within the simulation with the results averaged following fluid pathlines. Such a technique is ideally fitted for urban canopies as no homogeneous directions are assumed.

The LES equations for scalar transport are similarly obtained by spatially filtering the scalar transport equation. Neglecting molecular diffusivity, the filtered equation is:

$$\frac{\partial \tilde{T}}{\partial t} + u_j \frac{\partial \tilde{T}}{\partial x_j} = -\frac{\partial q_j}{\partial x_j} \quad (1.4)$$

Thus, closure expressions are also needed for scalar turbulent transport:

$$q_i = \tilde{T} u_i - \tilde{T} \tilde{u}_i \quad (1.5)$$

where q_i is the subgrid-scale heat flux per unit heat capacity. T is the temperature, and $\tilde{T}$ is the filtered temperature field that is numerically resolved in the LES model.
In the presented LES code the scalar equations are closed using a mixing length approach:

$$q_i = \frac{(c_s \Delta)^2}{\mathrm{Pr}_{SGS}} |\tilde{\mathbf{S}}| \frac{\partial \tilde{T}}{\partial x_i} \quad (1.6)$$

.
Optimization of natural ventilation in a buildings block of the city of Syracuse, Sicily.

More than 50% of the world's population now lives in urban areas, and this percentage is projected to increase in the future. The demands of this ever increasing population coupled with the current observed global warming trends make the impact of infrastructures on the health and comfort of inhabitants of urban areas a critical issue for the environmental quality and the quality of life of the cities inhabitants.

The reconstruction of a city block in Syracuse is a good opportunity to investigate building designs that reduce adverse impacts of increased population. For example, to avoid the use of air conditioning in this warm region of Sicily, this project uses LES to aide in the design of buildings that enhance natural ventilation. The geometry of buildings is optimized to create a maximum of turbulence, mostly in the courtyards. The fresh night breeze thus mixes with the accumulated heat of the day to cool down the area.

To compare the behavior of the wind in different geometries of the block, we use Large Eddy simulations (LES).

The main challenge is the heterogeneity and complexity of urban environments. When the rough surface interacts with the overlying atmospheric flow, the geometry of buildings or the spacing between them can lead to very complex dynamics. So, to achieve an accurate description of the turbulent flows in our domain, we have to take into account the effect of every single building of our block in Syracuse. For efficiency of computations, we wish to keep our grid regular, or not affected by the addition of the building. The effect of the buildings is thus represented by a force in the Navier-Stokes equations. Each building will be treated as a force that blocks the motion of the fluid; therefore the added force will be zero in the fluid and non-zero in the domain representing the obstacle. We can thus consider every kind of shapes.

The next step is to model the buildings block, adapt it to the requirements of the simulation. One limitation is the number of points that we can consider in our computational grid. We use the CSCS cluster to have the best possible computational power. The size chosen for a grid cell is 2m30 by 2m30 in the plane, and 1 meter vertically. This gives some limits to model thin walls; however we include those in the model, despite the alteration of their thickness.

Now, this block is part of an urban environment. Unfortunately, it is impossible to model the entire city. Nevertheless, we consider periodic boundary conditions. The idea is that the block repeats itself infinitely; the flow coming out on the right comes back inside the domain on the left side. Climatology of Syracuse tells us that the night breeze is fresh, and mostly comes from the north, which we will use in our simulations.

To gain some insight into the type of geometries one should consider, we start by studying simple blocks with a higher resolution. Different geometries are tested, namely:

- one where the buildings are all at the same height (Figure 1a),
- one where the buildings on the border of the block are the highest (Figure 1b),
- one where 2 of the buildings on the border of the block are the highest, leaving 2 lower walls (Figure 1c).

We observe that the last solution (c) leads to the best mixing within the city block. Indeed, the wind penetrates into the block via one of the lower walls, and it is then hits the 2 higher buildings before being canalized in the direction of the second lower building. It penetrates well into the courtyard before leaving the block. In the other solutions (a) and (b), the wind stays mostly over the block, penetrating very little into the courtyards. These simulation results can be used in the design of the entire block by using the buildings to create corners that will break the flow. It is also important to keep an exit for the wind on one side. Thus the city block design would have a side building that is lowered by one floor. Finally, we compare above design to the city blocks historical architecture (before any reconstruction) and to another situation, similar to the optimized one, but where all the buildings have the same height. In this last ituation, every higher building is lowered to the height of the rest of the buildings, leading to a lower volume of buildings, which should be favorable to better ventilation. The results show that the optimized solution has as good a mixing as the one with fewer high buildings. Therefore the optimized block design allows a higher population density without sacrificing the ventilation of the courtyards, and make use of the fresh night breeze to get rid of part of the accumulated heat of the day.

LES over EPFL campus for scalar roughness analysis

A typical modern urban canopy consists of agglomerate buildings, irregular streets, parking lots, motor-vehicles, and vegetation. Such aggregated rough surfaces disturb atmospheric flow, curve mean streamlines, generate large velocity gradients, sharp velocity discontinuities, flow separations and reattachments, recirculation zones, cavity regions, and cause inhomogeneous turbulence.

Arbitrary arrangement of non-uniform canopy surfaces must be catalogued and quantified in different patches or orientations. The relevant geometric physical parameters for an urban canopy are the zero-plane displacement, d_0 , which is used to indicate the obstacle height where wind can not penetrate and vertical wind velocity is zero, the scalar roughness for momentum z_0 , and the scalar roughness for heat flux z_{0h} are adopted to de-

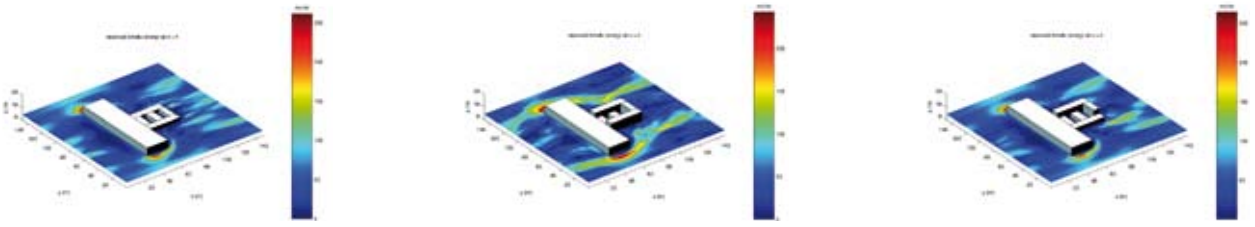

a) b) c)

Figure 1: Maps of turbulent mixing over the block in Syracuse for three proposed building configurations

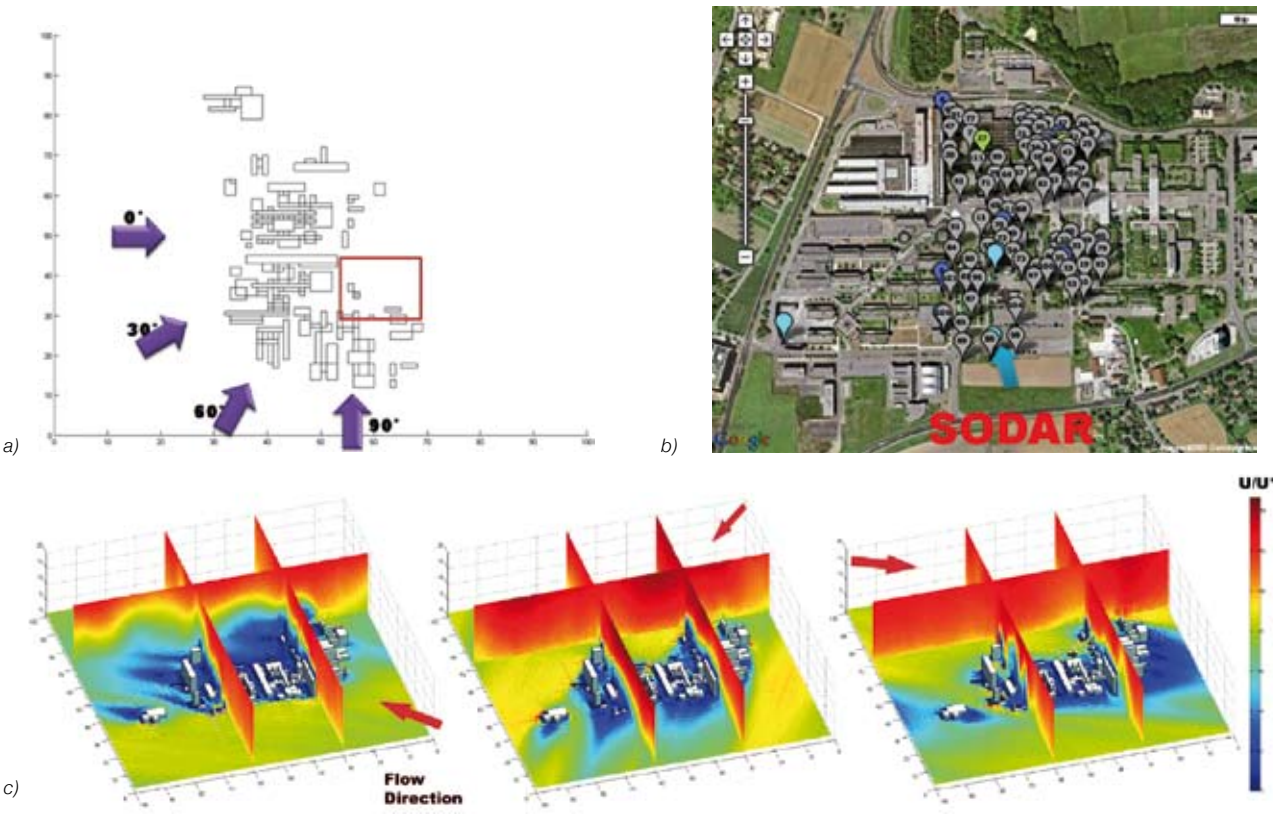

Fugure 2: a). EPFL campus building model of LES numerical computing domain; b). Satellite image of EPFL campus. (http://sensorscope.epfl.ch/map/), c) Slices over time averaged streamwise velocity field from 60° 150° and 240° wind directions

scribe ground surface physical characteristics. It would be naïve to expect a universal atmospheric flow pattern to exist in these disturbed flows and adopt a global representative scalar roughness value for momentum and heat flux for such a complex urban canopy. According to the relevant literature, d_0 is defined as approximately 2/3 of the averaged building height. However, LES provides valuable insight into the dependence of d_0 and scalar roughness on wind direction. Here we perform LES using 12 different wind direction sectors over EPFL campus.

The LES code, running at CSCS, computes a domain of with dimension of 1500m * 1500m * 400m, the numerical grids consists of 100*100*80 nodes, each node has physical dimension of 15m * 15m in horizontal space, and 5m in vertical space (Fig 2), and there are 127 building blocks implemented into the numerical computing domain. By tuning input wind directions by 30° over 0° ~ 360° into the computing domain, we are able to simulate and directly compute d_0 values according to the wind direction from the LES simulation results. Further, these measurements of d_0 can facilitate in the understanding of other relevant parameters that depend on wind angle of attack such as the momentum and scalar roughness height.

This approach, only available because of the high resolution LES computations, yields physical characteristics of the urban domain instead of empherical estimates that were deduced from previous works done for tall vegetation, bare soil etc.. However, after comparing with numerical simulation results from LES and SODAR measurement, (Fig 3), momentum roughness computed by LES shows relatively small value. This underestimate is likely due to the limits of the numerical computing domain. LES can only simulate influence of main bluff bodies, but not vegetation, and other subsidiary structures that are present in reality. Nevertheless

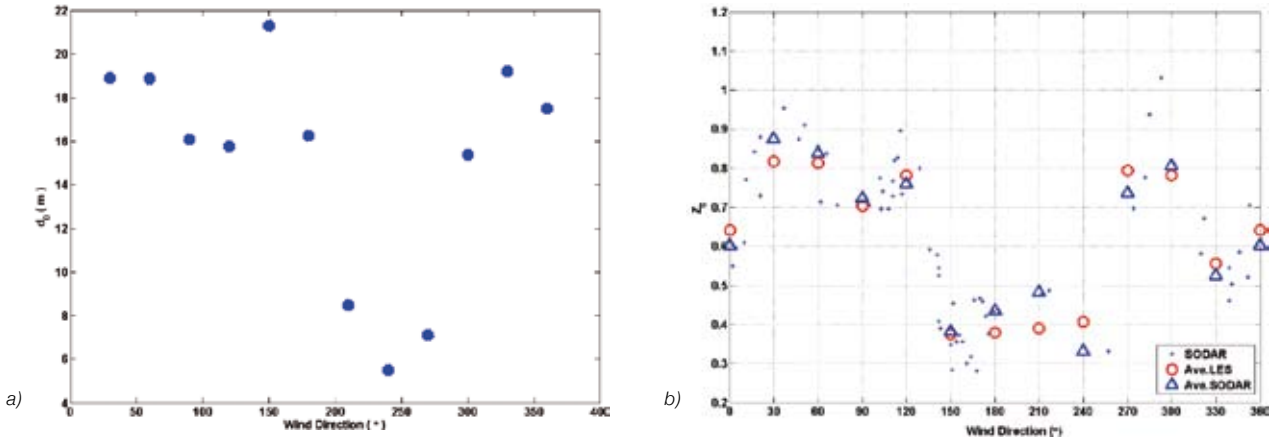

Figure 3. a) d_0 *value computed by LES in 12 wind directions. b) Scalar roughness comparison between measurement and numerical simulation.*

d_0 value can be considered as the influence from main building blocks, which are implemented inside of computing domain.

Summary

LES provides a valuable tool which can be used, given the proper computational resources, to investigate a variety of large scale flow phenomenon ranging from urban cnopies, to pollen transport to fate and transport of pollutants to land atmospheric interaction. In the above two examples LES is used to shed light on fundamental issues that face urban canopy research. One perspective involves design for more efficient use of energy and space, whilst the other involves accurately characterizing the urban canopy interaction in a new way that has never been done before. Only the continued availability of large computational resources makes such computations possible.

References

1. Lilly, D. K., 1967, The representation of small-scale turbulence in numerical simulation experiments. Proceedings, IBM Scienti¯c Computing Sympposium on Environmental Sciences, November 14-16, 1966, Thomas J. Watson Research Center, Yorktown Heights, N.Y., H.H. Goldstein, Ed., IBM Form No.320-1951, pp.195-210.
2. Lesieur, M., and Metais, O., 1996, New trends in large-eddy simulations of turbulence, Ann. Rev. Fluid Mech. 28, 45-82.
3. Mason, P.J., 1994, Large eddy simulation: A critical review of the technique. Quart. J. Roy. Metero. Soc., 120, 1-26.
4. Meneveau, C., and Katz, J., 2000, Scale-invariance and trubulence models for large-eddy simulation, Ann. Rev. Fluid Mech. 32, 1-32.

Crystallization, polymorphism and Nano-Machines from molecular dynamics

Prof. Michele Parrinello

Departement of Chemistry and Applied Biosciences, ETH Zürich, Switzerland

Freezing of a Lennard-Jones fluid

Davide Donadio, Federica Trudu and Michele Parrinello

In the absence of nucleation centers, moderately supercooled liquids are metastable, but after a finite time undergo homogeneous nucleation. This is described in simple terms by classical nucleation theory [1] in which spontaneous fluctuations lead to the formation of small crystallites. Most of these crystallites will eventually dissolve in the liquid, but at times one of them will exceed a certain critical size and initiate crystallization. In this picture, the critical nucleus is assumed spherical, and the nucleation barrier, which depends only on its size, is determined by a balance between surface and volume free energy terms. Although successful at describing nucleation qualitatively, CNT is oversimplified and fails in several cases [2].

Computer simulations have proven a useful tool to probe crystallization from the melt and to challenge the approximations of CNT [3,4]. Due to the characteristic time-scales of this process, the brute-force approach could be employed only for a deep supercooled liquid, and rare-events methods need to be employed to study nucleation close to coexistence [4]. In a recent investigation [5] we have employed transition path sampling molecular dynamics and metadynamics to study the crystallization of a Lennard-Jones fluid in a broad range of temperatures.

As lately confirmed by other researchers [6], we have shown that at shallow supercooling the assumption of spherical nuclei falls, as a consequence of the fast out-of-equilibrium growth conditions. Nevertheless the CNT prediction for the free energy barrier and the critical size of the nuclei can be adjusted to the simulation results if the growing nuclei are approximated by ellipsoids rather than spheres.

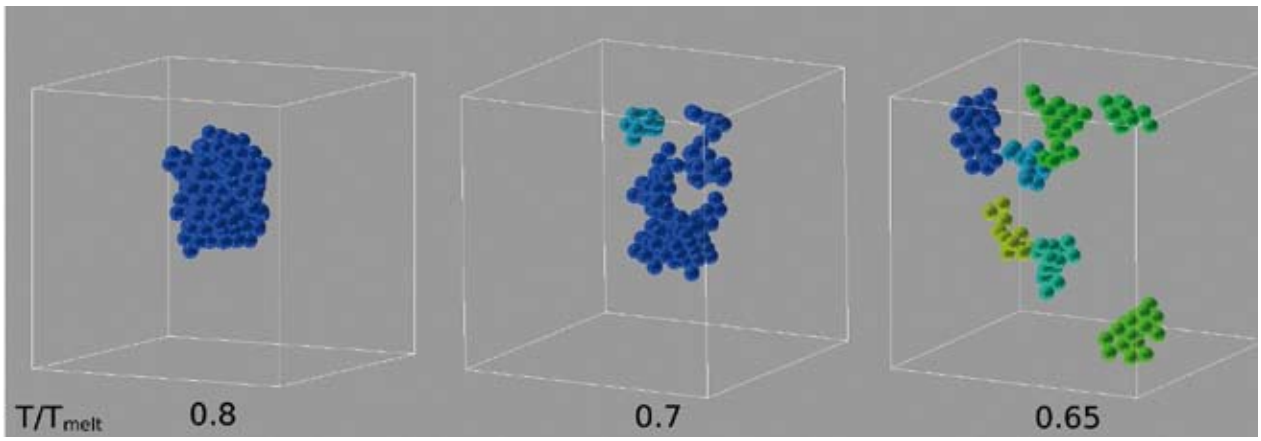

Figure 1: Snapshots along the freezing path of a Lennard-Jones fluid at different temperatures. Only the particles with a solid-like environment are shown.

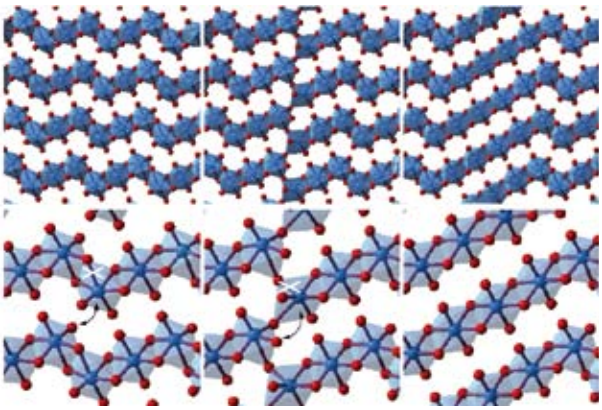

Figure 2: The details of a step along the transition from quartz to stishovite.

Even if with this latter assumption CNT captures the essential thermodynamic features of freezing, molecular dynamics simulations also show that the kinetics of the initial stages of the growth of crystalline embryos is characterized by the sudden formation of dense crystalline cluster of finite size. This feature is not predicted by classical kinetic theories that describe nucleation in terms of addition and removal of single particles.

At lower temperatures we observed a crossover from a classical nucleation regime to a more collective mechanism of freezing, influenced by the existence of a spinodal singularity. We provided direct evidences of the presence of a spinodal effect in crystallization, such as divergence in the characteristic fluctuation length and vanishing of the free energy barrier.

Pressure induced phase transitions of SiO_2 from metadynamics

Davide Donadio, R. Martonak and M. Parrinello

Silica is the main component of Earth's crust and a technologically very important material. Its phase diagram is characterized by the appearance of many metastable phases and marked hysteresis [7]. An understanding of its transition mechanisms offers the key to its complex behavior and properties. The high-pressure behaviour of silica has been the subject of several experiments supplemented by an intense theoretical activity, which lead to the discovery and characterisation of several new stable and metastable phases [8,9]. Nevertheless, the atomic-scale characterisation of the transition paths and the interpretation of some experimental results are still serious challenges.

We have devised an improvement of the metadynamics method [10] that allows for the simulation of pressure induced phase transitions of silica close to the experimental conditions. By combining metadynamics with classical and ab initio molecular dynamics we have successfully elucidated the subtle stepwise transition mechanisms that lead to the transformation of low-density 4-fold coordinated silica polymorphs to 6-fold high-density phases [11,12,13]. Our simulations shed light on the transformation path from quartz to stishovite [11,12], that occurs via the formation of two metastable phases that were previously observed in experiments. The analysis of the atomic-scale details of the transitions (Fig. 2) provides a valuable insight in the possible deformation mechanisms of the high-pressure phases of SiO_2 with broad implications in seismology and geosciences.

We also predict that on compression four-fold coordinated coesite will transform into the post-stishovite α-PbO-type phase – even within the stability domain of stishovite, and we are able to suggest how to modify the experimental protocols to observe such transition.

Computational Study of Molecular Nano-Machines

Paolo Raiteri, Giovanni Bussi, Clotilde S. Cucinotta and Michele Parrinello

In this project we focused on a bistable rotaxane which was specifically designed to achieve a photo-induced shuttling movement of its ring component in solution [14]. This compound has a

modular structure; its ring component R is a π-electron donating macrocycle, whereas its dumbbell component is made of several covalently linked units. They are a Ruthenium complex as the photosensitizer and stopper, a rigid spacer, and two π-electron accepting stations (A1 and A2, see figure 3), and a tetraarylmethane group as the terminal stopper. The Ru-based unit plays the dual role of a light-fueled power station and a stopper, whereas the mechanical switch consists of the two electron accepting stations and the electron-donating ring. Six hexafluorophosphate ions (PF_6^-) are present in the acetonitrile solution as the counter-anions of the positively charged rotaxane. The stable translational isomer of the Rotaxane in the ground state is the one in which the R component encircles A1.

The strategy devised to obtain the photoinduced shuttling movement of the ring between the two stations is based on a 'four stroke' synchronized sequence of electronic and nuclear processes. Light excitation of the photoactive unit is followed by the transfer of an electron from this unit to A1. After the reduction of this unit, with the consequent 'deactivation' of the A1 station, the ring moves by 1.3 nm towards the other station, A2. Eventually, a back electron-transfer from the 'free' reduced station to the oxidized unit restores the electron acceptor power to this radical cationic station. As a consequence of the electronic reset, thermally activated back movement of the ring takes place.

Due to the complexity of these systems and to the high activation barriers there is a time scale problem. In fact, the switching mechanism occurs on the time scale of milliseconds to minutes. This time scale cannot be simulated by straightforward MD. However, a combination of computer power and a wide range of novel computational techniques including classical molecular dynamics, umbrella sampling (US) in the Weighted Histogram Analysis Method approach, ab-initio Density functional theory based calculations and Coarse grained (CG) models rendered the study of this problem affordable.

The calculated free energy profile related to the ring movement confirmed the experimental findings about the relative stability of the different co-conformations in the two oxidation states of the bistable rotaxane. However, the observed shuttling kinetics could not be reproduced computationally if the role of the counter-anions was not explicitly taken into account. A combination of ab-

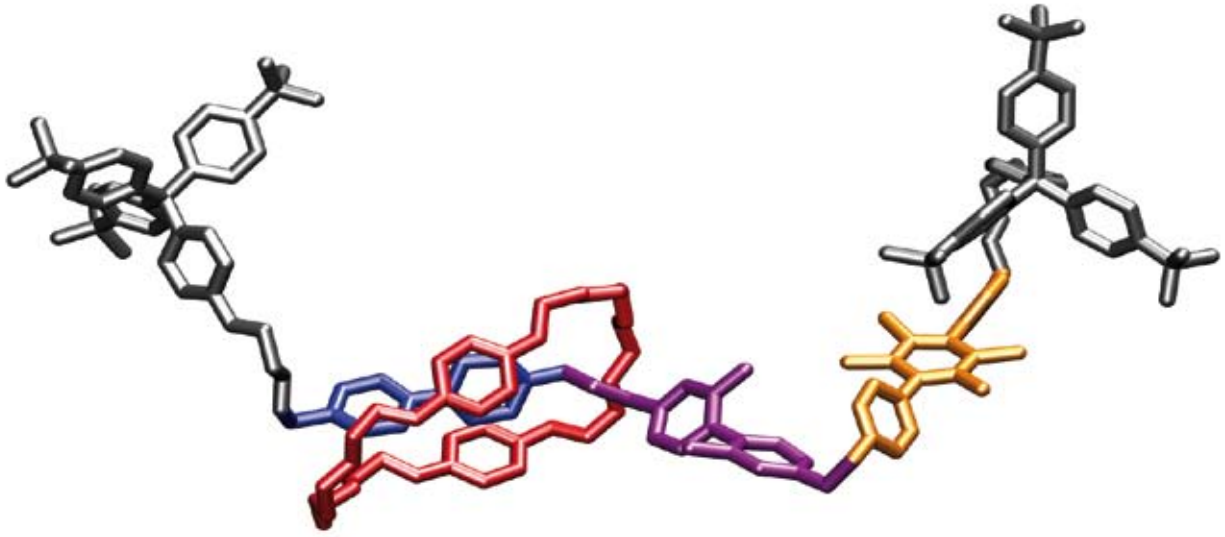

Figure 3: Licorice representation of the [2] Rotaxane studied in this project. The various building blocks are the electron donor macrocycle (red), the electron acceptor stations A1 (blue) and A2 (purple) the rigid spacer (yellow) and the stoppers (gray). In our simulation the Rull photosensitizer has been substituted with a copy of the other stopper).

initio and CG approaches, have, indeed, shown that the anions are strongly bonded to the axle of the dumbbell component, and that their decomplexation from the rotaxane framework may be the rate-limiting step in the translational isomerization process. US calculations have also demonstrated that the shuttling movement is almost barrierless in the absence of the counter-anions. Therefore, if the interaction between the positively charged rotaxane and its counter-anions could be weakened, e.g., by changing the nature of the solvent or the counter-anion, this molecular shuttle might work as a fast-switching, power-stroke nano-machine. Experiments in this direction are not straightforward because of solubility issues and difficulties related to counter-anion exchange for Rotaxane. Nonetheless, experiments to test this hypothesis are already underway in the laboratories of Prof. Balzani at the University of Bologna.

References

1. J. W. Gibbs (1878). Collected works. Vol. 1. Thermodynamics. Longmans, Green & Co., London.
2. P. G. Debenedetti (2006). Thermodynamics – When a phase is born. Nature, 441, 168.
3. W. C. Swope, H. C. Andersen (1990). 10^6 particle molecular dynamics study of homogeneous nucleation of crystals in a supercooled atomic liquid. Phys. Rev. B 41, 7042.
4. D. Moroni, P. R. ten Wolde, P. G. Bolhuis (2005). Interplay between structure and size in a critical crystal nucleus.
5. F. Trudu, D. Donadio, M. Parrinello (2006). Freezing of a Lennard-Jones fluid: from nucleation to spinodal regime. Phys. Rev. Lett. 97, 105701.
6. E. Sanz, C. Valeriani, D. Frenkel, M. Dijkstra (2007). Evidence of out-of-equilibrium crystal nucleation in suspensions of oppositely charged colloids. Phys. Rev. Lett. 99, 055501.
7. R. J. Hemley, C. T. Prewitt, K. J. Kingma (1994). Silica - Physical Behaviour, Geochemistry, and Materials Applications 41 (Rev. Mineral. Vol. 29, MSA,Washington DC).
8. K. J. Kingma, R. J. Hemley, H. K. Mao, D. R. Veblen (1993). New high-pressure transformation in α-quartz. Phys. Rev. Lett. 70, 3927.
9. J. Haines, J. M. Leger, F. Gorelli, M. Hanfland (2001). Crystalline post-quartz phase in silica at high pressure. Phys. Rev. Lett. 87, 155503.
10. R. Martonak, A. Laio, M. Parrinello (2003). Predicting crystal structures: The Parrinello-Rahman method revisited. Phys. Rev. Lett. 90, 075503.
11. R. Martonak, D. Donadio, A. R. Oganov, M. Parrinello (2006). Crystal structure transformations in SiO_2 from classical and ab initio molecular dynamics. Nat. Mater. 5, 623.
12. R. Martonak, D. Donadio, A. R. Oganov, M. Parrinello (2007). From 4- to coordinated silica: transformation pathways from metadynamics. Phys. Rev. B, 76, 014120.
13. D. Donadio, R. Martonak, P. Raiteri, M. Parrinello (2008). Influence of temperature and anisotropic pressure on the phase transitions in a-cristobalite. Phys. Rev. Lett. 100, 165502.
14. V. Balzani, M. Clemente-León, A. Credi, B. Ferrer, M. Venturi, A. H. Flood, J.F. Stoddart, Proc. Natl. Acad. Sci. USA 2006, 103, 1178-1183

Atomic Scale Modelling at Semiconductor-Oxide Interfaces

Prof. Alfredo Pasquarello

CSEA-ITP-SB, EPF Lausanne, Switzerland

The general goal pursued within the project *Atomic Scale Modelling at Semiconductor-Oxide Interfaces* consists in the computational study of atomic-scale phenomena in materials as far as both the structural and electronic properties are concerned. The aim is to complement experiment by providing a realistic description of the mechanisms occurring on the atomic and nanometer scale. This is achieved by accurately accounting for the interactions between atoms within a quantum mechanical description of the electronic structure, based on density functional theory. Currently, the research activity focuses on semiconductor-oxide interfaces [1-7] and on the catalytic growth of carbon nanotubes [8].

The major research project focused on defects affecting the electrical performance at the technologically relevant Si-SiO_2-HfO_2 gate stack. This gate stack is expected to replace the conventional Si-SiO_2 interface in new-generation silicon-based devices, provided remaining issues related to defects can be overcome. Our work aimed at determining the electronic defect levels with respect to the relevant band edges, in order to identify the nature of the defects responsible for the unsatisfactory electrical performance. A theoretical study of this nature faces several difficulties. These include on one hand the realization of a realistic model structure of the Si-SiO_2-HfO_2 gate stack (Fig. 1) and on the other hand the use of a sophisticated electronic-structure method in order to locate the defect levels within the band gap [1-2].

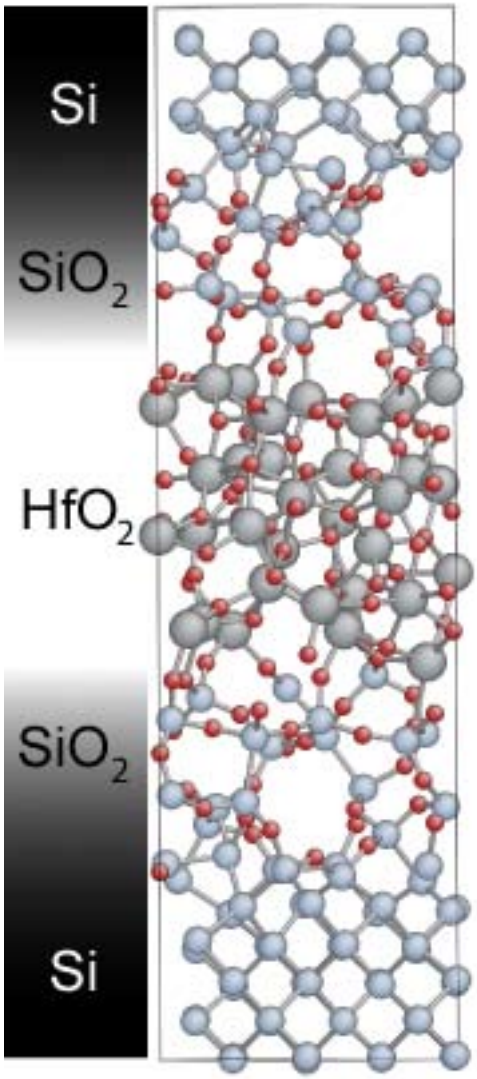

Figure 1: Atomic structure of a model structure of the Si-SiO_2-HfO_2 gate stack.

Indeed, it should be noted that state-of-the-art electronic methods based on semi-local approximations, such as the local density approximation or the generalized gradient approximation to density functional theory (DFT), are inappropriate for this purpose because electron band gaps are severely underestimated within those schemes. In

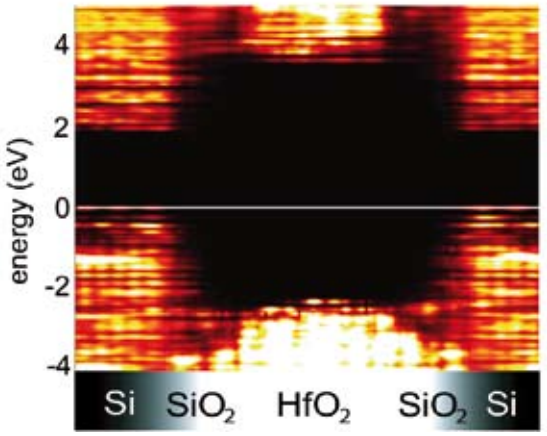

Figure 2: Band diagram of the Si-SiO_2-HfO_2 gate stack calculated with a hybrid density functional.

our study, we combined first principles molecular dynamics for model generation and hybrid density functionals for electronic-structure calculations, yielding a band diagram (Fig. 2) in close agreement with experiment. The availability of a reliable band diagram allows us then to study specific defect levels. In particular, we determined the charge transition levels of the oxygen vacancies located in the crystalline HfO_2 and in the noncrystalline transition region with respect to the silicon band edges. The study is complemented by the determination of the pinning levels associated to the oxygen vacancy levels. Our investigation reveals that the oxygen vacancies in crystalline monoclinic HfO_2 cannot be at the origin of the Fermi-level pinning. The energetics favor oxygen vacancies residing in the amorphous transition layer. Furthermore, the calculated pinning levels of these vacancies are consistent with experimental observations. We also studied oxygen vacancy migration in monoclinic HfO_2 and across its interface with SiO_2, finding that only the doubly positive charge state is eligible for long-range diffusion [3]. In addition to the oxygen vacancy defect, we also investigated the charge states of the hydrogen impurity and their most favorable location in the gate stack [4,5].

A second goal pursued within this project is the modeling of atomistic processes occurring during the catalytic growth of carbon nanotubes (CNTs). Carbon nanotubes are expected to become an important constituent of many technologies, in particular of future generation electronics. The inability of performing growth of CNTs with predetermined chirality indices, and thus electronic properties, is the major obstacle on the way to incorporating CNTs into electronic devices. The chemical vapor deposition (CVD) growth of CNTs catalyzed by metallic nanoparticles is believed to be the most promising approach for reaching this goal. For a long time, the catalyst composition has been limited to iron-group metals and their alloys. However, it has recently been shown that metallic nanoparticles of many other metals, including chemically inert coinage metals, are also able to act as catalysts in the CVD growth process. This called for a comprehensive study of the role of the metal catalyst chemical composition to achieve optimal growth conditions and enhance the preference for definite chiralities. Using first principles methods, we systematically studied the crucial steps of CVD growth of CNTs, the binding and the

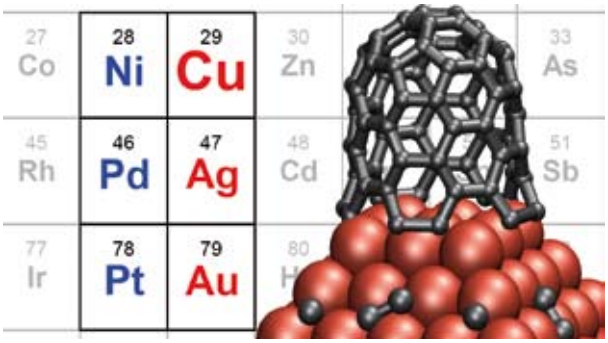

Figure 3: Schematic representation of the catalytic growth of carbon nanotubes. The investigated metals are shown in background.

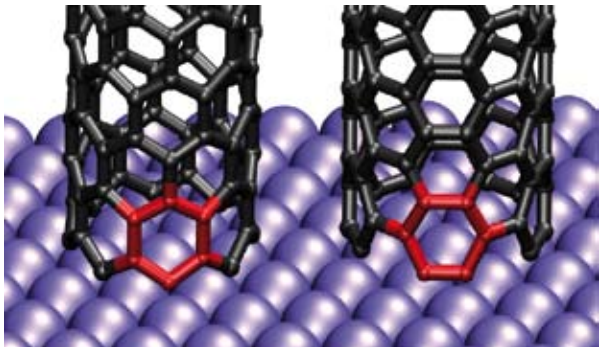

Figure 4: Growing nanotubes of different chirality: zigzag (left) and armchair (right).

diffusion of the carbon feedstock as well as the nucleation of CNTs (Fig. 3) [8]. Late transition (Ni, Pd, Pt) and coinage (Cu, Ag, Au) metal catalysts were investigated. For all metals, we considered various diffusion mechanisms including both surface and subsurface channels, finding the lowest activation barriers for carbon adatoms on nanoparticles of coinage metals. For these metals, our calculations further showed that the diffusion is restricted to the nanoparticle surface when diatomic carbon is initially obtained from the decomposition of the precursor gas. From the binding energies of armchair and zigzag edges of CNT fragments (Fig. 4), we inferred a high preference for the growth of armchair CNTs on Cu nanoparticles. These results indicate that coinage metal catalysts, in particular Cu, favor CVD growth of CNTs at low temperatures and with narrow chirality distributions.

References

1. P. Broqvist, A. Alkauskas, and A. Pasquarello, Appl. Phys. Lett. 92, 132911 (2008).
2. P. Broqvist and A. Pasquarello, Appl. Phys. Lett. 90, 082907 (2007).
3. N. Capron, P. Broqvist, and A. Pasquarello, Appl. Phys. Lett. 91, 192905 (2007).
4. J. Godet, F. Giustino, and A. Pasquarello, Phys. Rev. Lett. 99, 126102 (2007).
5. J. Godet, P. Broqvist, and A. Pasquarello, Appl. Phys. Lett. 91, 262901 (2007).
6. F. Devynck, F. Giustino, P. Broqvist, and A. Pasquarello, Phys. Rev. B 76, 075351 (2007).
7. F. Devynck, Z. Sljivancanin, and A. Pasquarello, Appl. Phys. Lett. 91, 061930 (2007).
8. O. V. Yazyev and A. Pasquarello, Phys. Rev. Lett. 100, 156102 (2008).

Atomistic simulation of surface-supported molecular nanostructures and of quasicrystal surfaces

Dr. Daniele Passerone

with Carlo Pignedoli

Swiss Federal Laboratories for Materials Testing and Research (EMPA), Duebendorf, Switzerland

General Interests

The main theme of our research is the application of advanced computational methods to the field of surface and interface science, with particular interest to applied nanochemistry and materials science experimentally developed at Empa. For periodic systems and slabs of medium size with adsorbates, and in particular in the case of metallic substrates, we adopt the codes q-Espresso and CPMD; for systems with more extended unit cell (up to 1000 atoms and more) like quasicrystals, we mostly adopt the code cp2k; a deeper insight into the chemical properties of the bonding of molecular nanostructures can be derived from gas phase calculations performed with the program Gaussian and GAMESS.

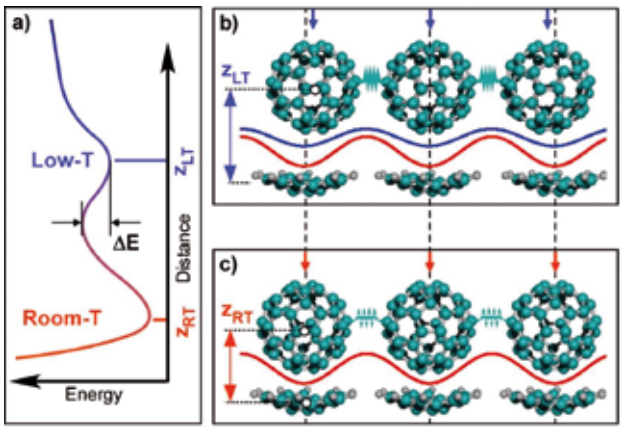

Figure 1: Schematic 1D model of the bistable behavior for a C_{60} island on a non-perfectly matched COR substrate

Projects performed at CSCS

Molecular nanostructures: the example of host-guest C_{60}-based systems [1]

Corannulene (COR) buckybowls were proposed as near ideal hosts for fullerene C_{60}, but direct complexation of C_{60} has remained a challenge in supramolecular chemistry. Experiments performed in our department at Empa reported the formation of surface-supported Corannulene-C_{60} host-guest complexes by deposition of C_{60} onto a COR lattice on Cu(110). Variable-temperature scanning tunneling microscopy studies reveal two distinctly different states of C_{60} on the corannulene host lattice, with different binding energies and bowl-ball separations. The transition from a weakly bound precursor state to a strongly bound host-guest complex is found to be thermally activated (fig. 1).

In order to understand the interaction between corannulene and fullerene, we performed high level MP2 calculations in the gas phase for these two molecules. We computed the binding energy with different basis sets and we corrected the results with respect to the basis set superposition error (BSSE) using the counterpoise method as implemented in the GAMESS code.

In order to compute the binding energy, we subtracted the energy of the single fragments from the total energy of the COR-C_{60} complex and we obtained 1 eV, 1.4 eV and 1.7 eV for the basis sets of 631-G, 631-G(d,p) and cc-pVdZ, respectively. After basis set superposition error (BSSE) correction, the results become 0.7 eV, 0.76 eV and 1.07 eV, respectively. We observe no significant charge transfer (<0.05 electrons both in the

Mulliken and in the Lowdin representation).
The experimental observation of a bistable behavior for small fullerene islands on a COR substrate suggests an analogy with the well-known Frenkel-Kontorova model [2]. When this model is applied to infinite overlayers with different natural lattice parameter with respect to the substrate, the system must find a compromise between lateral interactions and substrate pinning. This inter-play can generate commensurate regions, dislocations, and solitons.

In our case, the overlayer is a finite island of fullerenes on a COR substrate, which has a different set of lattice parameters. A single fullerene always prefers to sit in the minimum of the substrate potential, but an island of a few molecules can profit of the lateral cohesive energy. If, however, the equilibrium lateral distance within the island is different from the substrate periodicity, the C_{60} molecules must pay a price to the substrate potential. This 'price' is lower if the island is lifted from the substrate by a certain amount. The question is whether this behaviour could give rise to distinct stable or metastable states for the adsorbed island.

In order to verify this possibility, we generated a simple one-dimensional (1D) model for concurrent lateral and substrate potential interactions. The lateral interaction between two C_{60} at a distance r was taken as a realistic average potential, the substrate potential was modelled as a trigonometric function of period corresponding to the COR experimental lattice spacing, with an amplitude exponentially decaying with height. Using the above two potentials, the energy of an island made of N C_{60} molecules was minimized as a function of the position of the individual molecules. For a size of the C_{60} island larger or equal than N=6 there appears a bistability: two distinct minima of the potential energy are found. The absolute minimum corresponds to all fullerenes sitting at a height z=0 (the RT state deep in the COR bowl), and the secondary minimum to an island floating further above the surface.

Once the two minima were found, we used a two-point band optimization method to estimate the barrier between the two states [3]: the one with all balls at z=0 and the one with the majority of balls at a higher altitude. We show the corresponding results in Figure 2. We observe that for N=12 there is a barrier between the two states, that is lowered as the size of the chain is reduced (N=10 and N=8). Eventually, for N<6, we could not find "high" solutions anymore.

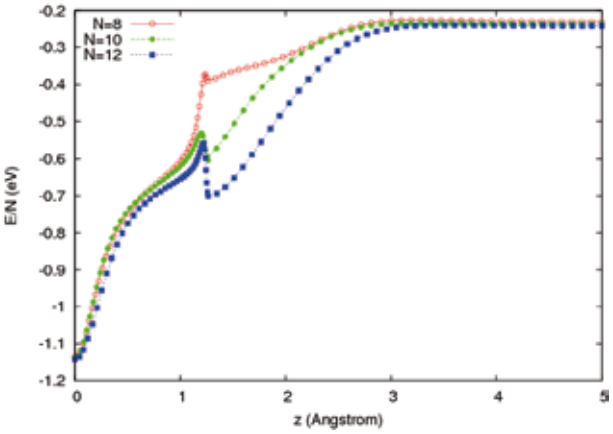

Figure 2: Bistable behavior as a function of height of the one-dimensional model presented in the text. With the model substrate potential a chain with N=12 fullerenes has two minima separated by a barrier of about 0.18 eV (blue). The energy of the secondary minimum increases and the barrier is lowered as the size of the chain is reduced to N=10 and N=8 (green curve and red curve, respec-tively).

Quasicrystals

Description

μAl_4Mn is a complex crystal that presents most of the peculiarities of the AlMn quasicrystalline system [4]. Recent experimental STM measurements at Empa revealed surprising features for the μAl_4Mn(0001) surface. From a low temperature STM scan at the surface it is evident the presence of terraces with height 0.5 (with respect to the lattice constant in the direction perpendicular to the surface). Less frequent steps of height 0.25 also occur (Fig. 1 top). Among the different theoretically possible terminations of the (0001) surface only two are observed experimentally namely z=0.25 (occurring with high probability) and z=0.5 (Fig 3). To unravel the origin of this unexpected finding and to model empirical potentials suitable

for large scale simulations of real AlMn quasicrystals, we performed ab initio DFT calculations using super-cells containing up to 600 atoms.

Achievements

For the ab initio calculations we used the cp2k code with Goedecker [5] pseudopotentials for Al and Mn (3s and 3p semicore electrons of Mn were included in the valence). A cutoff of 320 Ry for the plane wave expansion of the charge density was used.

We focused our attention on the z=0.5 (A) and z=0.25 (B) surfaces observed experimentally; we used the repeated slab geometry with a cell containing a bulk μAl4Mn unit with an additional layer in order to have both sides of the slab with (A) or (B) termination (see Fig 3 bottom).

Starting from the fully relaxed bulk structure (containing 100 Mn atoms and 458 Al atoms) we obtained slab A (128 Mn and 485 Al) and slab B (129 Mn and 482 Al). The calculation of the relative energy of surface A and B is a powerful tool to quantify the experimental evidence. However, for this particular system, this approach is not straightforward: the system is non stoichiometric so that addition of a surface layer do not correspond to an exact fraction of a bulk system. Moreover slabs A and B have a different number of atoms for both atomic species. The only way to define a relative stability for the two surfaces is to take into account the chemical potential of the atomic constituents: μ_{Al} and μ_{Mn}. Given the value of the chemical potentials and the total energy of each slab provided by the ab initio calculation, the relative stability of surface A with respect to surface B is defined by

$$\Delta E_{AB}=E_A-E_B-\Delta_{nAl}\mu_{Al}-\Delta_{nMn}\mu_{Mn}$$

Where Δ_{ni} is the difference between the number of atoms of “i” type in system B with respect to system A.

The value of μ_i is defined by the experimental conditions and only boundaries to it can be given by ab-initio calculations: the energy of an isolated atom of specie i defines the lower level of mi representing a system in equilibrium with a gas of atomic species. The energy of the most stable compound of species i define the highest possible value of μ_i where the system is in equilibrium e.g. with bulk Al and bulk Mn.

The surfaces observed experimentally are obtained by ion sputtering and subsequent annealing of a μAl_4Mn sample. A reasonable value for the chemical potentials of Al and Mn in this case is a value ranging from equilibrium with the bulk system and the energy cost of taking Al and Mn atoms directly form the surface of the crystal. To estimate μ_{Al} and μ_{Mn} in the case of extraction from the surface we calculated the formation energy of Al and Mn observed vacancies. In the extreme case of μ_{Al} and μ_{Mn} defined as the cost paid to form a surface vacancy our calculation reveal that formation of B is favored with respect to A by ~1.1 eV per surface unit confirming the experimental finding.

Work in progress

The ab initio calculations performed up to now will be used to fit a reliable empirical potential [6,7] that will allow simulating the surface tribological properties of real quasicrystalline AlMn systems. The analysis of the electronic structure of the optimized surfaces will allow a complete determination of the different features of the STM measurements.

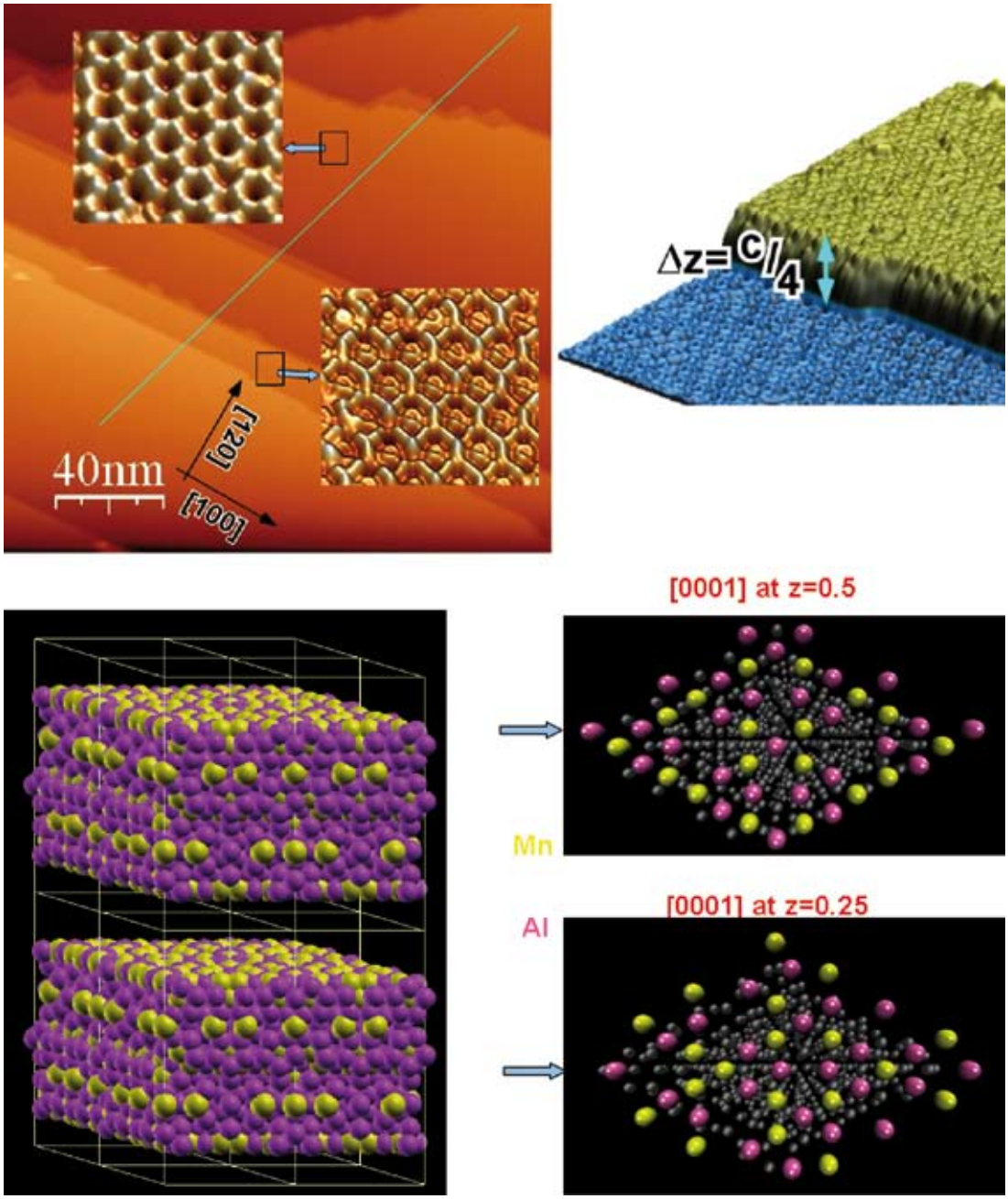

Figure 3 Top: STM scan of a mAl4Mn(0001) surface. The regions of different brightness are terraces divided by a step. Wide terraces are separated by a step of 0.5 c; narrow terraces are separated by a step of 0.25 c height (in the unit cell of μAl4Mn c=29.67 A). Bottom left: 2x2x2 repetition of the slab used for the surface calculations. Bottom right: surface layer for the z=0.5 surface (surface A) and for the z=0.25 surface (surface B). Yellow/pink balls are Mn/Al atoms.

References

1. W. Xiao, D. Passerone, P. Ruffieux, K. A. Mansour, O. Gröning, E. Tosatti, J. Siegel and R. Fasel, J. Am. Chem. Soc. 130, 4767 (2008).
2. Kontorova T.; Frenkel, Y. I.; Zh, Eksp. Teor. Fiz. 1938, 8.
3. Czerminski, R.; Elber, R. Int. J. Quantum Chem. 1990, Suppl. 24, 167.
4. C. B. Shoemaker, D. A. Keszler, D. P. Shoemaker, Acta Cryst. B45, 13 (1989)
5. S. Goedecker, M. Teter, and J. Hutter, Phys. Rev. B 54, 1703 (1996).
6. F. Ercolessi, J.B. Adams, Europhys. Lett. 26, 583 (1994)
7. P. Brommer, F. Gähler, Phil. Mag. 86, 753 (2006)

Modelling and Reconstruction of the North Atlantic-Climate System Variability (MONALISA-II)'

Dr. Christoph C. Raible

with T. F. Stocker, D. Hofer, T. Buehler, S. Kleppek, M. Renold, and K. Bieri

Climate and Environmental Physics, Physics Institute, University of Bern, and Oeschger Centre for Climate Change Research, Bern, Switzerland

Description

The project MONALISA-II is embedded in the National Centre of Competence in Research (NCCR) Climate. The project aims to improve our understanding of natural climate variability on decadal to centennial time scales during the last millennium focusing on the North Atlantic region. Climate reconstructions combining proxies from tree rings, ice cores, and documentary data deliver a first hint of climate variability of the past millennium [1]. However, reconstructions mainly suffer from the fact that they are sparsely resolved in space and time. Thus, to investigate the underlying mechanisms of decadal to centennial variations, climate model simulations are used in MONALISA-II. A set of different ensemble simulations are carried out at the Swiss National Supercomputing Centre with the Community Climate System Model, provided by the National Center for Atmospheric Research (Boulder, Co, USA). Three ensembles, each with six members covers the periods from 1000-1300, from 1640-1715, and from 1500-2000, respectively. Additionally, we conducted several sensitivity experiments with the focus on processes between atmosphere, ocean, and sea ice under different climate conditions. This allows us to detect thresholds which could be responsible for abrupt changes in the North Atlantic.

Achievements

A climatologic outstanding period during the last millennium is the Maunder Minimum (MM) from 1645-1715, which is characterized by low solar activity and a series of volcanic eruptions. This period was already a focus of the prior phase of the project. In an additional study, we investigated the mid-latitude cyclone characteristics, in particular the extreme behaviour in the MM ensemble simulations [4]. Proxy data [3] give evidence that storminess in Northern Europe substantially increased around the MM, compared with earlier and later time periods. These proxy results are compared with the MM simulations to gain insights of the underlying mechanisms. The modelling result suggests for winter that cyclones travel more zonally and shift southward in the MM relative to today (Fig. 1a). This means that the number of cyclones is on average decreased over northern Europe. Additional cyclone characteristics, like cyclone intensity and their extreme statistics, show that even in areas where the number of cyclones decreases the extreme cyclone intensity significantly increases in winter. We showed that the meridional temperature gradient (Fig. 1b) plays a key role in intensifying these extreme cyclones as well as the increase of lower level baroclinicity in the North Atlantic, when comparing the MM with today.

Another research focus is to the period 1500-2000. In particular, we investigated the teleconnection pattern in the Northern Hemisphere [2].

Reconstructions and the ensemble simulations from 1500-2000 suggest that the pattern and the connection strength (correlation between the centres of action) are not stable on decadal time scales in the North Atlantic-European region. Comparing the reconstructions with the simulations, we found that there might be a connection between the external natural (solar and volcanic) forcing and certain teleconnection pattern in the reconstruction, whereas the ensemble mean of the simulations gives no evidence for such a link. Preliminary tests, using the reconstruction method in the model world show that the method and the decrease of available proxy data lead to an underestimation of the variability of teleconnection patterns in the North Atlantic European region, mainly due to the fact that the number of degrees of freedom is reduced.

Another study deals with the mechanisms which generate and maintain a persistent decadal oscillation of the meridional overturning circulation (MOC) that we found in two of the six 1500-2000 simulations [7]. These oscillations only occur in the two simulations which are initialised by rather cold conditions leading to a completely sea ice covered Nordic Sea. The process involves an anomalous transport of salt and density in the North Atlantic subpolar gyre. Moreover, the North Atlantic Oscillation (NAO) connected to the MOC acts on the gyre circulation in which sea ice of the Labrador Sea generates a large local thermal anomaly increasing the meridional temperature gradient. The latter one leads to a NAO-like equivalent barotropic response of the atmospheric circulation via synoptic eddy activity, closing the positive feedback. For the first time, we found and explained a coupled atmosphere-ocean sea ice mode in a fully coupled general circulation model.

Sensitivity experiments with a freshwater forcing applied to the North Atlantic led to a series of publications within the last two years [5, 6]. One study deals with the robustness of the bipolar seesaw with respect to freshwater hosing experiments with and without global salt compensation [5]. Both forcing approaches strongly reduce the Atlantic MOC and led to a warming in the South. However, south to 40°S the compensated experiment exhibits a warming, whereas the experiment without compensation shows no signal. A further analysis shows that this warming is mainly due to heat

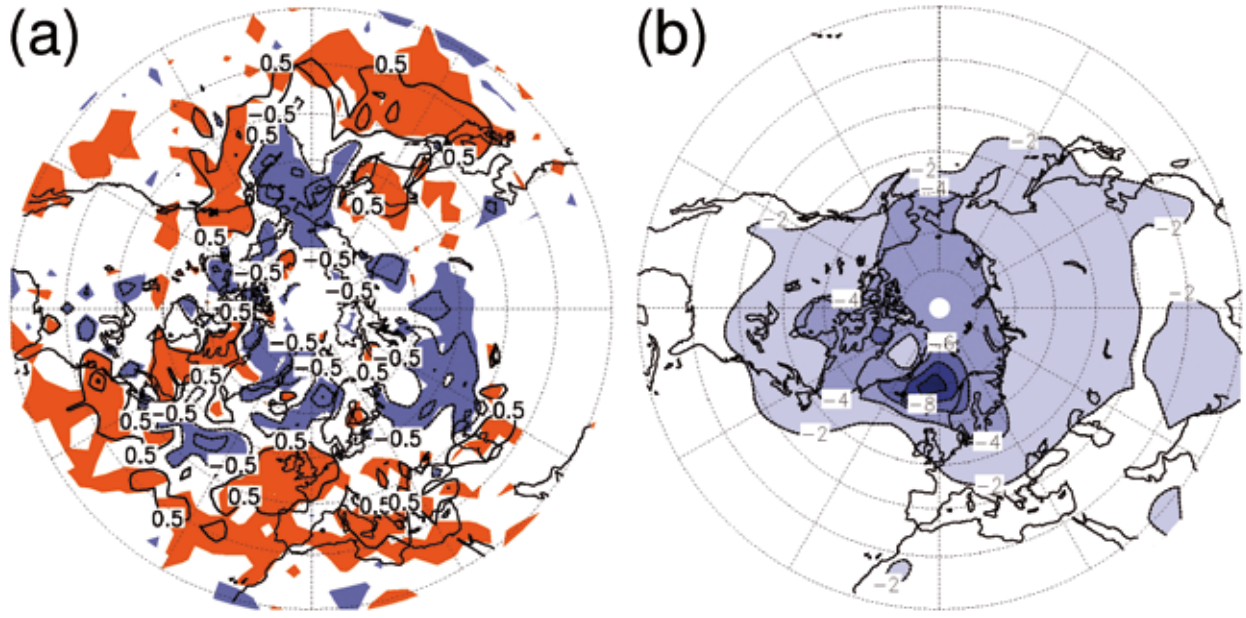

Figure 1: Simulated change in (a) cyclone density and (b) temperature between the ensemble of Maunder Minimum and the present day control simulation.

transport anomalies that are induced by the specific parameterization that represent eddy mixing. Additionally, these experiments enter in another study investigating the influence of a weakening of the Atlantic MOC on the tropical Pacific climate. Due to changes of tropical Atlantic SSTs the atmospheric circulation impacts the tropical eastern Pacific climate. The analysis further suggests that the existence of the present-day tropical Pacific cold tongue complex and the annual cycle in the eastern equatorial Pacific are partly controlled by the strength of the AMOC with possible implications on the interpretation of paleo-proxy data.

References

1. Casty, C., C. C. Raible, T. F. Stocker, H. Wanner, and J. Luterbacher, 2007: A European pattern climatology 1766 - 2000, Climate Dynamics, 29, 791-805
2. Raible, C. C., C. Casty, J. Luterbacher, A. Pauling, J. Esper, D. C. Frank, U. Büntgen, A. C. Roesch, P. Tschuck, M. Wild, P.-L. Vidale, C. Schär, H. Wanner, 2006: Climate variability-observations, reconstructions, and model simulations for the Atlantic-European and Alpine region from 1500-2100 AD, Climatic Change, 79, 9-29.
3. Raible, C. C., R. De Jong, T. F. Stocker, M. Yoshimori, 2008: On the ability of GCM simulations and the interpretation of wind and moisture-sensitive proxies, Pages Newsletter, 16, 10-11.
4. Raible, C. C., M. Yoshimori, T. F. Stocker, C. Casty, 2007: Extreme midlatitude cyclones and their implications to precipitation and wind speed extremes in simulations of the Maunder Minimum versus present day conditions, Climate Dynamics, 28, 409-423.
5. Stocker, T. F., A. Timmermann, M. Renold, O. Timm, «Effects of salt compensation on the climate model response in simulations of large changes of the Atlantic meridional overturning circulation, Journal of Climate, 20, 5912-5928, 2007
6. Timmermann, A., Y. Okumura, S.-I. An, A. Clement, B. Dong, E. Guilyardi, A. Hu, J. H. Jungclaus, M. Renold, T. F. Stocker, R. J. Stouffer, R. Sutton, S.-P. Xie, J. Yin, 2007: The influence of a weakening of the Atlantic meridional overturning circulation on ENSO, Journal of Climate, 20, 4899-4919.
7. Yoshimori, M., M. Renold, T. F. Stocker, and C. C. Raible, 2008: Simulated decadal oscillations of the Atlantic meridional overturning circulation in a cold climate state, Climate Dynamics, submitted.

Websites related to the MONALISA-2 project

NCCR-Climate: http://www.nccr-climate.unibe.ch

MONALISA-II: http://www.nccr-climate.unibe.ch/projects/project_en.html?ID=P%201.1

Fluid mechanics of avalanches

Martin Rentschler

Environmental Hydraulics Laboratory, ENAC, EPF Lausanne, Switzerland

Description

In nature, geophysical flows such as mudflows, lahars, snow avalanches and debris flows are potentially very destructive phenomena that regularly cause damage to infrastructure, houses and people. To understand the involved processes and to develop practical tools for engineers to predict these kind of events, we investigate the dynamics of these time-dependent flows of complex non-Newtonian fluids. To do so, we analyse numerically and experimentaly on the laboratory scale a given model fluid which mimics the behavior of these gravity driven flows. Using a simple shear experiment (Couette cell) we measure the rheological properties of the fluid which are used as parameters for the constitutive equation of our numerical model. We simulate then a time-dependent flow down an inclined plane. We finally compare the numerical results with laboratory experiments of a dam break down an inclined plane.

The fluids involved in gravity driven geophysical flows being two-phase materials, i.e. snow and air or soil and water, the rheological properties are still not fully understood. When the characteristic length and time scales of the different phases are on the same order of magnitude, there is a complex coupling between both phases that makes most continuum-mechanics models used so far of limited interest.

The other approach used here is to treat the mixture as a single phase fluid with a non-Newtonian rheological behavior. The most important feature of those geophysical flows is the existence of a yield stress. While the stress is below this threshold, the fluid stays at rest. Once the internal stress exceeds it, the mixture starts to flow like a viscous fluid. Below the yield stress, the viscosity should go to infinity in order to correctly represent the solid state of the material. In practice this is not possible, and so we have to limit the viscosity at some point. The characteristic timescale associated with this viscosity must be of orders of magnitude higher than the duration of the experiment so as to avoid any effects of the limited viscosity on the numerical computations.

In situ measurements of geophysical flows are very difficult and the uncertainties on the initial conditions impede the validation of models by those flows. To overcome this problem, we conduct well controled experiments on the lab scale using an alternative material, Carbopol, which mimics the viscoplastic behaviour of those mixtures. It allow us to perform quantitative comparisons with the proposed model. Our test case is the release of a finite amount of fluid on the top of an inclined plane, measuring the flow by capturing the three dimensional position of the free-surface in real time.

The first step in the development of a code able to simulate those geophysical flows is to predict correctly the laboratory experiment by measuring the shear-dependant viscosity function independently in the Couette cell. The temperature dependence is

eliminated by fixing the room temperature within 0.1 °C. This viscosity function is measured with a commercial rheometer and it takes the form of a Herschel Bulkley fluid.

Achievements

For the numerical simulation we used a standard biphasic Navier-Stokes solver thatwe equipped with a semi-implicit solver for the stokes part of the equation. With the numerical simulation we confirmed the existence of a plug layer over a highly sheared layer. The position of the surface between both states were subject of some scientific discussion.

The position of the front as well as its shape was well predicted, only the long term development of the front position didn't match. At this time of the flow one can observe in the numerical simulations that a very thin layer is still sheared, whereas most of the fluid already became a bulk. This flow behaviour in the experiment is not covered by the simulations, which might be due to some aberration of the rheology for flows in small length scales. This hypothesis is supported by the observation that Carbopol tends to form small scale inhomogeneities in the length scale of 10 to 100 micrometer.

The shape of the front is a phenomena that formerly was associated to surface tension. We could observe that even without surface tension such a shape can be observed. Analysing the velocity profiles, we found that it comes from a kind of rolling behaviour at the front of the flow. These results are subject to discussion and on the way to be published.

The simulation showed that for this type of flow it is sufficient to describe the properties of the fluid by a viscosity function which only depends on the shear rate. I.e. we are not forced to use a full stress tensor to characterize a fluid, but it is sufficient to treat it as an isotropic Reiner-Rivlin fluid. In the future, where we want to treat more complex fluids, i.e. granular suspensions, this may be no longer the case.

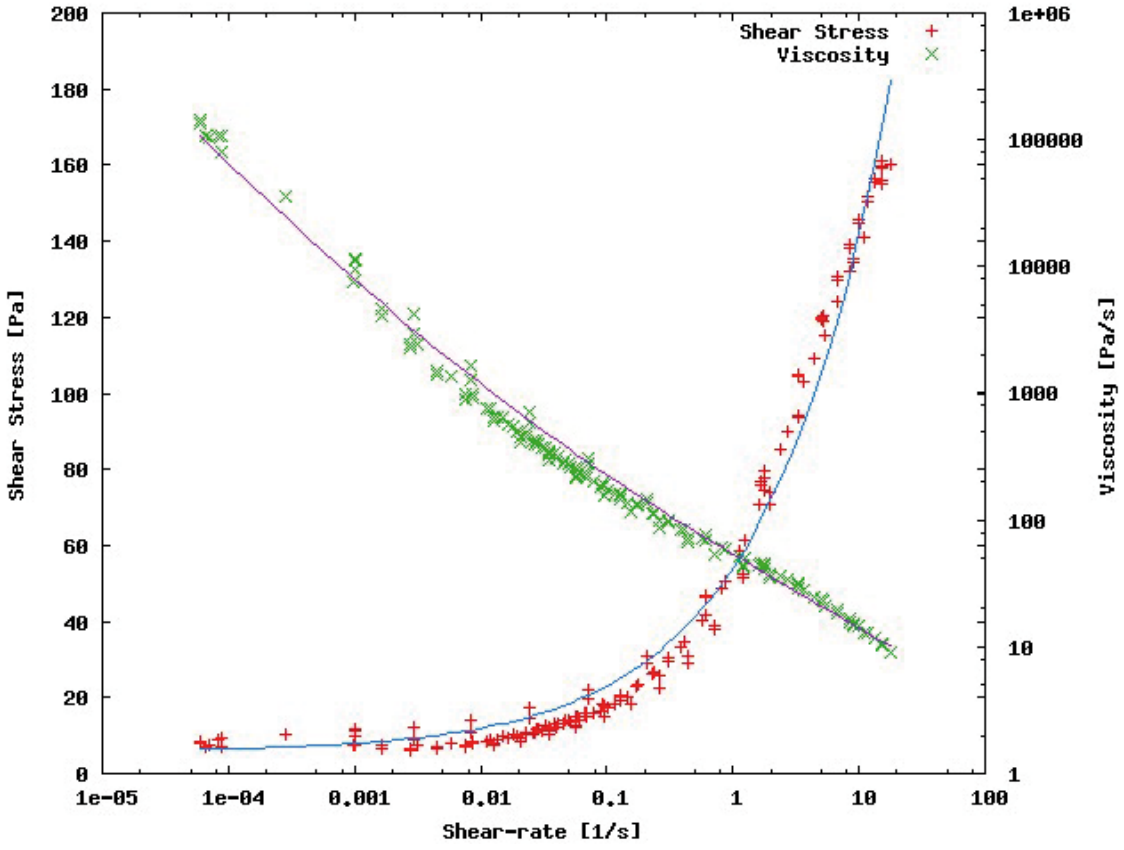

Figure 1: Shear-rate versus Viscosity and Stress. Measured data and theoretical curve.

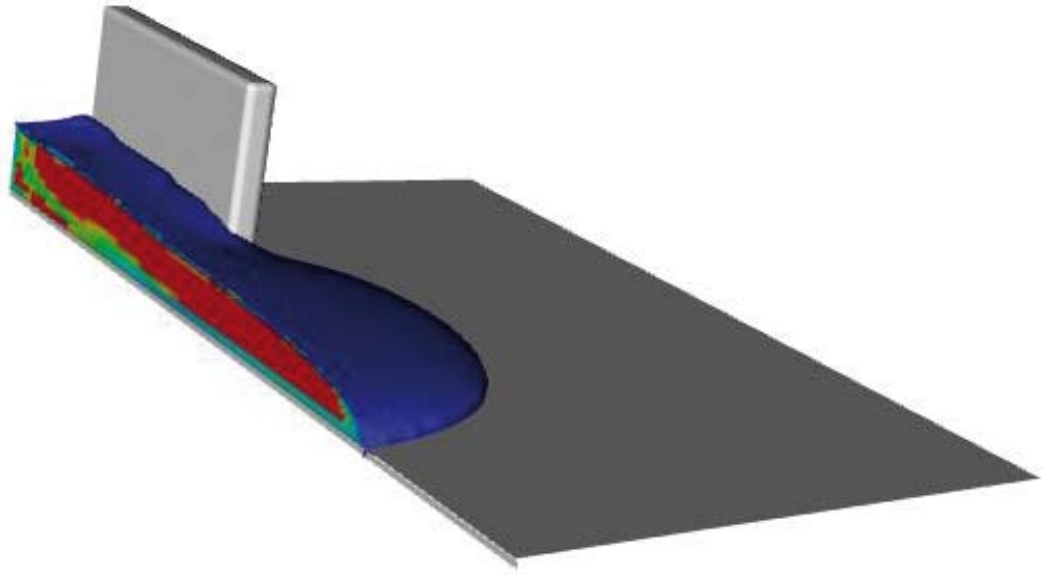

Figure 2: Flow of Carbopol down an inclined plane. The different colors indicate the different viscosities.

References

1. S. Cochard and C. Ancey: Tracking the free surface of time-dependent flows: Image processing for the dam-break problem, Experiments in Fluids 44 (2008) 59—71.
2. R. Croce, M. Griebel, and M.A. Schweitzer, A Parallel Level-Set Approach for Two-Phase Flow Problems with Surface Tension in Three Space Dimensions, Universität Bonn, Sonderforschungsbereich 611, Bonn, 2004.

Land-climate interactions: Modelling and analysis

Prof. Sonia I. Seneviratne

with Thierry Corti, Martin Hirschi, Eric Jäger, Andreas Roesch, Reto Stöckli, and Ryan Teuling

Institute for Atmospheric and Climate Science, ETH Zürich, Switzerland

Introduction

Our group investigates the role of land-climate interactions for the climate system, both at the regional and global scales. Our activities at CSCS encompass several research projects ranging from the coupling of the CLM regional climate model to the detailed vegetation/land model CLM (CLM-CLM or "CLM2"), to sensitivity experiments investigating the role of soil moisture, vegetation and snow for the modelling of extreme events, seasonal forecasting, and climate change projections. Funding for our research comes from several sources, in particular the CCES project MAIOLICA, SNF/NCCR-Climate, the EU-FP6 project CECILIA, and ETH core funding. We collaborate with several other groups, in particular with the ALPS-Climate project, within the CCES and NCCR-Climate programs, and as part of international research teams (CLM community, CECILIA, GLACE-2 project).
We maintain a regional (CLM / Climate Local Model) and a global (ECHAM5) climate model, also used by other groups at ETH Zurich and successfully run at CSCS (Cray XT3). Moreover, we maintain several land surface models (CLM / Community Land Model, Terra, Terra_LM, Biosphere-Atmosphere Transfer Scheme, Catchment Land Surface Model). We have conducted research at CSCS since July 2007.
Our current main modeling activities are as follows:

1. Coupling of the Climate Local Model (CLM) with the Community Land Model (CLM). The newly coupled model (CLM-CLM or "CLM2") will be the first of its type in terms of the combined high resolution (regional climate model) and high detail of the represented land/vegetation processes (dynamic vegetation processes, phenology, plant physiology). Significant resources are necessary for the testing of the new coupled version and the conducting of reference and sensitivity experiments. This work is performed as part of the CCES project MAIOLICA (http://www.cces.ethz.ch/projects/clench/MAIOLICA)
2. Investigation of the impact of land-climate interactions for regional and global climate. For this purpose, we use targeted sensitivity experiments with CLM-TERRA_LM, CLM-CLM and ECHAM5 for past, present and future climate. In particular, we focus on the role of land-atmosphere coupling for extreme events such as droughts, heatwaves, and heavy precipitation events, as well as possible modifications thereof with climate change. This work builds on past expertise (e.g. Seneviratne et al. 2006, Nature) and is conducted in coordination with several projects in our group (CECILIA, NCCR-Climate)
3. Analysis of the potential of land initialization (soil moisture, snow, vegetation) for seasonal forecasting, using both regional and global climate experiments. With this line of research, we aim to significantly improve the stand of seasonal forecasting, in particular in Europe,

by exploiting information linked with land persistence. We also work on this research with international teams, in particular as part of the GLACE-2 (Global Land-Atmosphere Coupling Experiment) experiment coordinated by NASA/GSFC

Background Information

Several studies have highlighted how land-atmosphere interactions can critically modulate climate variations on a range of temporal (seasonal to centennial) and spatial (local to global) scales. In particular, the role of soil moisture for precipitation and temperature in midlatitude and transitional climate zones has been highlighted in several investigations (e.g. Seneviratne and Stöckli 2008). These interactions are particularly important in the context of climate change, with shifts of climatic regimes significantly modifying the distribution of so-called “hot spots” of land-atmosphere coupling (Fig. 1). Recent results suggest that Central and Eastern Europe may become such a hot spot in the coming decades (Seneviratne et al. 2006a), and thus investigations in this region are particularly crucial.

Soil moisture is furthermore an important memory component of the climate system (e.g. Seneviratne et al. 2006b). Moreover, also snow and soil freezing play an important part for climate persistence. Thus, both soil moisture and snow may be critical for seasonal forecasting, and investigations on the potential of soil moisture and snow initialization are strongly needed, especially in Europe. Finally, other important land-atmosphere interactions within the framework of climate change involve interactions with the carbon cycle, and in particular links between CO2 assimilation and water use in plants. Only few climate models (in particular regional climate models) include a full description of these processes.

Current results and on-going research

Our research project started in July 2007. In this report, we present first results obtained in relation with our modeling activities at CSCS.

Several simulations with the CLM-TerraLM have been conducted since the beginning of the project, in particular: ensemble simulations at 50km (0.44o) resolution (1958-2006), experiments driven with ECMWF operation forecast analysis data (2002-2005), 4-year simulations at 50km resolution for the investigation of alternative cloud and precipitation parameterization schemes, and several simulations with uncoupled soil moisture at 50km resolution (1958-2006).

The analysis of the performed ensemble simulations and of existing CLM-TerraLM simulations from the ENSEMBLES FP6 project have allowed an assessment of the performance and intrinsic variability of the CLM-TerraLM model version (Jaeger et al. 2008a, Roesch et al. 2008). Though

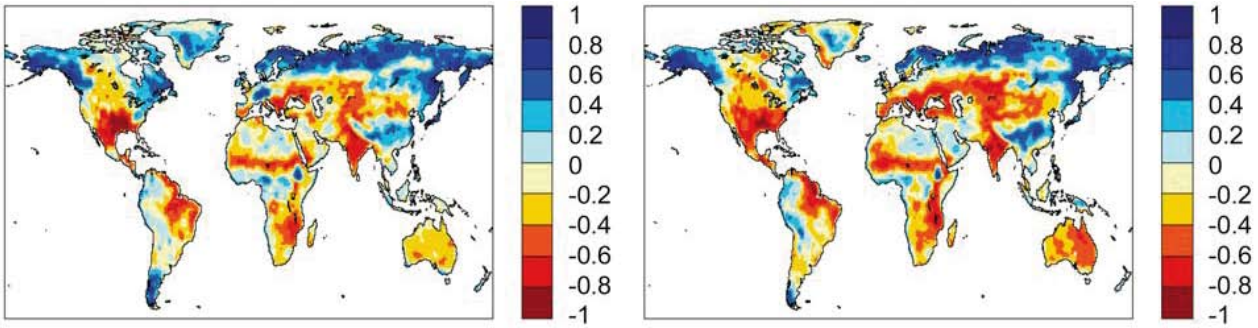

Figure 1: Correlation between June-July-August evapotranspiration and temperature in IPCC AR4 GCM simulations (ECHAM5, GFDL, HadCM3) for 1970-1990 (left) and 2080-2100 (right). Negative correlations (red) indicate strong land-atmosphere coupling (e.g. impact of soil moisture on temperature). Note the shift in land-atmosphere coupling taking place in Central Europe as a consequence of global warming, inducing a stronger impact of soil moisture on European climate with enhanced temperatures. [from Seneviratne et al. 2006a, Nature]

significant biases were identified, the model's overall land-atmosphere coupling characteristics appear realistic (Jaeger et al. 2008b, Fig. 2). Following this analysis, several sensitivity experiments with uncoupled soil moisture have been designed and are currently being performed. The purpose of these experiments is to investigate the respective role of interannual vs intraannual variability of soil moisture for the European climate.

In addition, simulations with the ECHAM5 GCM have been conducted for the GLACE2 experiment to which our group is contributing. The simulations are currently running and should be completed by the end of the year.

Finally, the coupling of the CLM-CLM ("CLM2") is underway. A beta version of the newly coupled version CLM-CLM is currently locally tested at ETH Zurich for performance optimization and testing of numerical stability. Once this preparatory test phase is completed, the CLM-CLM version will be ported to CSCS and long-term simulations will be conducted.

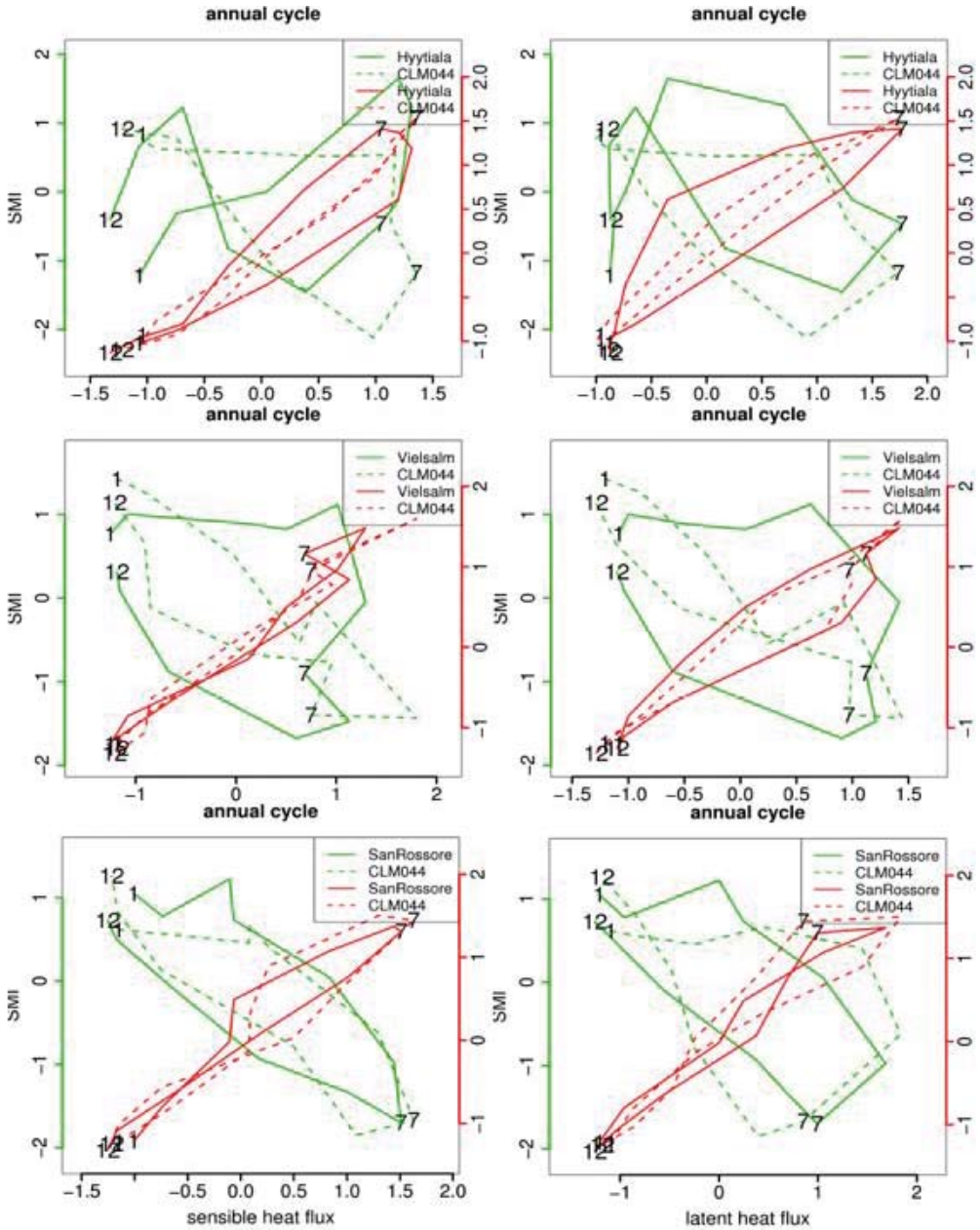

Figure 2: Validation of land-atmosphere coupling characteristics in CLM-TerraLM. Mean annual cycle (2002-2005) of sensible (left) and latent (right) heat fluxes as a function of standardized soil moisture (SMI, left y-axis) and radiation (right y-axis) for the Fluxnet stations Hyytiala (high latitude climate, boreal), Vielsalm (temperate climate, mixed vegetation) and San Rossore (mediterranean climate, evergreen). [from Jaeger et al. 2008b, in prep.]

References

1. Jaeger, E.B., I. Anders, D. Lüthi, B. Rockel, C. Schär, and S.I. Seneviratne, 2008a: Analysis of ERA40-driven CLM simulations for Europe. Meteor. Zeit., in press. (CLM special issue)
2. Jaeger, E.B., R. Stöckli, D. Lüthi, and S.I. Seneviratne, 2008b: Validation of planetary boundary layer fluxes of the CLM regional climate model with CarboEurope flux tower observations. In preparation.
3. Roesch, A., E.B. Jaeger, D. Lüthi, and S.I. Seneviratne, 2008: The analysis of CLM model biases in relationship to intra-ensemble model variability. Meteor. Zeit., in press. (CLM special issue).
4. Seneviratne, S.I., D. Lüthi, M. Litschi, and C. Schär, 2006a: Land-atmosphere coupling and climate change in Europe. Nature, 443, 205-209.
5. Seneviratne, S.I., R.D. Koster, Z. Guo, P.A. Dirmeyer, E. Kowalczyk, D. Lawrence, P. Liu, C.-H. Lu, D. Mocko, K.W. Oleson, and D. Verseghy, 2006b: Soil moisture memory in AGCM simulations: Analysis of Global Land-Atmosphere Coupling Experiment (GLACE) data. J. Hydrometeor., 7, 1090-1112
6. Seneviratne, S.I., and R. Stöckli, 2008: The role of land-atmosphere interactions for climate variability in Europe. In: Climate Variability and Extremes during the Past 100 years, Brönnimann et al. (eds.), Advances in Global Change Research, 33, Springer Verlag. (Book chapter)
7. Teuling, A.J., and S.I. Seneviratne, 2008: Contrasting spectral changes limit albedo impact on land-atmosphere coupling during the 2003 European heat wave. Geophys. Res. Lett., 35, L03401, doi:10.1029/2007GL032778.
8. Teuling, A.J., R. Uijlenhoet, B. van den Hurk, and S.I. Seneviratne, 2008: The functional role of soils in LSMs: A look using stochastic soil moisture models and ELDAS parameters. J. Hydrometeor., submitted.
9. van den Hurk, B., R. Haarsma, F. Selten, and S.I. Seneviratne, 2008: Impact of land-atmosphere coupling on European summer blocking events in a GCM experiment. J. Hydrometeor., submitted.

Reliability and degradation modelling of ultrathin dielectrics

Prof. Urs Sennhauser

with Matteo Farnesi Camellone, Joachim Reiner and Louis Schlapbach

Swiss Federal Laboratories for Materials Testing and Research (EMPA), Duebendorf, Switzerland

The essential limitations on gate insulators are related to the exponentially increasing gate current as the thickness of the oxide is reduced, and the effect of this current on both the functionality and reliability of de-vices and circuits. The leakage current is controlled by quantum-mechanical tunneling, either by Fowler-Nordheim tunneling at high gate voltage or by direct tunneling, at about 1-3 Volts but with ultra thin gate ox-ides (1-3 nm). The gate leakage current causes increased power consumption and may effect device and circuit functionality and reliability. This imposes a practical limit on oxide thickness. The rate of defect generation in the oxide is proportional to the current density flowing through it, and therefore the reliability margin for gateoxide breakdown has been drastically reduced as a consequence of device scaling. When the con-centration of defects reaches a critical value the system is irreversibly damaged and breakdown occurs. The idea of damage build-up to a critical value has been a key insight in leading to a predictive model of oxide reliability. However, this concept does not depend in any way on the physics of defect generation. Quantum mechanical models (ab-initio calculation) can be used to simulate the formation of atomic defects of a realistic material structure. Density Functional Theory [1] has been used to model and study the properties of alpha quartz and amorphous silica.

We used a norm conserving pseudopotential (Martin Troullier) for oxygen and a norm conserving (Goe-decker type) for silicon and the Generalized Gradient Approximation (GGA) to describe the exchange correlation energy. Several bulks of amorphous silica have been generated using a combination of classical and ab-initio molecular dynamics following the generation procedure of reference [2]. The interaction between silicon and oxygen atoms has been classically described by an empirical potential that has often been used to study static and dynamical properties of amorphous silica. The potential energy functions used to describe the interactions are completely empirical; the same interaction is used for bonded and non-bonded terms. This is the so called BKS potential [3] developed by van Beest, Kramer and van Santen by means of ab initio calculations.

The generated systems have been relaxed by Car and Parrinello quantum mechanical simulated annealing to reach the zero kelvin temperature. In order to check the structure of the generated systems we have analyzed several structural characteristics of the sample and compared them to experimental data. These structural characteristics are radial distribution functions, bond angles distributions and the static structure factor. In both calculations we applied periodic boundary conditions in space and we performed the calculations at the Gamma point only in the reciprocal space. Different species of defects in crystalline and

amorphous silica have been considered. Oxygen vacancies in different charged states (neutral and positive) have been studied. In the neutral case, after removing one oxygen atom from the crystalline or amorphous silica bulk, the structure of the system has been fully optimized leading to the formation of a Si-Si bond. If positively charged, the system relaxes to a configuration in which the unpaired electron is shared between the two partially coordinated silicon atoms. One of the two silicon atoms can reverse its direction. After overcoming an energy barrier it relaxes back and bonds to an oxygen which is threefold coordinated. The energy barriers involved in this mechanism have been explicitly evaluated by using ab-initio constrained molecular dynamics. The computed energy barriers have values in a range between 0.3-0.9 eV. In this configuration, called puckered configuration, the unpaired electron localizes on the silicon atom of the dangling bond and it can be detected using electron-paramagnetic-resonance (EPR) technique.

A model for electron trapping in amorphous silicon dioxide has been investigated. Electrons can be trapped by silicon atoms of the disordered network, leading to a significant distortion of the tetrahedron involved in the process [4]. The system has to overcome an energy barrier of 0.23 eV to allow the added electron to localize on the silicon atom.

Recently we started to study self trapped holes in amorphous silica dioxide bulk. Self trapped holes have been experimentally observed for the first time by Griscom [5] in 1989 and the first theoretical Hartree Fock calculations have been performed by Edwards [6] on a small cluster. Edwards showed that a hole localizes on a single oxygen atom in the silica cluster thus partially reproducing the experimental results of [5].

We performed unrestricted open shell Hartree Fock calculations on a bulk of amorphous silica in presence of a hole, we applied periodic boundary conditions (PBC) and we were able to localize the hole on a single oxygen atom of the disordered network. Hartree Fock calculations were required since the standard Density Functional Theory approximations, such as the local density approximation (LDA) or the generalized gradient approximation (GGA) often fail in describing electron/hole localization in silicon dioxide. This failure can be attributed partially to the incomplete cancellation of the unpaired electron self interaction. In addition, the Self Interaction Corrected (SIC) functional proposed by Vande Vondele and Sprik [7] has been applied to the system to successfully describe the hole localization [8].

Finally, the role of hydrogen in the degradation process of silicon dioxide has been investigated. The optimum geometries and the formation energies of different charged states of hydrogen (neutral, positive and negative) in amorphous and crystalline silica.

In conclusion, an extensive study of different kind of defects responsible for degradation of silicon dioxide has been carried out by using ab inito quantum mechanical techniques.

References

1. P.Hohennberg and W.Kohn Phys.Rev.B 136,864-871,1964.
2. M.Benoit et al.Eur.Phys.J. B13,631-636,2000.
3. B.W.H.van Beest et al.Phys.Rev.Lett.64,1955,1990.
4. M.Farnesi et al. in press Physical Review B.
5. D.L. Griscom PRB 40, 4224 (1989)
6. A.H Edwards PRL 71, 3190 (1993)
7. J.VandeVondele and M.Sprik Phys. Chem. Chem. Phys. 7, 1363, 2005
8. M.Farnesi et al. in preparation

The atomistic modeling of size effects in plasticity

Prof. Helena Van Swygenhoven

with Dr. P. M. Derlet

Materials Science and Simulation, ASQ/NUM, Paul Scherrer Institute, PSI Villigen, Switzerland

Description

Large scale molecular dynamics (MD) simulations are used to investigate plasticity in spatially confined structures [1]. Research is performed in the framework of NANOMESO, a research project financed through the international call between the EU and the NSF-USA (FP6-2007-NMP-NSF-1, nr 016710, 1 PhD and 1 post-doc) and in the framework of a Swiss SNF project (200021-100055/1, 1 PhD).

The main objective of NANOMESO is to address dislocation nucleation, propagation, and absorption mechanisms within a confined region such as a nanosized grain and to provide input for mesoscopic models of dislocation plasticity. The output is used by the other NANOMESO partners (more details can be found on web sites below). The main objective of the SNF project is to study the influence of the presence of dilute oxygen in confined interfaces.

All molecular dynamics (MD) simulations have been performed using our in-house MPI based parallel Fortran95 program called moldyPSI which operates on the Cray XT3 clusters. For ab- initio calculations performed on the XT3, the VASP package was used. The simulations involving oxygen have required the development of a new working tool within the framework of moldyPSI, based on a local chemical potential formalism. In what follows we highlight the achievements of the 2006-2007 CSCS computing period.

The atomistic modelling of dislocation activity within pure metallic nanocrystalline systems

To analyze the dislocation – grain boundary interaction processes and to study the influence of the grain boundary structure on these processes, MD simulations were performed on nanocrystalline Al samples containing 100 grains with a mean grain diameter of d=11.5 nm at a constant strain rate of 1e8/sec and constant temperature [2, 3]. All dislocation mediated slip events during the deformation were identified [4].

To study the local shear stress, the grain averaged stress tensor is determined from the atomic virial stress tensors of the fcc atoms within the grain. This averaged stress tensor is then used to calculate the grain averaged resolved shear stress for all 12 slip systems. Such a type of analysis has shown [4] that mesoscopic models of dislocation mediated plasticity in nanocrystals should take into account:

- a distribution of the slip plane areas for a given grain size.
- a distribution of the critical resolved shear stresses required to trigger slip events.
- the incorporation of a distribution of dislocation sources that are activated at shear stresses lower than that required for the dislocations to propagate.

Further analysis at the atomic scale of the slip events showed that during the deposition of dislo-

cation segments at the grain boundary, screw dislocations can circumvent local unfavorable GB structures by cross-slip [5]. An example for such a cross-slip process is shown in Fig.1. In this figure double cross-slip allowed the dislocation to avoid a region in the grain boundary that was under high compressive stresses. This mechanism constitutes an alternative depinning mechanism to that previously observed where dislocations remained on the same glide plane and depinned via a kinking mechanism.

Inspection of the sample for dislocation transmission revealed only a few cases in which slip was transferred through a GB into another grain. One interesting attempt of dislocation transmission through a general high angle grain boundary is shown in Fig. 2 [6]. The structure of the grain boundary shown in Fig. 2 consists of coherent regions (indicated in yellow) separated by regions of misfit. It is exactly at such a coherent region that the dislocation in grain 9 which deposits dislocation segments at the grain boundary to grain 11 is in part transmitted into grain 11. This observation points to the importance of the internal grain boundary structure for the transmission of slip, which can only be captured in three dimensional models of dislocation/grain boundary interaction.

To gain a more fundamental understanding of the nature of dislocation activity in metals, ab-initio calculations have been undertaken to investigate the origins of the strength of Ni, Al and Cu [7]. Past work has shown that the generalized-stacking-fault surface energy (GSFE) curve, which represents the energy dependency of rigidly shearing an fcc crystal at a (111) plane along a [–1–12] slip direction, can rationalize all published simulation work concerning dislocation activity within the metallic nanocrystalline environment. The ab-initio calculations revealed the relative insensitivity of the GSFE curve to the local complex stress envi-

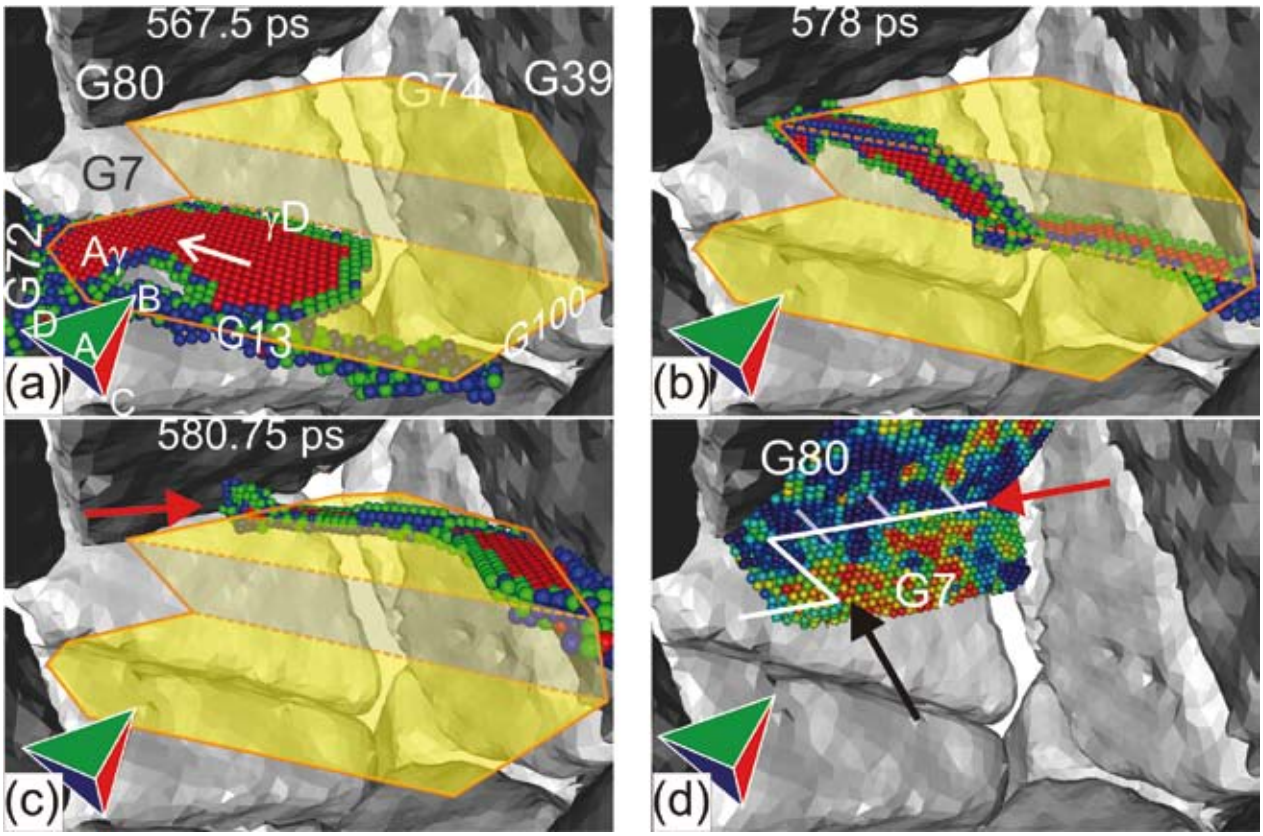

Figure 1: a) – c) Three snapshots of a full dislocation that cross-slips twice to avoid a compressive stress region of the neighbouring GB 86-7 shown in d). Only the non-FCC atoms within the central grain are shown to visualize the dissociated core of the full dislocation. In a) the triple junction line at which the full dislocation nucleates is displayed as the associated non-FCC atoms. In d) the atoms on the grain boundaries to grain 80 and 7 are colored according to the local hydrostatic stress, ranging from -1.5 GPa blue to 1.5GPa (red). The white line represents the region onto which the dislocation is deposited.

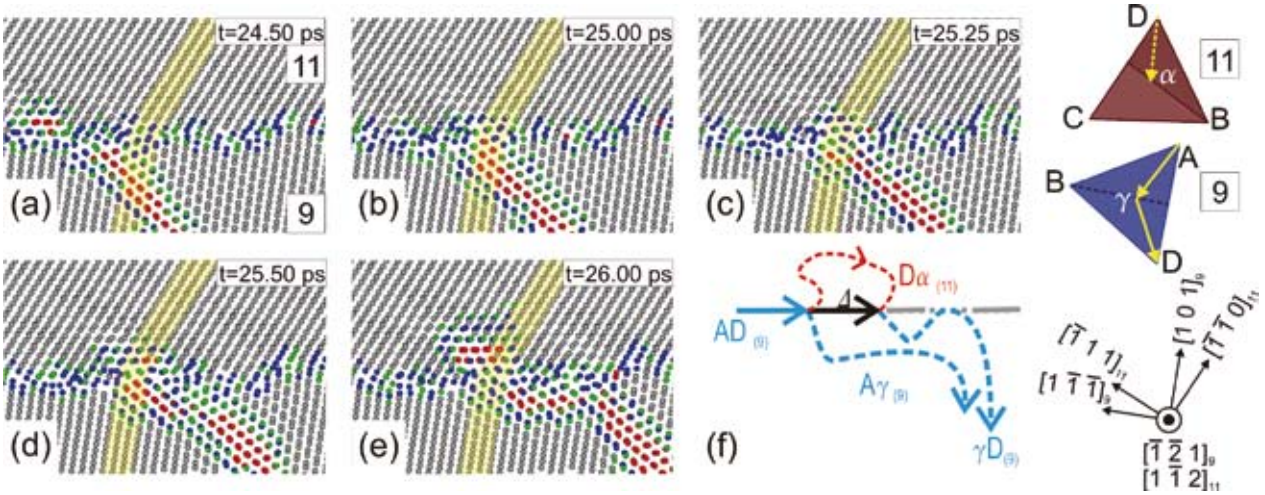

Figure 2: a)-e) temporal sequence of a dislocation transmission event at a coherent region during the passage of AD(c) in grain 9. The dislocation configuration of e) is shown schematically in f). The orientation of the slip systems of the two grains together with the identified Burgers vectors is shown on the Thompson tetrahedral.

ronment due to GBs, providing valuable information about the nature of cohesive bonding within these metals.

The modeling of dilute oxygen in confined interfaces

Most simulations investigating deformation mechanisms in metals have been performed on pure samples, making it difficult to extrapolate the results towards the experimental regime. Light impurities such as oxygen, hydrogen and carbon are naturally incorporated in interfaces during sample synthesis, and experimental studies have shown that they play a key role in the stability of the nanocrystalline structure under stress. For the case of O in Al, where oxidation occurs resulting in long-range electrostatic interactions and a dynamic charge transfer that depends on the local environment of each ion, it has not been possible to develop accurate atomistic potentials for use in routine large scale molecular dynamics simulations.

As a result, much of the present work has concentrated on the development of a new efficient and scalable algorithm to simulate the charge transfer between oxygen impurities and the surrounding metallic atoms [8]. In particular a local chemical potential approach that optimizes the charge on only those atoms expected to be ionic is developed. By doing so, the charge fluctuation problem experienced in regions far from any oxygen is solved, leading to a linear minimization problem of the electrostatic energy. In the dilute oxygen limit, such an approach can lead to at least an order of magnitude saving in computation. Ab-initio calculations of 108/109 atom Al/O configurations have been performed on Horizon to obtain oxygen defect energies to be used in an expanded materials data base for the development of a new Al/O empirical potential.

Simulations presently being performed using the above algorithm are investigating the effect that oxygen has on stress induced grain boundary migration as demonstrated in fig.3 where the stick-slip behaviour of a Σ75 GB is investigated as a function of O content. The work is performed in collaboration with Dr. O. Politano, Université de Bourgogne, Dijon, France.

Websites related to this large user project

http://mss.web.psi.ch/ for the activities of the group “Materials science and simulation”, ASQ/NUM department at the Paul Scherrer Institute.
http://www.mse.osu.edu/~andersonp/nanomeso.html for the EU-NSF funded consortium NANOMESO.

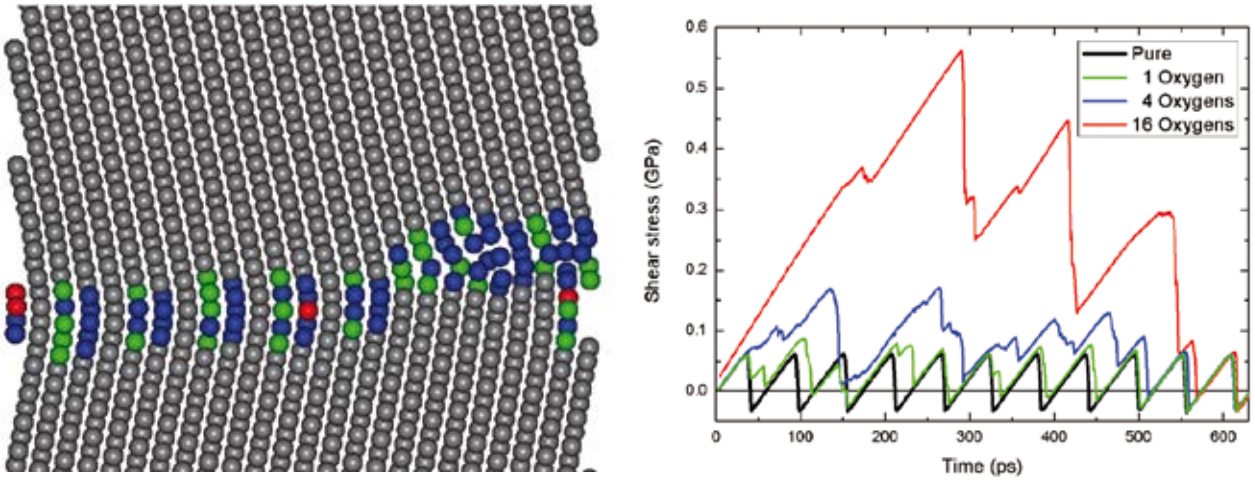

Figure 3: (a) Snapshot of a Σ75 grain boundary containing 16 O atoms located in the right-hand-side of the GB (yellow circles); (b) Shear stress (GPa) vs Time (ps) showing the influence of O on the stick-slip behavior.

References

1. Van Swygenhoven H, Weertman JR. Deformation in nanocrystalline metals. Materials Today 2006;9:24.
2. Van Swygenhoven H, Derlet PM, Froseth AG. Stacking fault energies and slip in nanocrystalline metals. Nature Materials 2004;3:399.
3. Van Swygenhoven H, Derlet PM, Froseth AG. Nucleation and propagation of dislocations in nanocrystalline fcc metals. Acta Materialia 2006;54:1975.
4. Bitzek E, Derlet PM, Andersen P, Van Swygenhoven H. The Stress-Strain Response of Nanocrystalline Metals: A Statistical Analysis of Atomistic Simulations. Acta Materialia 2008;56:4846.
5. Bitzek E, Brandl C, Derlet PM, Van Swygenhoven H. Dislocation Cross-Slip in Nanocrystalline FCC Metals. Phys. Re. Lett. 2008;100:235501.
6. Brandl C, Bitzek E, Derlet PM, Van Swygenhoven H. Slip transfer through a general high angle grain boundary in nanocrystalline aluminum. Applied Physics Letters 2007;91:111914.
7. Brandl C, Derlet PM, Van Swygenhoven H. General-stacking-fault energies in highly strained metallic environments: Ab initio calculations. Physical Review B 2007;76:054124.
8. Elsener A, Politano O, Derlet PM, Van Swygenhoven H. A local chemical potential approach within the variable charge method formalism. Modelling and Simulation in Materials Science and Engineering 2008;16.

Stellar Cosmic Engines in Galaxies

Dr. Rolf Walder

Observatoire de Genève, Université de Genève, Genève, Switzerland and Institut für Astronomie, ETH Zürich, Switzerland

Collaborators: Georges Meynet (Observatoire de Genève, Switzerland), Daniel Pfenniger (Observatoire de Genève, Switzerland), Doris Folini (ETH Zürich, Switzerland), Steven N. Shore (Università di Pisa, Italy), Andrei Bykov (Ioffe Institute, Russian Academy of Sciences, St. Petersburg, Russia), Randall J. LeVeque (University of Washington, Seattle, USA)

Themes

Stars deeply affect their environment – by means of winds, supernovae, and gamma-ray bursts. It suffices to see the fantastic shapes of supernova remnants and nebulae around massive stars to realize the deep impact stars have on the interstellar medium. The feed-back mechanisms between stars and gas regulate star formation, shape the chemical evolution of cosmic matter, and modify its dynamical properties. These mechanisms are at the heart of the physical understanding of how galaxies with their stellar and planetary population form and evolve. They are the general topic of this project.

A first focal point of the project are galactic wind bubbles, formed by winds and supernova explosions from big star clusters. We study numerically how such bubbles affect the distribution of chemical elements in the galaxy, the formation of new stars,

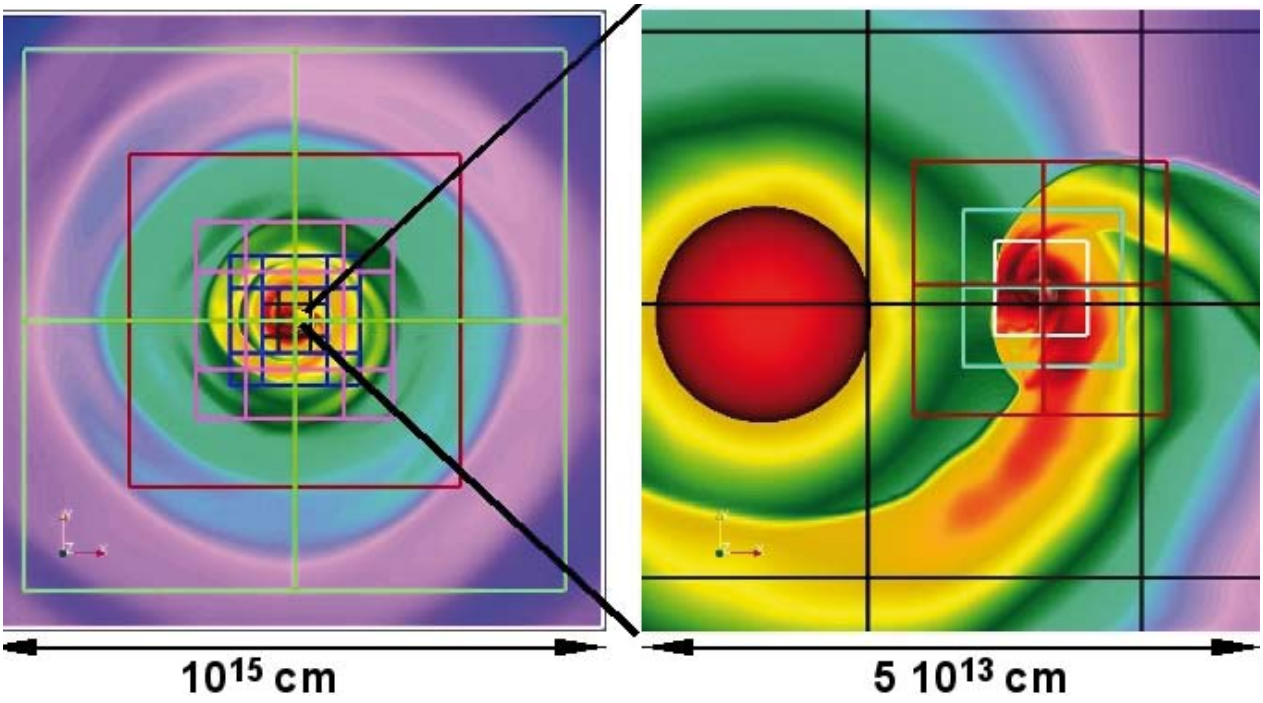

Figure 1: The grid structure of the nine levels of refinement, shown for the entire computational domain (left) and around the accreting WD (right). While the coarser grids of levels 1 through 6 are fixed in space, the meshes of levels 7 through 9 follow the orbiting WD. The RG is shown in red, the accreting WD in blue.

and the evolution of habitable zones in the universe. A second focal point are gamma-ray bursts, the most powerful engines in the universe since the big bang. We will numerically explore the suggestion that such bursts arise from massive, fast rotating stars.

The third focal point, supernovae Ia (SN Ia), we outline in more detail and present first results. SN Ia are thermonuclear bombs, burning within seconds about 1.4 solar masses (a Chandrasekhar mass) of carbon and oxygen to iron. The released energy is several 10^{51} ergs. In visible light, this event often outshines the host galaxy of the destroyed star. The energy emitted by SN Ia is always the same, which makes them – together with their brightness – the best distance indicators of the young and distant universe. In astrophysics, SN Ia are known as cosmological standard candles and as such are a crucial pillar of modern cosmology. Moreover, SN Ia produce about half of the iron group elements found in the universe.

Despite their key role, no progenitor star of an SN Ia has been identified so far. Several scenarios leading to an SN Ia have been suggested. A primary goal of this project is to scrutinize one particular progenitor scenario – recurrent novae - by means of high end numerical simulations.

Achievements

The recurrent nova RS Ophiuchi (RS Oph) is a binary star system, in which a white dwarf star (WD) accrets matter (mostly hydrogen) from the stellar wind of a red giant star (RG). If the WD manages to accrete enough mass to reach the Chandrasekhar stability limit (~ 1.4 solar masses), it will explode as an SN Ia. There are complications, however, which make a careful numerical study necessary. The accreted mass on the WD surface ignites periodically (every 22 years in RS Oph) and burns to helium. The burning is explosive and expells part of the accumulated matter. The crucial question is whether the nova expells more

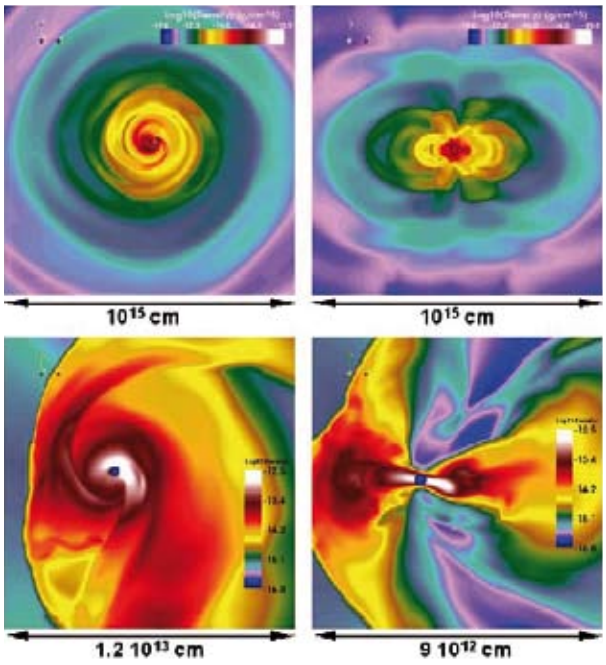

Figure 2: Density structure during the accretion phase. Shown is density (logarithmic scale, g/cm^3) in the orbital plane (xy-plane, left), and in a plane perpendicular to the orbit (yz-plane, right) for the entire computational domain (10^{15} cm a side, top) and a zoom around the accreting WD (10^{13} cm a side, bottom). Self-interacting high-density spirals dominate the inner region up to a few times the binary separation. The RG is shown in red, the WD in blue.

mass than was accumulated. Moreover, the evolutionary time scales of the entire system - evolution of individual stars, decay of orbit, time to potentially reach the Chandrasekhar limit - are all about 10 million years and are non-linearly coupled.

For the first time, we simulated RS Oph by means of 3D hydrodynamical simulations. Employing adaptive mesh techniques, we were able to resolve 7 orders of magnitude in space and time (see Fig. 1), a prerequisite for the achievement of the following results:

1. The WD collects about 10 % of the mass lost by the RG. The rest of the RG wind leaves the system in a systemic wind, which is highly structured by the orbital motion (Fig. 2). In the orbital plane, interacting Archimedian spirals form, in which mass is enhanced by an order of magnitude as compared to the undisturbed outflow. Normal to the orbital plane, the circumstellar matter is stratified by about a factor of 2.

2. In the vicinity of the accreting WD, a so called accretion disk is formed. Close to the star, energy and angular momentum are mostly dissipated in two strong spiral shocks. Further out, the dissipating shocks form a self-regulating network.

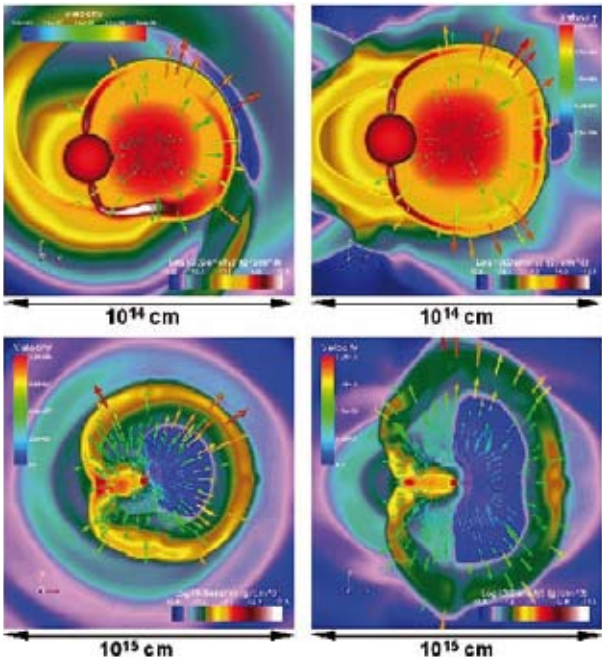

Figure 3: Density structure of the nova remnant. Shown are density (logarithmic scale, g/cm^3) and velocity (cm/s) in the orbital plane (xy-plane, left) and in a plane perpendicular to the orbit (yz-plane, right) at 29 hours (top panels) and 21 days (bottom panels) after explosion. The RG is shown in red, the WD in blue.

3. The systemic wind carries mass and angular momentum in a ratio that causes the stellar orbit to shrink by about 3% per million years. The change of the orbit thus is large compared with other relevant time scales. Combining the above accretion rate with nova explosion models, the Chandrasekhar limit is reached in about 10 million years. The lifetime of a RG is of the same order.
4. The nova explosion remnant is highly aspherical, a natural consequence of the density stratification normal to the orbital plane (Fig. 3). This finding corresponds well to observed radio-images. Also, the initial speed and deceleration of the blast wave correspond well with observations.

The insight gained by our simulations essentially helps to interpret the unique, panchromatic observations of the last nova outburst of RS Oph in February 2006. They confirm that RS Oph is indeed a prime candidate to evolve into an SN Ia. However, many questions remain open. To proceed, spectral emission shall be modeled that can be compared with observed data. Also, as the above results depend on the still uncertain system parameters, we perform simulations spaning the space of possible system parameters. In this way, we hope to further clarify the destiny of the system RS Ophiuchi.

References

1. R. Walder, D. Folini, S. N. Shore, 3D simulations of RS Oph: from accretion to nova blast. Astronomy&Astrophysics Letters, 2008, in press.
2. D. Folini, R. Walder, R. J. LeVeque, and J. M. Favre; Supersonic turbulence as an agent of structure formation in space. Proceedings of the 6th international Congress on Industrial and Applied Mathematics ICIAM07, Zurich, in press.
3. H. Couchman, D. Folini, G. Lake, and W. Petersen Astrophysical Simulations as Virtual Labs. SIAM News, October 21, 2007, (online version: http://www.siam.org/news/news.php?id=1227)
4. D. Folini and R. Walder; Supersonic turbulence in shock-bound interaction zones I: symmetric settings. Astronomy and Astrophysics, 459, 1-19, 2006.
5. G. Meynet and A. Maeder; Wind anisotropies and GRB progenitors. Astronomy and Astro-physics, 464, L11-L15, 2007
6. A. Maeder, G. Meynet, S. Ekstrom, R. Hirschi, and C. Georgy; Massive stars as cosmic engines through the ages. Cambridge University Press, IAU Symp. 250, F. Bresolin, P.A Crowther, and J. Puls, eds., in press.

List of Advanced Large Projects in Supercomputing (ALPS) 2007

Name	Organisation	Project Title
Jackson A.	ETH Zürich	Convection and Magnetic Field Gneration in Earth and Other Planets
Parrinello M.	ETH Zürich	Modelling Protein-Protein Interactions at the Atomic Level
Schär Ch.	ETH Zürich	Climate Change and the Hydrological Cycle from Global to European/Alpine Scales
Vogel V.	ETH Zürich	Towards Simulating a Cell Adhesion Site at Angstrom Resolution

List of Large User Projects 2006

Name	Organiszation	Project Title
Aemmer D.	ETH Zürich	Computational Science and Engineering in Nanoelectronic
Arbenz P.	ETH Zürich	Multi-level Micro-Finite Element Analysis for Human Bone Structure
Baiker A.	ETH Zürich	Hydrogenation reactions in heterogeneous enantioselective catalysis and homogeneous catalysis in supercritical CO_2
Bakowies D.	ETH Zürich	Atomizations energies from ab-inition calculations without empirical corrections
Besson O.	Uni Neuchâtel	Numerical solution of Navier Stokes equation in shallow domains
Brönimann S.	ETH Zürich	Climate and Stratospheric Ozone during the 20th century
Bürgi Th.	Uni Neuchâtel	Structure and enantiospecificity of chiral nanoparticles and interfaces
Cooper W.A.	EPF Lausanne	Computation of stellarator coils, equilibrium, stability and transport
Deubel D.	ETH Zürich	Quantum Chemical Studies of Transition Metal Anticancer Drugs
Folini D.	EMPA	Inverse modeling to monitor source regions of air pollutants
Gervasio F.	ETH Zürich	Charge transfer and oxidative damage to DNA
Hasenfratz P.	Uni Bern	Full QCD with 2 + 1 light chiral fermions
Hauser A.	Uni Genève	Photophysics and photochemistry of transition metal compounds: Theoretical Approaches
Helm L.	EPF Lausanne	Magnetic interactions in extended systems
Hutter J.	Uni Zürich	Development and application of ab-initio molecular dynamics methods
Joos F.	Uni Bern	Modelling CARBOn Cycle CLIMate Feedbacks (CARBOCLIM)
Kleiser L.	ETH Zürich	Numerical simulation of transitional, turbulent and multiphase flows
Koumoutsakos P.	ETH Zürich	Simulations using particle methods optimization of real world problems using evolutionary algorithms multiscale modelling, simulations and optimization of complex systems

Name	Organization	Project Title
Krajewski F.	ETH Zürich	Ab-initio simulation of the nucleation of silicon with a novel linear scaling electronic structure method
Läuchli A.	EPF Lausanne	Computational Studies of Strongly Correlated Electron System
Leriche E.	EPF Lausanne	Direct numerical simulation ot the buoyancy-driven turbulence in a cavity: the DNSBDTC project
Lüscher M.	CERN	Numerical lattice gauge theory
Maddocks J.	EPF Lausanne	Large-scale atomistic molecular dynamics simulations of DNA minicircles
Martonak R.	ETH Zürich	Crystal structure prediction from computer simulations
Meuwly M.	Uni Basel	Electronic Structure Calculations for Chemical Reactions involving Transition Metals
Oganov A.	ETH Zürich	Computational mineral physics and cristallography
Pasquarello A.	EPF Lausanne	Disordered network-forming materials
Passerone D.	Uni Zürich	Computational investigation of relevant photochemically active molecular switches
Poulikakos D.	ETH Zürich	Biothermofluidics for Cerebrospinal fluid diagnostic and control-development of a knowledge base Explosive vaporization phenomena in microenclosures
Raible Ch.	Uni Bern	Modelling and Reconstruction of North Atlantic Climate System Variability (MONALISA)
Raitieri P.	ETH Zürich	Computational study of molecular nano-machines
Röthlisberger U.	EPF Lausanne	Mixed quantum mechanics / molecular mechanics study of systems of biological interest
Schär Ch.	ETH Zürich	Modelling weather and climate on european and alpine scales
Schwierz C.	ETH Zürich	aLMO reanalysis and hindcast for the Alpine Region
Sennhauser U.	EMPA	Reliabilty and degradation physics of ultrathin dielectrics (Nanoxide)
Sljivancanin Z.	EPF Lausanne	Solid Surfaces and Interfaces
Van Lenthe H.	ETH Zürich	What genetic loci regulate bone strength?
Van Swygenhoven H.	PSI	The atomistic modeling of size effects in plasticity
Vogel P.	EPF Lausanne	Developing High-resolution Models How Mechanical force Changes Protein Function
Wild M.	ETH Zürich	Global Climate Change: Modelling Climate Dynamics on Decadal Time Scales

List of Large User Projects 2007

Name	Organisation	Project Title
Arbenz P.	ETH Zürich	Multi-level Micro-Finite Element Analysis for Human Bone Structure
Baiker A.	ETH Zürich	Hydrogenation reactions in heterogeneous enantioselective catalysis and homogeneous catalysis in supercritical CO_2
Bakowies D.	ETH Zürich	Atomisations energies from ab-initio calculations without empirical corrections
Behler J.	ETH Zürich	A Neutral-Network Representation of High-Dimensional ab-initio Potential-Energy Surfaces
Brönimann S.	ETH Zürich	Climate and Stratospheric Ozone during the 20th century
Bruneval F.	ETH Zürich	Crystal structure prediction from computer simulations
Bürgi Th.	Uni Neuchâtel	Structure and enantiospecificity of chiral nanoparticles and interfaces
Cooper W.A.	EPF Lausanne	Computation of stellarator coils, equilibrium, stability and transport
Deubel D.	ETH Zürich	Quantum Chemical Studies of Transition Metal Anticancer Drugs
Ensing B.	ETH Zürich	Multiscale modelling of proton conducting polymeric membranes
Fichtner W.	ETH Zürich	Computational Science and Engineering in Nanoelectronics
Folini D.	EMPA	Inverse modelling to monitor source regions of air pollutants
Fouchet L.	ETH Zürich	Dust in protoplannetary disks
Gervasio F.	ETH Zürich	Charge transfer and oxidative damage to DNA
Gödecker S.	Uni Basel	Atomistic simulations and electronic structure
Hasenfratz P.	Uni Bern	Full QCD with 2 + 1 light chiral fermions
Hauser A.	Uni Genève	Photophysics and photochemistry of transition metal compounds: Theoretical Approaches
Helm L.	EPF Lausanne	Magnetic interactions in extended systems
Hutter J.	Uni Zürich	Development and application of ab-initio molecular dynamics methods
Ianuzzi M.	PSI	Transport properties and microstructural changes in uranium dioxide
Joos F.	Uni Bern	Modelling CARBOn Cycle CLIMate Feedbacks (CARBOCLIM)
Kleiser L.	ETH Zürich	Numerical simulation of transitional, turbulent and multiphase flows
Koumoutsakos P.	ETH Zürich	Simulations using particle methods optimisation of real world problems using evolutionary algorithms multiscale modelling, simulations and optimisation of complex systems
Krack M.	ETH Zürich	Nitrogen reduction on pyrite surfaces
Krajewski F.	ETH Zürich	Ab-initio simulation of the nucleation of silicon with a novel linear scaling electronic structure method
Kröger M.	ETH Zürich	Computer-Aided Design of Nanostructured Interfaces for Biological Sensors
Läuchli A.	EPF Lausanne	Computational Studies of Strongly Correlated Electron System

Name	Organisation	Project Title
Lehning M.	WSL-SLF	Wind field simulations and snow drift modelling over steep terrain
Leyland P.	EPF Lausanne	Large scale compressible flow for aerothermodynamic studies
Lodziana Z.	EMPA	Computational investigation of complex hydrides for hydrogen storage
Lüscher M.	CERN	Numerical lattice gauge theory
Maddocks J.	EPF Lausanne	Large-scale atomistic molecular dynamics simulations of DNA minicircles
Mareda J.	Uni Genève	Molecular Modelling of Artificial Multifunctional Pores and their Catalytic Properties
Martonak R.	ETH Zürich	Crystal structure prediction from computer simulations
Meuwly M.	Uni Basel	Electronic Structure Calculations for Chemical Reactions involving Transition Metals
Oganov A.	ETH Zürich	Computational Crystallography: crystal structure prediction and simulation of planetary materials
Parlange M.	EPF Lausanne	Large-eddy-simulation studies of atmospheric boundary layer flow over complex terrain
Parrinello M.	ETH Zürich	Ab-initio study of proton diffusion in water-methanol solutions
Parrinello M.	ETH Zürich	Ab initio simulations of phase change materials
Pasquarello A.	EPF Lausanne	Atomic-Scale Modelling at Semiconductor-Oxide Interfaces
Passerone D.	Uni Zürich	Computational investigation of relevant photochemically active molecular switches
Passerone D.	EMPA	Atomistic simulation of surface-supported molecular nanostructures and of quaicrystal surfaces
Poulikakos D.	EMPA	Biothermofluidics for Cerebrospinal fluid diagnostic and control-development of a knowledge base Explosive vaporisation phenomena in microenclosures
Raible Ch.	Uni Bern	Modelling and Reconstruction of North Atlantic Climate System Variability (MONALISA)
Raitieri P.	ETH Zürich	Computational study of molecular nano-machines
Röthlisberger U.	EPF Lausanne	Mixed quantum mechanics / molecular mechanics study of systems of biological interest
Sbalzarini I.	ETH Zürich	Simulations of biological systems and development of a parallisation framework
Schär Ch.	ETH Zürich	Modelling weather and climate on european and alpine scales
Schwierz C.	ETH Zürich	aLMO reanalysis and hindcast for the Alpine Region
Seneviratne S.	ETH Zürich	Land-climate interactions: Modelling and analysis
Sennhauser U.	EMPA	Reliability and degradation physics of ultrathin dielectrics (Nanoxide)
Sljivancanin Z.	EPF Lausanne	Solid Surfaces and Interfaces

Name	Organisation	Project Title
Van Lenthe H.	ETH Zürich	What genetic loci regulate bone strength?
Van Mier J.	ETH Zürich	Investigation of 3D Size Effects in Concrete Using Lattice Models
Van Swygenhoven H.	PSI	The atomistic modelling of size effects in plasticity
Vogel P.	EPF Lausanne	Developing High-resolution Models How Mechanical force Changes Protein Function
Walder R.	ETH Zürich	Stellar Cosmic Engines in Galaxies

Impressum

CSCS Swiss National Supercomputing Centre
Via Canotnale
CH-6928 Manno
Switzerland
Tel +41 (0) 91 610 82 11
Fax +41 (0) 91 610 82 09
http://www.cscs.ch

Design, Production:
Dorothea Gerhardt

Printing:
OK Haller AG, Zürich

Print-run:
350


Scientific Report